Politechnika Krakowska im. Tadeusza Kościuszki | Szkoła Doktorska | Wydział Inżynierii Materiałowej i Fizyki | Wydział Inżynierii Środowiska i Energetyki

ROZPRAWA DOKTORSKA

mgr inż. Celina Ziejewska

Właściwości geopolimerów modyfikowanych odpadową stłuczką szklaną

Dyscyplina wiodąca: Inżynieria materiałowa

Dyscyplina dodatkowa: Inżynieria środowiska, górnictwo i energetyka

Promotor: dr hab. inż. Marek Hebda, prof. PK

Promotor pomocniczy: dr inż. Agnieszka Grela

Kraków, 2023

Autorka pracy jest stypendystką programu POLI DOCTUS realizowanego w ramach projektu pn. „*Droga do doskonałości - kompleksowy program wsparcia uczelni*” POWR.03.05.00-00-Z214/18 (zadanie nr 3), finansowanego przez Narodowe Centrum Badań i Rozwoju, umożliwiającego interdyscyplinarne kształcenie w Szkole Doktorskiej Politechniki Krakowskiej.

Doktorantka realizowała pracę w obrębie dwóch dyscyplin naukowych:

- Inżynieria materiałowa (dyscyplina wiodąca);
- Inżynieria środowiska, górnictwo i energetyka (dyscyplina dodatkowa).

Część badań przeprowadzono w ramach realizacji projektu pn. *„Opracowanie technologii druku 3D, konstrukcyjnych i elewacyjnych elementów prefabrykowanych wykonywanych z kompozytów betonowych i geopolimerów”,* numer umowy: POIR.04.01.04-00-0096/18-00, finansowanego ze środków Narodowego Centrum Badań i Rozwoju.

Kierownik projektu: dr hab. inż. Marek Hebda, prof. PK

Pragnę serdecznie podziękować mojemu promotorowi
Panu dr hab. inż. Markowi Hebdzie, prof. PK za wprowadzenie w świat nauki i badań naukowych, zaangażowanie na każdym etapie realizacji pracy i rozwoju naukowego. Dziękuję za nieustający optymizm, przekazaną wiedzę, cenne uwagi merytoryczne i wszechstronną pomoc.

Bardzo dziękuję mojej promotor pomocniczej
Pani dr inż. Agnieszce Greli za poświęcony czas, cenne uwagi, życzliwość oraz motywację do realizacji pracy.

Podziękowania składam również wszystkim osobom, z którymi współpracowałam w czasie realizacji pracy.

Szczególnie dziękuję moim kochanym Rodzicom za wsparcie, wiarę w moje możliwości i wiele więcej.

Spis treści

Streszczenie

Zmiany klimatyczne będące rezultatem m.in. efektu cieplarnianego stanowią istotne wyzwanie obecnego stulecia. W obliczu tych procesów konieczne staje się dążenie do ograniczenia antropogenicznej emisji gazów cieplarnianych, w tym w szczególności dwutlenku węgla, który stanowi ok. 80% wolumenu ich całkowitej ilości emitowanej do atmosfery. W związku z tym, stale rosnącym zainteresowaniem cieszą się geopolimery, materiały stanowiące niezwykle atrakcyjną alternatywę dla stosowanych konwencjonalnie materiałów budowalnych. Ich wytworzenie jest procesem o niższej energochłonności, pozwalającym na ograniczenie ilości emitowanego dwutlenku węgla do atmosfery, a także na zagospodarowanie odpadów i ochronę surowców naturalnych, w porównaniu do betonu wytworzonego z zastosowaniem tradycyjnego cementu portlandzkiego. Dodatkowo udowodniono, iż przy odpowiednim doborze materiałów bazowych oraz warunków procesu wytwarzania, geopolimery w porównaniu do betonów mogą charakteryzować się m.in. wyższą wytrzymałością na ściskanie i na zginanie oraz większą odpornością na warunki klimatyczne, w tym mrozoodpornością oraz odpornością chemiczną. Jednak do tej pory materiały geopolimerowe nie są jeszcze powszechnie stosowane m.in. ze względu na brak dostatecznej charakterystyki ich właściwości oraz określenia wpływu zmiennych stosowanych podczas procesu wytwarzania na produkt końcowy.

Celem naukowym prezentowanej rozprawy doktorskiej było opracowanie i analiza właściwości materiałów geopolimerowych modyfikowanych odpadową stłuczką szklaną. Dodatkowo celem utylitarnym było opracowanie sposobu wytwarzania, umożliwiającego zagospodarowanie materiałów odpadowych oraz produktów ubocznych procesów technologicznych. W celu realizacji przyjętych założeń wytworzono geopolimery spienione oraz niespienione na osnowie materiałów poprocesowych, odpadowych i/lub mineralnych takich jak: popiół lotny, łupek węglowy (po przeprowadzeniu obróbki mechanicznej i termicznej), metakaolin oraz hybrydy metakaolinu z łupkiem węglowym, zawierające dodatek brązowej odpadowej stłuczki szklanej. Wszystkie opracowane geopolimery scharakteryzowano z zastosowaniem szerokiego spektrum metod badawczych w celu określenia wpływu poszczególnych zmiennych, tj. udziału wagowego oraz wielkości cząstek zastosowanych frakcji stłuczki szklanej, rodzaju materiałów bazowych oraz komponentów, na finalne właściwości kompozytów geopolimerowych. Dodatkowo zrealizowane badania pozwoliły na wskazanie potencjalnych zastosowań zsyntetyzowanych materiałów. Zaproponowane rozwiązania wykazują potencjał możliwości ograniczenia ilości składowanych odpadów oraz produktów ubocznych procesów technologicznych. Sugerowany sposób

zagospodarowania odpadów oraz produktów ubocznych można uznać za innowacyjny i perspektywiczny. Wyniki zrealizowanych badań przedstawiono m.in. w cyklu czterech artykułów opublikowanych w recenzowanym, renomowanym czasopiśmie, indeksowanym w bazie Journal Citation Reports (JCR) oraz znajdującym się w wykazie czasopism naukowych Ministerstwa Edukacji i Nauki (MEiN).

Summary

Climate change resulting from among others the greenhouse effect constitutes a significant challenge of this century. Faced with these processes, it becomes necessary to pursue restriction of anthropogenic greenhouse gas emissions, in particular carbon dioxide, which constitutes approximately 80% of the volume of the total amount of greenhouse gas emissions into the atmosphere. Therefore, geopolymers, which are materials constituting extremely attractive alternatives to conventionally applicable building materials have been increasingly popular. Their manufacturing is a process characterized by lower energy consumption, allowing for a reduction in the amount of carbon dioxide emissions into the atmosphere, as well as waste management and preserving natural resources in comparison to concrete manufactured using Ordinary Portland Cement. Moreover, it has been proved that with the proper selection of base materials and manufacturing process conditions, geopolymers can be characterized by, for instance, higher compressive strength, higher flexural strength, and higher resistance to climatic conditions, including freeze-thaw resistance and chemical resistance compared to concrete. However, geopolymer materials are not commonly used yet, among others due to the lack of sufficient characteristics of their properties as well as determining the effect of variables used during the manufacturing process on the final product, up to now.

The scientific aim of the presented doctoral dissertation was to develop and analysis the properties of geopolymer materials modified with waste glass. Furthermore, the utilitarian objective was to develop their fabrication process, enabling the management of waste materials and byproducts of technological processes. In order to realise established objectives, foamed and non-foamed geopolymers on the base of post-process, waste and/or minerals materials, such as fly ash, coal gangue (after mechanical and thermal treatment), metakaolin and coal gangue-metakaolin hybrids, containing the addition of brown waste glass cullet were manufactured. All of the developed geopolymers were characterised using a broad spectrum of research methods to determine the influence of individual variables, such as weight ratios and particle size of applied fractions of waste glass, the type of base materials, and components on the final properties of the geopolymer composites. In addition, completed research enabled to determine the potential applications of the synthesized materials. The proposed solutions exhibit the capability to reduce the amount of landfilled waste and by-products of technological processes. Furthermore, the suggested way of waste management and by-products can be considered as innovative and prospective. The results of the completed study were presented among others in the

series of four scientific articles, published in peer-reviewed prestigious scientific journal, indexed in the Journal Citation Reports (JCR) database and contained in the Ministry of Education and Science list of scientific journals.

Wykaz publikacji wchodzących w skład rozprawy doktorskiej

Prezentowana rozprawa doktorska składa się z cyklu czterech powiązanych tematycznie publikacji, w których przedstawiono i szczegółowo omówiono rezultaty zrealizowanych prac badawczych. Artykuły opublikowano w recenzowanym czasopiśmie, indeksowanym w bazie Journal Citation Reports (JCR) oraz znajdującym się w wykazie czasopism naukowych Ministerstwa Edukacji i Nauki. Pełną treść publikacji wraz z materiałami uzupełniającymi załączono na końcu prezentowanej rozprawy doktorskiej. W celu zwiększenia przejrzystości i czytelności pracy, przyjęto następujące oznaczenia publikacji:

Załącznik 1 – oznaczenie *P1*

Marczyk, J., **Ziejewska, C.**, Gądek, S., Korniejenko, K., Łach, M., Góra, M., Kurek, I., Doğan-Sağlamtimur, N., Hebda, M., Szechyńska-Hebda, M. (2021) *Hybrid materials based on fly ash, metakaolin, and cement for 3D printing.* Materials, 14 (22). doi: 10.3390/ma14226874

Impact Factor$_{2021}$: 3.748

Punktacja MEiN: 140 pkt.

Załącznik 2 – oznaczenie *P2*

Ziejewska, C., Grela, A., Hebda, M. (2023) *Influence of waste glass particle size on the physico-mechanical properties and porosity of foamed geopolymer composites based on coal fly ash*. Materials, 16 (5). doi: 10.3390/ma16052044

Impact Factor$_{2023}$: 3.4

Punktacja MEiN: 140 pkt.

Załącznik 3 – oznaczenie *P3*

Ziejewska, C., Grela, A., Mierzwiński, D., Hebda, M. (2023) *Influence of waste glass addition on the fire resistance, microstructure and mechanical properties of geopolymer composites*. Materials, 16 (17). doi: 10.3390/ma16176011

Impact Factor$_{2023}$: 3.4

Punktacja MEiN: 140 pkt.

Załącznik 4 – oznaczenie *P4*

Ziejewska, C., Bąk, A., Hodor, K., Hebda, M. (2023) *Eco-Friendly coal gangue and/or metakaolin-based lightweight geopolymer with the addition of waste glass*. Materials, 16 (17). doi: 10.3390/ma16176054

Impact Factor$_{2023}$: 3.4

Punktacja MEiN: 140 pkt.

Spis ważniejszych skrótów, symboli i oznaczeń stosowanych w pracy

BET – metoda Brunauera, Emmeta i Tellera umożliwiająca wyznaczenie powierzchni właściwej materiału

CVAAS – (ang. *cold vapour atomic absorption spectrometry*) technika zimnych par w atomowej spektrometrii absorpcyjnej

DOC – (ang. *dissolved organic carbon*) zawartość rozpuszczonego węgla organicznego

DTA – (ang. *differential thermal analysis*) termiczna analiza różnicowa

FT-IR – (ang. *Fourier transform infrared spectroscopy*) spektroskopia fourierowska w podczerwieni

ICP-OES – (ang. *inductively coupled plasma – optical emission spectroscopy*) optyczna spektrometria emisyjna z plazmą wzbudzoną indukcyjnie

IUPAC – (ang. *International Union of Pure and Applied Chemistry*) Międzynarodowa Unia Chemii Czystej i Stosowanej

LCA – (ang. *life cycle assessment*) ocena cyklu życia produktów

LOI – (ang. *loss on ignition*) strata prażenia

obr./min – liczba obrotów na minutę, jednostka prędkości obrotowej

OPC – (ang. *Ordinary Portland Cement*) cement portlandzki

QMS – (ang. *quadrupole mas spectrometry*) kwadrupolowa spektrometria mas

RILEM – (fr. *Réunion Internationale des Laboratoires et Experts des Matériaux, systèmes de construction et ouvrages*) Międzynarodowa Unia Laboratoriów i Ekspertów w zakresie Materiałów Budowlanych, Systemów i Konstrukcji

ROI – (ang. *region of interest*) region zainteresowania, inaczej wybrany obszar obrazu poddany analizie

SEM – (ang. *scanning electron microscope*) skaningowy mikroskop elektronowy

t – tona

TDS – (ang. *total dissolved solids*) całkowita zawartość rozpuszczonych substancji stałych

TG – (ang. *thermogravimetry*) termograwimetria

w/s – (ang. *water to solid ratio*) stosunek wagowy cieczy do składników stałych, tzw. „*stosunek wodny*”

wag. – wagowo, udział wagowy [%]

XRD – (ang. *X-ray diffraction*) metoda dyfrakcji rentgenowskiej

XRF – (ang. *X-ray fluorescence*) metoda fluorescencji rentgenowskiej

MERYTORYCZNA CZĘŚĆ ROZPRAWY

1. Wprowadzenie

Żyjący około 2500 lat temu słynny grecki filozof Heraklit z Efezu głosił pogląd: „*Jedyną stałą rzeczą w życiu jest zmiana*” [1]. Pomimo upływu czasu paradygmat dynamicznej zmiany stanowiącej centralny element świata można uznać za aktualny, a jego przekaz można rozpatrywać zarówno w kontekście sytuacji osobistych jednostki, jak i globalnie. Do zadań współczesnej nauki należy nie tylko obserwacja zmieniającego się świata, reagowanie na pojawiające się potrzeby i problemy, skutki zmian, lecz także prognozowanie zmian umożliwiające podjęcie działań ukierunkowanych na określone aspekty.

Światowy rozwój gospodarczy i wzrost liczby ludności na świecie wiąże się z ciągłym wzrostem zapotrzebowania na żywność, wodę i materiały. Powoduje on również wzrost popytu na produkty budowalne m.in. wskutek intensyfikacji budownictwa mieszkaniowego, realizacji zaawansowanych projektów infrastrukturalnych oraz urbanizacji. Oszacowano, iż obecnie dostępna infrastruktura zaspokoi jedynie 40% globalnego zapotrzebowania prognozowanego na rok 2050. Wskazuje to na ogromne przyszłe zapotrzebowanie na beton, który już teraz zaraz po wodzie, cechuje się największym globalnym zużyciem. Każdego roku jego produkcja wynosi około 30 miliardów ton. W przemyśle budowlanym wykorzystanie betonu jest dwukrotnie wyższe niż wszystkich innych materiałów łącznie, jednocześnie beton jest kluczowy szczególnie dla krajów rozwijających się [2–8].

Podstawowym materiałem wiążącym stosowanym w produkcji konwencjonalnego betonu jest cement portlandzki (OPC). Obecnie powszechnie określany jest on mianem materiału niezrównoważonego i nieprzyjaznego środowisku ze względu na zużywanie surowców naturalnych w trakcie wytwarzania, wysoką energochłonność tego procesu, a także emisję znacznych ilości gazów cieplarnianych. Szacuje się, iż przemysł cementowy jest odpowiedzialny na zużycie istotnej ilości paliw kopalnianych, stanowiących ok. 12–15% całkowitej energii zużywanej przez przemysł [9, 10].

Antropogeniczna emisja olbrzymich ilości CO_2 jest poważnym wyzwaniem XXI wieku, który negatywnie wpływa na środowisko, powodując m.in. zmiany klimatyczne oraz globalne ocieplenie. Kwestia ta stanowi jeden z najistotniejszych problemów środowiskowych obecnych czasów. Obliczono, iż proces produkcyjny 1 t cementu powoduje sumarycznie emisję około 0,8–1,0 t CO_2, na co składa się 0,55 t CO_2 wynikającej z konieczności zastosowania około 1,5 t surowców naturalnych oraz 0,4 t CO_2 uwalnianej wskutek spalania paliw. Produkcja cementu ze względu na rozkład węglanu wapnia jest istotnym źródłem emisji tego gazu cieplarnianego, odpowiada za

około 6–8% całkowitej emisji dwutlenku węgla [11–13]. Dlatego istnieje konieczność opracowania nowych zrównoważonych materiałów dla inżynierii lądowej, które będą mogły zastąpić materiały stosowane konwencjonalnie, powodując efektywne obniżenie ilości emitowanego do atmosfery CO_2. Ponadto założenie to jest zgodne z wymaganiami narzuconymi przez Komisję Europejską, która zadecydowała o obligatoryjnej konieczności ograniczenia emisji gazów cieplarnianych o co najmniej 40% do 2030 r. w porównaniu do poziomu z 1990 r. [14].

Innym aspektem związanym z rozwojem gospodarczym jest rosnąca ilość produkowanych odpadów [15, 16]. Jednym z nich jest szkło odpadowe. Szkło dzięki posiadanym właściwościom takim jak m.in. odporność chemiczna, przezroczystość, i nie biodegradowalność jest materiałem szeroko rozpowszechnionym na całym świecie. Należy jednak podkreślić wysoką podatność szkła na kruszenie oraz stłuczenie. Powszechnie wiadomo, iż recykling szkła jest możliwy, natomiast proces ten jest złożony, głównie ze względu na wieloetapowość oraz wysoką energochłonność. Wiąże się z koniecznością transportu, sortowania, rozdrabniania, czyszczenia, przesiewania, przetapiania i formowania celem produkcji wyrobów szklanych. Wszystkie te etapy mogą wiązać się z zanieczyszczeniem środowiska. Dodatkowo należy podkreślić obecny trend polegający na stosowaniu domieszek m.in. metali ciężkich w procesie produkcji szkła celem poprawy poszczególnych właściwości materiału, które w czasie recyklingu mogą zostać uwolnione do środowiska [17]. Dane literaturowe z 2018 roku wskazują, iż całkowita ilość wyprodukowanego szkła na świecie wyniosła 130 milionów ton, natomiast globalny poziom recyklingu szkła jedynie 21% [18]. Według danych Eurostatu, czyli Urzędu Statystycznego Unii Europejskiej z 2020 roku, 19,1% odpadów opakowaniowych stanowiły odpady szklane. Ponadto w ostatnich latach widoczna jest tendencja wzrostu ilości produkowanych odpadów szkła opakowaniowego, przykładowo wzrost o 13,1% odnotowano w 2020 roku, względem danych z 2009 roku [19].

Niski poziom recyklingu produktów szklanych wynika przede wszystkim z wysokich wymagań dotyczących jakości surowca wejściowego podczas produkcji, co jest niezbędne w celu uzyskania wyrobów szklanych o wysokiej jakości końcowej. Odpady szklane o różnych kolorach mogą nie spełniać wymogów względem posiadanych właściwości po procesie odbarwiania, co utrudnia ich recykling ukierunkowany na wytwarzanie nowych wyrobów szklanych. Dodatkowy problem stanowi zróżnicowanie pod względem rodzaju oraz obecnych zanieczyszczeń szkła odpadowego trafiającego na składowiska odpadów. Dlatego opracowanie materiałów umożliwiających wykorzystanie szkła odpadowego pochodzącego z recyklingu, którego przetwarzanie stanowi obecnie poważne wyzwanie środowiskowe dla społeczeństwa, przyczyniłoby się

do zmniejszenia objętości składowisk odpadów, zagospodarowania odpadów, obniżenia emisji emitowanego CO_2, ograniczenia zużycia energii potrzebnej do wytopienia szkła, a także ochrony surowców naturalnych [20–26].

Wielu badawczy w swoich pracach udowodniło, iż proszek szklany ze względu na stosunkowo wysoką zawartość SiO_2 oraz właściwości amorficzne posiadał właściwości pucolanowe, wskazując na możliwość zastosowania tego materiału w przemyśle budowalnym [19, 27]. Aktywność pucolanowa szkła zależy m.in. od wielkości cząstek szkła i rośnie wraz z ich zmniejszeniem [28]. Ponadto wykazano, iż w zależności od wielkości cząstek odpady szklane mogą pełnić odmienną funkcję w betonie cementowym, tzn. mogą występować jako kruszywo grube (wielkość cząstek poniżej 14 mm), kruszywo drobne (wielkość cząstek poniżej 4,75 mm), prekursor (wielkość cząstek poniżej 0,6 mm) [29].

Ogromne ilości składowanych obecnie odpadów i produktów ubocznych procesów technologicznych pochodzą z przemysłu wydobywczego (górniczego), metalurgicznego oraz energetycznego. Przykładem takich materiałów są popioły lotne, łupki węglowe, a także żużle. Ich deponowanie może powodować problemy ekologiczne wskutek oddziaływania zanieczyszczeń na gleby, powietrze, wody powierzchniowe i podziemne, a także wymaga nakładów finansowych na poczet utworzenia oraz utrzymania składowisk, zajmujących ogromne obszary powierzchniowe [30, 31].

Materiały odpadowe i/lub poprocesowe mogą stanowić surowiec do produkcji materiałów geopolimerowych, polimerów nieorganicznych lub materiałów aktywowanych alkalicznie.

Termin geopolimer został opracowany przez Profesora Joseph'a Davidovits'a w 1972 roku [32]. Jednak Profesor Davidovits podkreślił w swojej pracy, iż jego odkrycie poprzedzone było osiągnięciami innych badawczy w zakresie badań materiałów glinokrzemianowych. Już w latach trzydziestych XX wieku prowadzono badania z zastosowaniem m.in. wodorotlenku sodu i potasu, których celem było ustalenie czy żużel wielkopiecowy zostanie związany po dodaniu go do cementu portlandzkiego. W czasie realizacji badań w 1940 roku belgijski naukowiec o nazwisku Purdon zaobserwował powstanie szybko wiążącego spoiwa w efekcie zastosowania dodatku alkaliów. Cementy żużlowe otrzymywane poprzez aktywację alkaliami, tzw. „*cementy Triefa*", stosowano w budownictwie na dużą skalę w latach 50-tych XX wieku. Następnie w 1957 roku ukraiński naukowiec Victor Glukhovsky, pracujący w Kijowskim Instytucie Inżynierii Lądowej w Związku Socjalistycznych Republik Radzieckich, stworzył recepturę otrzymywania spoiw żużlowych aktywowanych alkaliami. W kolejnych latach (60 i 70 XX

wieku) odniósł on wiele sukcesów badawczych skoncentrowanych wokół identyfikacji hydratów glinokrzemianu wapnia i sodu, a także hydratów krzemianu wapnia i sodu. Betony otrzymywane według tej technologii zostały przez naukowca nazwane mianem „*betonów krzemianowych glebowych*" (1959 r.), natomiast spoiwa otrzymały od niego nazwę „*cementów glebowych*" (1967 r.) [33].

W rysie historycznym rozwoju materiałów geopolimerowych podkreśla się również wkład innych naukowców tj.: Flint wraz ze współpracownikami (w 1946 roku wykazali możliwość ekstrakcji tlenku glinu z materiałów takich jak boksyty i glina), Borchert oraz Keidel (w 1948 roku zsyntetyzowali hydrosodalit Na–PS jako produkt reakcji kaolinitu w roztworze NaOH w temperaturze 100 °C), Howell (w 1963 roku z metakaolinu otrzymanego w wyniku kalcynacji kaolinu otrzymał zeolit typu A), zespół w składzie osobowym Besson, Caillère i Hénin (w 1969 roku dokonali syntezy hydrosodalitu z krzemianów warstwowych w roztworze NaOH w temperaturze 100 °C), Jean Paul Latapie wraz z Michel Davidovic (w 1972 roku potwierdzili możliwość wytworzenia ceramicznych, wodoodpornych płytek bez konieczności stosowania wypalania, co było możliwe dzięki reakcji przebiegającej pomiędzy kaolinitem (składnik gliny), a sodą kaustyczną, w temperaturze 150 °C) [33].

Ponadto niewątpliwie przełomowym osiągnięciem było opracowanie przez Joseph'a Davidovits'a technologii bazującej na geosyntezie w 1972 roku w laboratorium CORDI zlokalizowanego w Saint-Quentin we Francji, która została w późniejszym czasie opatentowana [33].

Synteza geopolimerów następuje w wyniku alkalicznej aktywacji prekursorów glinokrzemianowych zazwyczaj w temperaturze 20–120 °C, a proces ten nosi nazwę geopolimeryzacji [34]. Davidovits wskazał, iż geopolimery mogą występować w trzech podstawowych jednostkach strukturalnych w zależności od stosunku Si:Al, który wpływa na uporządkowanie bliskiego zasięgu:

- poli(sialan) - podstawowa jednostka łańcuchów polimerycznych to: –Si–O–Al–O–), gdy stosunek Si:Al jest równy 1,
- poli(silokso-sialan) - podstawowa jednostka łańcuchów polimerycznych to: –Si–O–Al–O–Si–O–), gdy stosunek Si:Al jest równy 2,
- poli(disilokso-sialan) - podstawowa jednostka łańcuchów polimerycznych to: –Si–O–Al–O–Si–O–Si–O–), gdy stosunek Si:Al jest równy 3 [35, 36].

Jednak należy podkreślić istnienie geopolimerów charakteryzujących się wartością stosunku Si:Al powyżej 3 w sytuacji, gdy stosowane są prekursory glinokrzemianowe z wysoką zawartością Si, a aktywacja alkaliczna przebiega z zastosowaniem

krzemianów [37]. Geopolimery składają się z tetraedrów $(SiO_4)^{4-}$ i $(AlO_4)^{5-}$ połączonych ze sobą za pomocą wspólnych atomów tlenu. Dodatkowe kationy takie jak Na^+, czy K^+ są obecne we wnętrzu szkieletów, celem zrównoważenia ujemnego ładunku [38]. Taka budowa geopolimerów sprawia, iż są one odporne na działanie podwyższonych temperatur [39, 40].

Empiryczny wzór geopolimerów przedstawiono poniżej [41]:

$$M_n[-(SiO_2)_z-AlO_2-]_n \cdot wH_2O \quad (1)$$

przy czym:

M – kation, tj. K^+ lub Na^+,

n – stopień polikondensacji,

z – współczynnik przyjmujący wartość 1, 2 lub 3, w zależności o stosunku Si:Al,

w – ilość moli wiązanej wody.

Źródłem pochodzenia kationów jest zwykle alkaliczny rozwór krzemianu składający się z mieszaniny wodorotlenków (sodu i/lub potasu) oraz roztworów krzemianów (roztwór krzemianu sodu, inaczej szkło wodne sodowe i/lub roztwór krzemianu potasu, inaczej szkło wodne potasowe). Wodorotlenek zasadowy rozpuszcza glinokrzemiany i korzystnie wpływa na wytrzymałość mechaniczną geopolimerów, natomiast roztwór krzemianu alkalicznego ma wpływ na stopień geopolimeryzacji oraz na wytrzymałość na ściskanie [42].

Prekursorami geopolimerowymi mogą być zarówno surowce mineralne, np. metakaolin lub glina [43], jak i materiały poprocesowe i/lub odpadowe np. popioły lotne pochodzące ze spalania węgla kamiennego [44] oraz węgla brunatnego [45], łupki węglowe [46], żużel wielkopiecowy [47], czerwony szlam [48], odpady gumowe [49], popiół z łusek ryżu [50], proszek ceglany [51], zużyte dachówki [52], odpady szklane [53], czy odpady ceramiczne [54]. Wszystkie omówione powyżej aspekty sprawiają, że geopolimery są ekologiczną alternatywą dla powszechnie stosowanych materiałów dla inżynierii lądowej, a ich zastosowanie umożliwia zmniejszenie ilości generowanego CO_2 aż o 70–90%, w porównaniu do cementu portlandzkiego [55].

Wśród geopolimerów można wyróżnić pianki geopolimerowe, czyli geopolimery o niskiej gęstości, charakteryzujące się porowatą strukturą. Takie spienione materiały można otrzymywać między innymi w efekcie zastosowania metody bezpośredniego spieniania, stosowania mikrosfer, czy stosowania zabiegu napowietrzania

z zastosowaniem pęcherzyków powierza. Jednak najczęściej stosowaną metodą jest bezpośrednie spieniane, które może mieć charakter chemiczny lub mechaniczny. Spienianie bezpośrednie chemiczne polega na wprowadzeniu do mieszanki substancji chemicznych, powszechnie nazywanych środkami spieniającymi, takich jak m.in. reaktywne proszki metali (na przykład proszek aluminium lub krzemu), czy nadtlenek wodoru (H_2O_2). W efekcie zastosowania środków chemicznych następuje wydzielanie się gazu, który powoduje powstanie porowatej struktury. Wytworzone w ten sposób pianki są niestabilne termodynamicznie, a wskutek napięcia powierzchniowego pomiędzy gazem, a zaprawą geopolimerową struktury porowate mogą się łączyć tworząc makropory. Jednak zbyt intensywne wydzielanie gazu może spowodować zapadnięcie się porowatej struktury geopolimeru [56–58].

Działanie H_2O_2 na zaprawę można przedstawić za pomocą poniższych równań [59]:

$$H_2O_2 + OH^- \rightarrow HO_2^- + H_2O \quad (2)$$

$$HO_2^- + H_2O_2^- \rightarrow H_2O + O_2 + OH^- \quad (3)$$

Natomiast przebieg reakcji spieniania mieszanki z zastosowaniem proszku Al można przedstawić następująco [9]:

$$Al + 3H_2O + OH^- \rightarrow Al(OH)_4^- + 3/2\ H_2 \quad (4)$$

Właściwości geopolimerów, jako produktów końcowych zależą od wielu czynników, m.in. właściwości prekursorów tj. składu chemicznego i stosunku Si:Al, wielkości i kształtu cząstek, ich reaktywności, a także od kompozycji mieszanek, warunków utwardzania oraz kondycjonowania, rodzaju i stężenia aktywatora alkalicznego, stosowanych dodatków, rodzaju i ilości środka spieniającego oraz stabilizującego (w przypadku materiałów spienionych) [60–62].

Stosunek Si:Al w geopolimerach determinuje ich właściwości, a w konsekwencji obszary ich zastosowań. Na rysunku 1 przedstawiono zależność pomiędzy budową sieci polimerowej, a zastosowaniem geopolimerów, zaproponowaną przez Profesora Joseph’a Davidovits’a.

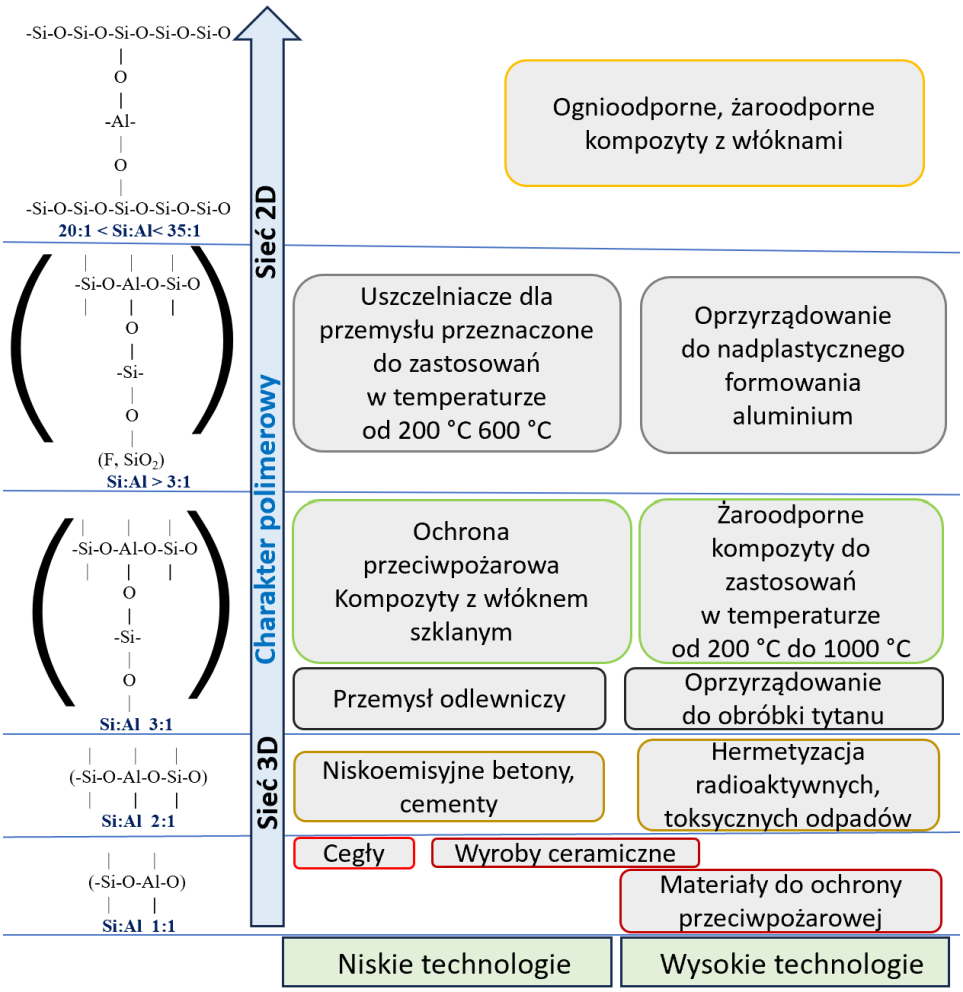

Rys. 1. Struktura geopolimerów, a możliwości ich zastosowania (opracowanie własne na podstawie literatury [63]).

Poli(sialany), w których stosunek Si:Al wynosi 1:1 są stosowane do produkcji ceramiki. Poli(silokso–sialany), czyli materiały odpowiadające stosunkowi Si:Al równemu 2:1, znajdują zastosowanie do produkcji cementów, betonów oraz mogą być stosowane do hermetyzacji materiałów niebezpiecznych. W przypadku materiałów charakteryzujących się stosunkiem Si:Al na poziomie 3:1 tj. poli(disilokso–sialany) wykazano, iż mogą być stosowane jako materiały do ochrony przeciwpożarowej, w przemyśle odlewniczym, do obróbki tytanu oraz jako kompozyty żaroodporne, przeznaczone do pracy w temperaturze od 200 °C do 1000 °C. Natomiast materiały o stosunku Si:Al wynoszącym powyżej 3 są stosowane jako uszczelniacze oraz oprzyrządowanie do formowania aluminium [63, 64]. Do innych zastosowań materiałów geopolimerowych można zaliczyć: materiały izolacyjne [65], materiały do stabilizacji gruntu [66], elementy stosowane celem izolacji akustycznej [67], filtry [68], ochrona przeciwogniowa [69], powłoki [70], chodniki oraz nawierzchnie dróg [71], elementy dekoracyjne [31], oraz doniczki [59].

2. Cel i zakres pracy

Celem naukowym pracy było opracowanie i analiza właściwości materiałów geopolimerowych wytworzonych na bazie surowców odpadowych, poprocesowych i/lub mineralnych modyfikowanych odpadową stłuczką szklaną, której obecne zagospodarowanie w przemyśle jest ograniczone. Realizacja celu pozwoliła na uzupełnienie informacji dotyczących możliwości integracji geopolimerów z odpadami szklanymi. Ponadto przyjęto cel utylitarny, którym było opracowanie sposobu wytwarzania kompozytów geopolimerowych umożliwiających zagospodarowanie materiałów odpadowych lub produktów ubocznych procesów technologicznych, a także wskazanie potencjalnych obszarów ich zastosowań. Zaproponowane rozwiązania są zgodne z koncepcją gospodarki o obiegu zamkniętym.

Materiałami wpisującymi się w przyjęte założenia i zastosowanymi w ramach badań przedstawionych w niniejszej rozprawie doktorskiej były: popiół lotny pochodzący ze spalania węgla kamiennego, łupek węglowy z kopalni węgla kamiennego Silesia (po przeprowadzeniu obróbki mechanicznej i termicznej), metakaolin oraz brązowa odpadowa stłuczka szklana.

Zakres pracy obejmował analizę literatury dotyczącą geopolimerów, ich aplikacyjności, możliwości zastosowania w ich produkcji odpadów, materiałów poprocesowych i mineralnych jako prekursorów geopolimerowych oraz zdefiniowania obecnego stanu wiedzy w zakresie kompozytów geopolimerowych z dodatkiem odpadów szklanych. Materiały bazowe scharakteryzowano m.in. poprzez określenie:

a. składu chemicznego metodą fluorescencyjnej spektrometrii rentgenowskiej,
b. powierzchni właściwej metodą sorpcji fizycznej,
c. gęstości metodą piknometrii helowej,
d. rozkładu wielkości cząstek metodą dyfrakcji laserowej,
e. wymywalności wodnej z uwzględnieniem pomiaru pH wyciągu wodnego,
f. promieniotwórczości naturalnej w zakresie stężenia izotopów naturalnie promieniotwórczych: ^{226}Ra, ^{228}Th, ^{40}K,
g. identyfikacji wiązań chemicznych w materiałach metodą FT–IR,
h. obserwacji morfologii cząstek z zastosowaniem skaningowego mikroskopu elektronowego oraz mikroskopu cyfrowego,
i. struktury materiałów, stabilności termicznej i zjawisk zachodzących podczas nagrzewania materiałów za pomocą sprzężonych metod analizy termicznej (DTA, TG, QMS oraz TG–FT-IR),

j. rentgenowskiej jakościowej i ilościowej analizy fazowej.

Następnie na podstawie wyników z przeprowadzonych badań wstępnych oraz w oparciu o dane literaturowe zaprojektowano przebieg empirycznych badań własnych. W kolejnych etapach przeprowadzono szereg syntez kompozytów geopolimerowych na bazie surowców naturalnych, materiałów poprocesowych i/lub odpadowych, przy zastosowaniu różnych zmiennych m.in. wielkości cząstek odpadowej stłuczki szklanej, ilości wprowadzonego dodatku, kompozycji mieszanek, rodzaju środka spieniającego. Tak otrzymane materiały scharakteryzowano z zastosowaniem spektrum badań umożliwiających określenie właściwości wytworzonych kompozytów geopolimerowych tj. m.in. przeprowadzono jakościową i ilościową analizę składu fazowego, zbadano efekty cieplne zachodzące podczas geopolimeryzacji oraz czas wiązania geopolimerów. Zdefiniowano także konsystencje mieszanek geopolimerowych, określono współczynnik przewodzenia ciepła λ, wyznaczono powierzchnie właściwe, gęstość, skład chemiczny, wymywalność oraz nasiąkliwość geopolimerów. Ponadto przeprowadzono analizę morfologii próbek na podstawie mikrofotografii wykonanych za pomocą skaningowego mikroskopu elektronowego oraz mikroskopu cyfrowego, zrealizowano badania tomograficzne geopolimerów, określono niepalność oraz właściwości mechaniczne materiałów poprzez przeprowadzenie badań wytrzymałości na zginanie, a także wytrzymałości na ściskanie. Sukcesywnie realizowane etapy prac badawczych pozwoliły na scharakteryzowanie właściwości materiałów, w zależności od sposobu ich wytworzenia. Na zakończenie w pracy wskazano potencjalne zastosowania otrzymanych materiałów.

3. Metodologia badań

3.1 Zastosowane materiały

Geopolimery wytworzono na bazie materiałów odpadowych, poprocesowych i/lub mineralnych takich jak: popiół lotny, metakaolin, szkło odpadowe, łupek węglowy. W dalszej części pracy syntetycznie opisano źródła pochodzenia zastosowanych w badaniach surowców.

- Popiół lotny pozyskano z elektrofiltrów z Elektrociepłowni Skawina.
- Metakaolin o nazwie handlowej Metakaolin KM 60 zakupiono od firmy Keramost z siedzibą w Republice Czeskiej.
- Łupek węglowy pochodził z kopalni węgla kamiennego Przedsiębiorstwa Górniczego "SILESIA" Sp. z o.o., zlokalizowanej w Czechowicach-Dziedzicach, w południowej Polsce.
- Brązową odpadową stłuczkę szklaną, uzyskaną ze szkła opakowaniowego, pozyskano od firmy Grabowski Export-Import (Sędziszowa, Polska). Wielkość cząstek dostarczonego materiału nie przekraczała 1200 µm. Celem dokładnego określenia wpływu zastosowanych frakcji wielkości cząstek na geopolimery, szkło odpadowe stosowano zarówno bezpośrednio w stanie wyjściowym (w publikacjach: P2, P3, P4), jak i po sortowaniu za pomocą zestawu sit i wytrząsarki laboratoryjnej na frakcje o wielkości cząstek: 200–1200 µm; 100–250 µm; 63–120 µm; 40–63 µm; 0,1–40 µm (w publikacjach: P2, P3). Stłuczki nie poddawano dodatkowemu czyszczeniu, co pozwoliło na redukcję ilości wody i energii elektrycznej oraz wymaganego nakładu pracy, tym samym zasobów finansowych, potrzebnych do przygotowania surowców. Proces przygotowania stłuczki odpadowej do badań schematycznie przedstawiono na rysunku 2.

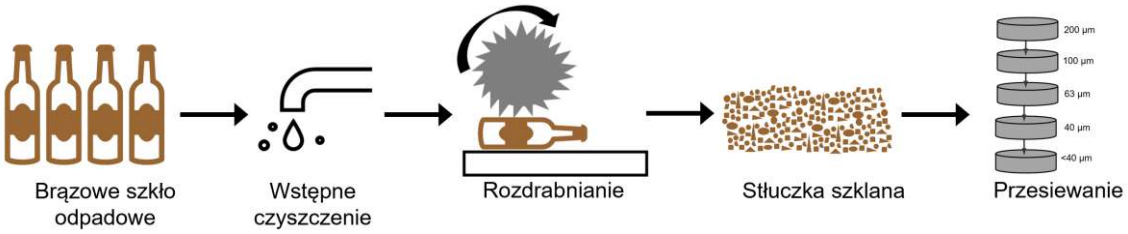

Rys. 2. Proces wytwarzania odpadowej stłuczki szklanej [na postawie publikacji P3].

Ponadto do wytworzenia geopolimerów zastosowano następujące produkty:

- wodorotlenek sodu (NaOH) w postaci płatków firmy Krakchemia S.A. (Kraków, Polska),
- szkło wodne sodowe R-145 (roztwór krzemianu sodu, Na_2SiO_3) o module molowym 2,5 firmy Chemi Kam sp. z o.o. (Będzin, Polska),
- proszek aluminium 5-7350 firmy Benda-Lutz (Skawina, Polska),
- nadtlenek wodoru (perhydrol, H_2O_2) o stężeniu procentowym 35% firmy Chempur (Piekary Śląskie, Polska),
- aldehyd syryngowy W404926 ($HOC_6H_2(OCH_3)_2CHO$) firmy Sigma-Aldrich (Saint Louis, Stany Zjednoczone Ameryki),
- cement CEM I 42,5R firmy Górażdże Cement S.A. Heidelberg Cement Group (Chorula, Polska),
- piasek rzeczny kwarcowy zakupiony od lokalnego dostawcy (Świętochłowice, Polska).

3.2 Wytworzenie próbek geopolimerowych

W ramach realizacji pracy wytworzono próbki zarówno spienione, jak i niespienione. Proces aktywacji alkalicznej przeprowadzono z zastosowaniem mieszaniny składającej się z 8-molowego roztworu wodorotlenku sodu oraz szkła wodnego sodowego R-145 (roztworu krzemianu sodu) o module molowym 2,5 zmieszanych w stosunku wag. 1:2,5. Autorzy wcześniejszych prac wykazali, że takie proporcje umożliwiły uzyskanie najniższych gęstości pianek geopolimerowych, przy zastosowaniu popiołu lotnego jako prekursora [20, 72]. Ponadto wyboru pomiędzy aktywatorem potasowym, a sodowym dokonano w oparciu o znacznie niższe koszty aktywatora sodowego [43]. Roztwór wodorotlenku sodu przygotowano z zastosowaniem wody wodociągowej, nie stosowano wody destylowanej. Jako środek spieniający w piankach geopolimerowych zastosowano proszek aluminium lub nadtlenek wodoru o stężeniu 35%. Przygotowany roztwór alkaliczny dokładnie mieszano i następnie pozostawiano w temperaturze pokojowej na 24 godziny w celu zapewnienia wyrównania się stężeń i osiągnięcia stałej temperatury mieszaniny. Stosunek cieczy do suchych składników tzw. „*stosunek wodny*" był stały i wynosił w/s=0,4 wag. [31].

Zasadniczo proces wytworzenia próbek spienionych obejmował następujące etapy:

1) mieszanie suchych składników (wybrane z następujących, w zależności od mieszanki: popiół lotny, metakaolin, łupek węglowy, piasek, stłuczka szklana, cement, stabilizator) przy wykorzystaniu mieszalnika planetarnego przez 2 minuty z prędkością obrotową 600 obr./min w celu uzyskania jednolitej mieszanki;
2) stopniowe wprowadzanie roztworu alkalicznego i dokładne mieszanie składników;
3) dodanie środka spieniającego (proszku aluminium lub 35% roztworu nadtlenku wodoru) i mieszanie pasty geopolimerowej przez 1 minutę*;
4) umieszczenie masy geopolimerowej w formach;
5) utwardzanie mieszanek geopolimerowych w suszarce laboratoryjnej przez 24 godziny w temperaturze 75 °C, przy ciśnieniu atmosferycznym;
6) rozformowanie próbek;
7) sezonowanie geopolimerów w temperaturze pokojowej przez 28 i 56 dni.

* Próbki niespienione wytworzono zgodnie z powyższym opisem, jednak z pominięciem wprowadzenia środka spieniającego (etap 3).

3.3 Zastosowane metody badawcze

Poniżej syntetycznie opisano metody badawcze zastosowane w celu scharakteryzowania zarówno właściwości surowców jak i wytworzonych materiałów geopolimerowych. Należy jednak podkreślić, iż zawarte w publikacjach wyniki stanowiły efekt realizacji 4-letnich badań naukowych, co wiązało się również ze zmiennym dostępem do poszczególnych urządzeń wynikającym m.in. z modernizacji aparatury badawczo-laboratoryjnej. W związku z tym w przypadku wybranych metod badawczych, badania przeprowadzono z zastosowaniem dwóch urządzeń pomiarowych, co wyszczególniono poniżej. Dokładny opis badań i przyjętych parametrów opisano w publikacjach P1, P2, P3, P4.

- Skład chemiczny określono metodą rentgenowskiej analizy fluorescencyjnej (XRF) z zastosowaniem spektrometru PANalytical Epsilon 3XLE (Malvern Panalytical, Almelo, Holandia) oraz spektrometru EDX–7200 (Shimadzu Corporation, Kioto, Japonia). Wyniki przedstawiono w formie składu tlenkowego.

- Pomiary techniką spektroskopii w podczerwieni z transformacją Fouriera (FT-IR) zrealizowano za pomocą spektrofotometru IRAffinity–1 S (Shimadzu, Kioto, Japonia) wyposażonego w przystawkę ATR Quest (Specec). W celu obniżenia poziomu szumów, prezentowane wyniki stanowiły średnią z 32 widm, zarejestrowanych w zakresie liczby falowej 4000–400 cm^{-1}. Badania przeprowadzono w temperaturze pokojowej. Widma przeanalizowano z wykorzystaniem bazy danych dostępnej w oprogramowaniu LabSolution FT-IR Shimadzu.

- Skład mineralogiczny określono z zastosowaniem metody dyfrakcji rentgenowskiej (XRD). Badania przeprowadzono na dyfraktometrze PANalytical Aeris z wykorzystaniem promieniowania CuKα. Dyfraktogramy rejestrowano w zakresie kątowym 10–100°(2θ) z krokiem pomiarowym 0,003° (2θ) oraz czasem zliczeń 340 s na krok pomiarowy. Zarejestrowane dyfraktogramy poddano analizie jakościowej oraz ilościowej (metodą Rietvelda) z zastosowaniem oprogramowania HighScore Plus oraz bazy danych International Centre for Diffraction Data (ICDD) PDF4+.

- Badania wymywalności przeprowadzono zgodnie z normą PN-EN 12457-2:2006 [73]. Przedmiot badań stanowiły surowce (metakaolin, popiół lotny) w stanie wyjściowym, w postaci proszku, oraz geopolimery rozdrobione na kawałki o wielkości nieprzekraczającej 10 mm w każdym z wymiarów. Porcję materiału z wodą dejonizowaną poddano wytrząsaniu z zastosowaniem wytrząsarki laboratoryjnej. Następnie uzyskane wyciągi wodne (eluaty) przefiltrowano i poddano analizom.

Przeprowadzono analizę fizykochemiczną obejmującą oznaczenie wartości pH metodą potencjometryczną zgodnie z normą PN-EN ISO 10523:2012 oraz określenie zawartości wody (wilgoci analitycznej) metodą wagową wg normy PN-EN 15934:2013-02 [74, 75]. Ponadto stężenie cynku, kadmu, miedzi, ołowiu, niklu, baru, chromu, arsenu, selenu, molibdenu i antymonu oznaczono metodą optycznej spektrometrii emisyjnej z plazmą wzbudzoną indukcyjnie (ICP-OES) zgodnie z normą PN-EN ISO 11885:2009 [76]. Zawartość rozpuszczonego węgla organicznego (DOC) w próbkach określono za pomocą spektroskopii w podczerwieni z transformacją Fouriera (FT-IR) wg normy PN-EN 1484:1999 [77]. Oznaczenie całkowitej zawartości rozpuszczonych substancji stałych (TDS) wykonano metodą grawimetryczną zgodnie z normą PN EN 15216:2010 [78]. Stężenie rtęci określono za pomocą techniki zimnych par w atomowej spektrometrii absorpcyjnej (CVAAS) wg normy PN-EN ISO 12846:2012 [79]. Zawartość jonów SO_4^{2-} i Cl^- określono przy użyciu metody chromatografii jonowej zgodnie z normą PN-EN ISO 10304-1:2009/AC:2012 [80].

- Morfologię surowców oraz geopolimerów obserwowano za pomocą skaningowych mikroskopów elektronowych (SEM): JEOL JSM5510LV (JEOL, Tokio, Japonia) oraz JEOL JSM–6390LV (JEOL, Tokio, Japonia). Przed badaniem na próbki nanoszono warstwę złota z wykorzystaniem napylarki próżniowej JOEL JEE–4X (JEOL, Tokio, Japonia).

- Gęstość właściwą określono metodą piknometryczną, stosując piknometr helowy Pycnomatic ATC (Thermo Fisher Scientific, Waltham, MA, Stany Zjednoczone Ameryki).

- Badania promieniotwórczości naturalnej przeprowadzono w zakresie stężenia izotopów naturalnie promieniotwórczych: ^{226}Ra, ^{228}Th, ^{40}K metodą spektrometrii promieniowania gamma przy użyciu urządzenia z detektorem germanowym o wysokiej czystości (ang. High-Purity Germanium detector – HPGe detector). Określono wskaźniki aktywności dla materiałów budowalnych, zgodnie z rozporządzeniem Rady Ministrów, z dnia 2 stycznia 2007 roku w „*sprawie wymagań dotyczących zawartości naturalnych izotopów promieniotwórczych potasu K–40, radu Ra–226 i toru Th–228 w surowcach i materiałach stosowanych w budynkach przeznaczonych na pobyt ludzi i inwentarza żywego, a także w odpadach przemysłowych stosowanych w budownictwie, oraz kontroli zawartości tych izotopów*” [81], według zależności:

$$f_1 = \frac{C_K}{3000\ Bq/kg} + \frac{C_{Ra}}{300\ Bq/kg} + \frac{C_{Th}}{200\ Bq/kg} \quad (5)$$

$$f_2 = C_{Ra}\ \text{[Bq/kg]} \quad (6)$$

w których:

C_K – stężenie promieniotwórcze izotopu potasu ^{40}K, wyrażone w Bq/kg,

C_{Ra} – stężenie promieniotwórcze izotopu radu ^{226}Ra, wyrażone w Bq/kg,

C_{Th} – stężenie promieniotwórcze izotopu toru ^{228}Th, wyrażone w Bq/kg,

f_1, f_2 – wskaźniki aktywności.

W uaktualnionym rozporządzeniu z dnia 17 grudnia 2020 r., wskaźnik stężenia promieniotwórczego izotopów promieniotwórczych *K–40, radu Ra–226 i toru Th–228* (wskaźnik I) wyznacza się zgodnie z przedstawioną powyżej zależnością na wskaźnik aktywności f_1 [82].

- Izotermy adsorpcji i desorpcji azotu wyznaczono w zakresie ciśnień względnych (P/P_0): $1*10^{-3}$ ÷ 0,95 z zastosowaniem analizatora sorpcji fizycznej Quantachrome Autosorb iQ - MP (Anton Paar, Graz, Austria). Przed realizacją pomiarów próbki odgazowano w temperaturze 300 °C umożliwiającej usunięcie wody oraz części zanieczyszczeń z powierzchni próbek, jednak niepowodującej zmian w strukturze materiału. Czas odgazowania każdej badanej próbki wynosił minimum 180 minut. Otrzymane wyniki pomiarów przeanalizowano z zastosowaniem programu Quantachrome ASiQwin. Powierzchnię właściwą określono m.in. metodą wielopunktową Brunauera-Emmetta-Tellera (BET) w zakresie ciśnień względnych P/P_0 od 0,05 do 0,30.
- Rozkład wielkości cząstek określono z zastosowaniem analizatora wielkości cząstek Fritsch Analysette 22 MicroTec plus (Fritsch GmBH, Idar-Oberstein, Niemcy) oraz analizatora wielkości cząstek PSA 1190 LD (Anton Paar, Graz, Austria). Przedstawione wyniki stanowiły średnią arytmetyczną z minimów 3 pomiarów dla każdego z badanych materiałów.
- Różnicową analizę termiczną (DTA), analizę termograwimetryczną (TG) i analizę wydzielanych produktów gazowych z materiału: m/z = 12 (C), m/z = 17 i 18 (H_2O), m/z = 28 (CO), m/z = 32 (O_2), m/z = 44 (CO_2), przeprowadzono z zastosowaniem urządzenia STA 449F3 sprzężonego z kwadrupolowym spektrometrem masowym QMS 403 (Netzsch-Gerätebau GmBH, Selb, Niemcy). Eksperymenty przeprowadzono w zakresie temperatur od 30 °C do 1000 °C. Próbki ogrzewano z prędkością 10 °C min^{-1} w atmosferze powietrza. Dane analizowano przy użyciu oprogramowania Proteus (Netzsch-Gerätebau GmBH, Selb, Niemcy).
- Badania wytrzymałości na ściskanie przeprowadzono zgodnie z normą PN-EN 12390-3:2019 z zastosowaniem próbek sześciennych wymiarach 50 mm × 50 mm × 50 mm, na

maszynie MATEST 3000 kN, model C-104 wyposażony w oprogramowanie Cyber-plus (MATEST S.p.A., Arcore, Włochy) oraz na urządzeniu MTS Criterion Model 43 (MTS Systems, Eden Prairie, MN, Stany Zjednoczone Ameryki) [83]. Wynik stanowił średnią arytmetyczną wraz z obliczonym odchyleniem standardowym z badania minimum 3 próbek dla każdej kompozycji. Geopolimery zbadano po 28 i/lub 56 dniach sezonowania w warunkach laboratoryjnych.

- Wytrzymałość na zginanie próbek określono zgodnie z normą PN-EN 12390-5:2019 [84]. W celu realizacji badań dla każdej kompozycji zsyntetyzowano minimum 3 próbki o wymiarach 200 mm × 50 mm × 50 mm. Próbki zbadano po 28 dniach sezonowania, z zastosowaniem hydraulicznej prasy do betonu (MATEST, Arcore, Włochy).
- Morfologię próbek obserwowano za pomocą mikroskopu cyfrowego Keyence VHX–E100 (Keyence, Osaka, Japonia), przy zastosowaniu różnych powiększeń.
- Gęstość próbek geopolimerowych określono metodą geometryczną jako stosunek masy do objętości próbki. Wynik dla każdej kompozycji stanowił średnią arytmetyczną przedstawioną wraz z odchyleniem standardowym z badania minimum 3 próbek. Masę zważono za pomocą wagi Radwag XA 60/220/Y (RADWAG, Radom, Polska) lub wagi Radwag PS 200/2000R2 (RADWAG, Radom, Polska). Objętość określono stosując odpowiedni wzór na objętość figury geometrycznej, przy czym wymiary próbek zmierzono za pomocą suwmiarki cyfrowej Limit 19014–0103 (Limit, Alingsås, Szwecja).
- Konsystencje mieszanek oznaczono z zastosowaniem metody stożka Novikowa zgodnie z normą PN-85-B-04500 oraz za pomocą metody stolika rozpływu w oparciu o normę PN-EN 1015-3:1999/A2:2006 [85, 86]. Wyniki stanowią średnią arytmetyczną z uwzględnionym odchyleniem standardowym z badania minimum 3 porcji zapraw dla każdej mieszanki.
- Nasiąkliwość próbek określono zgodnie z normą PN-88/B-06250 [87]. Badania zrealizowano na 3 próbkach dla każdej mieszanki o wymiarach 50 mm × 50 mm × 50 mm, po 28–dniowym okresie sezonowania. Na podstawie uzyskanych rezultatów obliczono średnią arytmetyczną oraz odchylenie standardowe.
- Porowatość, średni rozmiar i średnią gęstość komórek obliczono na podstawie mikrofotografii struktur geopolimerowych, przy użyciu oprogramowania ImageJ w wersji 1.53t.

Średnią gęstość komórek obliczono na podstawie zależności [88]:

$$N = \left[\frac{(nM^2)}{A}\right]^{\frac{3}{2}} \text{ [liczba komórek/cm}^3\text{]} \quad (7)$$

w której:

N – gęstość komórki,

n – liczba komórek widocznych na zdjęciu,

A – pole powierzchni analizowanej fotografii,

M – powiększenie.

- Badanie pod względem niepalności geopolimerów przeprowadzono według normy PN-EN ISO 1182:2020, stosując minimum 3 próbki dla każdej kompozycji po 28–dniowym czasie sezonowania [89]. Wynik badania stanowił średnią arytmetyczną ze zrealizowanych pomiarów wraz z obliczonym odchyleniem standardowym.
- Resztkową wytrzymałość na ściskanie wyznaczono na próbkach o wymiarach 50 mm × 50 mm × 50 mm po przeprowadzonym wcześniej badaniu niepalności. Testy zrealizowano na maszynie MATEST 3000 kN (MATEST, Arcore, Włochy). Przedstawiony wynik dla każdej z badanych kompozycji stanowił średnią arytmetyczną z badania minimum 3 próbek z uwzględnionym odchyleniem standardowym.
- Proces geopolimeryzacji zbadano z zastosowaniem systemu ujemnego współczynnika temperaturowego. Układ wykorzystany do rejestracji danych oraz przyjętą metodykę dokładnie opisano w publikacji [90].
- Analizę termograwimetryczną (TG/DTG) i spektroskopię w podczerwieni z transformacją Fouriera (FT-IR) przeprowadzono za pomocą urządzenia TG 209 F1 Libra (NETZSCH-Gerätebau GmbH, Selb, Niemcy) sprzężonego z spektrometrem FT-IR ALPHA (Bruker Optics GmbH, Ettlingen, Niemcy). W czasie pomiarów próbki ogrzewano od 25 °C do 1000 °C z szybkością ogrzewania 10 °C min^{-1} w atmosferze argonu. Widma FT-IR zarejestrowano w zakresie 4000–600 cm^{-1}.
- Współczynnik przewodzenia ciepła (λ) geopolimerów wyznaczono z zastosowaniem aparatu płytkowego HFM 446 Lambda (NETZSCH-Gerätebau GmBH, Selb, Niemcy). Pomiary przeprowadzono w trzech zakresach temperaturowych: 0–20 °C, 20–40 °C, 30–50 °C zgodnie z normą DIN EN 12667 [91].
- Badania tomograficzne przeprowadzono z zastosowaniem wysokorozdzielczego mikrotomografu komputerowego Phoenix nanotom S (Skaneateles, Nowy Jork, Stany

Zjednoczone Ameryki), wyposażonego w lampę rentgenowską o maksymalnym napięciu 180 kV. Analizę ilościową uzyskanych danych zrealizowano z zastosowaniem otwartego oprogramowania Fiji w wersji 1.53f51 i wtyczki Bone J przeznaczonej do analizy danych z pomiarów struktur porowatych. Centralna część próbek o wymiarach około 27 mm × 27 mm × 27 mm została wykorzystana do analizy jako obszar zainteresowania (ROI – ang. Region Of Interest).

4. Uzasadnienie połączenia publikacji w cykl

Realizowane w pracy doktorskiej badania podzielono na cztery etapy, co odzwierciedlono w numeracji i kolejności ukazywania się artykułów, stanowiących spójny cykl publikacji naukowych. Do najważniejszych zadań badawczych zrealizowanych w poszczególnych etapach zaliczono:

Etap 1. Charakterystyka surowców stosowanych w badaniach [P1].

Nowość naukowa: Szczegółowa charakterystyka metakaolinu i popiołu lotnego, weryfikacja ich właściwości pod względem możliwości zastosowania jako prekursorów geopolimerów. Dodatkowo przedstawiono możliwość druku geopolimerów oraz hybryd betonowo-geopolimerowych.

Mój wkład w powstanie publikacji polegał na: przygotowaniu materiałów do badań, wytworzeniu geopolimerów, przeprowadzeniu badań oraz analizie uzyskanych wyników.

Etap 2. Wytworzenie pianek geopolimerowych na osnowie popiołu lotnego oraz kompozytów zawierających odpadową stłuczkę szklaną. Charakterystyka stłuczki szklanej, stosowanej jako materiał bazowy. Określenie wpływu wielkości cząstek frakcji wprowadzonego dodatku oraz udziału wag. na właściwości geopolimerów spienionych: powierzchnię właściwą, morfologię, gęstość, wytrzymałość na ściskanie, wytrzymałość na zginanie, nasiąkliwość, porowatość, wymywalność [P2].

Nowość naukowa: Określono wpływ udziału wag. (0%, 10%, 20%, 30%) i wielkości cząstek różnych frakcji odpadów szklanych (0,1–1200 μm, 200–1200 μm, 100–250 μm, 63–120 μm, 40–63 μm; 0,1–40 μm) niepoddanych dodatkowemu czyszczeniu na właściwości pianek geopolimerowych wytworzonych bez zastosowania obróbki wysokotemperaturowej.

Mój wkład w powstanie publikacji polegał na: sformułowaniu problemu badawczego, opracowaniu koncepcji i metodyki badań, przygotowaniu materiałów do badań oraz wytworzeniu geopolimerów, przeprowadzeniu badań, analizie uzyskanych wyników, interpretacji i opracowaniu graficznym uzyskanych danych, przygotowaniu pierwszej wersji manuskryptu, przygotowaniu ostatecznej wersji manuskryptu, korekcie manuskryptu po recenzjach.

Etap 3. Synteza geopolimerów niespienionych z odpadową stłuczką szklaną, a następnie określenie wpływu zastosowanego udziału wag. oraz wielkości cząstek odpadów szklanych na: konsystencję mieszanek, przebieg procesu geopolimeryzacji, gęstość, skład mineralogiczny oraz chemiczny, powierzchnię właściwą, mikrostrukturę,

wytrzymałość na ściskanie, nasiąkliwość, niepalność, a także wytrzymałość na ściskanie oraz skład chemiczny po ekspozycji na wysoką temperaturę [P3].

Nowość naukowa: Określono wpływ dodatku szkła odpadowego o różnej wielkości cząstek (0,1–1200 μm, 200–1200 μm, 100–250 μm, 63–120 μm, 40–63 μm; 0,1–40 μm) i udziale wag. (0%, 10%, 20%, 30%) na niepalność wytworzonych na osnowie popiołu lotnego geopolimerów niespienionych.

Mój wkład w powstanie publikacji polegał na: sformułowaniu problemu badawczego, opracowaniu koncepcji oraz metodyki badań, przygotowaniu materiałów do badań, wytworzeniu geopolimerów, realizacji badań, analizie uzyskanych wyników, interpretacji i opracowaniu graficznym uzyskanych danych, przygotowaniu pierwszej wersji manuskryptu, przygotowaniu ostatecznej wersji manuskryptu, korekcie manuskryptu po recenzjach.

Etap 4. Wytworzenie kompozytów geopolimerów spienionych na osnowie łupka węglowego (po przeprowadzeniu procesu kruszenia, mielenia oraz kalcynacji) i/lub metakaolinu z dodatkiem odpadowej stłuczki szklanej. Charakterystyka łupka węglowego oraz dostosowanie sposobu przygotowania materiału do zastosowania jako prekursor w procesie geopolimeryzacji. Ocena wpływu zastosowania łupka węglowego i/lub metakaolinu jako materiałów bazowych, a także wpływu modyfikacji geopolimerów dodatkiem szkła odpadowego poprzez wyznaczenie: składu chemicznego, przewodności cieplnej, wytrzymałości na ściskanie, gęstości, właściwości termicznych, badania struktury, rozmieszczenia wprowadzonych dodatków w geopolimerach, porowatości zamkniętej i otwartej, anizotropii oraz homogeniczności materiałów. Wskazanie możliwości zastosowania opracowanych materiałów [P4].

Nowość naukowa: Zaprezentowano możliwość wytworzenia pianek geopolimerowych na osnowie łupka węglowego (po przeprowadzeniu obróbki mechanicznej i termicznej), wzmocnionych odpadami szklanymi. Ponadto wytworzono geopolimery na osnowie metakaolinu oraz hybryd (metakaolinu z łupkiem węglowym) oraz porównano ich właściwości. W badaniach zastosowano odpadową stłuczkę szklaną w stanie wyjściowym, bezpośrednio po dostarczeniu od producenta, niepoddaną dodatkowej obróbce.

Mój wkład w powstanie publikacji polegał na: sformułowaniu problemu badawczego, opracowaniu koncepcji badań, przygotowaniu materiałów do badań, wytworzeniu geopolimerów, opracowaniu metodyki badań, realizacji badań, analizie wyników, interpretacji i opracowaniu graficznym uzyskanych danych, przygotowaniu pierwszej

wersji manuskryptu, przygotowaniu ostatecznej wersji manuskryptu, korekcie manuskryptu po recenzjach.

5. Omówienie uzyskanych wyników badań

W tej części pracy esencjonalnie omówiono wyniki uzyskanych badań naukowych, przyjmując następującą kolejność: charakterystyka materiałów bazowych zastosowanych w badaniach (podrozdział 5.1), charakterystyka wytworzonych geopolimerów (podrozdział 5.2). Należy jednak podkreślić, iż wszystkie wyniki badań wraz ze szczegółowym ich omówieniem i analizą oraz z odniesieniami literaturowymi przedstawiono w publikacjach dołączonych do pracy jako załączniki.

5.1 Charakterystyka materiałów bazowych

Materiałami wyjściowymi zastosowanymi do syntezy geopolimerów były materiały odpadowe, poprocesowe i/lub mineralne takie jak: był popiół lotny (przedstawiony w publikacji: P1, P2, P3), metakaolin (przedstawiony w publikacji: P1, P4), szkło odpadowe (przedstawione w publikacji: P2, P3, P4), łupek węglowy (opisany w publikacji: P4).

5.1.1 Charakterystyka popiołu lotnego

Popiół lotny pochodzący ze spalania węgla kamiennego ze względu na skład chemiczny sklasyfikowano jako popiół krzemionkowy klasy F, zgodnie z normą ASTMC618 [92]. Obserwacja morfologii popiołu lotnego ujawniła, że charakteryzował się on w przybliżeniu kulistą morfologią cząstek, co jest korzystne pod względem zastosowania materiału w procesie geopolimeryzacji, ponieważ poprawia własności reologiczne mieszanki, zwiększając jej urabialność, a także zmniejsza zapotrzebowanie na substancje ciekłe oraz korzystnie wpływa na właściwości mechaniczne geopolimerów [44]. Wielkość cząstek popiołu lotnego mieściła się w zakresie od 1,3 μm do 32,5 μm. Gęstość popiołu wyznaczona z zastosowaniem piknometru helowego wyniosła 2,288 ± 0,001 g cm $^{-3}$. Szczegółowa analiza chemiczna odcieków uzyskanych podczas badania wymywalności wodnej popiołu wskazała obecność pierwiastków toksycznych, jednak występowały one w akceptowalnych według obowiązujących regulacji prawnych stężeniach. Odciek z badania popiołu był silnie zasadowy (wyznaczona wartość pH powyżej 12). W kolejnym etapie zrealizowano badania promieniotwórczości naturalnej popiołu, które ujawniły, iż stężenia radioaktywnych izotopów w materiale, takich jak: ^{40}K, ^{226}Ra i ^{228}Th mieściły się w dopuszczalnych zakresach, z wyjątkiem średniego poziomu

radioaktywności popiołu, który był nieznacznie wyższy od przyjętych akceptowalnych poziomów [P1].

Strata prażenia (LOI) popiołu lotnego wynosiła 3,3%, a więc uzyskana wartość mieściła się w dopuszczalnych limitach (od 3% do 6%, w zależności od kraju). Parametr ten wskazuje na zawartość niespalonego węgla w badanym materiale, który może absorbować wodę czy domieszki chemiczne wpływając na właściwości produktu końcowego [93–95]. Surowiec poddano również badaniom metodami analizy termicznej. W zakresie temperatur od 25 °C do 125 °C zarejestrowano efekty endotermiczne dla: m/z 17 i 18 (woda) oraz m/z 32 (tlen), związane z parowaniem. Znaczące efekty egzotermiczne zarejestrowano dla popiołu lotnego w zakresie temperatur od 400 °C do 700 °C, co powiązano z rozkładem materiału organicznego. Potwierdziły to wyniki zarejestrowanych metodą spektrometrii mas (QMS) jonów o określonym zakresie stosunku masy do ładunku elektrycznego: m/z 12 (węgiel) i m/z 44 (dwutlenek węgla) [P1].

W następnym etapie przeprowadzono badania z zastosowaniem metody FT-IR. Najbardziej intensywny efekt zarejestrowany na widmie popiołu lotnego przy liczbie falowej 1003 cm^{-1} przypisano asymetrycznym drganiom rozciągającym Si–O. Dodatkowo zidentyfikowano obecność wiązań Si–O, Si–Si, Si–O–Al, Al–O [P1].

W publikacji P2 zaprezentowano wyniki jakościowej i ilościowej analizy fazowej dyfrakcji promieni rentgenowskich. Analiza zarejestrowanego dyfraktogramu pozwoliła na identyfikację następujących faz krystalicznych w podanym udziale: 50,3% kwarcu (SiO_2), 45,0% mulitu ($Al_6Si_2O_{13}$), 2,1% hematytu (Fe_2O_3), 2,4% anhydrytu ($CaSO_4$) i 0,2% magnetytu (Fe_3O_4). Jednak przedstawione udziały procentowe należy traktować z pewnym przybliżeniem ze względu na występującą fazę amorficzną, wysokie tło i nakładające się na siebie odbicia [P2].

W kolejnym etapie wyznaczono izotermy adsorpcji - desorpcji azotu dla popiołu lotnego, które zidentyfikowano jako izotermy typu II z pętlą histerezy typu H3. Dodatkowo określono powierzchnię właściwą surowca metodą wielopunktową BET (w zakresie ciśnień względnych od 0,05 do 0,3), wynoszącą 7,804 $m^2\ g^{-1}$ [P2]. Na podstawie przedstawionych wyników badań popiołu lotnego stwierdzono, że surowiec ten można stosować jako prekursor materiałów geopolimerowych.

5.1.2 Charakterystyka odpadowej stłuczki szklanej

Analiza składu chemicznego brązowego, opakowaniowego szkła odpadowego zgodnie z oczekiwaniami ujawniła wysoką zawartość SiO_2 (68,8%), Na_2O (15,3%) oraz CaO (11,7%). Dodatkowo w ilości powyżej 1% zidentyfikowano: Al_2O_3 (1,6%) oraz MgO (1,3%). Pozostałe związki chemiczne występowały w ilości poniżej 1%. Obserwacja morfologii szkła odpadowego ujawniła, iż cząstki posiadały nieregularny kształt oraz wielkość, gładką powierzchnię i ostre krawędzie [P3].

Zarejestrowany dyfraktogram szkła odpadowego posiadał charakterystyczny efekt dyfrakcyjny o wysokiej intensywności, usytuowany w zakresie od 15° do 40° (2θ). Jego obecność oraz brak innych identyfikowalnych efektów dyfrakcyjnych wskazuje na amorficzny charakter badanego materiału [P2].

Ponadto w publikacji P2 przedstawiono wyniki pomiarów zrealizowanych z zastosowaniem laserowego analizatora wielkości cząstek. Średnia wielkość cząstek stłuczki szklanej w stanie dostawy wynosiła 550,1 ± 18,9 µm, przy czym rozkład wielkości cząstek był dwumodalny, z ekstremami dla cząstek o wielkości około 170 µm i 600 µm. Dodatkowo badaniom poddano stłuczkę odpadową po sortowaniu na frakcje o mniejszym zakresie wielkości cząstek. Średnia wielkość cząstek dla poszczególnych frakcji wynosiła: 584,9 ± 4,4 µm (dla frakcji o wielkości cząstek od 200 µm do 1200 µm), 155,2 ± 0,5 µm (dla frakcji o wielkości cząstek od 100 µm do 250 µm), 55,4 ± 1,2 µm (dla frakcji o wielkości cząstek od 63 µm do 120 µm), 33,3 ± 0,1 µm (dla frakcji o wielkości cząstek od 40 µm do 63 µm), oraz 19,8 ± 0,3 µm (dla frakcji o wielkości cząstek od 0,1 µm do 40 µm) [P2].

Dodatkowo zrealizowano badania z zastosowaniem analizatora sorpcji fizycznej, umożliwiające wyznaczenie powierzchni właściwej szkła odpadowego, wynoszącej 0,152 $m^2 g^{-1}$ dla stłuczki niesortowanej. Wraz ze zmniejszeniem wielkości cząstek szkła, powierzchnia właściwa rosła, osiągając maksymalną wartość wynoszącą 0,693 $m^2 g^{-1}$ dla frakcji zawierającej cząstki szkła o wielkości 0,1–40 µm [P2].

5.1.3 Charakterystyka metakaolinu

Cząstki metakaolinu obserwowane z zastosowaniem skaningowego mikroskopu elektronowego (SEM) charakteryzowały się kształtem zbliżonym do płatkowego, jednak o dość dużej nieregularności, porowatej strukturze, a także losowej geometrii. Dodatkowo zaobserwowano tendencję cząstek metakaolinu do tworzenia aglomeratów. Wielkość cząstek metakaolinu mieściła się w zakresie od 0,5 µm do 39,2 µm.

Wyznaczona gęstość metakaolinu wynosiła 2,566 ± 0,001 g cm^{-3}. W składzie chemicznym metakaolinu zidentyfikowano w największych ilościach: SiO_2 (54,9%) oraz Al_2O_3 (41,8%). Każdy z pozostałych związków chemicznych występował w ilości poniżej 1,2% [P1, P4].

Zrealizowane dla metakaolinu badania wymywalności wodnej ujawniły, że wszystkie toksyczne pierwiastki zidentyfikowane w odcieku występowały w ilościach mieszczących się w zakresach międzynarodowych limitów. Natomiast odciek surowca był lekko kwaśny, pH roztworu wynosiło 6. Strata prażenia metakaolinu wynosiła 0,7%. W rezultacie prowadzonych badań z zastosowaniem analizy termicznej, zaobserwowano niewielki spadek masy próbki. Na uzyskanym widmie FT-IR metakaolinu najbardziej intensywny efekt zarejestrowany dla długości falowej 1055 cm^{-1} przypisano drganiom Si–O–Si pochodzącym od minerałów krzemianowych, obecnych w materiale. Dodatkowo zidentyfikowano wiązania: Si–O, Si–Si, Si–O–Al, Al–O [P1].

Analiza mineralogiczna zrealizowana z zastosowaniem dyfraktometrii rentgenowskiej pozwoliła na identyfikację następujących faz: kwarcu (6,3%), kaolinitu (48,0%), illitu (20,6%), muskowitu (20,6%) oraz mulitu (4,6%). Ze względu na obecność fazy amorficznej, zauważalnej na dyfraktogramie w postaci tzw. amorficznego efektu „*halo*" występującego pomiędzy 15° a 40° 2θ, wskazane wartości udziału procentowego należy traktować jednie jako wartości szacunkowe [P4].

Ponadto przeprowadzone pomiary i analizy z zastosowaniem analizatora sorpcji fizycznej, ujawniły mezoporowaty charakter badanych materiałów. Natomiast powierzchnia właściwa surowca wyznaczona metodą BET wynosiła 13,370 $m^2\ g^{-1}$ [P4].

5.1.4 Charakterystyka łupka węglowego

Celem wyboru optymalnej temperatury kalcynacji rozdrobniony łupek węglowy, do średniej wielkości cząstek (D_{50}) równej 11,17 μm, zbadano z zastosowaniem sprzężonej metody analizy TG–FT-IR. Ubytek masy łupka węglowego przebiegał etapowo i związany był z następującymi kolejno procesami: usunięciem wody i desorpcją gazów znajdujących się na powierzchni materiału (maksymalny efekt zarejestrowano w temperaturze około 72 °C), utlenianiem (zarejestrowano maksimum efektu w temperaturze około 206 °C), dehydroksylacji kaolinitu i powstaniem metakaolinitu (z maksymalnym efektem występującym w temperaturze około 458 °C), oraz dwuetapowym procesem spalania związanym z rozkładem materii organicznej

(w zakresach temperatury od 631 °C do 864 °C i od 863 °C do 1049 °C). Zarejestrowany wykres widm FT-IR pozwolił na identyfikację produktów gazowych: CO_2, H_2O oraz CO we wszystkich charakterystycznych temperaturach, jednak intensywność ich emisji zmieniała się w zależności od temperatury. Na podstawie analizy uzyskanych wyników badań wykonanych z zastosowaniem metod analizy termicznej jako optymalną temperaturę kalcynacji łupka węglowego przyjęto 800 °C [P4].

Dodatkowo łupek węglowy przed i po procesie kalcynacji zbadano z zastosowaniem analizy składu chemicznego XRF, składu mineralogicznego XRD, gęstości metodą piknometrii helowej oraz powierzchni właściwej, objętości i rozmiarów porów występujących w materiale [P4].

Porównując skład chemiczny łupka węglowego przed i po procesie kalcynacji zauważono, że zasadnicza różnica polegała na wzroście zawartości Fe_2O_3 oraz zmniejszeniu zawartości SO_3. Niezależnie od zastosowanej obróbki termicznej, w składzie chemicznym materiału dominowały dwa związki chemiczne: SiO_2 oraz Al_2O_3. Natomiast różnica w składzie mineralogicznym pomiędzy łupkiem przed i po procesie kalcynacji polegała na obniżeniu zawartości kaolinitu (z 49,5% do 0,1%) i jednoczesnym zwiększeniu zawartości kwarcu (z 27,4% do 57,1%). Ponadto zastosowana obróbka termiczna spowodowała spadek powierzchni właściwej materiałów (z 8,043 $m^2\ g^{-1}$ do 4,150 $m^2\ g^{-1}$) oraz wzrost gęstości (z 2,273 ± 0,001 g cm^{-3} do 2,821 ± 0,001 g cm^{-3}) [P4].

5.2 Charakterystyka kompozytów geopolimerowych

Kolejnym etapem zrealizowanych prac badawczych była ocena wpływu modyfikacji geopolimerów spienionych dodatkiem odpadowej stłuczki szklanej. Etap ten został przedstawiony i dokładnie opisany w publikacji oznaczonej jako P2, pt. „*Influence of waste glass particle size on the physico-mechanical properties and porosity of foamed geopolymer composites based on coal fly ash*”. Pianki geopolimerowe wytworzono na osnowie popiołu lotnego, z dodatkiem piasku (10% wag.) i stłuczki szklanej (w ilości 10%, 20% oraz 30% wag.). Udział wag. wprowadzonego dodatku szkła odpadowego dobrano na podstawie analizy wcześniejszych prac, wskazujących, iż optymalna ilość dodatku powinna zawierać się w zakresie od 10% do 30% wag. [96–98]. Ponadto, dodatkową zmienną zastosowaną w badaniach, celem dokładniejszego poznania wpływu stłuczki szklanej na właściwości geopolimerów, była zróżnicowana wielkość cząstek wprowadzonego dodatku. Stłuczkę szklaną zastosowano zarówno bezpośrednio w stanie dostawy (cząstki o wielkości 0,1–1200 μm), jak i po sortowaniu na pięć frakcji: 200–1200 μm; 100–250 μm; 63–120 μm; 40–63 μm; 0,1–40 μm. Środkiem spieniającym

był proszek aluminium, stosowany w ilości 0,15% wag. względem suchych składników mieszanki (popiołu lotnego, piasku, odpadowej stłuczki szklanej).

Badania przeprowadzone z zastosowaniem analizatora sorpcji fizycznej ujawniły, iż powierzchnia właściwa próbki referencyjnej wynosiła 22,772 m^2 g^{-1}. Ponadto zaobserwowano wzrost powierzchni właściwej oraz zwiększenie reaktywności pucolanowej wraz ze zmniejszeniem wielkości cząstek szkła odpadowego. Modyfikacja geopolimerów polegająca na zastosowaniu niesortowanej odpadowej stłuczki szklanej, spowodowała wzrost powierzchni właściwej do 65% (w przypadku geopolimeru zawierającego 20% dodatku) względem próbki referencyjnej. Natomiast najwyższą powierzchnię właściwą zmierzono dla geopolimeru zawierającego 30% udziału wag. dodatku stłuczki szklanej o najmniejszych wielkościach cząstek, tj. mieszczących się w zakresie 0,1–40 μm. Uzyskane izotermy adsorpcji - desorpcji geopolimerów zgodnie z klasyfikacją IUPAC oznaczono jako izotermy typu IV z pętlą histerezy H3, co wskazuje na mezoporowatą strukturę materiałów, w której występują pory szczelinowe o średnicach w zakresie 2–50 nm.

Zrealizowane badania składu mineralogicznego pozwoliły na identyfikację zarówno faz krystalicznych (kwarcu, mulitu, hematytu), jak i fazy amorficznej (C–S–H w postaci rosenhanitu) we wszystkich badanych próbkach. Stwierdzono, iż zmiana ilości dodatku odpadów szklanych oraz stopnia ich rozdrobnienia miały znikomy wpływ na skład mineralogiczny geopolimerów. Stopień krystaliczności geopolimerów zmniejszał się wraz z rosnącym udziałem wag. stłuczki odpadowej w kompozytach.

Oszacowano, iż porowatość kompozytów ze stłuczką odpadową wynosiła od 50,3% do 68,5%, natomiast dla próbek odniesienia tj. niezawierających dodatku osiągnęła 50,5%. Stwierdzono, iż wprowadzenie szkła o wielkości cząstek w zakresie 0,1–1200 μm (niesortowana stłuczka szklana) w ilości do 20% wag. powoduje wzrost porowatości w stosunku do materiału odniesienia. Natomiast kompozyty z 30% wag. niesortowanego szkła odpadowego osiągnęły o ok. 9,5% niższą porowatość w porównaniu do próbek zawierających 20% wag. tego dodatku.

Jednym z podstawowych wyzwań dla materiałów spienionych, przeznaczonych do pełnienia funkcji konstrukcyjnych jest uzyskanie odpowiednich właściwości mechanicznych. W publikacji P2 przedstawiono wyniki badań wytrzymałości na ściskanie oraz wytrzymałości na zginanie, przeprowadzonych w celu określenia wpływu dodatku stłuczki szklanej na wytworzone materiały. Zaobserwowano, że próbki zawierające 20% oraz 30% niesortowanej odpadowej stłuczki po 28 dniach sezonowania charakteryzowały się najwyższą wytrzymałością na ściskanie ze wszystkich

wytworzonych materiałów. Wykazywały one 80% wzrost w porównaniu z materiałem odniesienia. Stwierdzono, iż przyczyną wyższej wytrzymałości na ściskanie geopolimerów z dodatkiem stłuczki szklanej w porównaniu do materiałów odniesienia może być wyższa aktywność pucolanowa takich materiałów wskutek większej dostępności rozpuszczalnego tlenku glinu i krzemionki. Dodatkowo zastosowanie niesortowanej stłuczki szklanej redukuje liczbę procesów w technologii wytwarzania geopolimerów, co jest korzystne pod kątem przyszłych zastosowań przemysłowych. Wyniki wytrzymałości na ściskanie były zgodne z wynikami porowatości próbek. Inną przyczyną wzrostu wytrzymałości na ściskanie może być wypełnienie porów przez wprowadzoną stłuczkę odpadową. Natomiast należy zaznaczyć, iż zastosowanie stłuczki w tej samej proporcji, ale charakteryzującej się inną wielkością cząstek skutkowało uzyskaniem odmiennych rezultatów, niż w przypadku niesortowanego szkła odpadowego.

Badania wytrzymałości na zginanie geopolimerów ujawniły, iż dodatek szkła odpadowego, niezależnie od zastosowanego udziału wag. oraz wielkości cząstek, miał negatywny wpływ na tę właściwość. Zauważano natomiast, iż wraz ze zmniejszeniem wielkości cząstek, negatywny wpływ zastosowanej stłuczki na wytrzymałość na zginanie zmniejszał się. Wielu badaczy w swoich pracach wskazało, iż wielkość cząstek szkła odpadowego powinna mieścić się w przedziale 38–75 μm celem uzyskania optymalnej wartości aktywności pucolanowej oraz umożliwienia rozpuszczania krzemionki w betonie [98]. W przeprowadzonych badaniach zaobserwowano, iż w przypadku zastosowania frakcji szkła odpadowego o wielkości cząstek mieszczących się w zakresach: 100–250 μm, 63–120 μm, 40–63 μm i 0,1–40 μm najwyższą wytrzymałość na zginanie osiągnięto przy zastosowaniu 20% wag. Przyczyną tego zjawiska jest rosnąca wartość stosunku Na_2O do SiO_2 wraz ze zwiększeniem udziału wag. dodatku szkła odpadowego. Natomiast po przekroczeniu optymalnej wartości, dodatkowe jony Na^+ obecne w materiale mogą spowodować wykwity, a także spadek wytrzymałości. W przypadku zastosowania większych cząstek, tj. frakcji szkła odpadowego zawierających cząstki o wielkościach mieszczących się w zakresach od 0,1 μm do 1200 μm oraz od 200 μm do 1200 μm, zaobserwowano tendencję do wzrostu wytrzymałości na zginanie wraz ze zwiększaniem udziału stłuczki, osiągając najlepsze rezultaty przy 30% udziale wag. dodatku, niemniej uzyskano wartości poniżej wyników wytrzymałości na zginanie dla materiałów odniesienia.

W celu weryfikacji bezpieczeństwa stosowania analizowanych geopolimerów, przeprowadzono badania wymywalności wodnej. Wyniki wskazały, iż wprowadzenie do geopolimerów odpadowej stłuczki szklanej miało niewielki wpływ na zawartość metali

ciężkich w odciekach, takich jak: Hg, Cd, Ni, Cr, Cu, Zn i As. Jedynie zbadane stężenie Pb było zauważalnie wyższe (o około 12 razy) dla geopolimerów z dodatkiem najmniejszej wielkości cząstek odpadów szklanych, w porównaniu do materiałów referencyjnych. Stwierdzono, iż zawartość wszystkich badanych metali niebezpiecznych w kompozytach geopolimerowych mieściła się w zakresie dopuszczalnych wartości wymywania dla odpadów obojętnych, zgodnie z Decyzją Rady Europejskiej 2003/33/WE, z wyjątkiem poziomu substancji rozpuszczonych ogółem, który przekraczał dopuszczalny zakres wartości dla odpadów obojętnych. Warto podkreślić, że poziom substancji rozpuszczonych ogółem mieścił się w limicie ustalonym dla odpadów innych niż niebezpieczne. Ponadto zawartość rozpuszczonych substancji stałych (TDS) odniesiono do porowatości i gęstości wytworzonych próbek. Na podstawie uzyskanych wyników stwierdzono, że w geopolimerach z 30% dodatkiem wag. różnej wielkości szkła odpadowego, najwyższą całkowitą zawartość TDS otrzymano dla próbek zawierających najmniejsze wielkości cząstek szkła (0,1–40 μm) oraz charakteryzujących się najwyższą porowatością i najmniejszą gęstością.

W kolejnym etapie prac zbadano strukturę próbek, co pozwoliło na sformułowanie wniosków, iż wraz ze wzrostem zawartości niesortowanej odpadowej stłuczki szklanej, uzyskane pory posiadały mniejsze średnice, a ich rozmieszczenie było bardziej zbliżone do homogenicznego. Dodatek stłuczki szklanej korzystnie wpłynął na jednorodność porów obecnych w strukturze geopolimerów. Materiały referencyjne, tj. niezawierające dodatku szkła odpadowego posiadały makropory, które mogą determinować niskie właściwości mechaniczne wyrobów. Ponadto wielkość porów zmniejszała się wraz ze zmniejszaniem wielkości zastosowanej odpadowej stłuczki szklanej.

Uzyskane wyniki badań szczegółowo opisane i zaprezentowane w publikacji P2 wykazały, iż zarówno zawartość, jak i wielkość cząstek odpadowej stłuczki szklanej mają wpływ na porowatą strukturę geopolimerów spienionych. Zmniejszenie wielkości porów oraz wzrost jednorodności ich rozmieszczenia można uzyskać poprzez: a) zwiększenie zawartości odpadów szklanych niesortowanych (o wielkości cząstek mieszczących się w zakresie 0,1 do 1200 μm) do 20% oraz 30%, b) zmniejszenie wielkości cząstek wprowadzonej stłuczki szklanej.

Kolejnym etapem pracy, który został szczegółowo omówiony w publikacji P3, pt. „*Influence of Waste Glass Addition on the Fire Resistance, Microstructure and Mechanical Properties of Geopolymer Composites*” było wytworzenie niespienionych kompozytów geopolimerów zawierających 0–30% udziału wag. brązowej odpadowej stłuczki szklanej o różnych wielkościach cząstek. Przyjęto dokładnie te same

udziały wag. (0%, 10%, 20%, 30%) oraz frakcje (0,1–1200 μm – niesortowane szkło odpadowe, 200–1200 μm, 100–250 μm, 63–120 μm i 40–63 μm, 0,1–40 μm) odpadowej stłuczki szklanej jak w publikacji P2, jednak tym razem wytworzono próbki niespienione. Pozwoliło to na szczegółowe omówienie wpływu analizowanego dodatku, zarówno na matrycę spienioną (publikacja P2), jak i niespienioną (publikacja P3).

W obecnych czasach wciąż toczy się nieustająca walka z pożarami, w efekcie której obrażenia, a nawet śmierć ponosi ogromna liczba osób. W raporcie przedstawionym przez organizację NSC (National Safety Council) oszacowano, iż w Stanach Zjednoczonych straż pożarna podejmuje działa związane z koniecznością gaszenia pożarów średnio co 23 sekundy, natomiast w ich efekcie ginie człowiek średnio co 3 godziny 8 minut [99]. Ponadto przewiduje się, że jedną z wielu konsekwencji globalnego ocieplenia klimatu, oddziaływującego na pogodę, spowodowanego m.in. przez emisję CO_2, będzie zwiększone prawdopodobieństwo zapłonu i wzrost częstotliwości występowania pożarów [100]. Dlatego tak istotne jest uwzględnianie odporności ogniowej na etapie projektowania i wyboru materiałów przeznaczonych do zastosowania w budownictwie. Naukowcy we wcześniejszych badaniach wykazali wyższą odporność materiałów geopolimerowych od stosowanego konwencjonalnie betonu, a także udowodnili, iż szkło odpadowe może mieć pozytywny wpływ na zwiększenie odporności ogniowej geopolimerów [101, 102]. Natomiast szczegółowy wpływ zawartości i wielkości cząstek tego dodatku m.in. na reakcję na ogień - niepalność geopolimerów nie został wcześniej poznany i dlatego autorzy publikacji P3 sformułowali go jako główny cel swoich badań. W publikacji P3 określono również konsystencje zapraw geopolimerów i zbadano efekty cieplne zachodzące w trakcie geopolimeryzacji z zastosowaniem termistora o ujemnym współczynniku temperaturowym. Ponadto określono skład mineralogiczny materiałów, zbadano ich właściwości mechaniczne, nasiąkliwość, gęstość, powierzchnię właściwą. Przeprowadzono badania odporności wytworzonych kompozytów na ekspozycję na temperaturę 750 °C i następnie wyznaczono średni ubytek masy oraz resztkową wytrzymałość na ściskanie geopolimerów. Dodatkowo zbadano wpływ działania wysokiej temperatury na skład chemiczny materiałów. Na podstawie otrzymanych wyników sklasyfikowano geopolimery pod względem ich niepalności.

Efekty cieplne zachodzące podczas geopolimeryzacji świeżych zapraw geopolimerowych oraz po 48 godzinach od momentu przygotowania zaprawy zarejestrowano za pomocą urządzenia termistorowego o ujemnym współczynniku temperaturowym. Otrzymane wyniki pozwoliły na obliczenie charakterystycznych wartości, takich jak: maksymalna temperatura uzyskana podczas procesu

geopolimeryzacji świeżej zaprawy geopolimerowej i odpowiadający jej czas, energię reakcji egzotermicznej, czas końca wiązania oraz różnicę temperatur pomiędzy maksymalnymi wartościami zarejestrowanych efektów cieplnych podczas geopolimeryzacji oraz po 48 godzinach utwardzania. Następnie porównano wyniki dla kompozytów geopolimerowych zawierających różną wielkość cząstek odpadowej stłuczki szklanej. Zauważono, iż dodatek 20% udziału wag. odpadowej stłuczki szklanej powodował skrócenie czasu wiązania geopolimerów, niezależnie od wielkości cząstek stłuczki. Szkło odpadowe charakteryzowało się wyższą zawartością wapnia niż zastępowany nim popiół lotny, co mogło pozytywnie wpłynąć na skrócenie czasu wiązania. Ponadto maksymalna zarejestrowana temperatura, energia reakcji egzotermicznej, a także różnica pomiędzy zarejestrowanymi efektami termicznymi były najwyższe w przypadku próbki zawierającej frakcje odpadowej stłuczki szklanej o najmniejszych wielkościach cząstek. Efekt ten powiązano z wyższym stopniem rozpuszczania mniejszych cząstek ze względu na ich wyższą powierzchnię właściwą, która może reagować z aktywatorem alkalicznym podczas aktywacji.

W celu określenia zdolności świeżych zapraw geopolimerowych do płynięcia zbadano ich konsystencje z zastosowaniem dwóch metod, tj. stożka Novikowa i stolika rozpływowego. Na podstawie uzyskanych wyników stwierdzono, że dodatek odpadów szklanych w ilości 20% wag. niezależnie od zastosowanych frakcji powodował uzyskanie konsystencji plastycznej. Natomiast wprowadzenie 30% wag. stłuczki odpadowej zawierającej frakcje o wielkości cząstek mieszczących się w zakresie 0,1–1200 μm oraz 200–1200 μm spowodował zmianę konsystencji świeżych zapraw geopolimerowych na rzadką oraz ciekłą, w przypadku odpowiednio metody stożka Novikowa i stolika rozpływowego. Zjawisko to wynika z większej zdolności popiołu do pochłaniania roztworu alkalicznego, niż cząstek szkła odpadowego. Jednak dodatek tej samej ilości (30% wag.) frakcji szkła odpadowego o mniejszych wielkościach cząstek spowodował uzyskanie konsystencji plastycznej. Mniejsze cząstki charakteryzują się większą powierzchną właściwą, której zdolność pochłaniania roztworu jest wyższa, niż większych cząstek i dlatego zastosowanie 30% wag. szkła, lecz o wielkościach cząstek w zakresie 100–250 μm, 63–120 μm, and 40–63 μm, 0,1–40 μm spowodowało uzyskanie konsystencji plastycznej.

Nasiąkliwość oraz gęstość zbadano dla próbek zawierających 10%, 20% oraz 30% wag. odpadowej stłuczki szklanej niesortowanej, tj. zawierającej cząstki o wielkości w zakresie 0,1–1200 μm. Zauważono silną zależność pomiędzy nasiąkliwością, a zawartością stłuczki szklanej. Nasiąkliwość próbek malała wraz ze wzrostem

zawartości stłuczki szklanej. Odwrotną zależność natomiast zauważono w przypadku gęstości geopolimerów, która wrastała wraz ze wzrostem zawartości szkła odpadowego.

W kolejnym etapie przeprowadzono jakościową rentgenowską analizę fazową geopolimerów, która pozwoliła na identyfikację następujących faz we wszystkich zbadanych materiałach: kwarcu (SiO_2), mulitu ($Al_6Si_2O_{13}$), CSH w postaci rosenhanitu ($Ca_3(Si_3O_8(OH)_2$), albitu ($NaAlSi_3O_8$) i anortytu ($CaAl_2Si_2O_8$). Porównując widma dyfrakcyjne zaobserwowano, iż zarejestrowane efekty dyfrakcyjne pochodzące od różnych geopolimerów zlokalizowane były w tych samych położeniach kątowych, lecz ich intensywność była zróżnicowana. Intensywność efektów dyfrakcyjnych była niższa w przypadku próbek z odpadową stłuczką szklaną, w porównaniu do materiału odniesienia oraz malała wraz ze zmniejszeniem wielkości cząstek odpadowej stłuczki szklanej. Zjawisko to powiązano z niższym stopniem krystaliczności geopolimerów.

Wszystkie izotermy otrzymane w rezultacie pomiarów przeprowadzonych z zastosowaniem analizatora sorpcji fizycznej sklasyfikowano jako izotermy adsorpcji – desorpcji typu IV z pętlami histerezy typu H3 (wg klasyfikacji IUPAC). Otrzymane rezultaty wskazują na obecność mezoporów we wszystkich zbadanych materiałach. Ponadto na podstawie zarejestrowanych wyników określono powierzchnie właściwe, a także objętości i rozmiary porów obecnych w geopolimerach. Zauważono, iż największą powierzchnią właściwą wyznaczoną metodą BET charakteryzował się materiał odniesienia (45,44 $m^2 g^{-1}$), natomiast dodatek niesortowanej odpadowej stłuczki szklanej (wielkość cząstek 0,1–1200 μm) spowodował zmniejszenie powierzchni właściwej kompozytów. Ponadto występowała zależność, wraz ze wzrostem udziału wag. odpadowej stłuczki szklanej niesortowanej w kompozytach geopolimerowych powierzchnia właściwa malała. Porównując wyniki uzyskane dla próbek zawierających 30% wag. odpadowej stłuczki szklanej o różnej wielkości cząstek zaobserwowano, iż powierzchnia właściwa zmniejszała się wraz ze zmniejszeniem wielkości cząstek odpadów szklanych. Dodatkowo występowała zauważalna zależność objętości oraz średnicy porów w geopolimerach, tj. im mniejsza wielkość cząstek oraz większy udział wag. wprowadzonego dodatku, tym mniejsza objętość oraz średnica porów w geopolimerach. Uzyskane wyniki były zgodne z obliczoną gęstością oraz wynikami z testów nasiąkliwości geopolimerów. Dodatek odpadowej stłuczki szklanej spowodował jednoczesne zmniejszenie nasiąkliwości wody, zmniejszenie wielkości i objętości porów, nieznaczny wzrost gęstości oraz zmniejszenie powierzchni właściwej. Badania ujawniły, iż dodatek szkła odpadowego zmniejszył porowatość geopolimerów, wytworzonych na osnowie popiołu lotnego i piasku, powodując uzyskanie próbek o wyższej gęstości, w porównaniu do materiału odniesienia.

Kolejnym etapem zrealizowanych prac badawczych była ocena wpływu wielkości cząstek oraz udziału wag. dodatku szkła odpadowego na wytrzymałość na ściskanie geopolimerów niespienionych. Zauważono korzystny wpływ dodatku odpadowej stłuczki szklanej na wytrzymałość na ściskanie, która była od 53% do 137% wyższa, w zależności od wariantu, niż dla próbek referencyjnych. Najkorzystniejszy udział wag. dodatku zależał od zastosowanej frakcji szkła odpadowego i wnosił 20% wag. dla próbek zawierających szkło o wielkości cząstek: 0,1–1200 μm, 200–1200 μm, 100–250 μm oraz 63–120 μm. Natomiast w przypadku frakcji zawierających mniejsze wielkości cząstek, tj. 63–40 μm i 0,1–40 μm najwyższe wyniki wytrzymałości na ściskanie uzyskano dla geopolimerów wytworzonych z 10% wag. dodatkiem szkła. Zjawisko to związane było z reaktywnością pucolanową stłuczki szklanej, która wzrasta wraz ze zmniejszeniem jej wielkości cząstek, co jest zgodne z wynikami uzyskanymi w czasie badań zapraw z zastosowaniem urządzenia termistorowego o ujemnym współczynniku temperaturowym. Mniejsze cząstki charakteryzują się wyższą powierzchnią właściwą, a więc większa powierzchnia jest dostępna dla aktywatora alkalicznego powodując wyższą reaktywność cząstek i efektywniejszy proces geopolimeryzacji. Popiół lotny charakteryzował się średnią wielkością cząstek wynoszącą 17,3 ± 2,5 μm i była ona mniejsza niż każdej z zastosowanych frakcji szkła odpadowego. Natomiast spośród stosowanych frakcji stłuczki, najmniejszą średnią wielkością cząstek (22,0 ± 0,3 μm) charakteryzowała się frakcja 0,1–40 μm szkła odpadowego. Zastąpienie szkłem odpadowym popiołu lotnego korzystnie wpływało na wytrzymałość na ściskanie geopolimeru, niezależnie od zastosowanej frakcji oraz udziału wag.

W dalszej części publikacji P3 poddano analizie mikrofotografie przedstawiające reprezentatywne próbki, wykonane za pomocą skaningowego mikroskopu elektronowego (SEM). Obserwacja morfologii geopolimerów ujawniła większą liczbę porów w próbkach referencyjnych, w porównaniu do kompozytów z dodatkiem odpadowej stłuczki szklanej, co jest zgodne z omówionymi wcześniej wynikami gęstości. Dodatkowo w osnowie geopolimerowej widoczne były nieliczne cząstki popiołu lotnego, wpływające negatywnie na właściwości mechaniczne kompozytów.

Kolejnym etapem pracy było określenie niepalności wytworzonych próbek geopolimerowych. Zgodnie z opisaną wcześniej metodyką badań (w podrozdziale 3.3 pt. „*Zastosowane metody badawcze*”) próbki umieszczono w piecu elektrycznym i poddano je nagrzaniu do temperatury 750 °C i następnie izotermicznemu wytrzymywaniu w tej temperaturze przez 30 min. Po tym czasie próbki chłodzono wewnątrz pieca. Procentowy ubytek masy badanych geopolimerów osiągał wartości mieszczące się w zakresie od 11,7% (dla próbek zawierających 30% wag. niesortowanej

stłuczki szklanej) do 17,7% (w przypadku próbek z 20% wag. dodatkiem frakcji o najmniejszej wielkości cząstek szkła odpadowego, tj. 0,1 –40 μm). Zauważono, iż wraz ze zmniejszeniem wielkości cząstek wprowadzonego dodatku wzrastał obliczony procentowy ubytek masy po testach niepalności. Zjawisko to powiązano z ilością wody zaabsorbowanej wewnątrz cząstek odpadów szklanych, która była tym większa im wyższy był stopień rozdrobnienia cząstek. Efekt ten wynikał z większej powierzchni właściwej mniejszych cząstek. Dodatkowo wyjaśniono, iż zmiany w badanych materiałach zależały od temperatury i obejmowały następujące zjawiska: 1/ poprawę wytrzymałości na ściskanie ze względu na reakcję nieprzereagowanych cząstek odpadów szklanych i kurczenie się porów (do 400 °C), 2/ przemiany związków żelaza (od 400 °C do 750 °C), 3/ tworzenie się nowych porów (od 400 °C do 600 °C), 4/ usuwanie porów podczas spiekania (od 600 °C do 750 °C), 5/ pękanie próbek (od 600 °C do końca badania) i skurcz (od 200 °C do końca badania) [103, 104]. Wszystkie wytworzone geopolimery, niezależnie od wielkości cząstek szła i ich udziału wag. sklasyfikowano jako materiały klasy $A1_{fl}$ według normy PN-EN ISO 1182:2020 [89].

Dodatkowo dla geopolimerów po badaniu niepalności przeanalizowano resztkową wytrzymałość na ściskanie. Na podstawie zarejestrowanych wyników stwierdzono, że zastosowanie szkła odpadowego poprawiło resztkową wytrzymałość na ściskanie o 221,6% i 164,7% w przypadku odpowiednio geopolimerów z największymi rozmiarami cząstek tj. 200–1200 μm oraz niesortowanych 0,1–1200 μm, w odniesieniu do niemodyfikowanych próbek referencyjnych. Kompozyty zawierające szkło odpadowe o większych rozmiarach cząstek charakteryzowały się wyższą resztkową wytrzymałością na ściskanie niż ich odpowiedniki zawierające mniejsze cząstki szkła. Kolejnym wnioskiem wynikającym z omawianych badań było ustalenie optymalnego udziału dodatku szkła zapewniającego uzyskanie najwyższych wyników wytrzymałości na ściskanie. Dla frakcji zawierających cząstki o rozmiarach: 0,1–1200 μm (stłuczka niesortowana), 200–1200 μm, 100–250 μm i 63–120 μm wynosił on 20% wag. Natomiast w przypadku zastosowania frakcji: 40–63 μm i 0,1–40 μm najwyższe wyniki uzyskano przy 10% wag. dodatku szkła odpadowego. Ponadto kompozycje z takimi udziałami wag. stłuczki wykazywały najwyższe wyniki dla obu parametrów, zarówno wytrzymałości na ściskanie, jak i resztkowej wytrzymałości na ściskanie geopolimerów.

Kolejny etap badań przedstawiony w publikacji P4 pt. *„Eco-Friendly Coal Gangue and/or Metakaolin-Based Lightweight Geopolymer with the Addition of Waste Glass”* koncentrował się na ocenie możliwości zastosowania łupka węglowego jako prekursora geopolimerów wzmocnionych odpadami szklanymi. Dodatkowo w celu porównania wpływu dodatku stłuczki szklanej na geopolimery wytworzone z różnych materiałów

bazowych, zsyntetyzowano również kompozyty na osnowie metakaolinu oraz hybryd metakaolinu z łupkiem węglowym zmieszanych w stosunku wag. 1:1. Jako materiały odniesienia zastosowano geopolimery na osnowie łupka węglowego i metakaolinu bez dodatku szkła odpadowego.

Bazując na wynikach przedstawionych w publikacjach P2 oraz P3, zastosowano optymalny udział stłuczki szklanej wynoszący 20% wag. Jako środek spieniający zastosowano nadtlenek wodoru (H_2O_2) o stężeniu 35%, w ilości 3% wag., natomiast jako stabilizator porowatej struktury zastosowano aldehyd syryngowy ($HOC_6H_2(OCH_3)_2$ CHO) w ilości 0,15% wag. W celu zwiększenia aktywności pucolanowej we wszystkich mieszankach geopolimerowych zastosowano dodatek 10% wag. cementu o wysokiej zawartości tlenku wapnia. Przedstawione ilości zastosowanego środka spieniającego oraz stabilizatora odnoszą się do masy suchych składników mieszanki.

Zgodnie z wynikami przedstawionymi w rozdziale 5.1 pt. „*Charakterystyka materiałów bazowych*” łupek węglowy poddano rozdrobnieniu mechanicznemu (do uzyskania wielkości cząstek D_{50}= 11,17 ± 0,36 μm) oraz obróbce temperaturowej (kalcynacja w temperaturze 800 °C przez 24h w piecu laboratoryjnym).

Wytworzone geopolimery poddano m.in. badaniom: analizy składu chemicznego i mineralogicznego, określono współczynnik przewodzenia ciepła λ, wyznaczono wytrzymałość na ściskanie i gęstość, przeprowadzono obserwację porowatych struktur pianek oraz badania porowatości z zastosowaniem wysokorozdzielczego mikrotomografu komputerowego, a także wyznaczono homogeniczność materiałów i stopień anizotropii.

W celu oceny składu mineralogicznego pianek geopolimerów przeprowadzono jakościową i ilościową rentgenowską analizę fazową. Uzyskane rezultaty badań ujawniły obecność faz takich jak: kwarc (SiO_2), kaolinit ($Al_2Si_2O_5(OH)_4$), mulit ($Al_6O_5(SiO_4)_2$), albit ($NaAlSi_3O_8$), muskowit ($KAl_2(Si_3Al)O_{10}(OH,F)_2$) oraz faza CSH w postaci rosenhanitu ($Ca_3Si_3O_9 \cdot H_2O$). Należy podkreślić brak identyfikowalnej fazy kaolinitu w składzie próbek wytworzonych na bazie łupka węglowego, co świadczy o redukcji wewnętrznej struktury kaolinitu w trakcie kalcynacji i powstaniu materiału o charakterze amorficznym. W trakcie geopolimeryzacji nastąpiła reakcja surowców z aktywatorem alkalicznym, w rezultacie czego utworzone zostały we wszystkich próbkach nowe fazy: CSH oraz albit. Szczególnie korzystna z punktu widzenia wytrzymałości na ściskanie geopolimerów jest obecność fazy CSH [64].

W kolejnej części badań przeprowadzono analizę struktury pianek geopolimerowych z zastosowaniem mikroskopu cyfrowego. Ocenie poddano rozmieszczenie porów

w materiałach, ich wielkość i kształt, spójność struktury, a także rozmieszczenie szkła odpadowego i stabilizatora w geopolimerach. Niezależnie od składu próbek stwierdzono jednorodny rozkład porów w strukturze pianek. Porównując próbki wytworzone na osnowie łupka węglowego z ich odpowiednikami wytworzonymi z zastosowaniem metakaolinu zauważano, że geopolimery na osnowie metakaolinu charakteryzowały się porowatością o bardziej regularnych kształtach i mniejszych rozmiarach. Dodatkowo w przypadku kompozytów z dodatkiem odpadowej stłuczki szklanej, zgodnie z oczekiwaniami dodatek ten był widoczny w strukturze porów, a więc ze względu na wielkość cząstek nie roztworzył się całkowicie. Ponadto w strukturze pianek na osnowie łupka węglowego zaobserwowano niewielkie niespójności i pęknięcia.

Przewodność cieplna materiałów spienionych stanowi istotną charakterystykę pod względem potencjalnego zastosowania wyrobów jako materiału izolacyjnego w budownictwie. Wyniki przeprowadzonych badań wykazały, że współczynnik przewodności cieplnej mieścił się w zakresie 0,079–0,117 W/(m·K). Dodatek materiałów odpadowych, tj. łupka węglowego, jak i odpadowej stłuczki szklanej powodował wzrost współczynnika λ do 25%, w porównaniu do geopolimerów wytworzonych na osnowie metakaolinu.

W dalszej części pracy [P4] określono wytrzymałość na ściskanie geopolimerów po 28 dniach sezonowania. Średnia wytrzymałość na ściskanie geopolimerów, uwzględniając odchylenie standardowe z pomiaru minimum trzech próbek, wynosiła od 0,70 ± 0,03 MPa (geopolimery na osnowie łupka węglowego) do 1,23 ± 0,05 MPa (kompozyty na osnowie metakaolinu z dodatkiem szkła odpadowego). Zastosowanie odpadowej stłuczki szklanej w kompozytach na osnowie metakaolinu oraz łupka węglowego spowodowało wzrost wytrzymałości na ściskanie o odpowiednio 9% oraz 54%, w porównaniu do geopolimerów wytworzonych z zastosowaniem tego samego prekursora, ale bez dodatku. Ponadto wprowadzony dodatek spowodował wzrost gęstości kompozytów. Zastosowanie metakaolinu jako prekursora materiałów geopolimerowych powodowało uzyskanie jednocześnie wyższej wytrzymałości na ściskanie oraz niższej gęstości, w porównaniu do próbek wytworzonych na osnowie łupka węglowego.

Reprezentatywne próbki geopolimerowe poddano badaniom z zastosowaniem rentgenowskiej mikrotomografii komputerowej (mikroCT) w celu oceny m.in.: homogeniczności rozkładu oraz udziału procentowego stłuczki szklanej oraz stabilizatora w piankach; porowatości z rozróżnieniem na pory otwarte i zamknięte; stopnia anizotropii oraz jednorodności geopolimerów (wyznaczonej w trzech kierunkach

XY, XZ, YZ). Wyniki potwierdziły, iż porowatość geopolimerów zależała od komponentów użytych w trakcie wytwarzania próbek. Zamiana łupka węglowego odpadową stłuczką szklaną powodowała obniżenie porowatości kompozytów, natomiast odwrotny efekt uzyskano stosując metakaolin. W strukturze wszystkich geopolimerów badanych z zastosowaniem mikrotomografii komputerowej dominowała porowatość otwarta, stanowiąca od 68,7% do 56,8% objętości materiału, natomiast udział porów zamkniętych wynosił od 0,3% do 1,8% objętości całych próbek. Struktura pianek była zbliżona do izotropowej.

Ostatnim badaniem, którego wyniki przedstawiono w publikacji P4 było wyznaczenie stopnia porowatości geopolimerów na podstawie wyników gęstości pozornej i gęstości właściwej próbek. Wyniki uzyskanych badań były spójne z rezultatami uzyskanymi z zastosowaniem mikrotomografii komputerowej. Obliczona porowatość dla geopolimerów przedstawionych w publikacji P4 mieściła się w zakresie 60,6% ÷ 81,2%. Potwierdzono, iż dodatek odpadowej stłuczki szklanej powoduje obniżenie porowatości kompozytu, zarówno w przypadku próbek wytworzonych z zastosowaniem metakaolinu, jak i łupka węglowego jako prekursorów geopolimerowych. Dodatkowo, zgodnie z wcześniej przedstawionymi wynikami, wyższą porowatością charakteryzowały się próbki wytworzone na osnowie metakaolinu niż na osnowie łupka węglowego.

Na podstawie wyników zrealizowanych badań wytworzone materiały geopolimerowe, z wyjątkiem geopolimerów na osnowie łupka węglowego z 20% udziałem wag. odpadowej stłuczki szklanej (ze względu na wyższą gęstość), zakwalifikowano do betonów lekkich klasy III zgodnie z klasyfikacją RILEM, które mogą znaleźć potencjalne zastosowanie np. jako warstwy izolacyjne oraz warstwy wypełniające przestrzenie np. wokół rur.

6. Podsumowanie i wnioski

W ramach realizacji prezentowanej rozprawy doktorskiej opracowano geopolimery na osnowie materiałów odpadowych, poprocesowych i/lub mineralnych takich jak: popiół lotny, łupek węglowy (po przeprowadzeniu obróbki mechanicznej i termicznej), metakaolin oraz hybryd metakaolinu z łupkiem węglowym, modyfikowanych odpadową stłuczką szklaną. W badaniach stosowano materiały, których obecne wykorzystanie jest ograniczone, takie jak łupek węglowy, popiół lotny i stłuczka szklana. Określono wpływ zmiennych tj. udziału wagowego oraz wielkości cząstek odpadowej stłuczki szklanej, rodzaju prekursora oraz kompozycji mieszanek na właściwości geopolimerów. Zrealizowane badania oraz analiza wyników umożliwiły sformułowanie następujących wniosków:

- Udział porowatości w strukturze spienionego geopolimeru zależy od zawartości oraz wielkości cząstek wprowadzanego szkła odpadowego i jest bardziej homogeniczny wraz ze wzrostem zawartości odpadowej stłuczki szklanej (do 30% wag.) i zmniejszeniem rozmiaru jej cząstek.
- Zastosowanie 20% wag. dodatku odpadowej stłuczki szklanej o wielkości cząstek 0,1–40 μm spowodowało uwolnienie największej energii reakcji egzotermicznej w trakcie procesu geopolimeryzacji w porównaniu do efektów zarejestrowanych dla pozostałych analizowanych frakcji.
- Konsystencję świeżych zapraw geopolimerowych zawierających do 20% wag. odpadów szklanych, niezależnie od zastosowanych w badaniach wielkości cząstek szkła odpadowego określono jako plastyczną. Zwiększenie zawartości stłuczki do 30% wag. o wielkości cząstek w zakresie 0,1–1200 μm oraz 200–1200 μm spowodowała zmianę konsystencji zaprawy na rzadką/ciekłą.
- Nasiąkliwość geopolimerów zarówno spienionych, jak i niespienionych zmniejszała się wraz ze wzrostem zawartości odpadowej stłuczki szklanej w geopolimerach.
- Dodatek 20% wag. szkła odpadowego o wielkości cząstek w zakresie 0,1–1200 μm w geopolimerach niespienionych powodował: zmniejszenie powierzchni właściwej o 4%, zmniejszenie całkowitej objętości porów o 19%, wzrost gęstości o 9% oraz zwiększenie wytrzymałości na ściskanie o 135,2% i 164,7% odpowiednio przed i po badaniu niepalności.
- Zastosowanie dodatku 20-30% wag. odpadowej stłuczki szklanej (średnia wielkość cząstek 550,1 μm) w piankach geopolimerowych spowodowało wzrost: powierzchni właściwej o 65-60%, gęstości o 6-9% oraz

wytrzymałości na ściskanie o ok. 80%, w porównaniu do materiałów referencyjnych.

- Dodatek odpadowej stłuczki szklanej w przypadku wszystkich badanych geopolimerów korzystnie wpływał na resztkową wytrzymałość na ściskanie, wyznaczoną po ekspozycji na temperaturę 750 °C. Ponadto wszystkie kompozyty geopolimerowe pod względem niepalności zakwalifikowano jako materiały klasy $A1_{fl}$.
- Substytucja metakaolinu zarówno szkłem odpadowym, jak i łupkiem węglowymi powodowała wzrost współczynnika przewodzenia ciepła pianek geopolimerowych.
- W strukturze pianek geopolimerowych dominowała porowatość otwarta (od 56,8% do 68,7%), a porowatość zamknięta wynosiła od 0,3% do 1,8%.
- Struktura pianek geopolimerowych była zbliżona do izotropowej, a rozmieszczenie porów i dodatków było homogeniczne.

Pełny opis zastosowanych materiałów bazowych oraz ich charakterystyki, metod badawczych, wyników badań wraz z dyskusją oraz przeglądem literatury dotyczącej podjętej tematyki badawczej zamieszczono w załącznikach [P1, P2, P3, P4].

7. Kierunki przyszłych badań

W dalszych etapach badań planowane jest przeprowadzenie analizy oceny cyklu życia wyrobów LCA (ang. Life Cycle Assessment). Takie podejście pozwoli na całościowe określenie wpływu materiałów na środowisko, uwzględniając proces pozyskania surowców, wytworzenia materiałów, ich eksploatacji oraz utylizacji. Dodatkowo zamierza się przeprowadzić analizę pod względem możliwości zastosowania zaprezentowanych rozwiązań na skalę przemysłową z uwzględnieniem kosztów wytworzenia, robocizny i wymagań aparaturowych.

Kolejnym kierunkiem przyszłych badań, który należy rozważyć jest ocena możliwości wytwarzania opracowanych mieszanek w technologii druku 3D, w formie prefabrykatów i/lub powłok ochronnych nanoszonych metodą natryskiwania.

Bibliografia

[1] J. Brimberg, S. Salhi, R. Todosijević, and D. Urošević, “Variable Neighborhood Search: The power of change and simplicity,” *Comput Oper Res*, vol. 155, 106221, 2023, doi: 10.1016/J.COR.2023.106221.

[2] C. R. Gagg, “Cement and concrete as an engineering material: An historic appraisal and case study analysis,” *Eng Fail Anal*, vol. 40, pp. 114–140, 2014, doi: 10.1016/J.ENGFAILANAL.2014.02.004.

[3] W. Ahmad, A. Ahmad, K. A. Ostrowski, F. Aslam, and P. Joyklad, “A scientometric review of waste material utilization in concrete for sustainable construction,” *Case Studies in Construction Materials*, vol. 15, e00683, 2021, doi: 10.1016/J.CSCM.2021.E00683.

[4] A. I. Fares, K. M. A. Sohel, K. Al-Jabri, and A. Al-Mamun, “Characteristics of ferrochrome slag aggregate and its uses as a green material in concrete – A review,” *Constr Build Mater*, vol. 294, 123552, 2021, doi: 10.1016/J.CONBUILDMAT.2021.123552.

[5] M. Nadi *et al.*, “Effect of natural graphite additions on the microstructural and mechanical behavior of metakaolin based geopolymer materials,” *Journal of Building Engineering*, 107562, 2023, doi: 10.1016/J.JOBE.2023.107562.

[6] R. Asghar, M. A. Khan, R. Alyousef, M. F. Javed, and M. Ali, “Promoting the green Construction: Scientometric review on the mechanical and structural performance of geopolymer concrete,” *Constr Build Mater*, vol. 368, 130502, 2023, doi: 10.1016/J.CONBUILDMAT.2023.130502.

[7] P. J. M. Monteiro, S. A. Miller, and A. Horvath, “Towards sustainable concrete,” *Nature Materials*, vol. 16, no. 7, pp. 698–699, 2017, doi: 10.1038/nmat4930.

[8] C. Ziejewska *et al.*, “3D Printing of Concrete-Geopolymer Hybrids,” *Materials,* vol. 15, no. 8, 2819, 2022, doi: 10.3390/MA15082819.

[9] Z. Zhang, J. L. Provis, A. Reid, and H. Wang, “Geopolymer foam concrete: An emerging material for sustainable construction,” *Constr Build Mater*, vol. 56, pp. 113–127, 2014, doi: 10.1016/J.CONBUILDMAT.2014.01.081.

[10] N. A. Madlool, R. Saidur, M. S. Hossain, and N. A. Rahim, “A critical review on energy use and savings in the cement industries,” *Renewable and Sustainable Energy Reviews*, vol. 15, no. 4, pp. 2042–2060, 2011, doi: 10.1016/J.RSER.2011.01.005.

[11] M. Alhawat, A. Ashour, G. Yildirim, A. Aldemir, and M. Sahmaran, “Properties of geopolymers sourced from construction and demolition waste: A review,” *Journal of Building Engineering*, vol. 50, 104104, 2022, doi: 10.1016/J.JOBE.2022.104104.

[12] X. Jiang, R. Xiao, Y. Ma, M. Zhang, Y. Bai, and B. Huang, “Influence of waste glass powder on the physico-mechanical properties and microstructures of fly ash-based geopolymer paste after exposure to high temperatures,” *Constr Build Mater*, vol. 262, 120579, 2020, doi: 10.1016/J.CONBUILDMAT.2020.120579.

[13] H.-W. Chang, T. Chang, F. Xiang, A. Mikhaylov, and A. Grigorescu, “Revisiting R&D intensity and CO2 emissions link in the USA using time varying granger causality test: 1870~2020,” *Heliyon*, vol. 9, no. 10, e20319, 2023, doi: 10.1016/J.HELIYON.2023.E20319.

[14] M. D. Ćirović, “Risk analysis of the european union 2030 greenhouse gas emission target compliance,” *International Journal of Global Warming*, vol. 16, no. 1, pp. 64–85, 2018, doi: 10.1504/IJGW.2018.094311.

[15] C. Mourou, M. Zamorano, D. P. Ruiz, and M. Martín-Morales, “Characterization of ceramic tiles coated with recycled waste glass particles to be used for cool roof applications,” *Constr Build Mater*, vol. 398, 132489, 2023, doi: 10.1016/J.CONBUILDMAT.2023.132489.

[16] C. Ziejewska *et al.*, “Eco-friendly zeolites for innovative purification of water from cationic dye and heavy metal ions.,” *J Clean Prod*, vol. 406, 136947, 2023, doi: 10.1016/J.JCLEPRO.2023.136947.

[17] R. Wang, Z. Zhang, X. Chen, L. Zhan, and Z. Xu, “Research on compound pollution characteristics and health risk evaluation of particulate matter and heavy metals in waste glass recycling process,” *Environmental Pollution*, p. 122570, 2023, doi: 10.1016/J.ENVPOL.2023.122570.

[18] P. Guo, W. Meng, H. Nassif, H. Gou, and Y. Bao, “New perspectives on recycling waste glass in manufacturing concrete for sustainable civil infrastructure,” *Constr Build Mater*, vol. 257, 119579, 2020, doi: 10.1016/J.CONBUILDMAT.2020.119579.

[19] E. Navaneetha, P. N. Rao, and A. Bahurudeen, “Compatibility of waste glass with other by-products for the production of sustainable concrete,” *Journal of Building Engineering*, vol. 80, 107922, 2023, doi: 10.1016/J.JOBE.2023.107922.

[20] D. Polat and M. Güden, “Processing and characterization of geopolymer and sintered geopolymer foams of waste glass powders,” *Constr Build Mater*, vol. 300, 124259, 2021, doi: 10.1016/J.CONBUILDMAT.2021.124259.

[21] R. M. Novais, G. Ascensão, M. P. Seabra, and J. A. Labrincha, “Waste glass from end-of-life fluorescent lamps as raw material in geopolymers,” *Waste Management*, vol. 52, pp. 245–255, 2016, doi: 10.1016/J.WASMAN.2016.04.003.

[22] R. Si, Q. Dai, S. Guo, and J. Wang, “Mechanical property, nanopore structure and drying shrinkage of metakaolin-based geopolymer with waste glass powder,” *J Clean Prod*, vol. 242, 118502, 2020, doi: 10.1016/J.JCLEPRO.2019.118502.

[23] Z. Bian, J.-X. Lu, Y. Huang, D. Xuan, G. Ou, and C. Sun Poon, “Recycling of waste glass in lightweight geopolymer using incineration bottom ash as a foaming agent: Towards energy conservation,” *Constr Build Mater*, vol. 400, 132632, 2023, doi: 10.1016/J.CONBUILDMAT.2023.132632.

[24] W. Dong, W. Li, and Z. Tao, “A comprehensive review on performance of cementitious and geopolymeric concretes with recycled waste glass as powder, sand or cullet,” *Resour Conserv Recycl*, vol. 172, 105664, 2021, doi: 10.1016/J.RESCONREC.2021.105664.

[25] E. Janowska-Renkas, M. Zdrojek, M. Kozioł, and A. Kaliciak-Kownacka, “Effect of composition of geopolymer composites containing fly ash and waste glass powder on their durability and resistivity demonstrated in presence of a nanocarbon additive in a form of graphene,” *Measurement*, vol. 211, 112616, 2023, doi: 10.1016/J.MEASUREMENT.2023.112616.

[26] S. Lei *et al.*, “Characteristics of lightweight geopolymers from microwave curing of basalt and waste glass powder mixtures,” *Constr Build Mater*, vol. 409, 133758, 2023, doi: 10.1016/J.CONBUILDMAT.2023.133758.

[27] K. Zheng, “Pozzolanic reaction of glass powder and its role in controlling alkali–silica reaction,” *Cem Concr Compos*, vol. 67, pp. 30–38, 2016, doi: 10.1016/J.CEMCONCOMP.2015.12.008.

[28] E. Gimenez-Carbo, L. Soriano, M. Roig-Flores, and P. Serna, “Characterization of Glass Powder from Glass Recycling Process Waste and Preliminary Testing,” *Materials*, vol. 14, no. 11, 2971, 2021, doi: 10.3390/MA14112971.

[29] A. Siddika, A. Hajimohammadi, M. A. Al Mamun, R. Alyousef, and W. Ferdous, “Waste Glass in Cement and Geopolymer Concretes: A Review on Durability and Challenges,” *Polymers,* vol. 13, no. 13, 2071, 2021, doi: 10.3390/POLYM13132071.

[30] S. K. Behera *et al.*, “Utilization of mill tailings, fly ash and slag as mine paste backfill material: Review and future perspective,” *Constr Build Mater*, vol. 309, 125120, 2021, doi: 10.1016/J.CONBUILDMAT.2021.125120.

[31] J. Mikuła, *Rozwiązania proekologiczne w zakresie produkcji : praca zbiorowa. T. 1, Nowoczesne materiały kompozytowe przyjazne środowisku*. Kraków: Wydawnictwo PK, 2014. Dostęp internetowy (12.11.2023): https://repozytorium.biblos.pk.edu.pl/resources/25728

[32] A. M. Elgarahy *et al.*, “Geopolymers as sustainable eco-friendly materials: Classification, synthesis routes, and applications in wastewater treatment,” *Sep Purif Technol*, vol. 324, 124631, 2023, doi: 10.1016/J.SEPPUR.2023.124631.

[33] J. Davidovits, *Geopolymer Chemistry and Applications 5 th edition*. Institut Géopolymère, 2020. Dostęp internetowy (01.10.2023): www.davidovits.info

[34] P. Kathirvel and S. Sreekumaran, “Sustainable development of ultra high performance concrete using geopolymer technology,” *Journal of Building Engineering*, vol. 39, 102267, 2021, doi: 10.1016/J.JOBE.2021.102267.

[35] X. Han, P. Zhang, Y. Zheng, and J. Wang, “Utilization of municipal solid waste incineration fly ash with coal fly ash/metakaolin for geopolymer composites preparation,” *Constr Build Mater*, vol. 403, 133060, 2023, doi: 10.1016/J.CONBUILDMAT.2023.133060.

[36] J. Davidovits, “Geopolymers - Inorganic polymeric new materials,” *Journal of Thermal Analysis*, vol. 37, no. 8, pp. 1633–1656, 1991, doi: 10.1007/BF01912193/METRICS.

[37] Q. Wan *et al.*, “Geopolymerization reaction, microstructure and simulation of metakaolin-based geopolymers at extended Si/Al ratios,” *Cem Concr Compos*, vol. 79, pp. 45–52, 2017, doi: 10.1016/J.CEMCONCOMP.2017.01.014.

[38] A. M. Tahwia, M. A. Ellatief, G. Bassioni, A. M. Heniegal, and M. A. Elrahman, “Influence of high temperature exposure on compressive strength and microstructure of ultra-high performance geopolymer concrete with waste glass and ceramic,” *Journal of Materials Research and Technology*, vol. 23, pp. 5681–5697, 2023, doi: 10.1016/J.JMRT.2023.02.177.

[39] Z. Pan, Z. Tao, Y. F. Cao, R. Wuhrer, and T. Murphy, “Compressive strength and microstructure of alkali-activated fly ash/slag binders at high temperature,” *Cem Concr Compos*, vol. 86, pp. 9–18, 2018, doi: 10.1016/J.CEMCONCOMP.2017.09.011.

[40] M. Lahoti, K. H. Tan, and E. H. Yang, “A critical review of geopolymer properties for structural fire-resistance applications,” *Constr Build Mater*, vol. 221, pp. 514–526, 2019, doi: 10.1016/J.CONBUILDMAT.2019.06.076.

[41] G. Yu and Y. Jia, “Microstructure and Mechanical Properties of Fly Ash-Based Geopolymer Cementitious Composites,” *Minerals,* vol. 12, no. 7, 853, 2022, doi: 10.3390/MIN12070853.

[42] M. M. A. B. Abdullah *et al.*, “Clay-Based Materials in Geopolymer Technology,” *Cement Based Materials*, 2018, doi: 10.5772/INTECHOPEN.74438.

[43] M. Łach *et al.*, “Process design for a production of sustainable materials from post-production clay,” *Materials*, vol. 14, no. 4, pp. 1–19, 2021, doi: 10.3390/MA14040953.

[44] K. Korniejenko, M. Łach, J. Marczyk, C. Ziejewska, N. P. Halyag, and G. Mucsi, “Fly ash as a raw material for geopolymerisation-mineralogical composition and morphology,” *IOP Conf Ser Mater Sci Eng*, vol. 706, no. 1, 2019, doi: 10.1088/1757-899X/706/1/012006.

[45] M. Idrees, A. Ameen, J. Shi, F. Saeed, and O. Gencel, “Preparation and performance optimization of eco-friendly geopolymers prepared from coarser lignite-based waste fly ash,” *Constr Build Mater*, vol. 391, 131804, 2023, doi: 10.1016/J.CONBUILDMAT.2023.131804.

[46] N. Mao, D. Wu, K. Chen, K. Cao, and J. Huang, “Combining experiments and molecular dynamics simulations to investigate the effects of water on the structure and mechanical properties of a coal gangue-based geopolymer,” *Constr Build Mater*, vol. 389, 131556, 2023, doi: 10.1016/J.CONBUILDMAT.2023.131556.

[47] B. Bayrak, S. A. Mostafa, A. Öz, B. A. Tayeh, G. Kaplan, and A. C. Aydın, “The effect of clinker aggregate on acid resistance in prepacked geopolymers containing metakaolin and quartz powder in the presence of ground blast furnace slag,” *Journal of Building Engineering*, vol. 69, 106290, 2023, doi: 10.1016/J.JOBE.2023.106290.

[48] T. Guo *et al.*, “Mechanical properties and microstructure of red mud-coal metakaolin geopolymer concrete based on orthogonal tests,” *Journal of Building Engineering*, vol. 79, 107789, 2023, doi: 10.1016/J.JOBE.2023.107789.

[49] G. Chen *et al.*, “Development of high performance geopolymer concrete with waste rubber and recycle steel fiber: A study on compressive behavior, carbon emissions and economical performance,” *Constr Build Mater*, vol. 393, 131988, 2023, doi: 10.1016/J.CONBUILDMAT.2023.131988.

[50] E. S. Poojalakshmi, J. Patel, B. Sunantha, B. S. Thomas, K. P. Ramaswamy, and R. Ahmad Khan, “Effect of mechanical activation on the properties of rice husk ash-based one part geopolymer,” *Mater Today Proc*, 2023, doi: 10.1016/J.MATPR.2023.04.306.

[51] P. Rovnaník, P. Rovnaníková, M. Vyšvařil, S. Grzeszczyk, and E. Janowska-Renkas, “Rheological properties and microstructure of binary waste red brick powder/metakaolin geopolymer,” *Constr Build Mater*, vol. 188, pp. 924–933, 2018, doi: 10.1016/J.CONBUILDMAT.2018.08.150.

[52] H. Ulugöl *et al.*, “Mechanical and microstructural characterization of geopolymers from assorted construction and demolition waste-based masonry and glass,” *J Clean Prod*, vol. 280, 124358, 2021, doi: 10.1016/J.JCLEPRO.2020.124358.

[53] D. Neeraj Varma and S. Prasad Singh, “Recycled waste glass as precursor for synthesis of slag-based geopolymer,” *Mater Today Proc*, 2023, doi: 10.1016/J.MATPR.2023.03.516.

[54] S. Dadsetan, H. Siad, M. Lachemi, O. Mahmoodi, and M. Sahmaran, “Optimization and characterization of geopolymer binders from ceramic waste, glass waste and sodium glass liquid,” *J Clean Prod*, vol. 342, 130931, 2022, doi: 10.1016/J.JCLEPRO.2022.130931.

[55] J. Davidovits, “False values on CO2 emission for geopolymer cement/concrete published in scientific papers,” 2015, Dostęp internetowy (19.09.2023): https://www.geopolymer.org

[56] A. Boros and T. Korim, “Development of Geopolymer Foams for Multifunctional Applications,” *Crystals*, vol. 12, no. 3, 386, 2022, doi: 10.3390/CRYST12030386.

[57] C. Bai *et al.*, “Fabrication and properties of slag-based geopolymer syntactic foams containing hollow glass microspheres,” *Mater Lett*, vol. 308, 131158, 2022, doi: 10.1016/J.MATLET.2021.131158.

[58] H. Alghamdi and N. Neithalath, “Synthesis and characterization of 3D-printable geopolymeric foams for thermally efficient building envelope materials,” *Cem Concr Compos*, vol. 104, 103377, 2019, doi: 10.1016/J.CEMCONCOMP.2019.103377.

[59] M. Szechyńska-Hebda, J. Marczyk, C. Ziejewska, N. Hordyńska, J. Mikuła, and M. Hebda, “Optimal Design of pH-neutral Geopolymer Foams for Their Use in Ecological Plant Cultivation Systems,” *Materials,* vol. 12, no. 18, 2999, 2019, doi: 10.3390/MA12182999.

[60] A. Kul *et al.*, “Characterization and life cycle assessment of geopolymer mortars with masonry units and recycled concrete aggregates assorted from construction and demolition waste,” *Journal of Building Engineering*, vol. 78, 107546, 2023, doi: 10.1016/J.JOBE.2023.107546.

[61] H. Korhonen, J. Timonen, S. Suvanto, P. Hirva, K. Mononen, and S. Jääskeläinen, “The Mechanical Properties of Geopolymers from Different Raw Materials and the Effect of Recycled Gypsum,” *Inorganics*, vol. 11, no. 7, 298, 2023, doi: 10.3390/INORGANICS11070298/S1.

[62] J. Liu, J. H. Doh, D. E. L. Ong, Z. Liu, and M. N. S. Hadi, “Methods to evaluate and quantify the geopolymerization reactivity of waste-derived aluminosilicate precursor in alkali-activated material: A state-of-the-art review,” *Constr Build Mater*, vol. 362, 129784, 2023, doi: 10.1016/J.CONBUILDMAT.2022.129784.

[63] Geopolymer Institute, “Why Alkali-Activated Materials are NOT Geopolymers ? – Geopolymer Institute,” *Geopolymer Camp*, 2017, doi: 10.13140/RG.2.2.34337.25441.

[64] J. Matsimbe, M. Dinka, D. Olukanni, and I. Musonda, “Geopolymer: A Systematic Review of Methodologies,” *Materials*, vol. 15, no. 19, 6852, 2022, doi: 10.3390/MA15196852.

[65] I. Kurek *et al.*, “Foamed Eco-Geopolymer Modified by Perlite and Cellulose as a Construction Material for Energy-Efficient Buildings,” *Energies*, vol. 15, no. 12, 2022, doi: 10.3390/EN15124297.

[66] F. Ayub and S. A. Khan, “An overview of geopolymer composites for stabilization of soft soils,” *Constr Build Mater*, vol. 404, 133195, 2023, doi: 10.1016/J.CONBUILDMAT.2023.133195.

[67] Y. X. Chen, K. M. Klima, H. J. H. Brouwers, and Q. Yu, “Effect of silica aerogel on thermal insulation and acoustic absorption of geopolymer foam composites: The role of aerogel particle size,” *Compos B Eng*, vol. 242, 110048, 2022, doi: 10.1016/J.COMPOSITESB.2022.110048.

[68] L. L. Duna *et al.*, “Performances of laterite-based geopolymer matrice filters on the bacteriological filtration of contaminated groundwater and microstructure,” *Journal of Water Process Engineering*, vol. 53, 103699, 2023, doi: 10.1016/J.JWPE.2023.103699.

[69] Q. Shuai *et al.*, “Fire resistance of phosphoric acid-based geopolymer foams fabricated from metakaolin and hydrogen peroxide,” *Mater Lett*, vol. 263, 127228, 2020, doi: 10.1016/J.MATLET.2019.127228.

[70] N. Yang, C. S. Das, X. Xue, W. Li, and J. G. Dai, “Geopolymer coating modified with reduced graphene oxide for improving steel corrosion resistance,” *Constr Build Mater*, vol. 342, 127942, 2022, doi: 10.1016/J.CONBUILDMAT.2022.127942.

[71] N. Ranjbar and M. Zhang, “Fiber-reinforced geopolymer composites: A review,” *Cem Concr Compos*, vol. 107, 2020, doi: 10.1016/J.CEMCONCOMP.2019.103498.

[72] P. Zhang, K. Wang, Q. Li, J. Wang, and Y. Ling, “Fabrication and engineering properties of concretes based on geopolymers/alkali-activated binders - A review,” *J Clean Prod*, vol. 258, 120896, 2020, doi: 10.1016/J.JCLEPRO.2020.120896.

[73] *PN-EN 12457-2:2006. Charakteryzowanie odpadów - Wymywanie - Badanie zgodności w odniesieniu do wymywania ziarnistych materiałów odpadowych i osadów - Część 2: Jednostopniowe badanie porcjowe przy stosunku cieczy do fazy stałej 10 l/kg w przypadku materiałów o wielkości cząstek poniżej 4 mm (bez redukcji lub z redukcją wielkości)*.

[74] *PN-EN ISO 10523:2012. Jakość wody. Oznaczanie pH*.

[75] *PN-EN 15934:2013-02. Osady ściekowe, uzdatnione bioodpady, gleba oraz odpady - Oznaczanie suchej masy poprzez oznaczanie zawartości suchej pozostałości lub zawartości wody*.

[76] *PN-EN ISO 11885:2009. Jakość wody - Oznaczanie wybranych pierwiastków metodą optycznej spektrometrii emisyjnej z plazmą wzbudzoną indukcyjnie (ICP-OES)*.

[77] *PN-EN 1484:1999. Analiza wody - Wytyczne oznaczania ogólnego węgla organicznego (OWO) i rozpuszczonego węgla organicznego (RWO)*.

[78] *PN EN 15216:2010. Charakteryzowanie odpadów - Oznaczanie całkowitej substancji rozpuszczonej (TDS) w wodzie i eluatach*.

[79] *PN-EN ISO 12846:2012. Jakość wody - Oznaczanie rtęci - Metoda absorpcyjnej spektrometrii atomowej (AAS) ze wzbogacaniem lub bez wzbogacania*.

[80] *PN-EN ISO 10304-1:2009/AC:2012. Jakość wody - Oznaczanie rozpuszczonych anionów za pomocą chromatografii jonowej - Część 1: Oznaczanie bromków, chlorków, fluorków, azotanów, azotynów, fosforanów i siarczanów*.

[81] "Rozporządzenie Rady Ministrów z dnia 2 stycznia 2007 r. w sprawie wymagań dotyczących zawartości naturalnych izotopów promieniotwórczych potasu K-40, radu Ra-226 i toru Th-228 w surowcach i materiałach stosowanych w budynkach przeznaczonych na pobyt ludzi i inwentarza żywego, a także w odpadach przemysłowych stosowanych w budownictwie, oraz kontroli zawartości tych izotopów." Dostęp internetowy (12.11.2023): https://isap.sejm.gov.pl/isap.nsf/DocDetails.xsp?id=WDU20070040029

[82] "Rozporządzenie Rady Ministrów z dnia 17 grudnia 2020 r. w sprawie materiałów budowlanych, w przypadku których oznacza się stężenie promieniotwórcze izotopów promieniotwórczych potasu K-40, radu Ra-226 i toru Th-232, wymagań dotyczących dokonywania tych oznaczeń oraz wartości wskaźnika stężenia promieniotwórczego, o której przekroczeniu informuje się właściwe organy." Dostęp internetowy (19.11.2023): https://isap.sejm.gov.pl/isap.nsf/DocDetails.xsp?id=WDU20210000033

[83] *PN-EN 12390-3:2019. Badania betonu - Część 3: Wytrzymałość na ściskanie próbek do badań*.

[84] *PN-EN 12390-5:2019. Badania betonu - Część 5: Wytrzymałość na zginanie próbek do badań*.

[85] *PN-85-B-04500. Zaprawy Budowlane. Badania cech fizycznych i wytrzymałościowych*.

[86] *PN-EN 1015-3:1999/A2:2006. Metody badań zapraw do murów - Określenie konsystencji świeżej zaprawy (za pomocą stolika rozpływu)*.

[87] *PN-88/B-06250. Beton zwykły*.

[88] T. Azdast and R. Hasanzadeh, "Increasing cell density/decreasing cell size to produce microcellular and nanocellular thermoplastic foams: A review," *https://doi.org/10.1177/0021955X20959301*, vol. 57, no. 5, pp. 769–797, 2020, doi: 10.1177/0021955X20959301.

[89] *PN-EN ISO 1182:2020. Badania reakcji na ogień wyrobów - Badanie niepalności*.

[90] D. Mierzwiński, M. Łach, M. Hebda, J. Walter, M. Szechyńska-Hebda, and J. Mikuła, “Thermal phenomena of alkali-activated metakaolin studied with a negative temperature coefficient system,” *J Therm Anal Calorim*, vol. 138, no. 6, pp. 4167–4175, 2019, doi: 10.1007/S10973-019-08471-7/FIGURES/8.

[91] *DIN EN 12667. Właściwości cieplne materiałów i wyrobów budowlanych - Określanie oporu cieplnego metodami osłoniętej płyty grzejnej i czujnika strumienia cieplnego - Wyroby o dużym i średnim oporze cieplnym*.

[92] *ASTMC618-22. Standard specification for coal fly ash and raw or calcined natural pozzolan for use in concrete*.

[93] H. J. Chen, N. H. Shih, C. H. Wu, and S. K. Lin, “Effects of the Loss on Ignition of Fly Ash on the Properties of High-Volume Fly Ash Concrete,” *Sustainability,* vol. 11, no. 9, p. 2704, 2019, doi: 10.3390/SU11092704.

[94] Z. Sun, A. Vollpracht, and H. A. van der Sloot, “pH dependent leaching characterization of major and trace elements from fly ash and metakaolin geopolymers,” *Cem Concr Res*, vol. 125, 105889, 2019, doi: 10.1016/J.CEMCONRES.2019.105889.

[95] T. S. Osholana, M. K. Dludlu, B. Oboirien, and R. Sadiku, “Enhanced reactivity of geopolymers produced from fluidized bed combustion bottom ash,” *S Afr J Chem Eng*, vol. 34, pp. 72–77, 2020, doi: 10.1016/J.SAJCE.2020.06.006.

[96] A. M. Tahwia, A. M. Heniegal, M. Abdellatief, B. A. Tayeh, and M. A. Elrahman, “Properties of ultra-high performance geopolymer concrete incorporating recycled waste glass,” *Case Studies in Construction Materials*, vol. 17, e01393, 2022, doi: 10.1016/J.CSCM.2022.E01393.

[97] M. Vafaei and A. Allahverdi, “High strength geopolymer binder based on waste-glass powder,” *Advanced Powder Technology*, vol. 28, no. 1, pp. 215–222, 2017, doi: 10.1016/J.APT.2016.09.034.

[98] A. Siddika, A. Hajimohammadi, W. Ferdous, and V. Sahajwalla, “Roles of Waste Glass and the Effect of Process Parameters on the Properties of Sustainable Cement and Geopolymer Concrete—A State-of-the-Art Review,” *Polymers,* vol. 13, no. 22, p. 3935, 2021, doi: 10.3390/POLYM13223935.

[99] S. Hall and B. Evarts, “Fire Loss in the United States During 2021,” 2022.

[100] S. J. Baker, “Fossil evidence that increased wildfire activity occurs in tandem with periods of global warming in Earth’s past,” *Earth Sci Rev*, vol. 224, 103871, 2022, doi: 10.1016/J.EARSCIREV.2021.103871.

[101] S. N. Abd Razak, N. Shafiq, L. Guillaumat, S. A. Farhan, and V. K. Lohana, “Fire-Exposed Fly-Ash-Based Geopolymer Concrete: Effects of Burning Temperature on Mechanical and Microstructural Properties,” *Materials*, vol. 15, no. 5, 2022, doi: 10.3390/MA15051884.

[102] S. Luhar and I. Luhar, “Valorisation of Waste Glasses for the Development of Geopolymer Mortar—Properties and Applications: An Appraisal,” *Journal of Composites Science 2022, Vol. 6, Page 30*, vol. 6, no. 1, 30, 2022, doi: 10.3390/JCS6010030.

[103] W. D. A. Rickard, A. Van Riessen, and P. Walls, “Thermal Character of Geopolymers Synthesized from Class F Fly Ash Containing High Concentrations of Iron and α-Quartz,” *Int J Appl Ceram Technol*, vol. 7, no. 1, pp. 81–88, 2010, doi: 10.1111/J.1744-7402.2008.02328.X.

[104] K. M. Klima, K. Schollbach, H. J. H. Brouwers, and Q. Yu, “Thermal and fire resistance of Class F fly ash based geopolymers – A review,” *Constr Build Mater*, vol. 323, p. 126529, 2022, doi: 10.1016/J.CONBUILDMAT.2022.126529.

Wykaz osiągnięć – dorobek naukowy

Dane bibliometryczne Autora rozprawy:

Wskaźnik Hirscha: 8 (wg Scopus), 9 (wg ResearchGate)

Całkowita liczba cytowań: 188 (wg Scopus), 217 (wg ResearchGate)

Sumaryczny Impact Factor: 67.718

Dane aktualne na dzień: 03.12.2023 r.

Numer ORCID: 0000-0002-6383-7639

Publikacje w czasopismach z listy Journal Citation Reports (JCR):

1) **Ziejewska Celina**, Bąk Agnieszka, Hodor Krzysztof, Hebda Marek: *Eco-Friendly coal gangue and/or metakaolin-based lightweight geopolymer with the addition of waste glass*. Materials. 2023, 16(17). DOI: 10.3390/ma16176054, IF: 3.4

2) **Ziejewska Celina**, Grela Agnieszka, Mierzwiński Dariusz, Hebda Marek: *Influence of waste glass addition on the fire resistance, microstructure and mechanical properties of geopolymer composites*. Materials. 2023, 16(17). DOI: 10.3390/ma16176011, IF: 3.4

3) **Ziejewska Celina**, Grela Agnieszka, Łach Michał, Marczyk Joanna, Hordyńska Natalia, Szechyńska-Hebda Magdalena, Hebda Marek: *Eco-friendly zeolites for innovative purification of water from cationic dye and heavy metal ions*. Journal of Cleaner Production. 2023, 406, 136947. DOI: 10.1016/j.jclepro.2023.136947, IF: 11.1

4) **Ziejewska Celina**, Grela Agnieszka, Hebda Marek: *Influence of waste glass particle size on the physico-mechanical properties and porosity of foamed geopolymer composites based on coal fly ash*. Materials. 2023, 16(5). DOI: 10.3390/ma16052044, IF: 3.4

5) Łach Michał, Pławecka Kinga, Marczyk Joanna, **Ziejewska Celina**, Hebdowska-Krupa Maria, Nykiel Marek, Hebda Marek, Miernik Krzysztof, Mierzwiński Dariusz, Korniejenko Kinga, Mikuła Janusz, Smoroń Krzysztof: *Use of diatomite from Polish fields in sustainable development as a sorbent for petroleum substances*. Journal of Cleaner Production. 389, 136100. DOI: 10.1016/j.jclepro.2023.136100, IF: 11.1

6) Marczyk Joanna, **Ziejewska Celina**, Korniejenko Kinga, Łach Michał, Marzec Witold, Góra Mateusz, Dziura Paweł, Sprince Andina, Szechyńska-Hebda Magdalena, Hebda Marek: *Properties of 3D printed concrete–geopolymer hybrids reinforced with aramid roving*. Materials. 2022, 15(17). DOI: 10.3390/ma15176132, IF: 3.4

7) Kurek Izabela, Florek Emilia, Gozdur Weronika, **Ziejewska Celina**, Marczyk Joanna, Łach Michał, Korniejenko Kinga, Duży Patrycja, Choińska Marta, Szechyńska-Hebda Magdalena, Hebda Marek: *Foamed eco-geopolymer modified by perlite and cellulose as a construction material for energy-efficient buildings*. Energies. 2022, 15(12). DOI: 10.3390/en15124297, IF: 3.2

8) Marczyk Joanna, **Ziejewska Celina**, Pławecka Kinga, Bąk Agnieszka, Łach Michał, Korniejenko Kinga, Hager Izabela, Mikuła Janusz, Lin Wei-Ting, Hebda Marek: *Optimizing the l/s ratio in geopolymers for the production of large-size elements with 3D printing technology*. Materials. 2022, 15(9). DOI: 10.3390/ma15093362, IF: 3.4

9) **Ziejewska Celina**, Marczyk Joanna, Korniejenko Kinga, Bednarz Sebastian, Sroczyk Piotr, Łach Michał, Mikuła Janusz, Figiela Beata, Szechyńska-Hebda Magdalena, Hebda Marek: *3D printing of concrete-geopolymer hybrids*. Materials. 2022, 15(8). DOI: 10.3390/ma15082819, IF: 3.4

10) Korniejenko Kinga, Figiela Beata, **Ziejewska Celina**, Marczyk Joanna, Bazan Patrycja, Hebda Marek, Choińska Marta, Lin Wei-Ting: *Fracture behavior of long fiber reinforced geopolymer composites at different operating temperatures*. Materials. 2022, 15(2). DOI: 10.3390/ma15020482, IF: 3.4

11) Marczyk Joanna, **Ziejewska Celina**, Gądek Szymon, Korniejenko Kinga, Łach Michał, Góra Mateusz, Kurek Izabela, Doğan-Sağlamtimur Neslihan, Hebda Marek, Szechyńska-Hebda Magdalena: *Hybrid materials based on fly ash, metakaolin, and cement for 3D printing*. Materials. 2021, 14(22). DOI: 10.3390/ma14226874, IF: 3.748

12) Korniejenko Kinga, Figiela Beata, Miernik Krzysztof, **Ziejewska Celina**, Marczyk Joanna, Hebda Marek, Cheng An, Lin Wei-Ting: *Mechanical and fracture properties of long fiber reinforced geopolymer composites*. Materials. 2021, 14(18). DOI: 10.3390/ma14185183, IF: 3.748

13) Łach Michał, Gado Reda A., Marczyk Joanna, **Ziejewska Celina**, Dogan-Saglamtimur Neslihan, Mikuła Janusz, Szechyńska-Hebda Magdalena, Hebda

Marek: *Process design for a production of sustainable materials from post-production clay*. Materials. 2021, 14(4). DOI: 10.3390/ma14040953, IF: 3.748

14) Szechyńska-Hebda Magdalena, Marczyk Joanna, **Ziejewska Celina**, Hordyńska Natalia, Mikuła Janusz, Hebda Marek: *Neutral geopolymer foams reinforced with cellulose studied with the FT-Raman spectroscopy*. IOP Conference Series: Materials Science and Engineering. 2019, 706. DOI: 10.1088/1757-899X/706/1/012017

15) Marczyk Joanna, **Ziejewska Celina**, Łach Michał, Korniejenko Kinga, Lin Wei-Ting, Hebda Marek: *Possibilities of using the 3D printing process in the concrete and geopolymers application*. IOP Conference Series: Materials Science and Engineering. 2019, 706. DOI: 10.1088/1757-899X/706/1/012019

16) Korniejenko Kinga, Łach Michał, Marczyk Joanna, **Ziejewska Celina**, Halyag Nóra Papné, Mucsi Gabor: *Fly ash as a raw material for geopolymerisation-mineralogical composition and morphology*. IOP Conference Series: Materials Science and Engineering. 2019, 706. DOI: 10.1088/1757-899X/706/1/012002

17) Szechyńska-Hebda Magdalena, Marczyk Joanna, **Ziejewska Celina**, Hordyńska Natalia, Mikuła Janusz, Hebda Marek: *Optimal design of pH-neutral geopolymer foams for their use in ecological plant cultivation systems*. Materials. 2019, 12(18). DOI: 10.3390/ma12182999, IF: 3.057

18) **Ziejewska Celina**, Marczyk Joanna, Szewczyk-Nykiel Aneta, Nykiel Marek, Hebda Marek: *Influence of size and volume share of WC particles on the properties of sintered metal matrix composites*. Advanced Powder Technology. 2019, 30(4). DOI: 10.1016/j.apt.2019.01.013, IF: 4.217

Pozostałe publikacje naukowe:

1) Gądek Szymon, Marczyk Joanna, **Ziejewska Celina**, Łach Michał: *The sustainability benefits derived from using additive manufacturing technologies*, Ukraine's current development, problems, and challenges: International Scientific and Practical Conference 2019. Mariupol, 2019.

2) **Ziejewska Celina**, Łach Michał, Mierzwiński Dariusz, Marczyk Joanna, Hager Izabela: *Development of innovative solutions through the collaboration industry enterprises with research institutions*, Ukraine's current development, problems

and challenges: International Scientific and Practical Conference 2019, Mariupol, 2019.

3) **Ziejewska Celina**, Hebda Marek, Nosal Przemysław: *Microstructural and mechanical properties of aluminium alloys joint fabricated by friction stir welding (FSW)*, CTU in Prague Faculty of Mechanical Engineering, 2018.

4) **Ziejewska Celina**, Nykiel Marek, Hebda Marek: *Badanie odporności na zużycie ścierne kompozytów na osnowie niskostopowej stali Astaloy CrL*, modyfikowanych dodatkiem węglika wolframu. Omnibuss Wiedza i technologia motorem gospodarki, 2017.

Udział w konferencjach naukowych – wystąpienia ustne:

1) Ogólnopolska Konferencja Interdyscyplinarna pn: „*COGITO CZ. VIII*"; 15–16.06.2023; Kraków. „*Wytwarzanie i właściwości proekologicznych materiałów aktywowanych alkalicznie*".

2) Ogólnopolska Konferencja Interdyscyplinarna pn: "*COGITO CZ. VIII*"; 15–16.06.2023; Kraków. Tytuł wystąpienia: „*Odpady górnicze i możliwości ich zagospodarowania*".

3) *Ogólnopolska Konferencja Młodych Naukowców pn. Nowe trendy w badaniach naukowych – wystąpienie młodego naukowca – Edycja V*; 22–24.06.2023; Kraków. Tytuł wystąpienia: „*Kompozyty geopolimerowe wytwarzane na bazie materiałów odpadowych*".

4) Konferencja międzynarodowa: *2nd International Conference on Environment, Technology and Management (ICETEM)*; Niğde Ömer Halisdemir University, 13–15.10.2022, Tytuł wystąpienia: „*Properties of waste glass-reinforced geopolymer composites*".

5) Konferencja międzynarodowa: *IV. International Turkic World Congress on Science and Engineering*; 23–24.06.2022; Niğde, Turcja. Tytuł wystąpienia: **„***The influence of glass waste on the properties of fly ash based geopolymer composites*".

6) Konferencja międzynarodowa: 3. International Baku Scientific Research Congress; 15–16.10.2021; Baku, Azerbejdżan. Tytuł wystąpienia: „*Fabrication and characterization of glass waste reinforced geopolymer foams*".

7) Konferencja międzynarodowa: Materials, Methods & Technologies 2021 23rd International Conference; 19–22.08.2021; Burgas, Bułgaria; Tytuł wystąpienia: „*Effect of waste glass powder on the physico-mechanical properties and microstructure of geopolymer composites*".

8) Konferencja międzynarodowa: TURK-COSE 2020: 2. International Turkic World Congress on Science and Engineering; 14–15.11.2020; Astana, Kazachstan. Tytuł wystąpienia: „*Influence of fibers addition on the mechanical properties of geopolymer composites*".

9) Konferencja ogólnopolska: Nowe Trendy w Badaniach Naukowych - Wystąpienie Młodego Naukowca Edycja I; 20–21.06.2020; Kraków. Tytuł wystąpienia: „*Materiały geopolimerowe w budownictwie - zielona alternatywa dla rozwiązań stosowanych tradycyjnie*".

10) Ogólnopolska Konferencja Interdyscyplinarna: OMNIBUS Część III; 11–12.06.2020; Kraków. Tytuł wystąpienia: „*Geopolimery - nowoczesne materiały przyjazne środowisku*".

11) Konferencja międzynarodowa: Susstainable development of Ukraine, challenges and ways of solution; 14–15.11.2019; Pryazovskyi State Technical University SHEI (PSTU), Ukraina.

12) Konferencja międzynarodowa: Student's Conference STC Faculty of Mechanical Engineering Czech Technical University in Prague; 11.04.2018, Praga, Czechy. Tytuł wystąpienia: „*Microstructural and mechanical properties of aluminium alloys joint fabricated by friction stir welding (FSW)*".

13) Konferencja ogólnopolska: Omnibuss, 27.06.2017, Częstochowa. Tytuł wystąpienia: „*Badanie odporności na zużycie ścierne kompozytów na bazie Astaloy CrL, modyfikowanych dodatkiem węglika wolframu*".

Udział w projektach badawczych:

1) 09.2022 – obecnie, udział w projekcie pn. "*Opracowanie kompozytów geopolimerowych jako materiału do ochrony niebezpiecznych wraków i innych krytycznych konstrukcji podwodnych przed korozją*", Narodowe Centrum Badań i Rozwoju, M-ERA.NET3/2021/71/MAR-WRECK/2022;

2) 10.2020 – obecnie, udział w projekcie pn. „*Droga do doskonałości - kompleksowy program wsparcia uczelni*" realizowanego w ramach Programu Operacyjnego Wiedza Edukacja Rozwój 2014-2020 współfinansowanego ze środków Europejskiego Funduszu Społecznego, WND-POWR.03.05.00-00-Z214/18;

3) 10.2022 – 10.2023, udział w projekcie pn. „*Smart Geopolymers*" (Inteligentne materiały geopolimerowe), Akronim: SMART-G, Źródło finansowania: 3. konkurs ERA-MIN 2 (Call 2019);

4) 03.2019 – 04.2022, udział w projekcie pn. "*Opracowanie technologii druku 3D konstrukcyjnych i elewacyjnych elementów prefabrykowanych wykonanych z kompozytów betonowych i geopolimerów*", Narodowe Centrum Badań i Rozwoju, POIR.04.01.04-00-0096/18-00;

5) 02.2018 – 06.2018, udział w projekcie pn. "*Development of ecofriendly composite materials based on geopolymer matrix and reinforced with waste fibers*", ELAC2015/T020721.

Staże, praktyki naukowe

1) Zagraniczny staż naukowy, 19.06.2023 – 19.07.2023, Riga Technical University (Ryga, Łotwa).

2) Zagraniczny staż naukowy, 16.11.2022 – 13.12.2022, Institut universitaire de technologie de Saint-Nazaire (Saint-Nazaire, Francja).

3) Zagraniczny staż naukowy, 15.08.2022 – 15.09.2022, Technical University of Liberec (Liberec, Czechy).

4) Zagraniczny staż naukowy, 29.10.2019 – 03.11.2019, Pryazovskyi State Technical University (Mariupol, Ukraina).

5) Staż przygotowujący do podjęcia obowiązków nauczyciela akademickiego, 26.02.2018 – 31.07.2018, Politechnika Krakowska im. Tadeusza Kościuszki (Kraków, Polska).

6) Staż w jednostce naukowej, 01.07.2017 – 30.09.2017, Polska Akademia Nauk Instytut Fizjologii Roślin im. Franciszka Górskiego (Kraków, Polska).

7) Praktyka zawodowa, 01.08.2016 – 31.08.2016, Instytut Odlewnictwa, Zespół Laboratoriów Badawczych (Kraków, Polska).

Wykaz innych aktywności naukowych

1. Pomoc w przygotowaniu stanowisk laboratoryjnych na Małopolskiej Nocy Naukowców 2023, wydarzeniu mającemu na celu popularyzację nauki, 29.09.2023, Politechnika Krakowska im. Tadeusza Kościuszki.
2. Pomoc w przygotowaniu oraz prezentacji stanowisk laboratoryjnych na Ogólnopolskim Dniu Inżynierii Materiałowej 2023, wydarzeniu mającemu na celu popularyzację inżynierii materiałowej, 17.03.2023, Politechnika Krakowska im. Tadeusza Kościuszki.
3. Uczestnictwo w komitecie organizacyjnym konferencji naukowej 2nd International Conference on Environment, Technology and Management (ICETEM), 13–15.10.2022, Department of Environmental Engineering of Nigde Omer Halisdemir University (Niğde, Turcja).
4. Pomoc w przygotowaniu oraz prezentacji stanowisk laboratoryjnych na Małopolskiej Nocy Naukowców 2022, wydarzeniu mającemu na celu popularyzację nauki, 30.09.2022, Politechnika Krakowska im. Tadeusza Kościuszki.

Ukończone kursy, szkolenia, aktywności rozwijające kompetencje merytoryczne

- Studia podyplomowe „Zarządzanie zasobami ludzkimi”, Centrum Szkolenia i Organizacji Systemów Jakości Politechniki Krakowskiej im. Tadeusza Kościuszki;
- Studium Pedagogiczne dla Asystentów i Doktorantów, Centrum Pedagogiki i Psychologii Politechniki Krakowskiej;
- „AgilePM Foundation”, szkolenie ukończone pozytywnym wynikiem egzaminu i uzyskaniem certyfikatu AgilePM Foundation, International AgilePM® Foundation;
- „PRINCE 2 Foundation 6th Edition”, Inprogress Szkolenia sp. z o.o.;
- „MS Project”, ZESPÓŁ EKSPERTÓW MANAGER Pelczar sp. j.;
- „Zarządzanie zespołem badawczym”, Centrum Organizacji Szkoleń i Konferencji SEMPER;
- „Zarządzanie projektami”; INPROGRESS sp. z o.o.;
- „Zarządzanie projektami”, Politechnika Krakowska im. Tadeusza Kościuszki, Centrum Wsparcia Projektów Zespół Pozyskiwania Funduszy;
- „Doskonalenie umiejętności miękkich”, COGNITY;
- „Geopolimery - nowoczesne i przyjazne środowisku materiały dla budownictwa”, Politechnika Krakowska im. Tadeusza Kościuszki;
- „Inventor Essentials and Fusion 360”; Autoryzowane Centrum Szkoleniowe Autodesk: Kompugraf Salon Grafiki Komputerowej S.C.;
- Szkolenie dotyczące obsługi spektrometru fluorescencji rentgenowskiej EDX-7200 z dyspersją energii, Shimadzu Corporation;
- Szkolenie dotyczące obsługi mikroskopu cyfrowego Keyence VHX-E100;
- Szkolenie dotyczące obsługi analizatora wielkości cząstek Anton-Paar PSA 1190LD; Anton Paar Poland sp. z o.o.;
- Szkolenie dotyczące obsługi analizatora sorpcji fizycznej Quantachrome Autosorb iQ-MP; Anton Paar Poland sp. z o.o.;
- Szkolenie dotyczące obsługi dyfraktometru Aeris; Malvern Panalytical B. V.

materials

MDPI

Article

Hybrid Materials Based on Fly Ash, Metakaolin, and Cement for 3D Printing

Joanna Marczyk [1], Celina Ziejewska [1], Szymon Gądek [1], Kinga Korniejenko [1], Michał Łach [1], Mateusz Góra [1,2], Izabela Kurek [1], Neslihan Doğan-Sağlamtimur [3], Marek Hebda [1,*] and Magdalena Szechyńska-Hebda [4,*]

1 Faculty of Material Engineering and Physics, Cracow University of Technology, Warszawska 24, 31-155 Kraków, Poland; joanna.marczyk@pk.edu.pl (J.M.); celina.ziejewska@pk.edu.pl (C.Z.); szymon.gadek@pk.edu.pl (S.G.); kinga.korniejenko@pk.edu.pl (K.K.); michal.lach@pk.edu.pl (M.Ł.); mateusz.gora@atmat.pl (M.G.); izabelakurek16@gmail.com (I.K.)
2 ATMAT Sp. z o.o., Siwka 17, 31-588 Kraków, Poland
3 Department of Environmental Engineering, Faculty of Engineering, Nigde Omer Halisdemir University, 51240 Nigde, Turkey; neslihandogansaglamtimur@gmail.com
4 Plant Breeding and Acclimatization Institute—National Research Institute, Radzików, 05-870 Błonie, Poland
* Correspondence: marek.hebda@pk.edu.pl (M.H.); szechynska@wp.pl (M.S.-H.); Tel.: +48-1262-83423 (M.H.)

Abstract: Nowadays, one very dynamic development of 3D printing technology is required in the construction industry. However, the full implementation of this technology requires the optimization of the entire process, starting from the design of printing ideas, and ending with the development and implementation of new materials. The article presents, for the first time, the development of hybrid materials based on a geopolymer or ordinary Portland cement matrix that can be used for various 3D concrete-printing methods. Raw materials used in the research were defined by particle size distribution, specific surface area, morphology by scanning electron microscopy, X-ray diffraction, thermal analysis, radioactivity tests, X-ray fluorescence, Fourier transform infrared spectroscopy and leaching. The geopolymers, concrete, and hybrid samples were described according to compressive strength, flexural strength, and abrasion resistance. The study also evaluates the influence of the liquid-to-solid ratio on the properties of geopolymers, based on fly ash (FA) and metakaolin (MK). Printing tests of the analyzed mixtures were also carried out and their suitability for various applications related to 3D printing technology was assessed. Geopolymers and hybrids based on a geopolymer matrix with the addition of 5% cement resulted in the final materials behaving similarly to a non-Newtonian fluid. Without additional treatments, this type of material can be successfully used to fill the molds. The hybrid materials based on cement with a 5% addition of geopolymer, based on both FA and MK, enabled precise detail printing.

Keywords: 3D printing; hybrids; fly ash; concrete; metakaolin

Citation: Marczyk, J.; Ziejewska, C.; Gądek, S.; Korniejenko, K.; Łach, M.; Góra, M.; Kurek, I.; Doğan-Sağlamtimur, N.; Hebda, M.; Szechyńska-Hebda, M. Hybrid Materials Based on Fly Ash, Metakaolin, and Cement for 3D Printing. *Materials* **2021**, *14*, 6874. https://doi.org/10.3390/ma14226874

Academic Editor: Antonino Recca

Received: 3 October 2021
Accepted: 8 November 2021
Published: 15 November 2021

1. Introduction

During the last several decades, the impact of Portland cement on the environment has been the subject of discussion for many researchers [1,2]. Portland cement is a traditional and indispensable material widely used in construction around the world [3,4]. Due to its main advantages, including resistance to fire, rust, and rot, as well as flexibility in molding and shaping, cement is one of the most frequently used materials in the construction industry [5–7]. However, cement production has led to negative environmental impacts. The process consumes a large number of raw materials and has high energy requirements, produces a large amount of carbon dioxide that is released into the atmosphere, and thus contributes to global warming [4–6,8]. This disadvantage leads to the need for the development of new alternative materials and methods, including geopolymer binders.

The term 'geopolymer' was first used by Joseph Davidovits in the 1970s [3,9]. It defines the class of inorganic polymers, usually received by mixing metakaolin, fly ash, or slag

with an alkaline activator [5,10,11] and containing the Al and Si tetrahedron network [12]. Metakaolin (MK) is a de-hydroxylated form of clay kaolin mineral [6–14], preferred in geopolymer production due to its bright color, easy control of the Si/Al ratio, and effectiveness of geopolymerization reactions; however, MK is relatively expensive [15]. Fly ash (FA), a by-product of coal power plants, is also a frequently used source material; however, its chemical composition is difficult to control, and the quality of FA depends on the type of coal and power-plant efficiency [16]. Commonly used alkaline activators are sodium hydroxide (NaOH), potassium hydroxide (KOH), or their combination, together with sodium silicate or potassium silicate [15,17,18]. The geopolymerization process occurs in three steps: (i) dissolution of the aluminosilicate material in an activator solution; (ii) transportation or diffusion of Al and Si ions and the formation of small, coagulated structures; and (iii) their polycondensation to form hydrated products [19,20]. Many natural minerals [21–23], calcined clays [24–26], and industrial by-products such as blast furnace slag [27], fly ash [28–32], rice husk ash [33], waste glass [34], and red mud [35] can be used as additional materials for the synthesis of geopolymers [17,36]. Therefore, geopolymer technology is an important solution for industrial waste utilization, the amount of which increases every year [8,17]. The reuse of by-product materials contributes to the reduction of greenhouse gas emissions and is an energy-saving and ecological alternative to Ordinary Portland Cement (OPC) [37–40].

The geopolymers and Portland cement have comparable properties [5,41,42]. They are characterized by high compressive strength [43], fire resistance [44], incombustibility, good resistance to chemical attack [45], high fracture toughness [46], low shrinkage [47], low thermal conductivity [44], low permeability [16], high stability at elevated temperatures [13], high strength-to-weight ratio, good durability and strong bonding, excellent heavy metal immobilization [12], resistance to freeze-thaw cycles [48], and low manufacturing energy consumption for construction purposes [49]. Their mechanical properties can be controlled in a wide range. Geopolymers have been successfully applied in a number of structural construction applications, such as beams, columns, slabs, tunnel linings, paving, etc.

A geopolymer hybrid is a combination of geopolymer and OPC or other binders, in order to produce material that combines the positive properties of OPC with the properties of alkali-activated materials or geopolymers. Hybrid OPC-geopolymer concrete has a lowered carbon footprint and improved ambient temperature curing while maintaining the positive properties of heavy metals immobilization, generally good mechanical properties, and high durability [50,51]. In the case of hybrid OPC-geopolymer concrete, generally of high FA content (70–90%) and low OPC content (10–30%), the clinker reaction products and reaction products from the glass phases of FA coexist. As the curing time progresses, when in combination, the (N,C)-A-S-H-type gels, called "hybrid gels", and aluminum-modified calcium silicate hydrate C-A-S-H-type gels densify the cementitious matrix and are responsible for the mechanical performance of this type of material [52].

In the construction industry, 3D printing is considered environmentally friendly, due to its offering designing freedom, automation, less waste generation, reduced raw material consumption, and lower labor cost [53]. Significant progress has been made toward the construction of 3D concrete printers (3DCP); the printing methods are focused mainly on the pumping and extrusion of cementitious pastes to generate buildable layers. An extrusion-based three-dimensional concrete printing (E3DCP) process has still not been widely applied, mainly due to technical hurdles related to materials development and processing challenges. The current, severely limited, scope of materials that can be used in the 3D printer includes rapid-hardening Portland cement (RHPC), calcium aluminate cement (CAC), magnesium oxychloride cement, fiber-reinforced cement polymer, and ultra-high-performance concrete (UHPC). It is urgently necessary to develop mixes that can be sufficiently fluid and at the same time have sufficient viscosity to retain their shape after the printing process. The printed layers must be self-supporting and free of those discontinuity flaws caused by unwarranted stiffness and insufficient cohesion. In E3DCP, shrinkage due to drying or post-processing is another limitation. Altogether, this results

in limited 3DCP applications. These methods still represent only 3% of the total additive manufacturing industry [54,55]. Supplementary cementitious materials (e.g., metakaolin or fly ash) are frequently utilized as a fractional replacement for cement to augment the desired rheological and packing properties. Geopolymers have also been recognized as a promising construction material for the 3D printing process due to their fast setting, the wide range of optimizable parameters, and their advantages in combination with substances modifying these properties [56].

None of the literature informs about the results of research on products made from concrete-geopolymer hybrids and their use in the 3D printing process. Therefore, we address in this article the development of materials based on hybrid geopolymers and OPC that can be used in the different methods of 3DCP.

2. Materials and Methods

2.1. Raw Materials

The commercial cement CEM I 42.5R from the cement plant Górażdże Cement S.A. (Heidelberg Cement Group, Chorula, Poland) was used for the experiments. According to manufacturer protocol, in appropriate proportions, after very fine grinding and homogenization, the raw material was heated (cyclone heat exchangers) and then sintered (rotary furnace; raw material temperature 1450 °C, flame and gas temperatures 2000 °C). The material remained in the high-temperature zone for approx. 30 min. The temperature of cement clinker at the exit of the furnace was approx. 900–1300 °C. Then it was subjected to intensive cooling, down to a temperature of about 100 °C. As a result, the cement clinker (in the form of hard sintered lumps) was obtained. The product, with the addition of gypsum, was ground in a ball mill to a very fine powder (CEM I Portland cement). This cement meets the standard requirements according to PN-EN 197-1 [57], and the properties described in the Declaration of Performance No. 1487-CPR-027-02. Cement conforms to the IBDiM Technical Recommendation No. RT/2010-02-0060/1.

The fly ash (FA) from the combined heat and power plant in Skawina (Skawina CHP Coal Power Plant, Skawina, Poland) and metakaolin (MK) KM 60 (Keramost, Kadaň, Czech Republic) were used as raw materials for geopolymers production. The pulverization process of FA was used to uniform the chemical composition and particle size, as FA was collected from different mechanical and electrostatic precipitators and zones. MK was prepared via the dehydroxylation of kaolin to remove the chemically bonded hydroxyl ions, according to the procedure described earlier [58–60]. The raw materials were mixed with commercial quartz sand with a chemical composition: 90.0–90.3% SiO_2, max. 0.2% Fe_2O_3, 0.08–0.1% TiO_2, 0.4–0.7% Al_2O_3, 0.17% CaO, 0.01% MgO.

2.2. Characterization of Raw Materials

The chemical composition of starting materials was analyzed using X-ray fluorescence (PANalytical Epsilon 3 XLE, Malvern Panalytical, Lelyweg 1, Almelo, The Netherlands) according to PN-EN 1744-1+A1:2013 [61].

The mineralogical characterization was carried out using X-ray diffraction (XRD) PANalytical Aeris (Malvern Panalytical, Lelyweg 1, Almelo, The Netherlands), using CuKα radiation. Samples were scanned in the angular range from 10° to 70° (2θ) at 0.003° (2θ) step size and a time per step of 340 s. The qualitative and quantitative analysis was performed against the ICDD (International Center for Diffraction Data, PDF-4) catalog and the HighScore Plus software (PANalytical).

The structural properties were determined using a Fourier transform infrared spectroscopy (FTIR) spectrometer (Shimadzu IRAffinity-1S, Kioto, Japan) equipped with the ATR Quest (Specec) adapter. The wavenumber range was 4000 cm^{-1} to 400 cm^{-1}. A total of 32 spectra was averaged to reduce noise levels. The spectra were analyzed using a database with Shimadzu LabSolution FTIR software.

Water content was determined by the weight method in accordance with the standard, PN-EN 15934:2013 [62].

The pH value was determined using the potentiometric method (2.0–12.0 measuring range with 0.2 uncertainty) in accordance with the standard, PN-EN ISO 10523:2012 [63].

Water-leaching tests were carried out in accordance with PN-EN 12457-2:2006 [64]. In the aqueous extracts, the pH was also determined.

The concentrations of natural radioactivity (^{40}K, ^{226}Ra, ^{228}Th) in the raw materials were tested using the high-resolution gamma spectrometry method. A device was equipped with a high-purity germanium detector (HPGe). In accordance with the regulation of the Council of Ministers, in the case of "requirements regarding the content of natural radioactive isotopes in raw materials and materials used in buildings for human and livestock habitation, as well as in industrial waste used in construction, and the control of the content of these isotopes", building materials are qualified on the basis of two activity indicators, defined according to the following relationships [65]:

$$f_1 = \frac{C_K}{3000\text{Bq/kg}} + \frac{C_{Ra}}{300\text{Bq/kg}} + \frac{C_{Th}}{200\text{Bq/kg}}$$
$$f_2 = C_{Ra} \quad (1)$$

where C_K, C_{Ra}, and C_{Th} are the isotope concentrations of potassium ^{40}K, radium ^{226}Ra and thorium ^{228}Th, expressed in Bq kg^{-1}.

The morphology of the raw material particles was observed via a scanning electron microscope (JEOL JSM5510LV, JEOL, Tokyo, Japan). Particles of fly ash and metakaolin were stuck onto carbon tape to ensure good conductivity. The samples were coated with a layer of gold, using a vacuum evaporator (BS300).

The particle size distribution of fly ash and metakaolin was carried out using a laser particle size analyzer (FRITSCH ANALYSETTE 22 MicroTec plus, Fritsch GmBH, Idar-Oberstein, Germany). The volume-size distribution was expressed as D_{10}, D_{50} (median), and D_{90}.

The true density of the raw materials was determined using a helium pycnometer (Pycnomatic ATC, Thermo Fisher Scientific, Waltham, MA, United States).

The specific surface area was determined as a function of relative pressure with the BET (Brunauer–Emmett–Teller) method, using a physical sorption analyzer, Quantachrome Autosorb iQ—MP (Anton Paar company, Graz, Austria). The pore volume and the average pore size were determined by nitrogen adsorption/desorption using the BJH (Barrett–Joyner–Halenda) technique. The sample degassing temperature was 300 °C, the rate 20 °C min^{-1}, and the soak time 180 min. Volume measurements of nitrogen adsorption and desorption were carried out at relative pressures (p/p_0) in the range from 0.021 to 0.994 for 44 measuring points. The results were analyzed using the ASiQwin software.

Differential thermal analysis (DTA), coupled with thermogravimetry (TG, DTG) and evolved gas analysis (QMS), was performed with NETZSCH STA 449F3 and quadrupole mass spectrometry QMS 403 (Netzsch GmBH, Selb, Germany). The experiments were carried out in the temperature range from 30 °C to 1000 °C. Samples were heated at 10 °C min^{-1} in an air atmosphere. The data were analyzed using Proteus software (Netzsch). The TG curve is the change in mass loss and the DTA curve is the mass loss rate as a function of temperature [66,67].

2.3. Preparation of Geopolymer Specimens

FA or MK was mixed with sand in a 1:1 proportion and then activated. The activator solution consisted of 10 M sodium hydroxide and the aqueous solution of sodium silicate (R-145, a molar ratio of 2.5 and density of 1.45 g cm^{-3}). The ratio of sodium hydroxide solution to sodium water glass was fixed at 1:2.5. Ingredient-mixing for 15 min in a low-speed mixer was performed 24 h before use, to allow the equilibration of a constant concentration and temperature. Six geopolymer types were designed, depending on composition and the liquid-to-solid ratio (Table 1).

Table 1. Type of geopolymer samples.

Sample	Composition, wt. %			Liquid/Solid Ratio
	FA: Sand 1:1	MK: Sand 1:1	10M NaOH: Water Glass 1:2.5	
FA-0.245	80.32	-	19.68	0.25
FA-0.280	78.12	-	21.88	0.28
FA-0.350	74.07	-	25.93	0.35
MK-0.350	-	74.07	25.93	0.35
MK-0.375	-	72.73	27.27	0.38
MK-0.400	-	71.43	28.57	0.40

The ingredients were mixed in a GEOLAB cement mortar mixer (Geolab, Warsaw, Poland) for 15 min to a homogeneous paste. The fresh geopolymer pastes were formed in the molds with the size of 50 mm × 50 mm × 50 mm for compressive strength test; 71 mm × 71 mm × 71 mm for the abrasion resistance test; 200 mm × 50 mm × 50 mm for the flexural strength test. Molds were shaken to remove the trapped air. The specimens were cured at 24 h at 75 °C, and then de-molded and stored at ambient conditions.

2.4. Characterization of Geopolymers

The compressive strength of the geopolymers after curing for 1 and 28 days was tested in accordance with the PN-EN 12390-3:2019 standard [68] on a testing machine, a MATEST 3000 kN (Model C-104 with Cyber-plus evolution program, MATEST S.p.A., Arcore, Italy).

A flexural strength test of geopolymer samples after curing for 28 days was acquired in accordance with the PN-EN 12390-5:2019 standard with a concrete press (MATEST).

The surface abrasion resistance test was conducted in accordance with the PN-EN 13892-3:2015 standard [69] using the Böhme abrasion test abrader. The samples were weighed, placed on the steel test disc, and 20 g of abrasive powder (artificial corundum) was spread over the grinding path. During the test, the sample was subjected to 16 abrasion cycles consisting of 22 revolutions. After every 22 revolutions, the abrasive powder was replaced with fresh powder. The specimen was turned about the vertical axis by 90° after each cycle. The samples were weighed after the experiment was completed. The average weight loss and volume decrease were calculated as follows:

$$\text{Surface abrasion weight loss, } \% = \frac{w_1 - w_2}{w_1} \times 100 \quad (2)$$

where w_1 was the initial weight of the sample; w_2 was the final weight of the sample [5].

$$\text{Volumetric abrasion losses } (\text{cm}^3\ 50\ \text{cm}^{-2}),\ \Delta V = \Delta m/\rho \quad (3)$$

where Δm was the weight loss after 16 cycles; ρ was the density in g cm^{-3} [70].

The fire resistance test of the geopolymers was acquired in accordance with the PN-EN ISO 1182:2020 standard [71] in an electric furnace. The samples were dried at 60 °C and then cooled to ambient temperature. The test was carried out for 30 min at 750 °C. The weight of the specimens was measured before and after the experiment. The weight loss was expressed as a percentage of the initial sample weight [72]:

$$\textit{Loss of mass, } \% = 100 \times \left[1 - \frac{\textit{mass after experiment}}{\textit{mass before experiment}}\right]. \quad (4)$$

2.5. Hybrid Preparation

Geopolymer-based hybrids, made of both fly ash and metakaolin, were prepared from the CEM I 42.5R cement solution and the geopolymer mass. CEM I 42.5R cement solution was prepared in the amount of 5 wt %. Geopolymer mixtures made on the basis of fly ash

contained an additive of sand (1:1) and the liquid-to-solid ratio was 0.28. Geopolymers made with a base of metakaolin contained an additive of sand (1:1), and the liquid-to-solid ratio was 0.35. Concrete control (without geopolymers) was made with a base of cement and sand in the proportion of 1:1, and the water-to-solid ratio was 0.125.

The GALAXY printer supplied by the ATMAT company (ATMAT, Kraków, Poland) was used for the printing process. About 50 kg of each tested material was prepared for printing. The printing process was carried out at an ambient temperature, with a printing speed of 150 mm s^{-1}. The diameter of the nozzle was 15 mm, and the thickness of the applied layers was 10 mm.

2.6. Statistical Analysis

All data are the average of three to six repetitions. The standard deviation was calculated and is presented.

3. Results and Discussion

3.1. Characterization of Raw Materials

CEM I 42.5R was selected for the tests. It has a composition compliant with the requirements of PN-EN 197-1 [57]. Dry Portland cement is a white/grey, odorless, fine-ground material. The particle size was 5–30 μm. The specific density was 3.11 g cm^{-3}, and the bulk density 1.42 t m^{-3}. The main component was cement clinker (95%: alit, $3CaO•SiO_2$, ref. code: 00-016-0407; belit, $2CaO•SiO_2$, ref. code: 00-033-0303; tricalcium aluminate $3CaO•Al_2O_3$, ref. code: 00-038-1429; brownmillerite $4CaO•Al_2O_3•Fe_2O_3$, ref. code: 00-011-0124) mixed with gypsum (max. 5%, $CaSO_4•2H_2O$, ref. code: 00-006-0047), which was used as a setting-time regulator. The sulfate content (as SO_3) reached the value of 3.24% (with the norm not exceeded, 4.00%), the chloride content (as Cl^-), 0.06% (max. 0.100%), the alkali content (as Na_2Oeq), 0.75%. The content of soluble chromium (VI) in the cement, due to its natural composition, was below 0.0002% of the total dry weight. The content of individual clinker phases has a significant impact on the course of the hydration process, an exothermic reaction of cement (clinker) with water. The amount of the total heat effect is determined by the presence of alite and tricalcium aluminate. On the other hand, alite and belite are the phases responsible for the buildup of strength. Therefore, in the early period of hydration, the presence of alite is of key importance for strength, while the content of belite over a longer period of time determines the strength. The pH of the studied cement was 11.0–13.5 at a temperature of 20 °C in water for a water–material ratio of 1:2. The melting-point value for cement was >1250 °C.

Fly ash (FA) and metakaolin (MK) were considered as important raw materials for geopolymer production; however, both FA and MK's suitability for geopolymerization reactions depended on their physical properties. The particles of FA had approximately spherical morphology, which is beneficial in order to achieve a successful geopolymerization process (Figure 1A and Figure S1A,C,E in Supplementary Materials). It improves the rheological properties of the mixture, increasing its workability. In addition, it reduces the need for liquid substances and has a beneficial effect on the mechanical properties of geopolymers [73]. In contrast, the particles of MK were in the form of irregular flakes with random geometry, rough and porous surface texture, and tend to form agglomerates (Figure 1B and Figure S1B,D,F in Supplementary Materials). The morphology of both materials seems to be typical, as described earlier [74]. FA and MK also had different particle-size distributions (Figure 1C, Table S1 in Supplementary Materials). The FA particle size ranged from 1.3 to 32.5 μm, with 90% particles of less than 30 μm and a distribution width of D_{50} 22.3 μm; the MK particle size ranged from 0.5 to 39.2 μm, with 90% of the particles' size exceeding 30 μm, and a distribution width of D_{50} 18 μm. Along with a decrease in the particle size, the density and mechanical properties of the geopolymer have increased. The phenomenon is attributable mainly to the greater surface area available for chemical reactions. The smaller particles have a larger surface area in comparison to the volume and, thus, higher reactivity, including the rate of dissolution of the monomers, i.e., silicate

and aluminate, consequently showing a more effective geopolymerization process [75–78]. Furthermore, the porosity is the lowest at the smallest particle size and the voids can be better filled within fine particles, leading to denser and stronger geopolymer products [79]. In earlier studies, we showed the beneficial effect of grinding the raw materials, even if the process is energy-intensive; the reduction of particle size and the increase of specific surface area were crucial to obtaining the higher reaction rate of the precursor, more reacted final material and the proper mechanical properties of the geopolymer products [80]. The size reduction throughout the milling process is recognized as a mechanical activation of the material, resulting in an increase in compressive strength [75,79]. Another way is separating in different fractions to enable smaller particles [81]. On the other hand, if gases can be released from the raw materials through the voids between particles in a larger fraction, they do not affect the mechanical strength as much as when they destroy the compactness of the material, leaving it with lower density and lower compressive and bending strength.

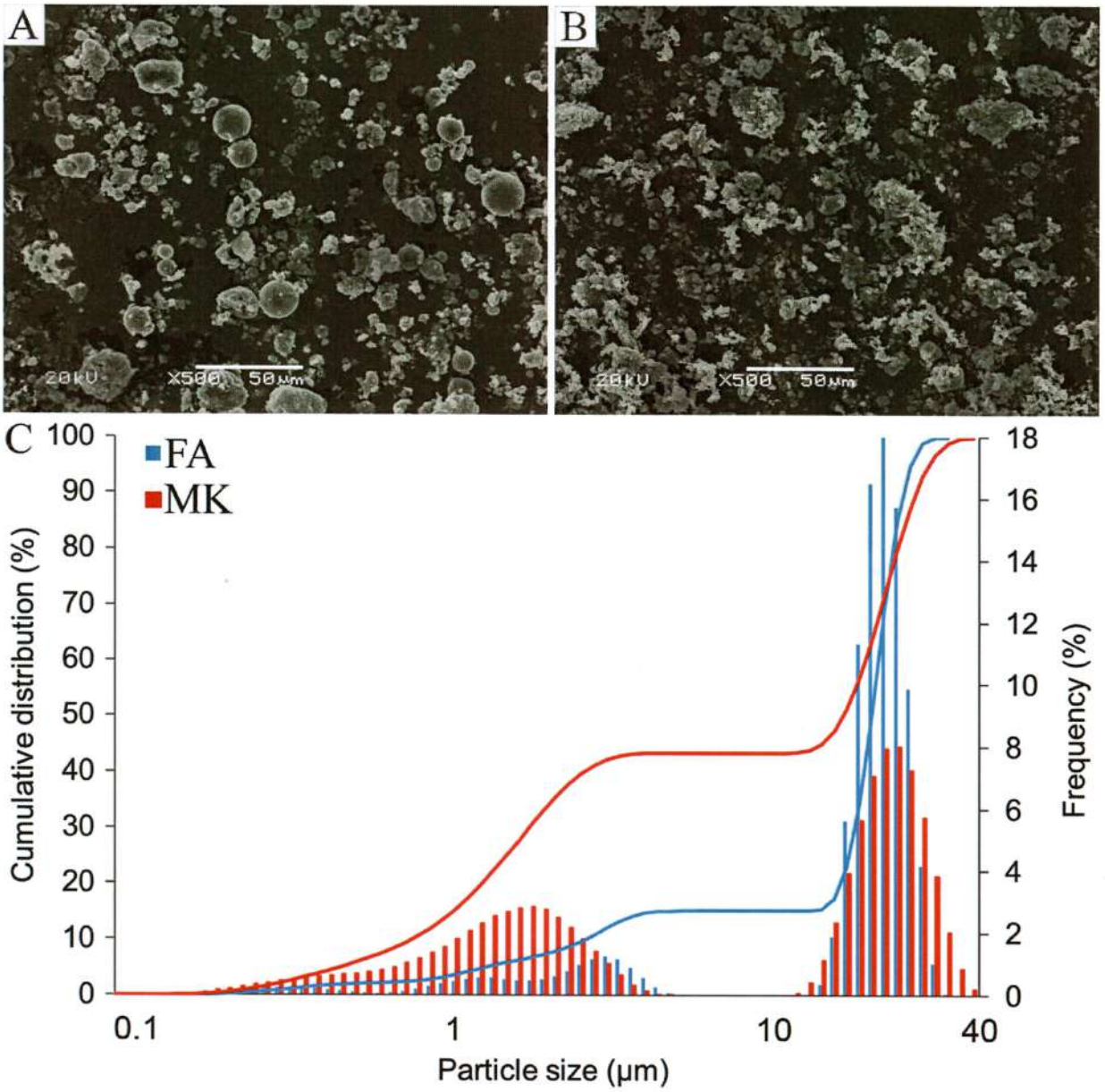

Figure 1. SEM micrographs (**A**,**B**) and particle size distribution (**C**) of fly ash and metakaolin. (**A**)—fly ash morphology, (**B**)—metakaolin morphology, (**C**)—particle size distribution described by cumulative distribution (lines) and frequency (bars).

The density of the FA was 2.288 ± 0.001 g cm^{-3}, whereas the MK density of 2.566 ± 0.001 g cm^{-3} was compliant with the specifications presented by the manufacturer (2.50–2.80 g cm^{-3}) and other authors [82,83].

To yield information concerning the effects of surface porosity and particle size for the FA and MK, external area and pore area evaluations were conducted (Table 2 and Table S1 in Supplementary Materials, Figure S2 in Supplementary Materials). Depending on the method, the value of the surface area for FA was in the range of 10.431–14.616 m^2 g^{-1}, and for MK the range was 12.999–21.415 m^2 g^{-1}, while the pore volume was 0.026–0.027 cm^3 g^{-1} and 0.140–0.142 cm^3 g^{-1} for FA and MK, respectively (Table 2, Figure S2 in Supplementary Materials). Similarly, the pore size was 2.134 nm for FA and 2.975 nm for MK. Therefore, the materials were defined as mesoporous, according to IUPAC classification [84–87], with slit-like interparticle pores [88–90] (Figure S1E,F in Supplementary Materials).

Table 2. Textural characteristics of fly ash and metakaolin, BET—specific surface area analysis method; BJH—pore size and volume analysis method.

Parameter	FA	MK
Single-Point BET (m^2 g^{-1})	10.431	12.999
Multi-Point BET (m^2 g^{-1})	12.760	15.315
Surface Area BET (m^2 g^{-1})	14.616	21.415
Total pore volume BJH (cm^3 g^{-1})	0.026	0.140
Pore volume BJH (cm^3 g^{-1})	0.027	0.142
Average pore diameter BJH (nm)	2.134	2.975

Fly ash and metakaolin are considered important raw materials for geopolymer production, as SiO_2 and Al_2O_3 are their main chemical constituents (Table 3). The analysis of the chemical composition of FA and MK showed a high content of silica and alumina, which exceeded 70% and 90% in FA and MK, respectively. However, considering the Si:Al ratio, it is important to note that the raw materials before geopolymerization had Si:Al ratios of 3.26 and 2.17 for FA and MK samples, respectively. The mechanical properties of the geopolymers became increasingly elastic with the increasing total SiO_2 content in the raw materials. On the other hand, homogeneity of the microstructure meant a compressive strength increase along with the Si:Al ratio [59]. Thus, although the total Si content can improve the properties of MK-originated geopolymers rather than FA-originated geopolymers, the final effect may be the complementary result of both factors—not only the total content of the Si and Al components but also their relationship to each other. The element differentiating significantly between both raw materials was calcium content; FA had a higher calcium content (5.120%, classified as class F), while a much lower content was found in MK (0.490%). The effect of calcium on geopolymer produced from metakaolin and fly ash is usually positive; a composite system with geopolymer gel and calcium–silicate–hydrate gel can co-exist when the calcium content increases [91]. The presence of CaO, together with MgO, which was much higher in FA than MK (Table 3), can contribute to increased pH value in the range of 10.0–13.0 [92]. Indeed, the leachate for raw materials was highly alkaline (pH value > 12.0) for FA, and slightly acidic (pH value = 6.0) for MK at a temperature of 20 °C; the high pH value was primarily due to the hydrolysis of lime, which yields free hydroxyl ions. Furthermore, numerous accessory minerals of Ba, Sr, Zn, Pb, V, Cr, Cu, Ni, Rb, Ga, Zr, Te, As, Sb, Sn, and Y were typical components of FA, while they were present to a lesser extent in MK (Table 3). Accordingly, the more rich and complex composition of FA resulted in more abundant total dissolved substances in the FA leachate when compared to that of MK (Supplementary Materials Table S2). Generally, FA is a hazardous material collected from coal production as an unburned residual; thus, its potentially detrimental role in polluting the environment should be carefully recognized. However, the detailed chemical analysis of leachate from raw materials revealed the presence of toxic elements at an acceptable level, in the case of both FA and MK (according to EU Decision 2003/33/EC [93], and Chinese National Standard GB 5085.3-2007 [94]),

even if a much higher content of Sb, Ba, Cr, Cr(VI), Mo, Hg, Se, chlorides, fluorides, and sulfates were detected in FA (Supplementary Materials Table S2). Similarly, the ^{40}K, ^{226}Ra, and ^{228}Th radioactivity of FA and MK were below the international limits (EU report [95]); they slightly exceeded an average radioactivity level for FA, but not for MK, as produced in Europe (622–793 Bq kg^{-1} for ^{40}K; 126–191 Bq kg^{-1} for ^{226}Ra; and 89–91 Bq kg^{-1} for ^{232}Th) [96] (Supplementary Materials Table S3).

Table 3. Fly ash and metakaolin chemical compositions (X-ray fluorescence), loss on ignition (LOI), and mineral phases as calculated from the XRD data (Figure S3 in the Supplementary Materials) with the Rietveld method results.

Main Minerals, %			Accessory Minerals, ppm			Mineral Phases, %		
	FA	MK		FA	MK		FA	MK
SiO_2	48.220	52.430	BaO	800.0	99.7	Quartz	42.0	9.4
TiO_2	1.110	0.310	SrO	600.0	103.5	Mullite	52.5	5.8
Al_2O_3	26.130	42.750	Zn	199.7	37.1	Hematite	2.6	-
Fe_2O_3	7.010	1.200	Pb	146.4	151.7	Magnetite	1.0	-
MnO	0.090	0.012	V	274.2	34.6	Anhydrite	1.2	-
MgO	1.720	0.175	Cr	171.4	-	Rutile	0.7	-
CaO	5.120	0.490	Cu	129.8	15.3	Illite-2M1	-	43.4
Na_2O	1.615	0.000	Ni	109.6	-	Kaolinite-1A	-	41.4
K_2O	3.480	1.300	Rb	184.0	156.6			
P_2O_5	0.700	0.440	Ga	31.6	57.6			
SO_3	1.110	0.030	Zr	209.0	84.0			
Cl	0.090	0.060	Te	40.1	22.5			
LOI	3.284	0.722	As	-	20.4			
			Sb	20.6	-			
			Sn	45.2	37.0			
			Y	49.1	17.7			

A greater value for loss on ignition (LOI), an indicator of the residual carbon content [97], was observed in the case of FA (3.284%) than in MK (0.722%) (Table 3) and, similarly, the dissolved organic carbon (DOC) level was higher in FA leachates (Supplementary Materials Table S2). Many countries have recently tended to institute more strict specifications for the limit on LOI (ranging from 3% to 6%) for quality assurance. Although obtained LOI values are common (e.g., [98,99]), it is worth noticing that the residual carbon present in fly ash can absorb water and chemical admixtures (e.g., superplasticizer, air-entraining agent), reducing their efficiency or even resulting in a changed air–void system in the concrete. The LOI results were confirmed by higher FA instability and organic decomposition, along with a temperature rise during thermal analysis (Figure S3 in Supplementary Materials). Although the FA and MK samples showed low weight loss (Figure S3A in Supplementary Materials) and related thermal effects (Figure S3B in Supplementary Materials) in the temperature range from 25 °C to 400 °C, the extreme differences between both materials were recorded at 400–700 °C, with the maximum at 583 °C (Figure S3A–H in Supplementary Materials). Significant mass loss and exothermal effects were recorded for FA, but they were not observed for MK. These resulted from organic material decomposition due to C (*m*/*z* 12, Figure S3C in the Supplementary Materials), and CO_2 (*m*/*z* 44, Figure S3H in the Supplementary Materials) products were recorded with the QMS method. A similar pattern of changes in the temperature range of 400–700 °C was not found for H_2O (*m*/*z* 17 and 18, Figure S2D,E in the Supplementary Materials), CO (*m*/*z* 28, Figure S2F in the Supplementary Materials), and O_2 (*m*/*z* 32, Figure S2G in the Supplementary Materials). For H_2O and O_2, only the evaporation effects were recorded in the temperature range from 25 °C to 125 °C, with higher values for FA. This can result from capillary effects, which occur due to the higher adhesive and cohesive forces interacting

between the H_2O (and O_2) and the internal surface of pores in raw-material particles. This finding is confirmed by the FA microstructure, described above, i.e., smaller particle size, particles' total pore volume, and average pore diameter, which altogether influence the total surface area (much smaller for FA). Such microstructures allow keeping the H_2O (and O_2) molecules more closely bonded to the FA pore surface than to bigger particles and the pores of MK at room temperature. When the temperature rises, adsorbed water (and dissolved O_2) can be removed to the atmosphere to a greater extent. In contrast, the water is able to penetrate the MK easily through the larger number of capillary channels, and a higher water amount can be removed to the atmosphere at room temperature. This effect is also compatible with higher Ca content in FA. The greater bonding energy of the calcium, the reduction of the repulsive forces between the particles, the van der Waal's forces, and the greater misfit of the calcium ion and its hydration shell would tend greatly to reduce the number of water layers that could be adsorbed.

The qualitative results of XRD (Figure S4 in the Supplementary Materials) and their quantitative analysis with the Rietveld method (Table 3), performed for FA, revealed the presence of phases rich in Si and Al, such as mullite ($Al_6Si_2O_{13}$, ref. code: 00-015-0776) and quartz (SiO_2, ref. code: 01-075-8320). Furthermore, hematite (Fe_2O_3, ref. code: 04-002-7501), magnetite (Fe_3O_4, ref. code: 04-022-0447), anhydrite ($CaSO_4$, ref. code: 00-003-0163), and rutile (TiO_2, ref. code: 04-015-7316) were recorded for FA in decreasing order of presence. In MK, a different phase composition was recorded, with the main phases, rich in Si and Al, consisting of illite (K, H_3O) $Al_2Si_3AlO_{10}(OH)_2$, ref. code: 00-026-0911), kaolinite ($Al_2Si_2O_5(OH)_4$, ref. code: 00-058-2004), quartz, and mullite. The different forms of Si/Al in FA and MK suggest the various potentials for geopolymerization processes [86–88]. The mullite and quartz phases in FA may not dissolve readily in an alkaline solution and, as a result, can lower the geopolymerization's effectiveness. On the other hand, the crystalline quartz phase, due to the aluminosilicate compounds, can improve the physical and mechanical properties of geopolymers [99]. The kaolinite in MK may demonstrate an incomplete calcination process, which is dependent on the temperature treatment [80,100,101]. The asymmetrical hump appearing clearly in the range of 20–30° (2θ) is commonly identified in MKs and indicates an amorphous phase related to aluminosilicate glass (Figure S4 in the Supplementary Materials) [85,102]. In the case of MK, the crystalline structure can be broken down to form an amorphous phase during calcination, at a temperature lower than that necessary to generate a liquid phase and produce glass on cooling. However, the illite in MK has significant K_2O content and, in the case of geopolymerization of the reacting minerals (dissolution and polycondensation), it can have a significant effect on the increase in strength of the geopolymerization products [25,103]. Moreover, it is worth noticing that the mineral composition can result in lower adhesive and cohesive forces interacting between the H_2O and the internal surface of pores in MK particles (as described above), because kaolinite and illite favor the more rapid water sorption/desorption.

The results were confirmed by the FTIR spectrum (Figure 2, Table S4 in the Supplementary Materials). FTIR spectra contain information on the mineralogical composition as each mineral component has a unique absorption pattern in the mid-IR range and, thus, they are widely used for the study of aluminosilicates. The most intense band was recorded for both FA and MK at approximately 1000–1100 cm^{-1}. FA was characterized by the maximum vibration at wavenumber 1003 cm^{-1}, related to the asymmetric Si-O stretching vibrations occurring in the aluminosilicate structures [73]. In MK, the main band, centered at 1055 cm^{-1}, was associated with the Si-O-Si vibrations originating from silicate minerals present in the material [104]. The band intensity around 1100 cm^{-1}, related to the asymmetrical stretching vibration peak for the Si-O bond, was higher for MK than FA. Altogether, this is in agreement with a higher total content of silica in MK (Table 3). Moreover, common peaks found at 793 cm^{-1}, associated with Si-O bending vibrations, peak at 699 cm^{-1} with Si-Si vibrations, peak at 547 cm^{-1} with Si-O-Al vibrations, and peak at 418 cm^{-1} with Al-O vibrations; all were higher for MK and were thus related to the higher total content of Si and Al. Similar shifts in raw materials have been observed

previously [38,85,88]. Considering the mineral phase content, FA was characterized by the maximum vibration at wavenumber 1003 cm^{-1} and the bending vibration at 793 cm^{-1} and 781 cm^{-1} that can be attributed to the presence of quartz [38,105]. The presence of mullite in FA was represented by the band around 557 cm^{-1} related to the substitution of Al for Si in the mullite structure, and furthermore by the shift of the main band around 1000 cm^{-1} (in comparison to MK bands) and thus the marking band at 915 cm^{-1} associated with the presence of aluminum in the octahedral position, characteristic of mullite. MK phases can be assigned by the main band centered at 1055 cm^{-1} for kaolinite and 537–529 cm^{-1}, 1023–1027 cm^{-1}, and 1066–1070 cm^{-1} for illite.

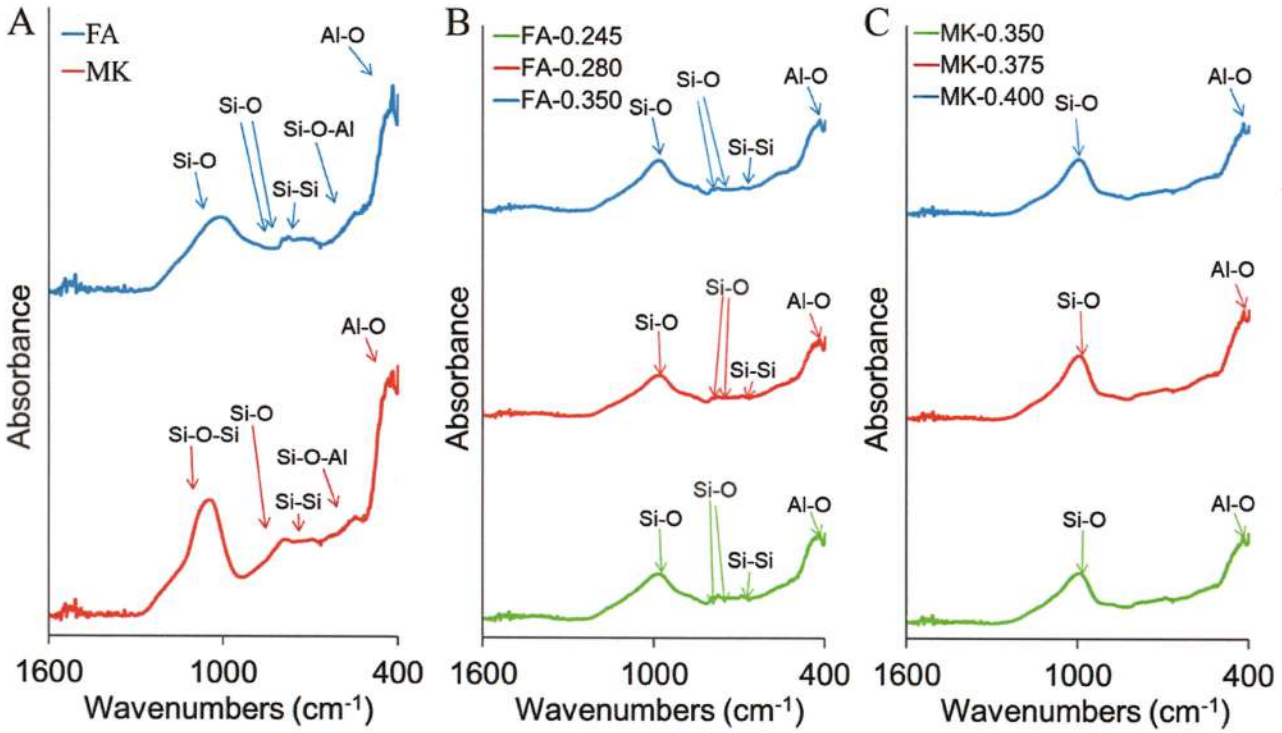

Figure 2. FTIR spectra of fly ash and metakaolin (**A**), as well as geopolymers produced from fly ash (**B**) and metakaolin (**C**), mixed with sand and NaOH: water glass in ratio 0.245, 0.280 and 0.350 for FA, and 0.350, 0.375, and 0.400 for MK. Complete spectra are presented in Figure S5 in the Supplementary Materials.

3.2. *Properties of Concrete and Geopolymers*

Different cement powders are used in industrial installations for the production of binding materials, e.g., ready-mixed concrete of classes C 16/20—C 40/50 and higher, SCC self-compacting mortars, and concrete for large- and small-sized prefabricates. It is used both in professional conditions and by individual users for indoor and outdoor construction. In our experiments, we used cement powder, which required 27.2% water to achieve standard consistency. The beginning of the setting time of concrete was 227 min (with the normative requirement $\geq$ 60 min). The compressive strength after 2 days was 28.4 MPa (with the normative requirement $\geq$ 20 MPa), while after 28 days, it was 60.8 MPa (with the normative requirement $\geq$ 42.5 MPa $\leq$ 62.5 MPa). The volume stability was 0.6 mm (with the requirement $\leq$ 10 mm). The specific surface of the concrete was 4187 $cm^2\ g^{-1}$.

Due to their excellent properties, geopolymer products have been used, among others, as refractory materials [42,100], thermal insulation [106], construction [107], and 3D printing [108]. Among the diverse range of potential applications, geopolymers can also be used as technologically advanced composites in planes, ships, the nuclear power industry [109], biomaterials, or ecological utilization, replacing plastic [58,59,110]. In our experiments, the raw materials for geopolymers were mixed with commercial sand, the

composition of which includes SiO_2 90.0–90.3%, Fe_2O_3 max. 0.2%, TiO_2 0.08–0.1%, Al_2O_3 0.4–0.7%, CaO 0.17%, and MgO 0.01% (particle size: < 50 µm). The liquid-to-solid mass ratio was maintained at 0.245, 0.280 and 0.350 for FA, while at 0.350, 0.375, and 0.400 for MK (Table 1). Compared to concrete, the setting time at room temperature was longer for geopolymers, up to 405 min (initial setting time)—630 min (final setting time) for fly ash-based geopolymers, and up to 323 min (initial setting time)—522 min (final setting time) for metakaolin-based geopolymers (Table S5, Supplementary Materials). It is worth noting that the setting time could be adjusted in a wide range, along with the changes in temperature during the setting process, the duration of mixing of ingredients before setting process and, in a narrower range, along with the changes in the liquid to solid ratio and geopolymer composition resulting from different raw materials (FA and MK). In the first case, an increase from room temperature to the temperature of 75 °C can reduce the setting time by even one order of magnitude. Prolonging mixing from 15 min to 30 min can shorten the setting time twice. Moreover, changing the liquid-to-solid ratio from 0.245 to 0.350 for FA and from 0.350 to 0.400 for MK can extend the setting time by approximately 40% and 25%, respectively. In differently composed geopolymers, the range of changes was slightly greater for FA pastes mixed for 15 min and kept at 75 °C during the setting time measurement (27–46 min) than MK geopolymers under the same conditions (28–39 min). The results were confirmed by the consistency of fresh geopolymer mortars, determined by the flow table method and the Novikov cone method (Table S6, Supplementary Materials). The mortars consistency can be defined as dense-plastic for FA-0.245, FA-0.280, and MK-0.350; plastic for MK-0.375 and MK-0.400; and liquid for FA-0.350, suggesting that the liquid-to-solid ratio chosen for FA geopolymers influences its properties in more extreme ranges than the ratio chosen for MK geopolymers.

The FTIR spectra of geopolymers produced from fly ash and metakaolin, with a different liquid-to-solid ratio and curing for 28 days, generally showed a similar pattern to raw materials and to each other (independently of the liquid-to-solid ratio), although a lower intensity and number of bands were detected for geopolymers, particularly for MK-originated geopolymers (Figure 2, Figure S5 in the Supplementary Materials). The most intensive bands for geopolymers were those found at around 1000 cm^{-1}, related to the vibration of Si-O(Si) (Table S4 in the Supplementary Materials). However, a significant difference from the raw materials was the shift of these bands from 1003 cm^{-1} to 989 cm^{-1} for FA-originated geopolymers and from 1055 cm^{-1} to 992 cm^{-1} for MK-originated geopolymers. This indicated the formation of new amorphous aluminosilicate gel phases during the geopolymerization process. The position at around 1000–1100 cm^{-1} is indicative of the silica structure and, thus, with increasing values of wavenumbers around 990, lower Si atoms at the tetrahedral position, relating to enriched Si-O at the tetrahedral position. At the same time, the raw material bands at 547 cm^{-1}, representing the vibration of Si-O-Al, are reduced in the geopolymer material (Table S4 in the Supplementary Materials); similarly, the band absorbance at 418 cm^{-1} and adjacent bands, relating to the vibration of Al-O, is lowered (Figure S5 in the Supplementary Materials). To conclude, the formation of both FA- and MK-originated geopolymer material is favored in one direction to form a poly(silate-siloxo) (-Si-O-Al-O-Si-O-) structure, in which is the ratio Si:Al = 2; a poly(silate-disiloxo) (-Si-O-Al-O-Si-O-Si-O) structure, Si:Al = 3; or even additional sialate links, when Si:Al > 3; rather than in the direction to form poly(silate) (-Si-O-Al-O-), in which ratio Si:Al = 1. Positive ions (Na^+, K^+, Ca^{2+}) must be present in such framework cavities to balance the negative charge of Al^{3+} in IV-fold coordination. Therefore, an FA-originated geopolymer structure was not surprising, as a much higher content of positive ions was available already in FA (raw material). In MK-originated geopolymers, the arrangement consisted of a more equal share of individual structures, due to the vibration around Si-Si 690 cm^{-1} and bending vibration Si-O around 793 cm^{-1} and 783 cm^{-1} being reduced; thus, the relative effect of the Al-O bonds increased. The effect correlated with the Si:Al ratio for FA versus MK raw materials, as the Si:Al ratio of 3.26 and 2.17 were calculated for FA and MK, respectively (before the geopolymerization

process). Additionally, one can conclude that by calculating the Si:Al ratio of raw materials, the formation of the structure during the geopolymerization process can be predicted.

With the increase in the Si:Al ratio, geopolymers generally show higher mechanical properties due to the increased Si-O-Si bonds and residual silica as reinforcement. Therefore, the positive mechanical effect was expected due to the chemical arrangement of fly ash components (Table 3, Figures S4 and S5, Table S4 in the Supplementary Materials) and was confirmed by the structure of FA-originated geopolymers (Figure 1, Figure S6 in the Supplementary Materials). Indeed, analysis of the compressive strength, flexural strength, and abrasion resistance showed better mechanical properties of the FA geopolymers in comparison with the MK geopolymers, provided that the geopolymers were cured for 28 days (Table 4).

Table 4. Mechanical properties of geopolymers produced from fly ash and metakaolin after 1 and 28 days of curing, represented by compressive strength (MPa) after 1 day and 28 days of curing, as well as flexural strength (MPa) and abrasion resistance (cm^3 50 cm^{-2} and %) after 28 days of curing. The representative photos of the samples after tests are presented in Figure S6 in the Supplementary Materials.

Sample	Compressive Strength		Flexural Strength	Abrasion Resistance	
	1 Day	28 Days	28 Days	28 Days	28 Days
FA-0.245	44.73 ± 8.05	39.55 ± 3.29	7.58 ± 0.54	26.27 ± 9.67	7.20 ± 2.64
FA-0.280	41.71 ± 11.27	47.47 ± 1.12	9.38 ± 0.36	36.07 ± 2.21	9.81 ± 0.67
FA-0.350	25.45 ± 2.75	40.43 ± 7.20	5.68 ± 0.33	14.22 ± 1.72	3.82 ± 0.46
MK-0.350	68.34 ± 2.64	53.24 ± 3.78	6.25 ± 0.56	12.40 ± 0.04	3.34 ± 0.04
MK-0.375	61.40 ± 7.90	34.65 ± 4.69	4.50 ± 0.02	30.17 ± 13.24	8.50 ± 3.96
MK-0.400	24.62 ± 0.52	34.23 ± 3.26	4.29 ± 0.67	18.24 ± 4.29	4.70 ± 1.14

When compared to the results of the compressive strength test performed 1 day after the geopolymerization reaction, a different effect was observed, indicating the solidification process of the geopolymer as a chemical reaction, with the generation of new structures. Incomplete geopolymer formation after 24 h of curing at 20 °C is a common phenomenon, and the formation of aluminosilicate networks with the transition from hexa-coordinated Al(VI) to tetra-coordinated Al(IV) during the following days was identified [111]. Therefore, considering the changing parameters after the geopolymerization process, it is necessary to adjust the length of the curing period and specify them in the time-function parameters of geopolymer products. Although the liquid (activators) to solid (raw materials) mass ratio did not influence the geopolymer structure significantly (similar FT-IR spectra, Figure 2 and Figure S5 in the Supplementary Materials), it was a key factor affecting the compressive strength of geopolymers [9] (Table 4). Values ranged between 25.45–68.34 MPa for FA and MK geopolymer products cured for 1 day and 28 days. Along with the improved amount of liquids/a reduced amount of used raw materials (L/S increase from 0.245 to 0.350 for FA and from 0.350 to 0.400 for MK), the compressive strength decreased ~43% and 64%, respectively, for FA and MK, after the first day of curing (Table 4). Although the change of L/S ratio from 0.33 to 0.60 can reduce the final compressive strength, even up to 60% [9] in our studies, this effect was slightly counteracted in the geopolymers FA-0.28 and FA-0.35 with the passage of time since the compressive strength improvement was observed on the 28th day of curing (14% and 59%, respectively). Thus, one can conclude that the compressive strength of cured FA geopolymers did not depend on the L/S ratio. In contrast, the compressive strength of MK-originated geopolymers increased along with time only for MK-0.4 (39%), while for MK-0.350 and MK-0.375 it significantly decreased (32% and 44%, respectively). In this case, the differences remained significant between MK-0.350 and MK-0.400 (up to 34%), and it can be concluded that the L/S ratio is a factor of great importance for MK-originated geopolymers (Table 4). This is due to the excess of activator solution increasing the water quantity in the mix; thus, improper shrinkage

along with time led to crack formation. This adverse effect of water on geopolymerization is reported elsewhere [16,39,102,112,113]. In conclusion, the L/S ratio should be optimized in each case when the composition of raw materials is changed. These statements are also reinforced by a comparison of FA and MK geopolymers as a product of reactions performed at the same L/S ratio (0.350). The compressive strength was lower for the FA geopolymer than the MK geopolymer and the experiments showed an FA geopolymer morphology with more of a cracking structure (Figure S6 in the Supplementary Materials).

The L/S ratio affected the flexural strength (bending strength) of the specimens in the same way due to more cracks, resulting in a more fragile structure of the samples. FA and MK had a flexural strength higher for FA-0.245 and FA-0.280 when compared to FA-0.350, MK-0.375, and MK-0.400, while a comparison between FA-0.350 and MK-0.350 showed the better mechanical properties of MK-0.350 (Table 4). Thus, it can be stated that the highest flexural strength is developed for a geopolymer with a lower L/S ratio, and FA required a lower L/S ratio than MK for a successful geopolymerization process. Although the flexural strength was analyzed after 28 days, it was suggested that the effect of the alkaline solution-to-binder ratio on the flexural strength of the geopolymer mortar can stabilize within 7 days [114], and an increasing alkaline solution-to-binder ratio has a negative effect on the flexural strength.

Generally, the mechanical properties tested during a surface abrasion resistance test also followed compressive and flexural strength changes (Table 4), and this is in agreement with the fact that the abrasion resistance increased along with the decrease in the ratio of L/S [115]. The only exception was MK-0.350, with the lowest parameter values.

3.3. Concrete and Geopolymer Hybrid Materials and Their 3D Printing

The above-described research was aimed at selecting the protocol and choosing the parameters allowing their implementation to produce optimal geopolymer products that could potentially be used for printing composite materials using the 3D printing system. The effect of the cement-to-geopolymer ratio on preparing the optimal consistency of mortar and thus defined setting time should be the main factor. However, the influence of both the duration of mixing time and the temperature of the mixture on the setting time could also be critical, considering the 3D printing conditions, because the material is mixed and heated as a result of friction immediately before feeding it to the printing nozzle. Therefore, the final print result depends not only on the fixed printer parameters but also on the mass sensitivity to mechanical and physical factors. A pilot test was designed to include both different cement-to-geopolymer ratios and parameters indirectly influencing the setting time. With the introduction of cement to geopolymer mortar, the setting time of the hybrid material was shortened (Figure S7, Supplementary Materials) as expected due to the differences in the setting time of both components (227 min for concrete and 630 min for geopolymer (Table S5, Supplementary Materials)). Surprisingly, this effect was sharp and linear only in the range of 5–30% cement in the hybrid material. Higher cement content (95% and 100%) prolonged the setting time in comparison to the results obtained for the range 5–30%. Further experiments were performed preferentially for materials based on FA-0.280 + 5% cement and MK-0.350 + 5% cement due to the best mechanical properties described earlier for geopolymers (Table 4). The general effect for both materials was similar, independently of the type of raw material used (Table S7, Supplementary Materials). However, the setting time for the hybrid materials based on MK-0.350 + 5% cement was shorter than the setting time for hybrid materials based on FA-0.280 + 5% cement, even if the liquid-to-solid ratio could suggest an opposite tendency. The differences in the setting time of hybrids were higher when the temperature of fresh mortars increased (Table S7, Supplementary Materials) and was related to differences in the setting time of geopolymers (MK vs. FA, mixed 15 min and measured at RT (Table S5, Supplementary Materials)). In both cases, the final result was determined by a few factors: (1) the higher porosity and specific surface area of MK than FA requires more water for the same workability of MK and FA materials (Figure 1, Table 2, Table S1 and Figure S2,

Supplementary Materials); (2) the microstructure causes water to be more strongly absorbed in FA (van der Waals forces) while evaporating more easily at room temperature from MK (Figure S3, Supplementary Materials); (3) the values of the consistency of fresh geopolymers indicated that the FA geopolymer was more plastic than the MK geopolymer (Table S6, Supplementary Materials). Moreover, the results were consistent with the particle size distribution of the raw materials. The fluidity of paste with bigger and more round particles is lower [116], as observed for FA-originated material, in contrast to metakaolin's smaller particles with a larger surface area and rough shape that may lead to interlocking between particles in the fresh paste. The interparticle forces are influential in regulating the rheology of the suspension at the high solid concentration. The net interparticle forces are governed by the sum of the attractive van der Waals and the electrostatic repulsive forces. With a change in particle size, both are altered and the interparticle forces with a finer particle are stronger, resulting in increased viscosity [117]. The above results clearly demonstrate that an appropriate selection of the production parameters allows for wide control of the initial and final setting times of the produced material compositions. On the other hand, the properties of geopolymer hybrids, such as density, compressive strength, and flexural strength, are significantly dependent on the content of the added amount of cement (Figure S8 in Supplementary Materials). The mechanical properties confirmed the correct choice of the materials, based on FA-0.280 + 5% cement and MK-0.350 + 5% cement, as the best mechanical properties of geopolymers (Table 4) were followed by the best mechanical properties of hybrid materials.

A GALAXY printer (ATMAT company) was used for the printing of (1) geopolymers based on FA-0.280 and MK-0.350, (2) hybrid materials based on FA-0.280 and MK-0.350 with the addition of 5% cement, (3) hybrid materials based on cement with the addition of 5% FA-0.280 and MK-0.350, and (4) cement. Tests based on materials with various compositions indicated that the consistency of all mixtures was suitable for transport through the printer elements, ensured continuous feeding through a nozzle in the 3D printing process, and allowed the mixture to form individual layers of printed detail. However, not all materials were suitable for printing standard details. Geopolymers or hybrids based on a geopolymer matrix with the addition of 5% cement did not allow for obtaining the set dimensional parameters of the details, due to the plasticity of mortar and/or because setting time was inappropriate, and the walls of the detail were unstable. This effect was independent of the type of raw material used (FA and MK) (Figure 3A–D). Traces of residues after applying individual layers of the printed detail were seen even if the walls spilled. The materials behaved similarly to a non-Newtonian fluid. It was also found that the mixtures based on metakaolin (Figure 3B,D) had a lower spread than the tested counterpart compositions based on fly ash (Figure 3A,C). The results were confirmed by the lower values of buildability (shape stability) of the samples. This means that the ability of wet mortar to resist deformation during the layer-by-layer fabrication process was low [118]. Based on the obtained results of the setting time (Supplementary Materials Tables S5 and S7), it can be concluded that the use of this type of mixture will be effective in 3D printing technology after introducing additional modifications to the device, allowing it to heat the applied layer by volume or locally. Without additional treatments, this type of material can also be successfully used in applications aimed at the free and accurate filling of an empty or scaffold-reinforced mold. On the other hand, the use of hybrids based on cement with a 5% addition of geopolymer, based on both FA and MK, allowed for precise detail printing (Figure 3E,F). The obtained results from the visual evaluation in terms of maintaining the geometry of the shape and the quality of the printout were significantly better, compared to the results obtained for the sample printed from cement (Figure 3G). Similarly, the buildability parameters of the samples were much better. These results required that the first layer of concrete should have enough yield strength to sustain the weight of itself and the subsequent higher layers. The printed layers must be self-supporting and free of discontinuity flaws caused by insufficient cohesion or lack of continuity of material feeding. The printed layers of materials must be stacked

stably to build a solid object (buildability). Furthermore, the extrudability is related to the workability of the mortar mixes. Therefore, the fresh mortar mixes dedicated to the printing process must display especially high flowability and workability during the pumping stage, whereas the requirements are just the opposite after deposition [119].

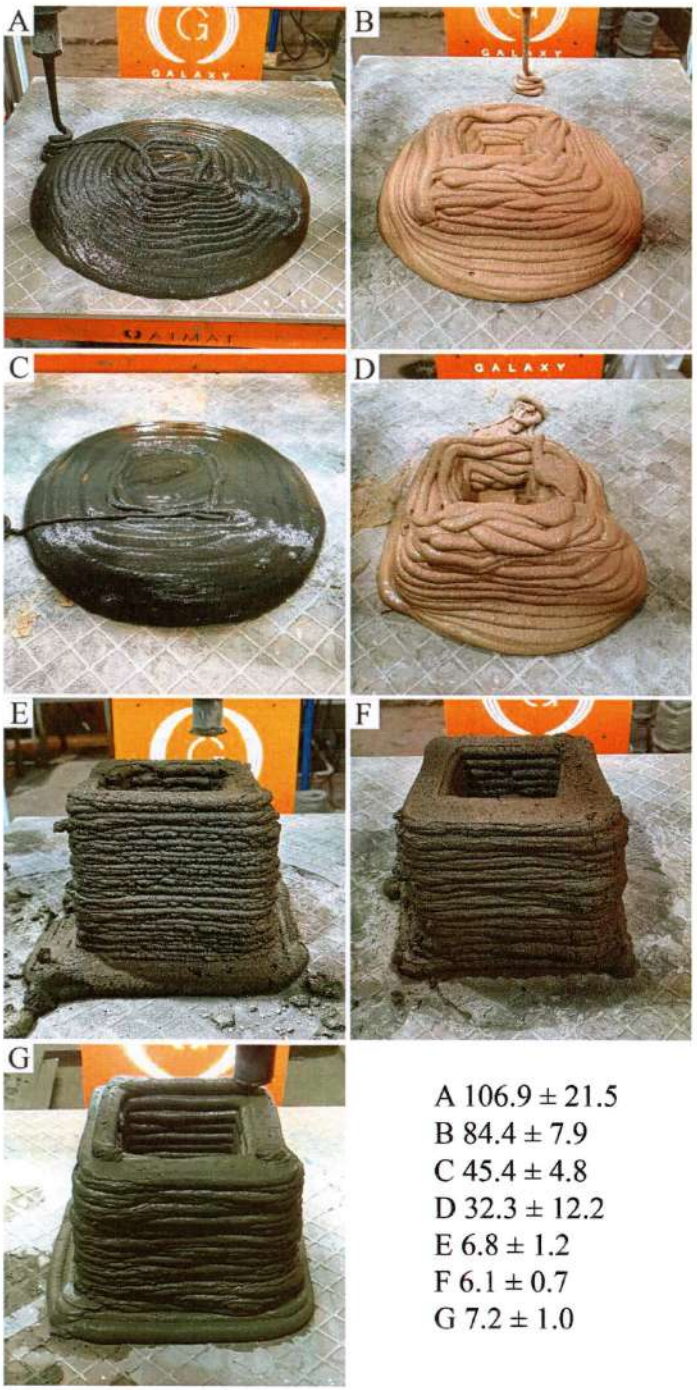

Figure 3. Details produced with the 3D printing method from materials with different compositions: (**A**) geopolymer based on fly ash FA-0.280; (**B**) geopolymer based on metakaolin MK-0.350, (**C**) 95% geopolymer based on fly ash FA-0.280 and 5% cement, (**D**) 95% geopolymer based on metakaolin MK-0.350 and 5% cement, (**E**) 5% geopolymer based on fly ash FA-0.280 and 95% cement, (**F**) 5% geopolymer based on metakaolin MK-0.350 and 95% cement, (**G**) cement. The values denote sample buildability (%).

4. Conclusions

We present herein the development of concrete-geopolymer hybrids that are suitable for 3DCP methods and dedicated to using environmentally friendly building materials. The aim was to classify raw materials and geopolymers, as well as the design of protocols for the production of a wide range of hybrid materials with different physicochemical properties during printing but ultimately retaining the best mechanical properties as the target, including compressive strength. The compressive strength of geopolymer binders and hybrid materials were dependent on many variables in our studies, including (but not limited to): (1) the mineralogical and chemical composition of the aluminosilicate resources of the raw materials, including the Si:Al ratio, Ca, accessory minerals, dissolved organic carbon, water content, and pH; (2) the structural properties of the raw materials, with an emphasis on morphology, particle size distribution, true density, and specific surface area; (3) the physical properties of the raw materials, e.g., thermal behavior and radioactivity level. CEM I 42.5R (particle size 5–30 μm, the specific density 3.1 g cm^{-3}), fly ash (spherical particles, 90% of them being < 30 μm, density 2.3 g cm^{-3}), and metakaolin (irregular flake-shaped particles, 90% of them being > 30 μm, 2.6 g cm^{-3}) were used as the raw materials.

The variables that should be selected to promote the geopolymerization process, i.e., greater surface area, the volume of pores, and content of silica and alumina, were found in MK, while a higher pH value, the Si:Al ratio, calcium content, and water absorption were observed in FA. In contrast, the properties reducing the geopolymerization efficiency, i.e., higher loss on ignition and the presence of dissolved organic carbon, confirmed by the thermal instability, were higher in FA. Diverse properties were not a limiting factor in the geopolymerization process. The chemical arrangement of FA-originated geopolymers (the increased Si-O-Si bonds with residual silica as reinforcement) provided better mechanical properties (compressive strength, flexural strength, and abrasion resistance) after 28 days of curing.

Similarly, many factors during the preparation process affected the properties of geopolymers and hybrid materials, which in turn determined the 3D printing process in our studies: (1) the proportion of raw materials, the liquid-to-solid ratio, the water to binder ratio; (2) the duration of mixing time and the temperature of the mixture; (3) rheology modifiers, accelerators or retarders of the setting time; (4) curing time. Therefore, changes in the liquid-to-solid ratio from 0.245 to 0.350 for FA and from 0.350 to 0.400 for MK extended the setting time by 40% and 25%, respectively. This resulted, at least, from the capillary effects (the adhesive and cohesive forces interacting between the H_2O and the internal surface of pores) being higher in FA particles (higher Ca content, smaller particle size, the particles' total pore volume, average pore diameter, allowing them to keep the H_2O molecules more closely bonded; it is only when the temperature rises that adsorbed water can be removed into the atmosphere to a greater extent) than MK particles (the water is able to penetrate easily through the bigger particles and pores of the MK; a higher water quantity can be removed to the atmosphere at room temperature). Paste temperature, when increased from room temperature to a temperature of 75 °C, reduced the setting time by even one order of magnitude, while the prolongation of its mixing from 15 min to 30 min shortened the setting time twice as much. Along with an increased amount of L/S, the compressive strength decreased by ~43% and 64% after the first day of curing, for FA and MK, respectively. In the following days of curing, the effect was counteracted in the wide range of the L/S ratio for FA-originated geopolymers, but not MK-originated geopolymers. With the introduction of cement to geopolymer mortar in the range of 5–30%, the setting time of the hybrid material was shortened, while the content of cement in the range of 95% and 100% prolonged the setting time. Many other variables, as optimized earlier, can also modify the physico-mechanical properties of the final product, e.g.: (1) the type and formulation of the alkaline activator and the content of alkaline ions in the activator; the fraction of silicate to hydroxide compounds in the activator [26,120]; (2) the formulation of aggregates [75–78,80]; and (3) specific modifications, including

reinforcing additives [59,121], agents controlling the geopolymer macrostructure [58,59], and curing conditions.

The results of the 3D printing of cement-geopolymer hybrids were presented for the first time. Geopolymers or hybrids based on a geopolymer matrix with the addition of 5% cement resulted in a high setting time, and the final materials behaved similarly to a non-Newtonian fluid. The use of this type of mixture is recommended in 3D printing technology after heating the printed elements. Without additional treatments, this type of material can be successfully used to fill the molds. In contrast, hybrid materials based on cement with a 5% addition of geopolymer, based on both FA and MK, enabled precise detail printing. Future work should consist of the optimization of printing. Particularly when the geopolymer binder is 3D-printed, the number of effective factors on the product strength is expanded by: (1) the printing method, size and geometry of printing nozzle, the number of nozzles; (2) the printing parameters, which include the resolution of layers, mainly Z-layer thickness, degree, and shape of the extrusion (circular, ovular or rectangular), linear rates of extrusion, the orientation of manufacture (vertical or horizontal), retraction; (3) mass sensitivity to mechanical and physical factors.

Altogether, our findings demonstrate a great ability to achieve the classification of geopolymers for different 3D-printing methods and imply the significance of different factors in the compressive strength of the final product. However, mixture design and the appropriate selection of ingredients in laboratory conditions are costly and time-consuming; therefore, to achieve the desired mechanical properties and to support the usage of FA in the building industry, data can be applied in future research using data-driven methods involving artificial intelligence and machine learning methods, as well as reliable, precise, and accurate mathematical equations [56,122,123].

Supplementary Materials: The following are available online at https://www.mdpi.com/article/10.3390/ma14226874/s1, Figure S1. SEM micrographs of fly ash and metakaolin at different magnifications (100×, 200×, 1000×). A,C,E—fly ash morphology, B,D,F—metakaolin morphology. Figure S2. The nitrogen adsorption–desorption isotherms of fly ash and metakaolin. Adsorption isotherms exhibit shapes that depend on the intensity of the adsorbate-adsorbent interaction and on the pore size. According to the IUPAC classification, N2 sorption isotherms can be classified as type IV, which indicates the presence of mesopores. The hysteresis loops are of type H3 for slit-like interparticle pores. Figure S3. Thermal decomposition of the fly ash and metakaolin during heating from ambient temperature to 1000 °C: A—thermogravimetry (TG, solid lines) and DTG (derivative thermogravimetry, dashed lines) curves; B—differential thermal analysis (DTA) curves; C–H—curves of evolved gas analysis (Quadrupole Mass Spectrometry) for C—*m*/*z* 12, H_2O—*m*/*z* 17 and 18, CO—*m*/*z* 28, O_2—*m*/*z* 32, CO_2—*m*/*z* 44, respectively. Figure S4. XRD patterns of fly ash and metakaolin. Figure S5. Complete FTIR spectra of raw materials, i.e., fly ash and metakaolin (A), as well as geopolymers produced from fly ash (B) and metakaolin (C), mixed with sand and NaOH:water glass in ratio 0.245, 0.280 and 0.350 for FA, and 0.350, 0.375, and 0.400 for MK. The spectra correspond to Figure 2. Figure S6. Photographs of representative geopolymer samples after an analysis of compressive strength after 1 day and 28 days of curing, as well as flexural strength and abrasion resistance after 28 days of curing. Photographs of fly ash- and metakaolin-based geopolymers with the same liquid-to-solid ratio of 0.35 were compared. Figure S7. Initial and final setting time (min) of hybrid samples based on fly ash FA-0.280 and the different contents of cement. The duration of the ingredient-mixing before the test was set to 15 min and the experiment was carried out at room temperature, according to the EN 196-2: 2005 + A1: 2008 standard with 600 cm^{-3} of mortar. Standard error did not exceed 10%. Figure S8. Density (A), compressive strength (B), and flexural strength (C) of printed hybrid samples based on fly ash (FA-0.280), depending on the content of the added cement and carried out at room temperature. The duration of ingredients mixing before the test was set to 15 min. The tests were carried out according to the EN 196-2: 2005 + A1: 2008 standard with 600 cm^{-3} of mortar. Standard error did not exceed 10%. Table S1. The particle size distribution width (μm) of the fly ash and metakaolin. The distribution width corresponded to the data presented on Figure 1C in the main text. The D_{50}, the median, has been defined as the diameter where half of the population lies below this value. Similarly, 90 percent of the distribution lies below the D_{90}, and 10 percent of the population lies below the D_{10}. Table S2. Composite of the water leachates

tested for fly ash and metakaolin presented in mg L^{-1}. Table S3. Natural radioactivity testing of raw materials presented in Bq kg^{-1}. Table S4. Main FTIR bands of raw materials i.e., fly ash and metakaolin (A) as well as geopolymers produced from fly ash (B) and metakaolin (C) mixed with sand and NaOH: water glass in ratio 0.245, 0.280 and 0.350 for FA, and 0.350, 0.375, and 0.400 for MK. The bands are related to Figure 2 and Supplementary Materials Figure S5. Table S5. Initial and final setting time (min) of geopolymer samples based on fly ash and metakaolin tested at 75 °C. The duration of ingredient-mixing before the test was 15 and 30 min. The tests were carried out according to the EN 196-2: 2005 + A1: 2008 standard with 600 cm^{-3} of mortar. Standard error did not exceed 10%. Table S6. Consistency of fresh geopolymer mortars determined by the flow table method (mm) and the Novikov cone method (mm). The duration of ingredient-mixing was 15 min, room temperature. The flow table method was carried out according to the EN 1015-3. 1500 cm^{-3} of mortar was taken into the mold, the measurement was taken as the average mortar spreading (mean diameter) measured in two directions perpendicular to each other (diameter 1 and diameter 2). According to the EN 1015-3-6 standard, the mortar consistency is defined as: dense-plastic with the value < 140, plastic for the values in the range of 140–200, and liquid with the value > 200. Novikov's cone method was performed according to the PN-85/B-04500 standard, by determining the resistance of the mortar to a free-immersion cone with a mass of 300 g in about 1 dm^3 of mass. The measurement value corresponds to the depth of the cone immersion into the geopolymer mortar and is read in centimeters along the cone. Standard error did not exceed 10%. Table S7 Initial and final setting time (min) of hybrid samples based on fly ash FA-0.280 and metakaolin MK-0.350 with 5% addition of cement, carried out at room temperature and 75 °C. The duration of ingredient-mixing before the test was set to 15 min and the experiment was carried out at room temperature, according to the EN 196-2: 2005 + A1: 2008 standard, with 600 cm^{-3} of mortar. Standard error did not exceed 10%.

Author Contributions: Conceptualization, K.K., M.Ł. and M.H.; Data curation, J.M., C.Z., S.G., M.G., I.K. and N.D.-S.; Formal analysis, M.H. and M.S.-H.; Funding acquisition, K.K. and M.Ł.; Investigation, J.M., C.Z., S.G., M.G. and I.K.; Methodology, J.M., K.K., M.Ł., M.H. and M.S.-H.; Resources, K.K., M.Ł., M.H. and M.S.-H.; Visualization, J.M., M.H. and M.S.-H.; Writing—original draft, J.M., N.D.-S., M.H. and M.S.-H.; Writing—review & editing, M.H. and M.S.-H. All authors have read and agreed to the published version of the manuscript.

Funding: This work has been supported by the Growth Operational Programme 2014–2020, IV Increasing the research potential, 4.1.4: 'Application projects', funded by the National Centre for Research and Development in Poland, within the framework of the grant: "Development of 3D printing technology for construction and facade prefabricated elements made of concrete composites and geopolymers", grant no. POIR 04.01.04-00-0096/18-00.

Institutional Review Board Statement: Not applicable.

Informed Consent Statement: Not applicable.

Data Availability Statement: Not applicable.

Conflicts of Interest: The authors declare no conflict of interest. The funders had no role in the design of the study; in the collection, analyses, or interpretation of data; in the writing of the manuscript, or in the decision to publish the results.

References

1. Ferreira, E.G.A.; Yokaichiya, F.; Rodrigues, M.S.; Beraldo, A.L.; Isaac, A.; Kardjilov, N.; Franco, M.K.K.D. Assessment of Greener Cement by employing thermally treated sugarcane straw ashes. *Constr. Build. Mater* **2017**, *141*, 343–352. [CrossRef]
2. Abrão, P.C.R.A.; Cardoso, F.A.; John, V.M. Efficiency of Portland-pozzolana cements: Water demand, chemical reactivity and environmental impact. *Constr. Build. Mater.* **2020**, *247*, 118546. [CrossRef]
3. Wu, Y.; Lu, B.; Bai, T.; Wang, H.; Du, F.; Zhang, Y.; Cai, L.; Jiang, C.; Wang, W. Geopolymer, green alkali activated cementitious material: Synthesis, applications and challenges. *Constr. Build. Mater.* **2019**, *224*, 930–949. [CrossRef]
4. Schneider, M.; Romer, M.; Tschudin, M.; Bolio, H. Sustainable cement production-present and future. *Cem. Concr. Res.* **2011**, *41*, 642–650. [CrossRef]
5. Yan, B.; Duan, P.; Ren, D. Mechanical strength, surface abrasion resistance and microstructure of fly ash-metakaolin-sepiolite geopolymer composites. *Ceram. Int.* **2017**, *43*, 1052–1060. [CrossRef]
6. Celik, A.; Yilmaz, K.; Canpolat, O.; Al-mashhadani, M.M.; Aygörmez, Y.; Uysal, M. High-temperature behavior and mechanical characteristics of boron waste additive metakaolin based geopolymer composites reinforced with synthetic fibers. *Constr. Build. Mater.* **2018**, *187*, 1190–1203. [CrossRef]

7. Lahoti, M.; Wijaya, S.F.; Tan, K.H.; Yang, E.H. Tailoring sodium-based fly ash geopolymers with variegated thermal performance. *Cem. Concr. Compos.* **2020**, *107*, 103507. [CrossRef]
8. Singh, N.B.; Middendorf, B. Geopolymers as an alternative to Portland cement: An overview. *Constr. Build. Mater.* **2020**, *237*, 117455. [CrossRef]
9. Lahoti, M.; Tan, K.H.; Yang, E.H. A critical review of geopolymer properties for structural fire-resistance applications. *Constr. Build. Mater.* **2019**, *221*, 514–526. [CrossRef]
10. Ling, Y.; Wang, K.; Wang, X.; Hua, S. Effects of mix design parameters on heat of geopolymerization, set time, and compressive strength of high calcium fly ash geopolymer. *Constr. Build. Mater.* **2019**, *228*, 116763. [CrossRef]
11. Zhang, H.Y.; Kodur, V.; Qi, S.L.; Cao, L.; Wu, B. Development of metakaolin-fly ash based geopolymers for fire resistance applications. *Constr. Build. Mater.* **2014**, *55*, 38–45. [CrossRef]
12. Ji, Z.; Pei, Y. Bibliographic and visualized analysis of geopolymer research and its application in heavy metal immobilization: A review. *J. Environ. Manag.* **2019**, *231*, 256–267. [CrossRef]
13. Lahoti, M.; Wong, K.K.; Yang, E.H.; Tan, K.H. Effects of Si/Al molar ratio on strength endurance and volume stability of metakaolin geopolymers subject to elevated temperature. *Ceram. Int.* **2018**, *44*, 5726–5734. [CrossRef]
14. Cheng, T.W.; Lee, M.L.; Ko, M.S.; Ueng, T.H.; Yang, S.F. The heavy metal adsorption characteristics on metakaolin-based geopolymer. *Appl. Clay Sci.* **2012**, *56*, 90–96. [CrossRef]
15. Mohseni, E. Assessment of Na2SiO3 to NaOH ratio impact on the performance of polypropylene fiber-reinforced geopolymer composites. *Constr. Build. Mater.* **2018**, *186*, 904–911. [CrossRef]
16. Wongpa, J.; Kiattikomol, K.; Jaturapitakkul, C.; Chindaprasirt, P. Compressive strength, modulus of elasticity, and water permeability of inorganic polymer concrete. *Mater. Des.* **2010**, *31*, 4748–4754. [CrossRef]
17. Belmokhtar, N.; Ammari, M.; Brigui, J.; Allal, L.B. Comparison of the microstructure and the compressive strength of two geopolymers derived from Metakaolin and an industrial sludge. *Constr. Build. Mater.* **2017**, *146*, 621–629. [CrossRef]
18. Akono, A.T.; Koric, S.; Kriven, W.M. Influence of pore structure on the strength behavior of particle- and fiber-reinforced metakaolin-based geopolymer composites. *Cem. Concr. Compos.* **2019**, *104*, 103361. [CrossRef]
19. Komnitsas, K.; Zaharaki, D. Geopolymerisation: A review and prospects for the minerals industry. *Miner. Eng.* **2007**, *20*, 1261–1277. [CrossRef]
20. Abdel-Gawwad, H.A.; Abo-El-Enein, S.A. A novel method to produce dry geopolymer cement powder. *HBRC J.* **2016**, *12*, 13–24. [CrossRef]
21. Wang, A.; Liu, H.; Hao, X.; Wang, Y.; Liu, X.; Li, Z. Geopolymer Synthesis Using Garnet Tailings from Molybdenum Mines. *Minerals* **2019**, *9*, 48. [CrossRef]
22. Lin, W.T.; Korniejenko, K.; Hebda, M.; Łach, M.; Mikuła, J. Engineering properties of ternary cementless blended materials. *Int. J. Eng. Technol. Innov.* **2020**, *10*, 191–199. [CrossRef]
23. Grela, A.; Łach, M.; Bajda, T.; Mikuła, J.; Hebda, M. Characterization of the products obtained from alkaline conversion of tuff and metakaolin. *J. Therm. Anal. Calorim.* **2018**, *133*, 217–226. [CrossRef]
24. Selmani, S.; Sdiri, A.; Bouaziz, S.; Joussein, E.; Rossignol, S. Effects of metakaolin addition on geopolymer prepared from natural kaolinitic clay. *Appl. Clay Sci.* **2017**, *146*, 457–467. [CrossRef]
25. Prasanphan, S.; Wannagon, A.; Kobayashi, T.; Jiemsirilers, S. Reaction mechanisms of calcined kaolin processing waste-based geopolymers in the presence of low alkali activator solution. *Constr. Build. Mater.* **2019**, *221*, 409–420. [CrossRef]
26. Gado, R.A.; Hebda, M.; Łach, M.; Mikuła, J. Alkali Activation of Waste Clay Bricks: Influence of The Silica Modulus, SiO_2/Na_2O, H_2O/Na_2O Molar Ratio, and Liquid/Solid Ratio. *Materials* **2020**, *13*, 383. [CrossRef]
27. Huang, X.; Huang, T.; Li, S.; Muhammad, F.; Xu, G.; Zhao, Z.; Yu, L.; Yan, Y.; Li, D.; Jiao, B. Immobilization of chromite ore processing residue with alkali-activated blast furnace slag-based geopolymer. *Ceram. Int.* **2016**, *42*, 9538–9549. [CrossRef]
28. Toniolo, N.; Boccaccini, A.R. Fly ash-based geopolymers containing added silicate waste. A review. *Ceram. Int.* **2017**, *43*, 14545–14551. [CrossRef]
29. Bohra, V.K.J.; Nerella, R.; Madduru, S.R.C. Material properties, processing & characterization of fly ash based geopolymer. *Mater. Today Proc.* **2019**, *19*, 2617–2621. [CrossRef]
30. Doğan-Sağlamtimur, N.; Bilgil, A.; Szechyńska-Hebda, M.; Parzych, S.; Hebda, M. Eco-Friendly Fired Brick Produced from Industrial Ash and Natural Clay: A Study of Waste Reuse. *Materials* **2021**, *14*, 877. [CrossRef]
31. Lin, W.T.; Lin, K.L.; Chen, K.; Korniejenko, K.; Hebda, M.; Łach, M. Circulation Fluidized Bed Combustion Fly Ash as Partial Replacement of Fine Aggregates in Roller Compacted Concrete. *Materials* **2019**, *12*, 4204. [CrossRef]
32. Grela, A.; Łach, M.; Mikuła, J.; Hebda, M. Thermal analysis of the products of alkali activation of fly ash from CFB boilers. *J. Therm. Anal. Calorim.* **2016**, *124*, 1609–1621. [CrossRef]
33. Kaur, K.; Singh, J.; Kaur, M. Compressive strength of rice husk ash based geopolymer: The effect of alkaline activator. *Constr. Build. Mater.* **2018**, *168*, 188–192. [CrossRef]
34. Burciaga-Díaz, O.; Durón-Sifuentes, M.; Díaz-Guillén, J.A.; Escalante-García, J.I. Effect of waste glass incorporation on the properties of geopolymers formulated with low purity metakaolin. *Cem. Concr. Compos.* **2020**, *107*, 103492. [CrossRef]
35. Toniolo, N.; Rincón, A.; Avadhut, Y.S.; Hartmann, M.; Bernardo, E.; Boccaccini, A.R. Novel geopolymers incorporating red mud and waste glass cullet. *Mater. Lett.* **2018**, *219*, 152–154. [CrossRef]

36. Koshy, N.; Dondrob, K.; Hu, L.; Wen, Q.; Meegoda, J.N. Synthesis and characterization of geopolymers derived from coal gangue, fly ash and red mud. *Constr. Build. Mater.* **2019**, *206*, 287–296. [CrossRef]
37. Nath, P.; Sarker, P.K. Flexural strength and elastic modulus of ambient-cured blended low-calcium fly ash geopolymer concrete. *Constr. Build. Mater.* **2017**, *130*, 22–31. [CrossRef]
38. Juenger, M.C.G.; Winnefeld, F.; Provis, J.L.; Ideker, J.H. Advances in alternative cementitious binders. *Cem. Concr. Res.* **2011**, *41*, 1232–1243. [CrossRef]
39. Nguyen, K.T.; Ahn, N.; Le, T.A.; Lee, K. Theoretical and experimental study on mechanical properties and flexural strength of fly ash-geopolymer concrete. *Constr. Build. Mater.* **2016**, *106*, 65–77. [CrossRef]
40. Wang, Y.C.; Zhao, J.P. Facile preparation of slag or fly ash geopolymer composite coatings with flame resistance. *Constr. Build. Mater.* **2019**, *203*, 655–661. [CrossRef]
41. Zhang, Z.; Provis, J.L.; Reid, A.; Wang, H. Geopolymer foam concrete: An emerging material for sustainable construction. Constr. *Build. Mater.* **2014**, *56*, 113–127. [CrossRef]
42. Zhang, H.Y.; Kodur, V.; Wu, B.; Cao, L.; Wang, F. Thermal behavior and mechanical properties of geopolymer mortar after exposure to elevated temperatures. *Constr. Build. Mater.* **2016**, *109*, 17–24. [CrossRef]
43. Ng, C.; Alengaram, U.J.; Wong, L.S.; Mo, K.H.; Jumaat, M.Z.; Ramesh, S. A review on microstructural study and compressive strength of geopolymer mortar, paste and concrete. *Constr. Build. Mater.* **2018**, *186*, 550–576. [CrossRef]
44. Shuai, Q.; Xu, Z.; Yao, Z.; Chen, X.; Jiang, Z.; Peng, Z.; An, R.; Li, Y.; Jiang, X.; Li, H. Fire resistance of phosphoric acid-based geopolymer foams fabricated from metakaolin and hydrogen peroxide. *Mater. Lett.* **2020**, *263*, 1–4. [CrossRef]
45. Zhuang, H.J.; Zhang, H.Y.; Xu, H. Resistance of geopolymer mortar to acid and chloride attacks. *Procedia Eng.* **2017**, *210*, 126–131. [CrossRef]
46. Sanjayan, J.G.; Nazari, A.; Pouraliakbar, H. FEA modelling of fracture toughness of steel fibre-reinforced geopolymer composites. *Mater. Des.* **2015**, *76*, 215–222. [CrossRef]
47. Ling, Y.; Wang, K.; Fu, C. Shrinkage behavior of fly ash based geopolymer pastes with and without shrinkage reducing admixture. *Cem. Concr. Compos.* **2019**, *98*, 74–82. [CrossRef]
48. Zhao, R.; Yuan, Y.; Cheng, Z.; Wen, T.; Li, J.; Li, F.; Ma, Z.J. Freeze-thaw resistance of Class F fly ash-based geopolymer concrete. *Constr. Build. Mater.* **2019**, *222*, 474–483. [CrossRef]
49. Zhang, Y.J.; Wang, Y.C.; Xu, D.L.; Li, S. Mechanical performance and hydration mechanism of geopolymer composite reinforced by resin. *Mater. Sci. Eng. A* **2010**, *527*, 6574–6580. [CrossRef]
50. Wijaya, M.F.; Olivia, M.; Wibisono, G.; Saputra, E.; Wang, S. Characteristics of geopolymer hybrid concrete in peat water. *IOP Conf. Ser. Mater. Sci. Eng.* **2019**, *615*, 012120. [CrossRef]
51. Barboza-Chavez, A.C.; Gómez-Zamorano, L.Y.; Acevedo-Dávila, J.L. Synthesis and Characterization of a Hybrid Cement Based on Fly Ash, Metakaolin and Portland Cement Clinker. *Materials* **2020**, *13*, 1084. [CrossRef]
52. Rojas-Duque, O.; Espinosa, L.M.; Robayo-Salazar, R.A.; Mejía de Gutiérrez, R. Alkali-Activated Hybrid Concrete Based on Fly Ash and Its Application in the Production of High-Class Structural Blocks. *Crystals* **2020**, *10*, 946. [CrossRef]
53. Marczyk, J.; Ziejewska, C.; Łach, M.; Korniejenko, K.; Lin, W.T.; Hebda, M. Possibilities of using the 3D printing process in the concrete and geopolymers application. *IOP Conf. Ser. Mater. Sci. Eng.* **2019**, *706*, 012019. [CrossRef]
54. Xia, M.; Sanjayan, J. Method of formulating geopolymer for 3D printing for construction applications. *Mater. Des.* **2016**, *110*, 382–390. [CrossRef]
55. Siddika, A.; Mamun, A.A.A.; Ferdous, W.; Saha, A.K. 3D-printed concrete: Applications, performance, and challenges. *J. Sustain. Cement-Based Mater.* **2020**, *9*, 127–164. [CrossRef]
56. Bagheri, A.; Cremona, C. Formulation of mix design for 3D printing of geopolymers: A machine learning approach. *Mater. Adv.* **2020**, *1*, 720. [CrossRef]
57. PN-EN 197-1. Cement—Part 1: Composition, Specification and Conformity Criteria for Common Cements. 2014. Available online: https://standards.iteh.ai/catalog/standards/cen/64f4e2ca-0c2e-4f68-8c50-16f9f69bc572/pren-197-1 (accessed on 12 November 2021).
58. Szechyńska-Hebda, M.; Marczyk, J.; Ziejewska, C.; Hordyńska, N.; Mikuła, J.; Hebda, M. Neutral geopolymer foams reinforced with cellulose studied with the FT-Raman spectroscopy. *IOP Conf. Ser. Mater. Sci. Eng.* **2019**, *706*, 012017. [CrossRef]
59. Szechyńska-Hebda, M.; Marczyk, J.; Ziejewska, C.; Hordyńska, N.; Mikuła, J.; Hebda, M. Optimal Design of pH-neutral Geopolymer Foams for Their Use in Ecological Plant Cultivation Systems. *Materials* **2019**, *12*, 2999. [CrossRef]
60. Mierzwiński, D.; Łach, M.; Hebda, M.; Walter, J.; Szechyńska-Hebda, M.; Mikuła, J. Thermal phenomena of alkali-activated metakaolin studied with a negative temperature coefficient system. *J. Therm. Anal. Calorim.* **2019**, *138*, 4167–4175. [CrossRef]
61. PN-EN 1744-1:2010+A1:2013 Tests for Chemical Properties of Aggregates. Chemical Analysis. Available online: https://standards.iteh.ai/catalog/standards/sist/b1e5043b-1edc-49e8-9409-ed59a5808203/sist-en-1744-1-2010a1-2013 (accessed on 9 January 2013).
62. PN-EN 15934:2012 Sludge, Treated Biowaste, Soil and Waste—Calculation of Dry Matter Fraction after Determination of Dry Residue or Water Content. Available online: https://standards.iteh.ai/catalog/standards/cen/c7e440f9-c400-4318-8ee5-637e7f127c5d/en-15934-2012 (accessed on 22 August 2012).
63. PN-EN ISO 10523:2012 Water Quality—Determination of pH. Available online: https://standards.iteh.ai/catalog/standards/cen/8e85ce30-e43b-4af1-a586-386403da6b56/en-iso-10523-2012 (accessed on 15 February 2012).

64. PN-EN 12457-2:2002 Characterisation of Waste—Leaching-Compliance Test for Leaching of Granular Waste Materials and Sludges—Part 2: One Stage Batch Test at a Liquid to Solid Ratio of 10 L/kg for Materials with Particle Size below 4 mm (without or with Size Reduction). Available online: https://standards.iteh.ai/catalog/standards/cen/db6fbdf3-1de7-457c-a506-46c4898e3f09/en-12457-2-2002 (accessed on 18 September 2002).
65. Łach, M.; Hebdowska-Krupa, M.; Stefańska, A.; Stefanek, J.; Stanek, A.; Mikuła, J.; Hebda, M. Characterisation of post-production raw material from the Raciszyn II deposit as a material suitable for the production of alkaline-activated materials. *J. Therm. Anal. Calorim.* **2019**, *138*, 4551–4559. [CrossRef]
66. Kalak, T.; Kłopotek, A.; Cierpiszewski, R. Effective adsorption of lead ions using fly ash obtained in the novel circulating fluidized bed combustion technology. *Microchem. J.* **2019**, *145*, 1011–1025. [CrossRef]
67. Hebda, M.; Laska, M.; Szechyńska-Hebda, M. Application of a device used for observation of controlled thermal processes in a furnace: Examples of delubrication, oxidation, melting, pyrolysis, and combustion. *J. Therm. Anal. Calorim.* **2013**, *114*, 1099–1109. [CrossRef]
68. PN-EN 12390:2019 Testing Hardened Concrete. Available online: https://standards.iteh.ai/catalog/standards/cen/ae7e6a86-1cbc-455e-8b2a-8964be9087f9/en-12390-2-2019 (accessed on 26 June 2019).
69. PN-EN 13892-3:2014 Methods of Test for Screed Materials—Part 3: Determination of Wear Resistance—Böhme. Available online: https://standards.iteh.ai/catalog/standards/cen/e92c20b0-6afa-4ab6-a2dd-9240e13a7ba4/en-13892-3-2014 (accessed on 17 December 2014).
70. Akgün, Y.; Yazıcıoğlu, O.F. The Abrasion Resistance of Mortars Containing Natural Zeolite Analcime. *Eur. J. Eng. Nat. Sci.* **2019**, *3*, 6–11.
71. PN-EN ISO 1182:2020 Reaction to Fire Tests for Products—Non-Combustibility Test. Available online: https://standards.iteh.ai/catalog/standards/sist/36888eed-5e43-41c3-ad45-9078a16a66ba/sist-en-iso-1182-2020 (accessed on 16 July 2020).
72. Aboulayt, A.; Jaafri, R.; Samouh, H.; Idrissi, A.C.E.; Roziere, E.; Moussa, R.; Loukili, A. Stability of a new geopolymer grout: Rheological and mechanical performances of metakaolin-fly ash binary mixtures. *Constr. Build. Mater.* **2018**, *181*, 420–436. [CrossRef]
73. Korniejenko, K.; Łach, M.; Marczyk, J.; Ziejewska, C.; Halyag, N.P.; Mucsi, G. Fly ash as a raw material for geopolymerisation-mineralogical composition and morphology. *IOP Conf. Ser. Mater. Sci. Eng.* **2019**, *706*, 1–8. [CrossRef]
74. Sujjavanich, S.; Suwanvitaya, P.; Chaysuwan, D.; Heness, G. Synergistic effect of metakaolin and fly ash on properties of concrete. *Constr. Build. Mater.* **2017**, *155*, 830–837. [CrossRef]
75. Assi, L.N.; Deaver, E.E.; Ziehl, P. Effect of source and particle size distribution on the mechanical and microstructural properties of fly Ash-Based geopolymer concrete. *Constr. Build. Mater.* **2018**, *167*, 372–380. [CrossRef]
76. Li, Z.; Gao, Y.; Zhang, J.; Zhang, C.; Chen, J.; Liu, C. Effect of particle size and thermal activation on the coal gangue based geopolymer. *Mater. Chem. Phys.* **2021**, *267*, 124657. [CrossRef]
77. Almutairi, A.L.; Tayeh, B.A.; Adesina, A.; Isleem, H.F.; Zeyad, A.M. Potential applications of geopolymer concrete in construction: A review. *Case Stud. Constr. Mater.* **2021**, *15*, e00733. [CrossRef]
78. Pawluczuk, E.; Kalinowska-Wichrowska, K.; Jiménez, J.R.; Fernández-Rodríguez, J.M.; Suescum-Morales, D. Geopolymer concrete with treated recycled aggregates: Macro and microstructural behavior. *J. Build. Eng.* **2021**, *44*, 103317. [CrossRef]
79. Traven, K.; Češnovar, M.; Ducman, V. Particle size manipulation as an influential parameter in the development of mechanical properties in electric arc furnace slag-based AAM. *Ceram. Int.* **2019**, *45*, 22632–22641. [CrossRef]
80. Łach, M.; Gado, R.A.; Marczyk, J.; Ziejewska, C.; Dogan-Saglamtimur, N.; Mikuła, J.; Szechyńska-Hebda, M.; Hebda, M. Process design for a production of sustainable materials from post-production clay. *Materials* **2021**, *14*, 953. [CrossRef]
81. Horvat, B.; Ducman, V. Influence of Particle Size on Compressive Strength of Alkali Activated Refractory Materials. *Materials* **2020**, *13*, 2227. [CrossRef]
82. Kaminska, K.; Dzierwa, P. The influence of compaction and saturation on the compressibility of colliery waste. *Therm. Sci.* **2019**, *23*, 1345–1355. [CrossRef]
83. Górski, M.; Wielgus, N.; Loska, K.; Kozioł, M.; Landrat, M.; Ścierski, W.; Pikoń, K. Characteristics of Metakaolin-Based Geopolymer with Cathode Ray Tube Glass. *Polymers* **2021**, *13*, 1149. [CrossRef]
84. Sing, K. Reporting Physisorption Data for Gas/Solid Systems with Special Reference to the Determination of Surface Area and Porosity. *Pure Appl. Chem.* **1985**, *57*, 603–619. [CrossRef]
85. El Alouani, M.; Alehyen, S.; El Achouri, M.; Taibi, M. Comparative study of the adsorption of micropollutant contained in aqueous phase using coal fly ash and activated coal fly ash: Kinetic and isotherm studies. *Chem. Data Collect.* **2019**, *23*, 1–8. [CrossRef]
86. Liang, G.; Zhu, H.; Zhang, Z.; Wu, Q. Effect of rice husk ash addition on the compressive strength and thermal stability of metakaolin based geopolymer. *Constr. Build. Mater.* **2019**, *222*, 872–881. [CrossRef]
87. Nežerka, V.; Bílý, P.; Hrbek, V.; Fládr, J. Impact of silica fume, fly ash, and metakaolin on the thickness and strength of the ITZ in concrete. *Cem. Concr. Compos.* **2019**, *103*, 252–262. [CrossRef]
88. Luo, H.; Law, W.W.; Wu, Y.; Zhu, W.; Yang, E.H. Hydrothermal synthesis of needle-like nanocrystalline zeolites from metakaolin and their applications for efficient removal of organic pollutants and heavy metals. *Microporous Mesoporous Mater.* **2018**, *272*, 8–15. [CrossRef]

89. Thommes, M.; Kaneko, K.; Neimark, A.V.; Olivier, J.P.; Rodriguez-Reinoso, F.; Rouquerol, J.; Sing, K.S.W. Physisorption of gases, with special reference to the evaluation of surface area and pore size distribution (IUPAC Technical Report). *Pure Appl. Chem.* **2015**, *87*, 1051–1069. [CrossRef]
90. Chen, F.; Zhang, Y.; Liu, J.; Wang, X.; Chu, P.K.; Chu, B.; Zhang, N. Fly ash based lightweight wall materials incorporating expanded perlite/SiO2 aerogel composite: Towards low thermal conductivity. *Constr. Build. Mater.* **2020**, *249*, 118728. [CrossRef]
91. Guo, X.; Sji, H. Metakaolin-, fly ash- and calcium hydroxide-based geopolymers: Effects of calcium on performance. *Adv. Cem. Res.* **2015**, *27*, 559–566. [CrossRef]
92. Pantazopoulou, E.; Zouboulis, A. Chemical toxicity and ecotoxicity evaluation of tannery sludge stabilized with ladle furnace slag. *J. Environ. Manag.* **2018**, *216*, 257–262. [CrossRef]
93. Council of the European Union and 2003/33/EC. *Council Decision Establishing Criteria and Procedures for the Acceptance of Waste at Landfills Pursuant to Article 16 of and Annex II to Directive 1999/31/EC*; EUR-lex, European Union: Luxembourg, 2003; Available online: https://eur-lex.europa.eu/legal-content/EN/TXT/?uri=uriserv%3AOJ.L.2003.011.01.0027.01.ENG&toc=OJ%3AL%3A2003%3A011%3ATOC (accessed on 16 January 2003).
94. Wei, Y.; Wang, J.; Wang, J.; Zhan, L.; Ye, X.; Tan, H. Hydrothermal processing, characterization and leaching toxicity of Cr-added 'fly ash-metakaolin' based geopolymer. *Constr. Build. Mater.* **2020**, *251*, 118931. [CrossRef]
95. Kaiser, S. Radiological protection principles concerning the natural radioactivity of building materials. *Radiat. Prot.* **1999**, *112*, 1–16.
96. Gupta, M.; Mahur, A.K.; Varshney, R.; Sonkawade, R.G.; Verma, K.G.; Prasad, R. Measurement of natural radioactivity and radon exhalation rate in fly ash samples from a thermal power plant and estimation of radiation doses. *Radiat. Meas.* **2013**, *50*, 160–165. [CrossRef]
97. Chen, H.-J.; Shih, N.-H.; Wu, C.-H.; Lin, S.-K. Effects of the Loss on Ignition of Fly Ash on the Properties of High-Volume Fly Ash Concrete. *Sustainability* **2019**, *11*, 2704. [CrossRef]
98. Sun, Z.; Vollpracht, A.; van der Sloot, H.A. pH dependent leaching characterization of major and trace elements from fly ash and metakaolin geopolymers. *Cem. Concr. Res.* **2019**, *125*, 105889. [CrossRef]
99. Osholana, T.S.; Dludlu, M.K.; Oboirien, B.; Sadiku, R. Enhanced reactivity of geopolymers produced from fluidized bed combustion bottom ash. *S. Afr. J. Chem. Eng.* **2020**, *34*, 72–77. [CrossRef]
100. Zenabou, N.N.M.; Benoit-Ali, N.; Zekeng, S.; Rossignol, S.; Melo, U.C.; Tchamba, A.B.; Kamseu, E.; Leonelli, C. Improving insulation in metakaolin based geopolymer: Effects of metabauxite and metatalc. *J. Build. Eng.* **2019**, *23*, 403–415. [CrossRef]
101. Kocak, Y. Effects of metakaolin on the hydration development of Portland–composite cement. *J. Build. Eng.* **2020**, *31*, 101419. [CrossRef]
102. Xie, J.; Kayali, O. Effect of initial water content and curing moisture conditions on the development of fly ash-based geopolymers in heat and ambient temperature. *Constr. Build. Mater.* **2014**, *67*, 20–28. [CrossRef]
103. Xu, H.; van Deventer, J.S.J. The geopolymerisation of alumino-silicate minerals. *Int. J. Miner. Process.* **2000**, *59*, 247–266. [CrossRef]
104. Clausi, M.; Fernández-Jiménez, A.M.; Palomo, A.; Tarantino, S.C.; Zema, M. Reuse of waste sandstone sludge via alkali activation in matrices of fly ash and metakaolin. *Constr. Build. Mater.* **2018**, *172*, 212–223. [CrossRef]
105. Ismail, I.; Bernal, S.A.; Provis, J.L.; San Nicolas, R.; Hamdan, S.; van Deventer, J.S.J. Modification of phase evolution in alkali-activated blast furnace slag by the incorporation of fly ash. *Cem. Concr. Compos.* **2014**, *45*, 125–135. [CrossRef]
106. Carabba, L.; Moricone, R.; Scarponi, G.E.; Tugnoli, A.; Bignozzi, M.C. Alkali activated lightweight mortars for passive fire protection: A preliminary study. *Constr. Build. Mater.* **2019**, *195*, 75–84. [CrossRef]
107. Silva, G.; Kim, S.; Aguilar, R.; Nakamatsu, J. Natural fibers as reinforcement additives for geopolymers—A review of potential eco-friendly applications to the construction industry. *Sustain. Mater. Technol.* **2020**, *23*, e00132. [CrossRef]
108. Panda, B.; Tan, M.J. Experimental study on mix proportion and fresh properties of fly ash based geopolymer for 3D concrete printing. *Ceram. Int.* **2018**, *44*, 10258–10265. [CrossRef]
109. Cui, X.M.; Liu, L.P.; He, Y.; Chen, J.Y.; Zhou, J. A novel aluminosilicate geopolymer material with low dielectric loss. *Mater. Chem. Phys.* **2011**, *130*, 1–4. [CrossRef]
110. Pangdaeng, S.; Sata, V.; Aguiar, J.B.; Pacheco-Torgal, F.; Chindaprasirt, P. Apatite formation on calcined kaolin-white Portland cement geopolymer. *Mater. Sci. Eng. C* **2015**, *51*, 1–6. [CrossRef]
111. Chen, L.; Wang, Z.; Wang, Y.; Feng, J. Preparation and Properties of Alkali Activated Metakaolin-Based Geopolymer. *Materials* **2016**, *9*, 767. [CrossRef]
112. Barbosa, V.F.F.; MacKenzie, K.J.D.; Thaumaturgo, C. Synthesis and characterisation of materials based on inorganic polymers of alumina and silica: Sodium polysialate polymers. *Int. J. Inorg. Mater.* **2000**, *2*, 309–317. [CrossRef]
113. Jonbi, J.; Fulazzaky, M.A. Modeling the water absorption and compressive strength of geopolymer paving block: An empirical approach. *Meas. J. Int. Meas. Confed.* **2020**, *158*, 107695. [CrossRef]
114. Elyamany, H.E.; Abd Elmoaty, A.E.M.; Elshaboury, A.M. Setting time and 7-day strength of geopolymer mortar with various binders. *Constr. Build. Mater.* **2018**, *187*, 974–983. [CrossRef]
115. Ramujee, K.; Potharaju, M. Permeability and abrasion resistance of geopolymer concrete. *Indian Concr. J.* **2014**, *88*, 34–43. [CrossRef]
116. Kim, H.K.; Hwang, E.A.; Lee, H.K. Impacts of metakaolin on lightweight concrete by type of fine aggregate. *Constr. Build. Mater.* **2012**, *36*, 719–726. [CrossRef]

117. Singh, D.B.; Kumar, N.; Kaushal, D.R.; Sharma, A.K.; Yadav, J.K. Effect of solid concentration and grain size on the rheology of fly ash slurries. *Mater. Today-Proc.* **2021**, *46*, 10904–10908. [CrossRef]
118. Chen, Y.; Veer, F.; Copuroglu, O.A. Critical Review of 3D Concrete Printing as a Low CO_2 Concrete Approach. *Heron* **2017**, *62*, 167–194. [CrossRef]
119. Salam, N.M.; Ma, G.; Ijaz, N.; Wang, L. Importance and potential of cellulosic materials and derivatives in extrusion-based 3D concrete printing (3DCP): Prospects and challenges. *Constr. Build. Mater.* **2021**, *291*, 123281. [CrossRef]
120. Łach, M.; Mierzwiński, D.; Korniejenko, K.; Mikuła, J.; Hebda, M. Geopolymers as a material suitable for immobilization of fly ash from municipal waste incineration plants. *J. Air Waste Manag.* **2018**, *68*, 1190–1197. [CrossRef] [PubMed]
121. Korniejenko, K.; Figiela, B.; Miernik, K.; Ziejewska, C.; Marczyk, J.; Hebda, M.; Cheng, A.; Lin, W.T. Mechanical and Fracture Properties of Long Fiber Reinforced Geopolymer Composites. *Materials* **2021**, *14*, 5183. [CrossRef] [PubMed]
122. Khan, M.A.; Zafar, A.; Farooq, F.; Javed, M.F.; Alyousef, R.; Alabduljabbar, H.; Khan, M.I. Geopolymer Concrete Compressive Strength via Artificial Neural Network, Adaptive Neuro Fuzzy Interface System, and Gene Expression Programming with K-Fold Cross Validation. *Front. Mater.* **2021**, *8*, 621163. [CrossRef]
123. Dao, D.V.; Ly, H.B.; Trinh, S.H.; Le, T.T.; Pham, B.T. Artificial Intelligence Approaches for Prediction of Compressive Strength of Geopolymer Concrete. *Materials* **2019**, *12*, 983. [CrossRef]

Article

Hybrid materials based on fly ash, metakaolin, and cement for 3D printing

Joanna Marczyk[1], Celina Ziejewska[1], Szymon Gądek[1], Kinga Korniejenko[1], Michał Łach[1], Mateusz Góra[1,2], Izabela Kurek[1], Neslihan Doğan-Sağlamtimur[3], Marek Hebda[1]*, Magdalena Szechyńska-Hebda[4]*

[1] Faculty of Material Engineering and Physics, Cracow University of Technology, Warszawska 24, 31-155 Kraków, Poland
[2] ATMAT Sp. z o.o., Siwka 17, 31-588 Kraków, Poland
[3] Department of Environmental Engineering, Faculty of Engineering. Nigde Omer Halisdemir University, Nigde, Turkey
[4] Plant Breeding and Acclimatization Institute - National Research Institute, Radzików, 05-870 Błonie, Poland
* Correspondence: mhebda@pk.edu.pl, szechynska@wp.pl, tel.: +48 126283423

Supplementary Materials

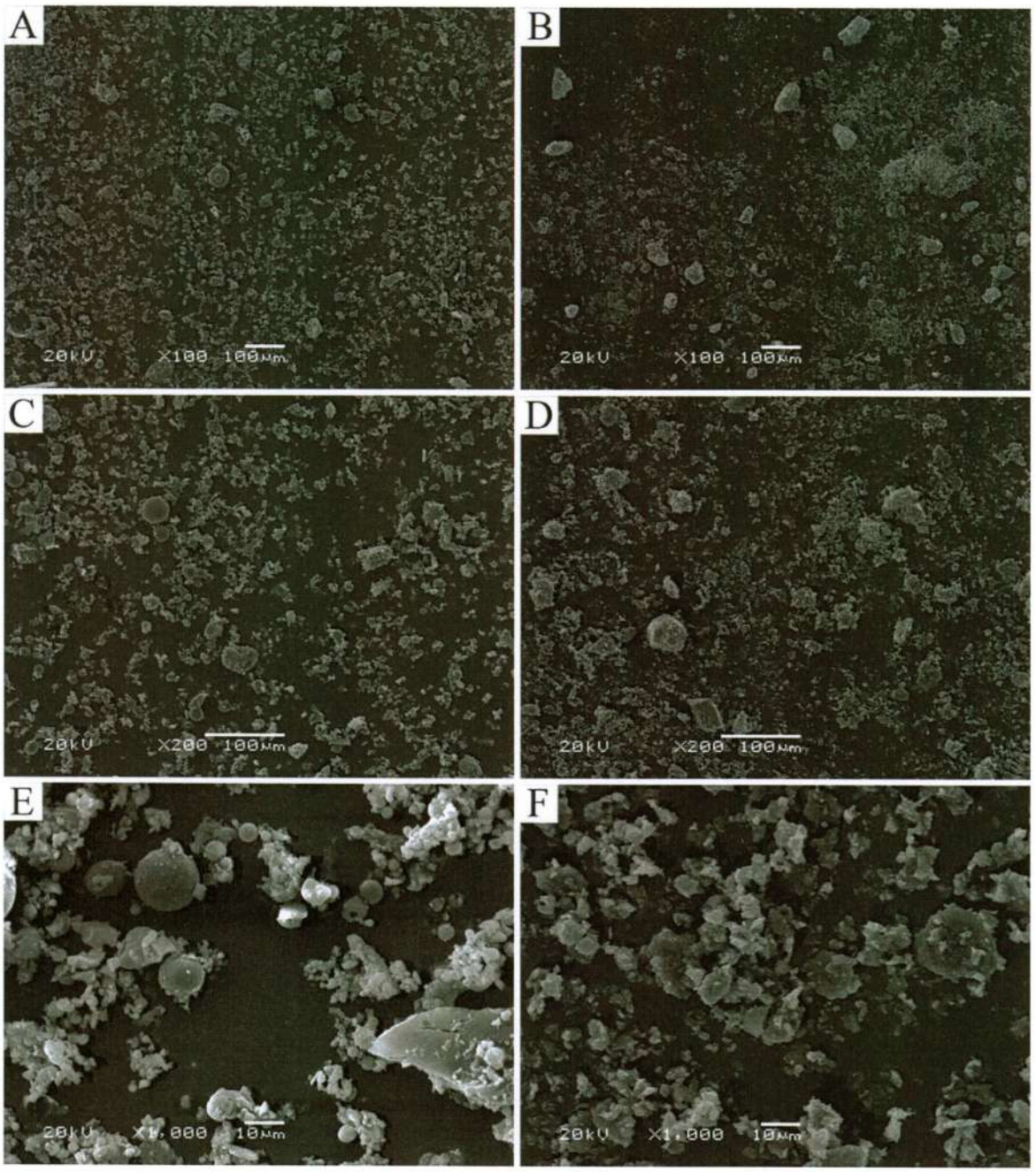

Figure S1. SEM micrographs of fly ash and metakaolin at different magnifications (100x, 200x, 1000x). A, C, E - fly ash morphology, B, D, F - metakaolin morphology.

Table S1. The particle size distribution width (μm) of the fly ash and metakaolin. The distribution width corresponded to data presented on Figure 1C in the main text. The D_{50}, the median, has been defined as the diameter where half of the population lies below this value. Similarly, 90 percent of the distribution lies below the D_{90}, and 10 percent of the population lies below the D_{10}.

Distribution width	FA	MK
D5	1.3	0.5
D10	2.8	0.8
D25	18.9	1.5
D50 (median)	22.3	18
D75	25.4	25.4
D90	28.2	30.8
D95	29.6	33.9
D99	32.5	39.2

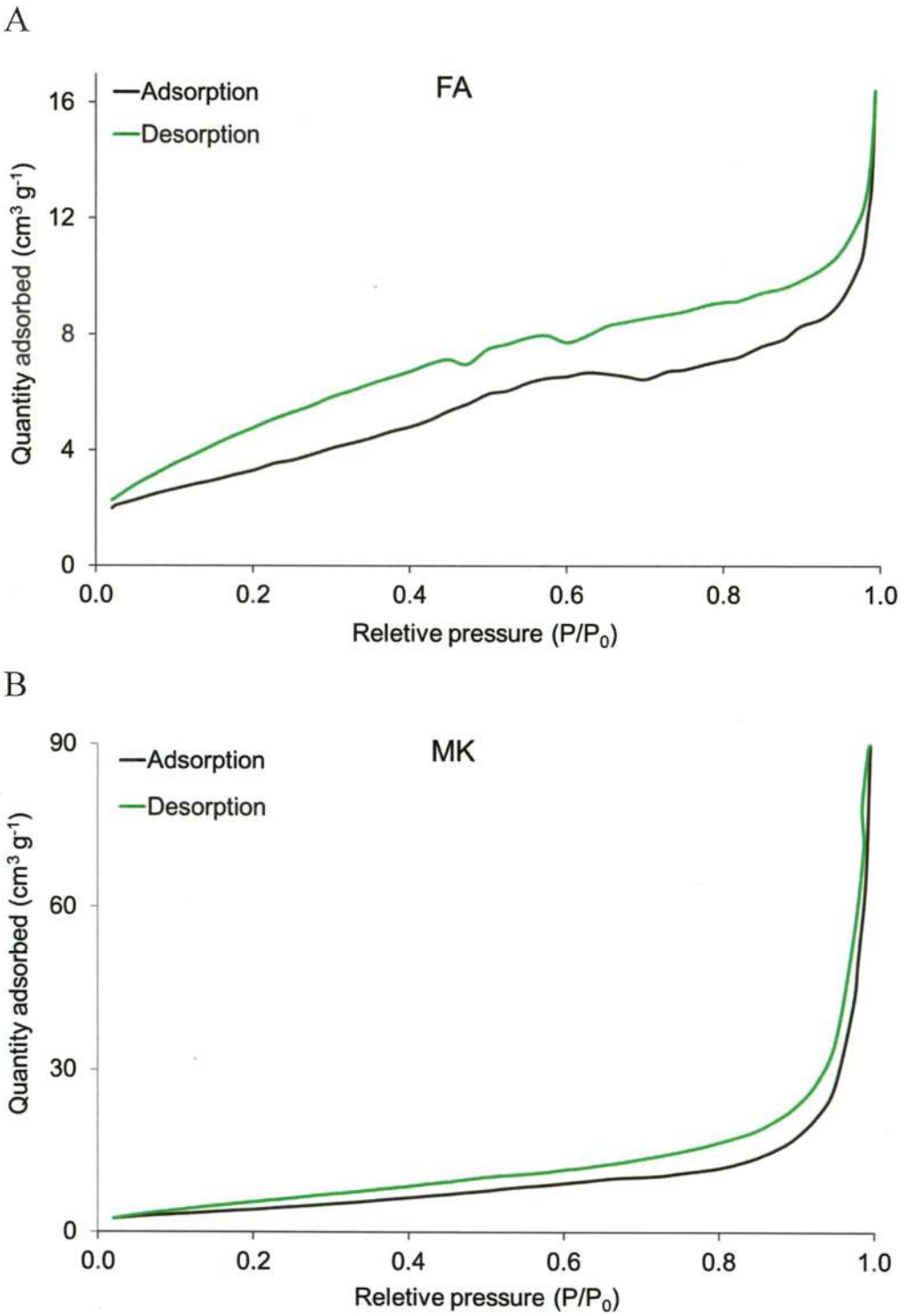

Figure S2. The nitrogen adsorption–desorption isotherms of fly ash and metakaolin. Adsorption isotherms exhibit shapes that depend on the intensity of the adsorbate-adsorbent interaction and on the pore size. According to the IUPAC classification, N2 sorption isotherms can be classified as type IV, which indicates the presence of mesopores. The hysteresis loops are of type H3 for slit-like interparticle pores.

Table S2. Composite of the water leachates tested for fly ash and metakaolin presented in mg l^{-1}.

Component	FA	MK
Sb	< 0.01	< 0.005
As	< 0.01	0.018
Ba	0.66	0.051
Cr	0.12	< 0.005
Cr(VI)	0.12	< 0.01
Zn	< 0.03	< 0.03
Cd	< 0.001	< 0.001
Cu	< 0.005	< 0.005
Mo	0.29	0.0068
Ni	< 0.005	< 0.005
Pb	< 0.005	< 0.005
Hg	< 0.001	< 0.001
Se	0.030	< 0.005
chlorides	20	< 5
fluorides	2.4	0.78
sulphates	414	44
DOC (dissolved organic carbon)	3.6	2.8
total dissolved substances	1390	100

Table S3. Natural radioactivity testing of raw materials presented in Bq kg^{-1}.

Determinable parameter	FA	MK
Potassium activity concentration (^{40}K)	814.06 ± 73.27	353.77 ± 31.84
Radium activity concentration (^{226}Ra)	194.33 ± 23.32	75.83 ± 9.10
Thorium activity concentration (^{228}Th)	100.95 ± 28.27	128.61 ± 36.02

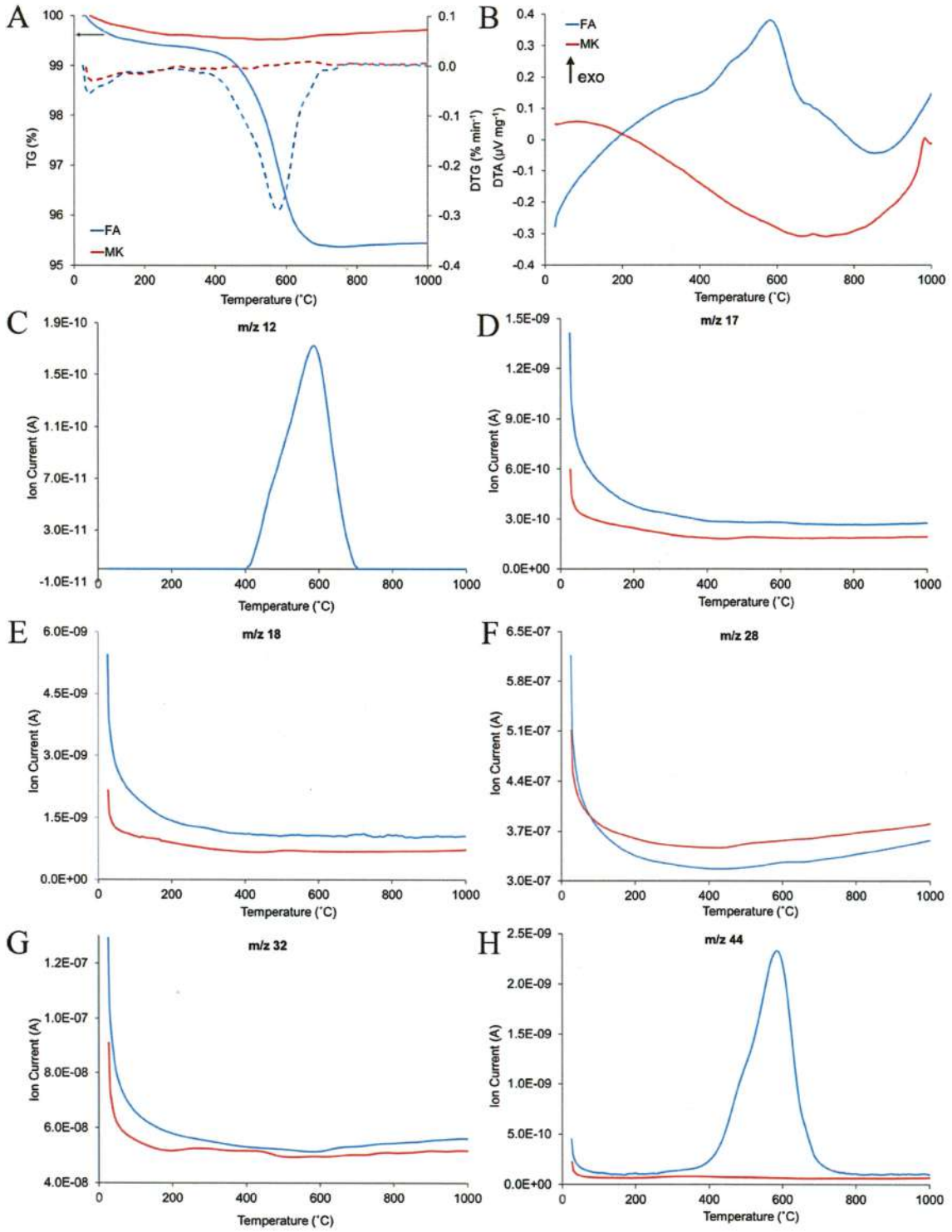

Figure S3. Thermal decomposition of the fly ash and metakaolin during heating from ambient temperature to 1000 °C: A – thermogravimetry (TG, solid lines) and DTG (derivative thermogravimetry, dashed lines) curves; B – differential thermal analysis (DTA) curves; C-H – curves of evolved gas analysis (Quadrupole Mass Spectrometry) for C - *m*/*z* 12, H_2O - *m*/*z* 17 and 18, CO - *m*/*z* 28, O_2 - *m*/*z* 32, CO_2 - *m*/*z* 44, respectively.

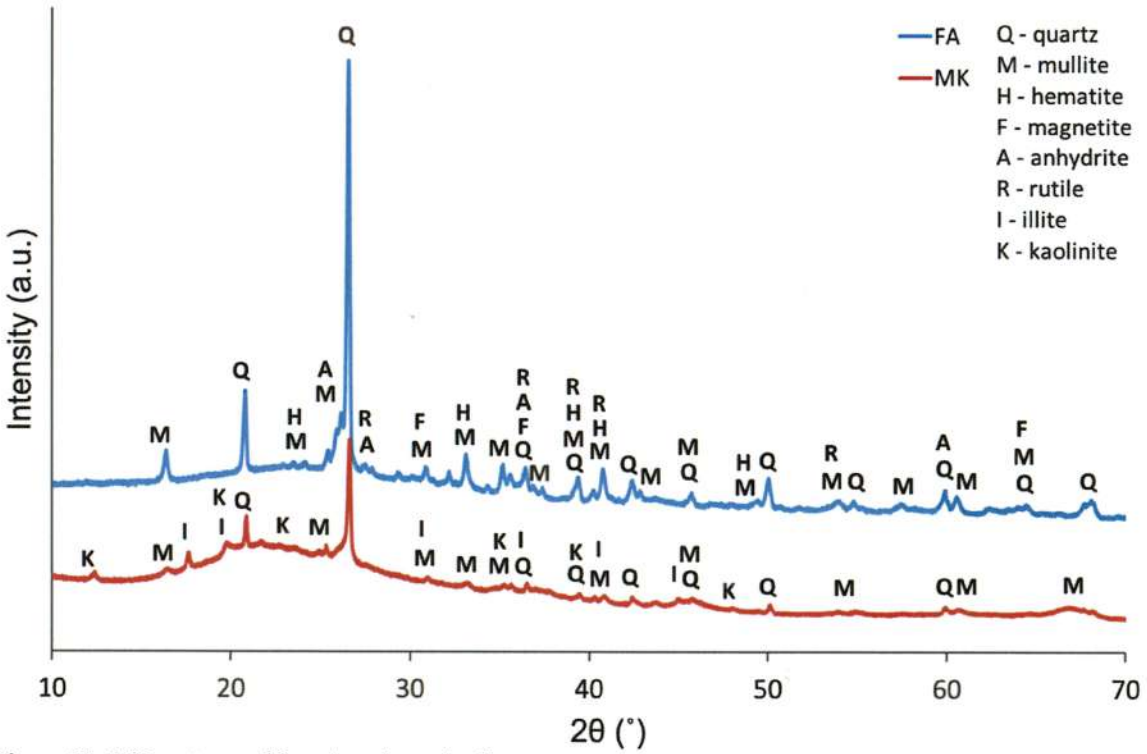

Figure S4. XRD patterns of fly ash and metakaolin.

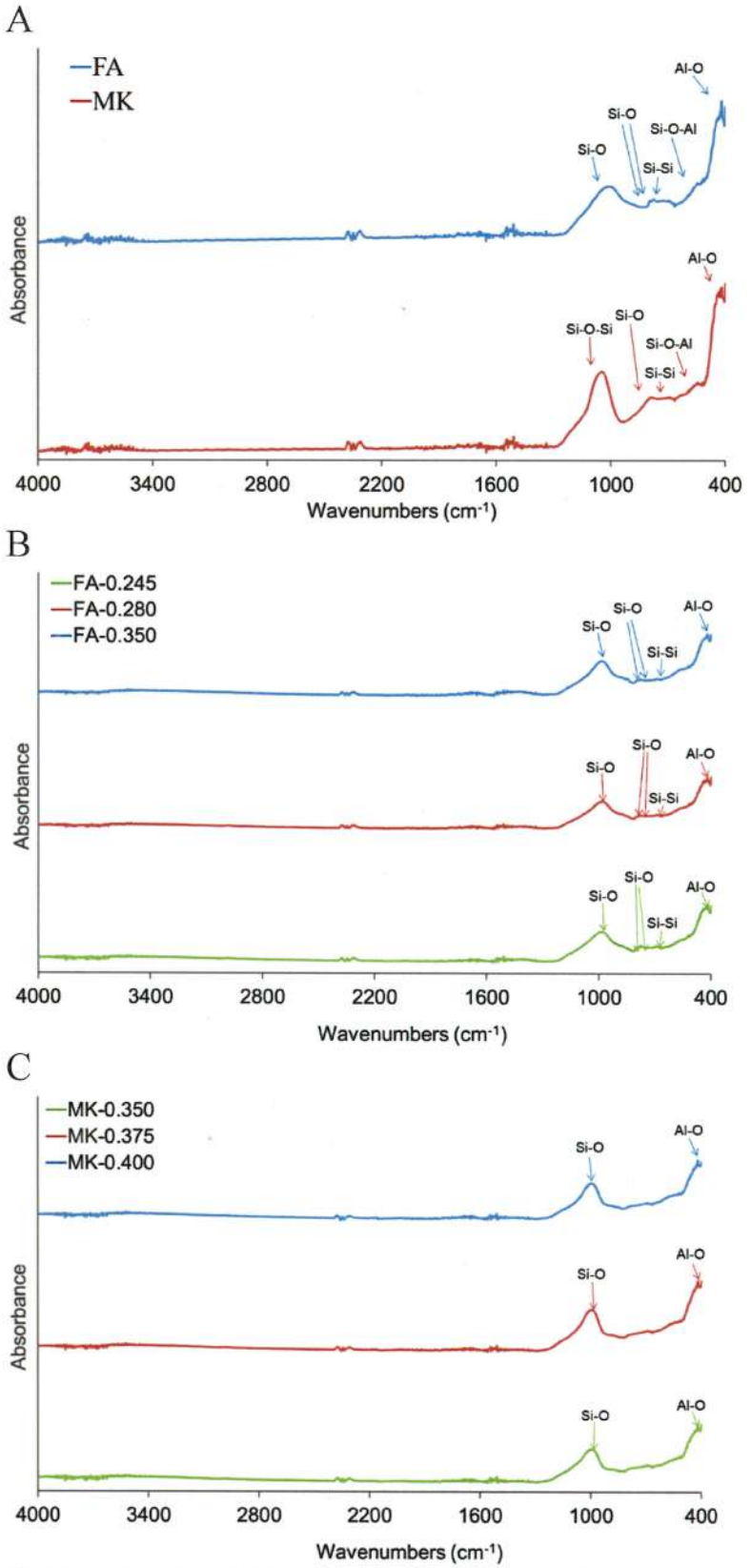

Figure S5. Complete FTIR spectra of raw materials i.e. fly ash and metakaolin (A) as well as geopolymers produced from fly ash (B) and metakaolin (C) mixed with sand and NaOH : water glass in ratio 0.245, 0.280 and 0.350 for FA, and 0.350, 0.375, and 0.400 for MK. The spectra correspond to Figure 2.

Table S4. Main FTIR bands of raw materials i.e. fly ash and metakaolin (A) as well as geopolymers produced from fly ash (B) and metakaolin (C) mixed with sand and NaOH : water glass in ratio 0.245, 0.280 and 0.350 for FA, and 0.350, 0.375, and 0.400 for MK. The bands are related to Figure 2 and Supplementary Materials Figure 5.

Sample	Wavenumber	Vibration band
	Raw materials	
FA	1003 cm-1	Vibration of Si-O
	793 cm-1 and 781 cm-1	Bending vibration of Si-O
	699 cm-1	Vibration of Si-Si
	547 cm-1	Vibration of Si-O-Al
	418 cm-1 and adjacent bands	Vibration of Al-O
MK	1055 cm-1	Vibration of Si-O-Si
	793 cm-1	Bending vibration of Si-O
	699 cm-1	Vibration of Si-Si
	547 cm-1	Vibration of Si-O-Al
	418 cm-1 and adjacent bands	Vibration of Al-O
	Geopolymers	
FA	989 cm-1	Vibration of Si-O
	793 cm-1 and 783 cm-1	Bending vibration of Si-O
	690 cm-1	Vibration of Si-Si
	420 cm-1	Vibration of Al-O
MK	992 cm-1	Vibration of Si-O
	420 cm-1	Vibration of Al-O

Sample	Before test	After test	
		1 day of curing	28 days of curing
Compressive strength			
FA			
MK			
Flexural strength			
FA			
MK			
Abrasion resistance			
FA			
MK			

Figure S6. Photographs of representative geopolymer samples after the analysis of: compressive strength after 1 day and 28 days of curing, as well as flexural strength and abrasion resistance after 28 days of curing. Photographs of fly ash- and metakaolin-based geopolymers with the same liquid-to-solid ratio of 0.35 were compared.

Table S5. Initial and final setting time (min) of geopolymer samples based on fly ash and metakaolin tested at 75 °C. The duration of ingredients mixing before test was 15 and 30 minutes. The tests were carried out according to the EN 196-2: 2005 + A1: 2008 standard with 600 cm^3 of mortar. Standard error did not exceed 10%.

Sample	Initial time	Final time	Initial time	Final time	Initial time	Final time
	15 min + RT		15 min + 75 °C		30 min + 75 °C	
FA-0.245			27	34		
FA-0.280	405	630	32	40	14	18
FA-0.350			40	46		
MK-0.350			28	33		
MK-0.375	323	522	35	38	29	34
MK-0.400			37	39		

Table S6. Consistency of fresh geopolymer mortars determined by flow table method (mm) and the Novikow cone method (mm). The duration of ingredients mixing was 15 minutes, room temperature. The flow table method was carried out according to the EN 1015-3. 1500 cm^3 of mortar was taken into the mould, the measurement was taken as the average mortar spreading (mean diameter) measured in two directions perpendicular to each other (diameter 1 and diameter 2). According to the EN 1015-3-6 standard, the mortar consistency is defined as: dense-plasticic with the value < 140, plasticic for the values in the range of 140-200, and liquid with the value > 200. The Novikov`s cone method was performer according to the PN-85/B-04500 standard, by determining the resistance of the mortar to a freely immersion cone with a mass of 300 g in about 1 dm^3 of mass. The measurement value corresponds to the depth of the cone immersion into the geopolymer mortar and is read in centimeters along the cone. Standard error did not exceed 10%.

Sample	Flow table method			Novikov`s cone method
	Diameter 1	Diameter 2	Mean	
FA-0.245	100	105	103	100
FA-0.280	135	140	138	800
FA-0.350	255	260	258	1100
MK-0.350	105	110	108	350
MK-0.375	150	145	148	250
MK-0.400	180	180	180	100

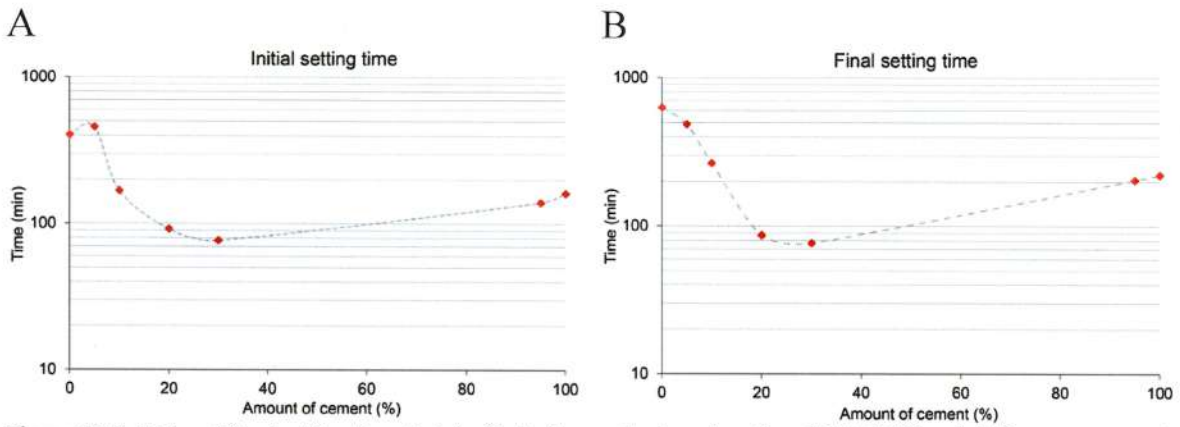

Figure S7. Initial and final setting time (min) of hybrid samples based on fly ash FA-0.280 and different content of cement. The duration of ingredients mixing before test was set to 15 minutes and experiment was carried out at room temperature according to the EN 196-2: 2005 + A1: 2008 standard with 600 cm^3 of mortar. Standard error did not exceed 10%.

Table S7 Initial and final setting time (min) of hybrid samples based on fly ash FA-0.280 and metakaolin MK-0.350 with 5% addition of cement. carried out at room temperature and 75 °C. The duration of ingredients mixing before test was set to 15 minutes and experiment was carried out at room temperature according to the EN 196-2: 2005 + A1: 2008 standard with 600 cm^{-3} of mortar. Standard error did not exceed 10%.

Sample	Initial time	Final time	Initial time	Final time
	RT		75 °C	
FA-0.280 + 5% cement	459	486	49	55
MK-0.350 + 5% cement	366	403	31	44

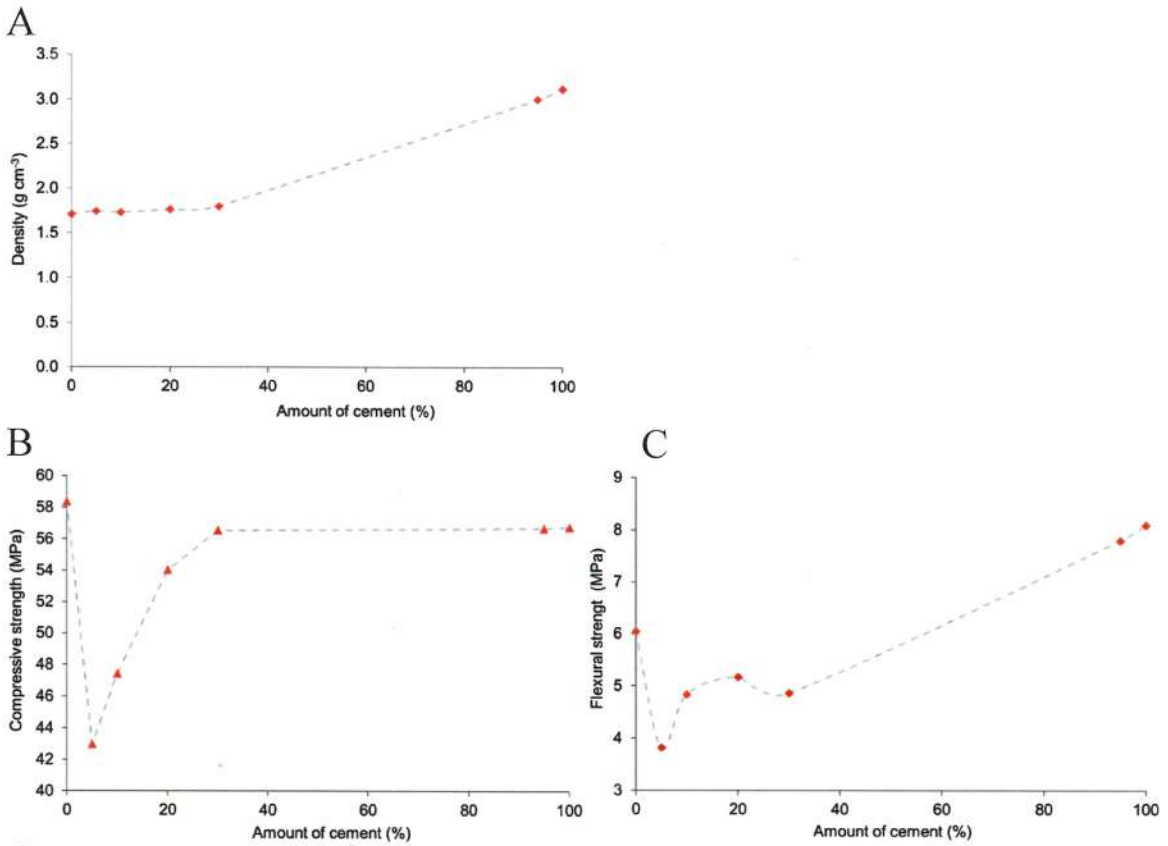

Figure S8. Density (A), compressive strength (B), and flexural strength (C) of printed hybrid samples based on fly ash (FA-0.280) depending on the content of the added cement and carried out at room temperature. The duration of ingredients mixing before test was set to 15 minutes. The tests were carried out according to the EN 196-2: 2005 + A1: 2008 standard with 600 cm^{-3} of mortar. Standard error did not exceed 10%.

Załącznik 2 – oświadczenia współautorów dotyczące publikacji P1

Kraków, dn. 23.11.2023 r.

OŚWIADCZENIE – PUBLIKACJA P1

Oświadczam, iż mój wkład w powstanie publikacji pt.: „*Hybrid Materials Based on Fly Ash, Metakaolin, and Cement for 3D Printing*" opublikowanej w czasopiśmie *Materials* w 2021 roku, nr DOI: 10.3390/ma14226874 jest zgodny z informacją zawartą w poniższej tabeli.

Jednocześnie oświadczam, iż wyrażam zgodę na wykorzystanie wyżej wymienionej publikacji jako część rozprawy doktorskiej mgr inż. Celiny Ziejewskiej.

Autor	Wkład w powstanie publikacji
Joanna Marczyk	Przygotowanie mieszanek geopolimerowych, wytwarzanie geopolimerów metodą odlewania, wytwarzanie geopolimerów i hybryd betonowo-geopolimerowych z zastosowaniem technologii druku 3D. Przeprowadzenie badań i analiza wyników: rentgenowskiej jakościowej i ilościowej analizy fazowej (XRD), obserwacji morfologii surowców i geopolimerów z zastosowaniem skaningowego mikroskopu elektronowego (SEM), analizy wielkości cząstek, badań z zastosowaniem analizatora sorpcji fizycznej, wyznaczania czasu początku i końca wiązania. Badanie konsystencji świeżych zapraw geopolimerowych metodą stożka Novikowa oraz metodą stolika rozpływowego. Przygotowanie materiałów i analiza uzyskanych wyników stabilności termicznej i zjawisk zachodzących podczas nagrzewania materiałów za pomocą sprzężonych metod analizy termicznej (DTA, TG, QMS). Przygotowanie pierwszej wersji manuskryptu, opracowanie metodyki badań, wizualizacja uzyskanych danych.

Celina Ziejewska	Przygotowanie mieszanek geopolimerowych, wytwarzanie geopolimerów metodą odlewania, wytwarzanie geopolimerów i hybryd betonowo-geopolimerowych z zastosowaniem technologii druku 3D. Przeprowadzenie badań i analiza wyników: rentgenowskiej jakościowej i ilościowej analizy fazowej (XRD), gęstości właściwej, obserwacji morfologii surowców i geopolimerów z zastosowaniem skaningowego mikroskopu elektronowego (SEM), analizy wielkości cząstek, wyznaczania czasu początku i końca wiązania. Badanie konsystencji świeżych zapraw geopolimerowych metodą stożka Novikowa oraz metodą stolika rozpływowego. Przygotowanie materiałów i analiza uzyskanych wyników: składu chemicznego metodą rentgenowskiej spektroskopii fluorescencyjnej (XRF), identyfikacji wiązań chemicznych metodą spektroskopii w podczerwieni z transformatą Fouriera (FTIR), wymywalności wodnej, promieniotwórczości naturalnej w zakresie stężenia izotopów naturalnie promieniotwórczych: ^{226}Ra, ^{228}Th, ^{40}K oraz stabilności termicznej i zjawisk zachodzących podczas nagrzewania materiałów za pomocą sprzężonych metod analizy termicznej (DTA, TG, QMS).
Szymon Gądek	Przygotowanie mieszanek betonowo-geopolimeorwych, wytwarzanie geopolimerów i hybryd betonowo-geopolimerowych z zastosowaniem technologii druku 3D.
Kinga Korniejenko	Sformułowanie problemu badawczego, opracowanie koncepcji badań, opracowanie metodyki badań, pozyskanie finansowania na poczet zrealizowanych badań i kosztów publikacyjnych.
Michał Łach	Sformułowanie problemu badawczego, opracowanie koncepcji badań, opracowanie metodyki badań, pozyskanie zasobów na poczet zrealizowanych badań.
Mateusz Góra	Udział w badaniach i analizie wyników hybryd betonowo-geopolimerowych, weryfikacja danych.
Izabela Kurek	Przeprowadzenie badań i analiza wyników hybryd betonowo-geopolimerowych: wytrzymałości na zginanie, wytrzymałości na ściskanie, gęstości, czasu początku i końca wiązania.
Marek Hebda	Sformułowanie problemu badawczego, opracowanie koncepcji badań, pozyskanie finansowania na poczet zrealizowanych badań i kosztów publikacyjnych, opracowanie metodyki badań, wizualizacja uzyskanych danych, zarządzanie zespołem badawczym, nadzór merytoryczny nad prowadzonymi badaniami, przygotowanie pierwszej wersji manuskryptu, przygotowanie ostatecznej wersji manuskryptu, korekta manuskryptu po recenzjach.

Magdalena Szechyńska-Hebda	Opracowanie metodyki badań, nadzór merytoryczny nad prowadzonymi badaniami, pozyskanie zasobów na poczet zrealizowanych badań wizualizacja uzyskanych danych, przygotowanie pierwszej wersji manuskryptu, przygotowanie ostatecznej wersji manuskryptu, korekta manuskryptu po recenzjach.

.....
podpis oświadczającego
mgr inż. Joanna Marczyk

.....
podpis oświadczającego
mgr inż. Celina Ziejewska

.....
podpis oświadczającego
mgr inż. Szymon Gądek

.....
podpis oświadczającego
dr inż. Kinga Korniejenko

.....
podpis oświadczającego
dr hab. inż. Michał Łach, prof. PK

.....
podpis oświadczającego
mgr inż. Mateusz Góra

.....
podpis oświadczającego
mgr inż. Izabela Kurek

.....
podpis oświadczającego
dr hab. inż. Marek Hebda, prof. PK

.....
podpis oświadczającego
dr hab. inż. Magdalena Szechyńska-Hebda, prof. IB PAN

Magdalena Szechyńska-Hebda	Opracowanie metodyki badań, nadzór merytoryczny nad prowadzonymi badaniami, pozyskanie zasobów na poczet zrealizowanych badań wizualizacja uzyskanych danych, przygotowanie pierwszej wersji manuskryptu, przygotowanie ostatecznej wersji manuskryptu, korekta manuskryptu po recenzjach.

.....
podpis oświadczającego
mgr inż. Joanna Marczyk

.....
podpis oświadczającego
mgr inż. Celina Ziejewska

.....
podpis oświadczającego
mgr inż. Szymon Gądek

.....
podpis oświadczającego
dr inż. Kinga Korniejenko

Podpisano przez/ Signed by:
MATEUSZ
GÓRA
Data/ Date: 27.11.2023 13:02
mSzafir

.....
podpis oświadczającego
dr hab. inż. Michał Łach, prof. PK

.....
podpis oświadczającego
mgr inż. Mateusz Góra

.....
podpis oświadczającego
mgr inż. Izabela Kurek

.....
podpis oświadczającego
dr hab. inż. Marek Hebda, prof. PK

.....
podpis oświadczającego
dr hab. inż. Magdalena Szechyńska-Hebda, prof. IB PAN

Location: Nigde, date 27.11.2023

Prof. Neslihan Doğan-Sağlamtimur
Nigde Omer Halisdemir University

STATEMENT

I declare that for the work entitled: "*Hybrid Materials Based on Fly Ash, Metakaolin, and Cement for 3D Printing*" published in the scientific journal *Materials* in 2021, DOI number: 10.3390/ma14226874, my participation consisted of substantive supervision of research and participation in writing the first version of the manuscript.

Furthermore, I consent to the use of this manuscript as a part of the doctoral dissertation of Celina Ziejewska, BEng, MSc.

.....

Signature of the co-author of the publication

materials

MDPI

Article

Influence of Waste Glass Particle Size on the Physico-Mechanical Properties and Porosity of Foamed Geopolymer Composites Based on Coal Fly Ash

Celina Ziejewska [1], Agnieszka Grela [2] and Marek Hebda [1,*]

[1] Faculty of Materials Engineering and Physics, Cracow University of Technology, Warszawska 24, 31-155 Cracow, Poland
[2] Faculty of Environmental and Power Engineering, Cracow University of Technology, Warszawska 24, 31-155 Cracow, Poland
* Correspondence: marek.hebda@pk.edu.pl

Abstract: In order to protect the environment and counteract climate change, it is necessary to take any actions that enable a reduction in CO_2 emissions. One of the key areas is research focused on developing alternative sustainable materials for construction to reduce the global demand for cement. This work presents the properties of foamed geopolymers with the addition of waste glass as well as determined the optimal size and amount of waste glass for improving the mechanical and physical features of the produced composites. Several geopolymer mixtures were fabricated by replacing coal fly ash with 0%, 10%, 20%, and 30% of waste glass by weight. Moreover, the effect of using different particle size ranges of the addition (0.1–1200 µm; 200–1200 µm; 100–250 µm; 63–120 µm; 40–63 µm; 0.1–40 µm) in the geopolymer matrix was examined. Based on the results, it was found that the application of 20–30% of waste glass with a particle size range of 0.1–1200 µm and a mean diameter of 550 µm resulted in approximately 80% higher compressive strength in comparison to unmodified material. Moreover, the samples produced using the smallest fraction (0.1–40 µm) of waste glass in the amount of 30% reached the highest specific surface area (43.711 m^2/g), maximum porosity (69%), and density of 0.6 g/cm^3.

Keywords: geopolymer; waste glass; particle size; compressive strength; leachability

Citation: Ziejewska, C.; Grela, A.; Hebda, M. Influence of Waste Glass Particle Size on the Physico-Mechanical Properties and Porosity of Foamed Geopolymer Composites Based on Coal Fly Ash. *Materials* **2023**, *16*, 2044. https://doi.org/10.3390/ma16052044

Academic Editor: Xiaoshuang Shi

Received: 31 January 2023
Revised: 24 February 2023
Accepted: 27 February 2023
Published: 1 March 2023

1. Introduction

Global economic development and perpetual growth in the world population are both connected with a continuing increase in the demand for food, water, and materials, especially for the construction industry. The worldwide annual production of cement reached 4.4 billion tons and 1.39 billion tons in 2021 and 1995, respectively [1,2]. Thus, the production of this material has increased more than threefold in a matter of 26 years and it has been estimated that 3 tons of concrete are manufactured each year per every person around the world [3]. Moreover, global warming and climate change are considered the most significant environmental issues of this millennium. Cement production, due to the decomposition of calcium carbonate ($CaCO_3$) into lime (CaO), is one of the main sources of carbon dioxide (CO_2) emissions, and therefore has a significant impact on climate change [4]. It is estimated that it generates approximately 7% of entire worldwide CO_2 anthropogenic emissions [5]. Therefore, there is an immediate need to develop new sustainable materials that will cause an effective reduction in the amount of the most common greenhouse gas, CO_2 emitted into the atmosphere [6]. Furthermore, this assumption is consistent with requirements imposed by the European Commission, which decided to reduce greenhouse gas emissions by at least 40% by 2030 compared to the level of 1990 [7].

Another important issue and serious problem nowadays is the storage of an enormous amount of post-process waste derived from extractive, metallurgical, and power industries.

Their landfill may result in ecological problems due to the impact of pollutants on soils, surface water, and groundwater. In addition, it requires financial outlays, as well as poses a risk of self-ignition. Fly ash ranks among the most substantial waste from the furnaces in coal combustion plants. Polish industry generates about 5 million tons of fly ash annually, with only a small part of it recycled [8,9].

Therefore, the prospect of using such waste products after processing as a base material for the production of geopolymers should be emphasized [10]. Geopolymer is an inorganic polymeric material obtained from silica-aluminate materials, such as metakaolin [11], fly ash [12], silica fume [13], clay [14], and red mud [15] by the geopolymerization process [16]. The geopolymer primary structure consists of $[SiO_4]^{4-}$ and $[AlO_4]^{5-}$ anions linked by an oxygen atom [17]. Geopolymers are currently becoming increasingly popular in the scientific community as well as the construction industry due to their properties, such as high fire resistance (they show stability up to 1000–1200 °C) [18], great mechanical properties, including good compressive (even more than 100 MPa) and flexural strength (up to 25 MPa) [19], frost resistance (even at the level of F300) [20], excellent dimensional stability [21], and acid resistance [22]. However, apart from the technical issues offered by geopolymers, their positive impact on the environment should also be considered. Geopolymerization is a low-cost technology, which enables the use of waste materials, reduces energy consumption, as well as decreasing the total carbon dioxide footprint because high temperatures are not required in the geopolymer manufacturing process and therefore CO_2 emissions are reduced by around 70% compared to in the process to manufacture Ordinary Portland Cement (OPC) [23–25]. Due to their properties, geopolymers are becoming more and more widely used in various industries, in applications such as materials capable of immobilization toxic substances [26], construction materials [27], structural materials [28], and protective coatings [29].

Glass is a widely used material all over the world [30] because of its properties, such as transparency [31] and chemical durability [32]. According to the literature data, the total global production of glass reached approximately 89.4 Mt in 2007 [33]. However, many end-of-life glass products or glass waste are landfilled [34,35]. The global recycling rate of waste glass reached only 21% in 2018 [36], whereas in China it was about 50% in 2021 [37] and Australia achieved 59% in 2020–2021 [38]. The rest of the material has been continuously accumulating in landfills for years because it is a non-flammable and non-biodegradable material. Waste glass may be reused in the glass industry, however, an insufficient quantity of reused glass results from, among other things, requirements for the quality of the raw material, which is necessary to obtain high-quality products. Moreover, multicolored waste glass might not meet requirements in regards to its properties after the deinking process, making it difficult to recycle it into new glass products. However, the use of recycled glass would contribute to reducing landfill volumes, managing waste, reducing CO_2 emissions, protecting the energy required to melt glass, and saving natural resources [39–41]. It was found that the addition of 10 % of glass cullet in the furnace during glass manufacturing decreases energy consumption by 3%, as well as CO_2 emissions by around 5%.

As waste glass contains large amounts of silica and alumina, it may be an alternative source of building materials. Studies indicate the possibility of using waste glass for geopolymer production [33,39]. The addition of waste glass powder can positively affect the mechanical properties of geopolymers [28,33,42,43], or their fire resistance [8]. Additionally, glass cullet can be used to produce geopolymer foams [41,42,44], as well as nonporous materials [45,46].

Waste glass is commonly used as an additive in concrete. The most beneficial effect is achieved through the application of waste glass with a particle size of 75 μm [47]. In general, there is a tendency to use waste glass characterized by small particle sizes, as a pozzolan and fine aggregate in concrete manufacturing [48]. Shi et al. [49] stated that the pozzolanic activity of waste glass is higher the finer particle size is. However, there is still a research gap relating to the application of waste glass in geopolymer foam.

In general, one of the most popular methods for producing geopolymer foam with glass is the application of the sintering process. Badanoiu et al. [50] investigated geopolymer foam based on red mud and cullet obtained using thermal treatment at 600–800 °C for 1 h. Similarly, other authors [41] used temperatures ranging from 600 °C to 750 °C for 1 h during the manufacture of geopolymers with waste glass particle sizes of 23 and 72 μm, whereas Tramontin Souza et al. [51] used temperature treatment at 900 °C for 30 min. Moreover, Siddika et al. [52] applied a sintering process for geopolymer with a particle size of D50 = 25 μm waste glass for 10–60 min at 800 °C. However, high-temperature treatment is associated with high energy consumption and carbon dioxide emissions. Therefore, there is a possibility to obtain geopolymer foam with waste glass without using the sintering process. Zhang et al. [53] explored geopolymer foams with three particle sizes of waste glass, D50 = 49.2 μm, 159.1 μm, and 302.1 μm, cured at 20–100 °C, and found that finer particles influenced the higher level of geopolymerization and improved compressive strength. Ruan et al. [54] proved that aluminium powder is a suitable foaming agent for geopolymers obtained at low temperatures (80 °C). However, to date, no study has focused on the impact of the percentage content and particle size of five different fractions of waste glass in the range between 0–1200 μm on the properties of produced foamed geopolymer composites, obtained without the application of a high-temperature treatment, and the presented work purposes complement the existing lack of information. Furthermore, researchers in previous studies [33,44,55] had used only glass waste after cleaning, without contamination. However, these proceedings required water and energy consumption, as well as having a negative impact on the environment due to the wastewater generated. Wang et al. [44,56] studied the influence of contaminated waste glass fines on the concrete behavior at 10 wt% substitutions of sand. It was found that the application of such a quantity of unwashed waste glass does not cause a higher environmental risk than the use of traditional concrete. Therefore, in the present work, unwashed waste glass with different particle diameters was used in the range of: 0.1–1200 μm; 200–1200 μm; 100–250 μm; 63–120 μm; 40–63 μm; 0.1–40 μm, with a weight fraction of from 0 to 30%, was used as an additive to geopolymers to evaluate the effect of the applied amount on the properties of produced samples. Density, porosity, specific surface area, mineralogical composition, morphology, leachability, water absorption, and mechanical properties, such as flexural strength and compressive strength were investigated. Moreover, the effect of partially replacing river sand and coal fly ash with waste glass was described.

2. Materials and Methods

2.1. Materials

Coal fly ash (with the chemical composition presented in Table 1) was supplied by the Skawina Coal Power Plant (Skawina, Poland) and it was labeled as Class F fly ash in accordance with the ASTMC618 standard [57]. The loss of ignition (LOI) of coal fly ash was 3.284 and this parameter is usually used to evaluate the residual carbon content [58]. The quartz sand was supplied by an indigenous company (Świętochłowice, Poland). Sodium silicate (Na_2SiO_3) R-145 was purchased from Chemi Kam sp. Z o.o. (Będzin, Poland). The waste glass (WG) that was applied in this study (with the chemical composition shown in Table 1) was sourced from a local supplier Grabowski Import-Export (Sędziszowa, Poland). The waste glass was derived from unserviceable brown bottles. The company crushed and ground the glass waste to obtain particles size smaller than 12 mm. Using a set of sieves and a laboratory shaker, the delivered glass waste was divided into fractions: 0.1–1200 μm; 200–1200 μm; 100–250 μm; 63–120 μm; 40–63 μm; 0.1–40 μm.

Table 1. Chemical composition of coal fly ash and waste glass.

Compound (%)	Material	
	Coal Fly Ash	Waste Glass
SiO_2	48.22	73.40
Al_2O_3	26.13	1.43
Fe_2O_3	7.01	-
FeO	-	0.45
CaO	5.12	11.30
K_2O	3.48	0.20
Na_2O	1.62	11.96
MgO	1.72	1.25
SO_3	1.11	-
TiO_2	1.11	-
P_2O_5	0.70	-
MnO	0.090	-
Cl	0.09	-

2.2. Samples Preparation

To provide a homogeneous mixture, all dry components (coal fly ash, waste glass, sand) were mixed for 2 min in a GEOLAB cement mortar mixer (GEOLAB, Warsaw, Poland). Alkali activator solution was then added to the starting materials. A mix of sodium hydroxide solution of 8 M and an aqueous solution of sodium silicate was used as an alkaline activator in a proportion of 2.5:1. The solution was prepared 24 h before use to provide complete mixing of the ingredients and reach a constant temperature. The liquid-to-solid ratio (L/S) was set at the level of 0.4 to get proper workability. The final step before the casting of samples was adding aluminum powder (5-7350 type, Benda-Lutz, Skawina, Poland) as a foaming agent (0.15% by weight). Mixtures were then put into wooden molds of the appropriate shapes and sizes. Geopolymer samples were heated in the drying apparatus (Chemland) for 24 h at 75 °C. After demolding, samples were cured at ambient conditions for 28 days.

Varied weight ratios and different particle sizes of waste glass were added to the geopolymer mixture to evaluate the effect of the used addition on the properties of the samples. The compositions of geopolymer mixtures were fixed based on the previous studies, which indicates that waste glass should be applied in quantities of 10% to 30% [47,59,60]. Therefore, three different weight ratios of waste glass were used in geopolymers: 10%, 20%, and 30%, which correspond to the calculated theoretical SiO_2/Al_2O_3 mole ratios of 5.19, 6.07, and 7.22, respectively. As a reference, a sample without added glass with a theoretical SiO_2/Al_2O_3 molar ratio of 4.48 was used. Moreover, the Na_2O/SiO_2 molar ratios were 0.14, 0.15, 0.16, and 0.17 for samples with 0%, 10%, 20%, and 30% of waste glass, respectively. The composition of the designed geopolymer samples is given in Table 2.

2.3. Analytical Methods for Raw Materials and Geopolymers Characterization

The mineralogical composition of the raw materials and geopolymers was determined by a PANalytical Aeris diffractometer (Malvern Panalytical, Almelo, The Netherlands) using Cu Kα radiation, scanning range from 10° to 100° 2θ, step size 0.003° (2θ), and measurement time per step of 340 s. High Score Plus software version 4.8 (PANalytical) equipped with the ICDD (International Center for Diffraction Data, PDF4+) database was used to identify the diffraction patterns.

The particle size distribution of the raw materials was measured using a Particle Size Analyser PSA 1190 LD (Anton Paar, Graz, Austria).

The morphology of the raw materials and geopolymers samples were examined using a Keyence VHX-E100 digital microscope (Keyence, Osaka, Japan) as well as a scanning electron microscope JEOL JSM-6390LV (JEOL, Tokyo, Japan).

Table 2. The composition of the evaluated geopolymer samples.

Designation of Samples	Composition			
	Waste Glass Quantities (%)	Waste Glass Particle Size (μm)	Coal Fly Ash (%)	Sand (%)
REF	-	-	90	10
A10	10	0.1–1200	80	10
B10	10	200–1200	80	10
C10	10	100–250	80	10
D10	10	63–120	80	10
E10	10	40–63	80	10
F10	10	0.1–40	80	10
A20	20	0.1–1200	70	10
B20	20	200–1200	70	10
C20	20	100–250	70	10
D20	20	63–120	70	10
E20	20	40–63	70	10
F20	20	0.1–40	70	10
A30	30	0.1–1200	60	10
B30	30	200–1200	60	10
C30	30	100–250	60	10
D30	30	63–120	60	10
E30	30	40–63	60	10
F30	30	0.1–40	60	10

The specific surface area of the raw materials and geopolymers was determined by the Brunauer–Emmett–Teller (BET) gas adsorption method. Before registering adsorption-desorption isotherms, the specimens were degassed at 300 °C for 24 h to remove expendable vapors and gases adsorbed on the sample surface. Nitrogen adsorption-desorption isotherms of the investigated materials were recorded using Autosorb-iQ/MP Quantachrome Instruments gas sorption analyzers (Anton Paar company, Graz, Austria).

The density of the produced geopolymers was calculated by the geometric method as the ratio of the mass to the volume of the samples. The masses of the specimens were measured using a Radwag XA 60/220/Y balance (RADWAG, Radom, Poland).

The samples intended for use in testing the mechanical properties had dimensions of 50 mm × 50 mm × 50 mm, and 200 mm × 50 mm × 50 mm for the compressive and flexural strength tests, respectively. Compressive strength tests were carried out according to the PN-EN 12390-3:2019 standard using a MATEST 3000 kN machine (MATEST S.p.A., Arcore, Italy). Flexural strength tests were performed in accordance with the PN-EN 12390-5:2019 standard on a concrete press (MATEST S.p.A., Arcore, Italy).

The leaching assessment was conducted according to the PN-EN 12457-4:2006 standard. The pH of the water extract was analyzed by the potentiometry method, at a temperature of 21.9–23.2 °C. The concentrations of zinc, cadmium, copper, lead, nickel, barium, chromium, arsenic, selenium, molybdenum, and antimony were determined by Inductively Coupled Plasma Optical Emission Spectrometry (ICP-OES). The dissolved organic carbon (DOC) content of samples was characterized by Fourier Transform Infrared Spectroscopy (FTIR). Determination of the total dissolved solids (TDS) was made by the gravimetric method. The mercury concentration was defined by Cold Vapor Atomic Absorption (CVAA) spectroscopy. The SO_4^{2-} and Cl^- ion content was measured using the ion chromatography method.

The water absorption tests were conducted in accordance with PN-88/B-06250 "Ordinary concrete" on 5 cm geopolymer cubes. The following relationship was used:

$$n_w = \frac{G_2 - G_1}{G_1} \cdot 100\ [\%] \quad (1)$$

where n_w is water absorption; G_1 is the average mass of dry samples; and G_2 is the average mass of the samples saturated with water.

ImageJ software version 1.53t was used to calculate the porosity, average cell size, and cell density of materials, using 2D photographs of geopolymer structures.

The average cell density of samples was determined based on the following equation:

$$N = \left[\frac{(nM^2)}{A}\right]^{\frac{3}{2}} [\text{cells/cm}^3] \quad (2)$$

where N is the cell density; n is the number of cells in the SEM image; A is the area of the analyzed image; and M is the magnification [61].

Regardless of the research method used and the type of materials analyzed, the measurements were performed with at least three repetitions.

3. Results and Discussion

3.1. Properties of Raw Materials

X-ray diffraction (XRD) patterns of the coal fly ash and glass waste used in the experiment as raw materials are shown in Figure 1. The qualitative X-ray diffraction analysis of coal fly ash enabled the identification of the following crystalline phases: quartz (SiO_2 card no.: 01-089-8936), mullite ($Al_6Si_2O_{13}$, card no.: 00-015-0776), hematite (Fe_2O_3, card no.: 01-079-0007), anhydrite ($CaSO_4$, card no.: 01-085-6123), and magnetite (Fe_3O_4, card no.: 01-080-6407). However, the coal fly ash also contained a broad hump in the range from 15° to 30° 2θ, suggesting the existence of amorphous components, which are primarily in charge of the reactiveness of the raw materials [62]. Quantitative X-ray analysis of the coal fly ash enabled a determination of the content of individual phases, whose shares were respectively: 50.3% SiO_2, 45.0% $Al_6Si_2O_{13}$, 2.1% Fe_2O_3, 2.4% $CaSO_4$, and 0.2% Fe_3O_4. The results of the quantitative analysis can only be considered as approximate values due to the existence of the amorphous phase, the high intensity of background noise, and overlapping reflections. The XRD pattern of the waste glass indicates that this is a completely amorphous material, different from the coal fly ash.

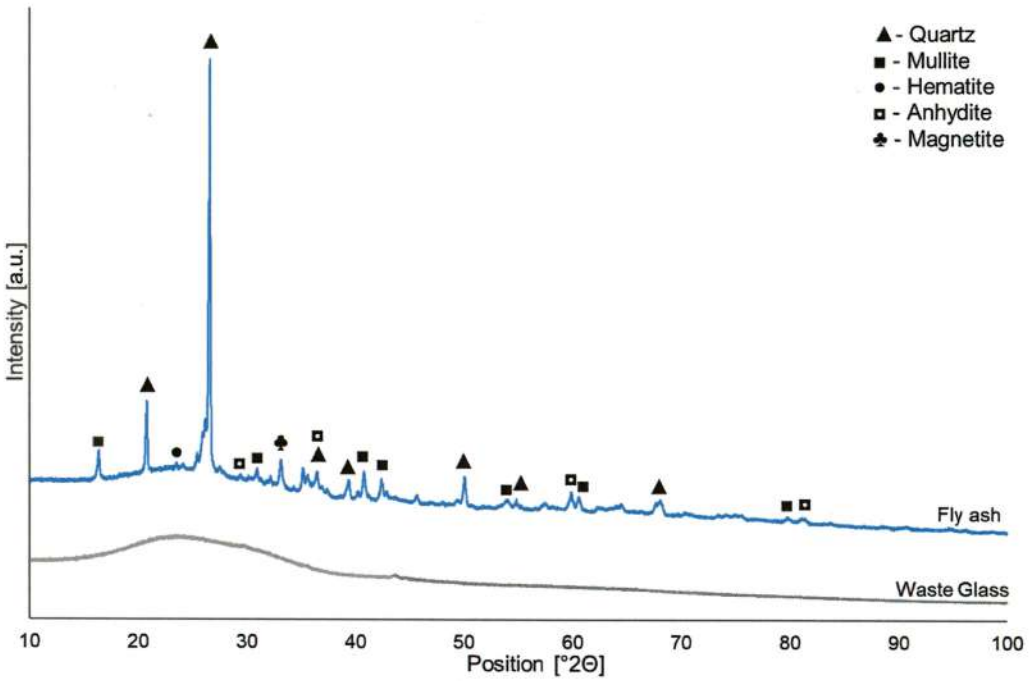

Figure 1. XRD patterns of waste glass and coal fly ash.

Figure 2 presents the particle size distribution of the coal fly ash and waste glass before and after separation into different fractions. Coal fly ash has the smallest average particle size among all used starting materials. Moreover, Table S1 in Supplementary Materials demonstrates the averaged results of the size distribution of coal fly ash and waste glass used in this study.

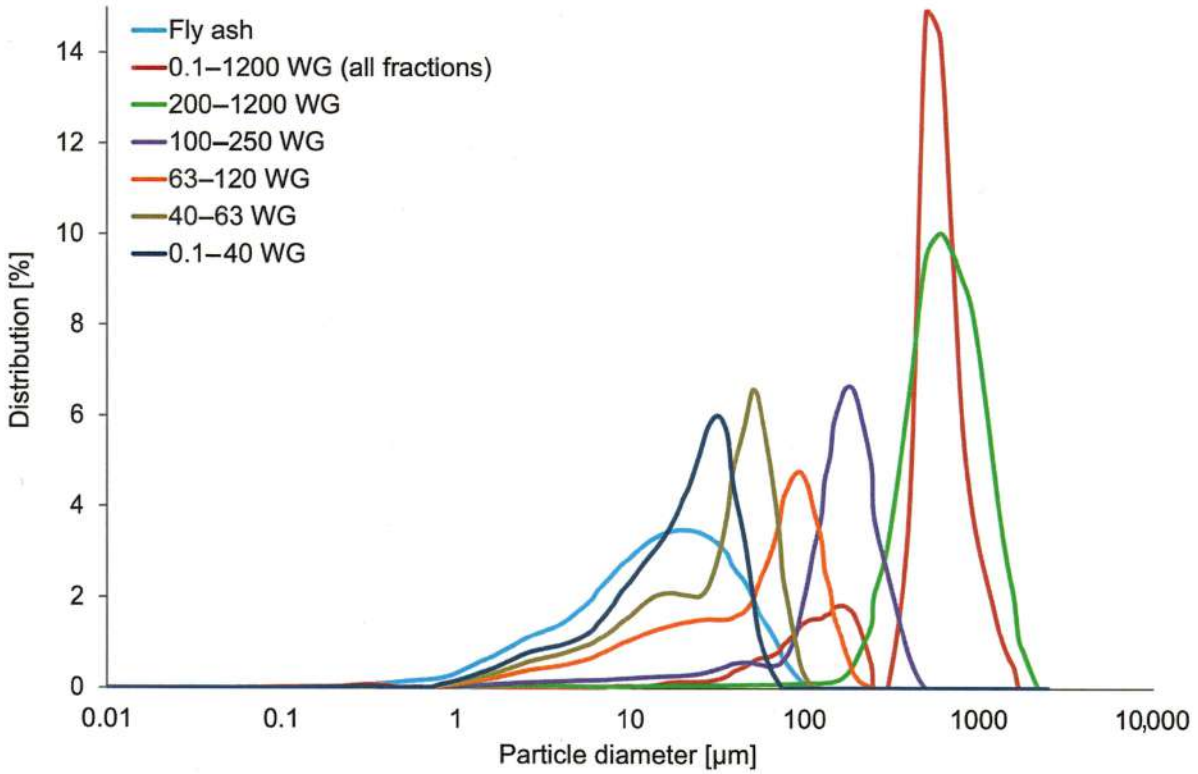

Figure 2. The particle size distribution of coal fly ash and glass waste before and after the division into different fractions.

The coal fly ash was characterized by comparable median and mean values (12.3 ± 1.3 µm and 17.3 ± 2.5 µm, respectively) and a small span range, which indicates an approximately normal particle size distribution [57]. Conversely, the as-delivered waste glass is distinguished by higher variations in this regard, with a mean particle size of 550.1 ± 18.9 µm. As can be seen in Figure 2, the particle size distribution curve of the unsorted waste glass consists of two peaks, representing particles about 170 µm and 600 µm in size. Moreover, in the case of the waste glass after division into fractions, the mean particle size was 584.9 ± 4.4 µm, 155.2 ± 0.5 µm, 55.4 ± 1.2 µm, 33.3 ± 0.1 µm, and 19.8 ± 0.3 µm, which was adequate for 0.1–1200 WG, 100–250 WG, 63–120 WG, 40–63 WG, and 0.1–40 WG. The obtained results were in line with expectations.

Figure 3a–g illustrates the morphology of the raw materials. The as-delivered waste glass consisted of particles of varying shapes and sizes (Figure 3a). Furthermore, the obtained images also confirmed the effectiveness of sieving concerning the obtained particle size and distribution of waste glass. The coal fly ash consisted of many porous particles of various sizes and shapes, such as spherical, irregular, and angular, but consisted predominantly of spherical particles. Such a morphology of coal fly ash has a beneficial effect on the geopolymerization process, as it enhances its reactivity [63].

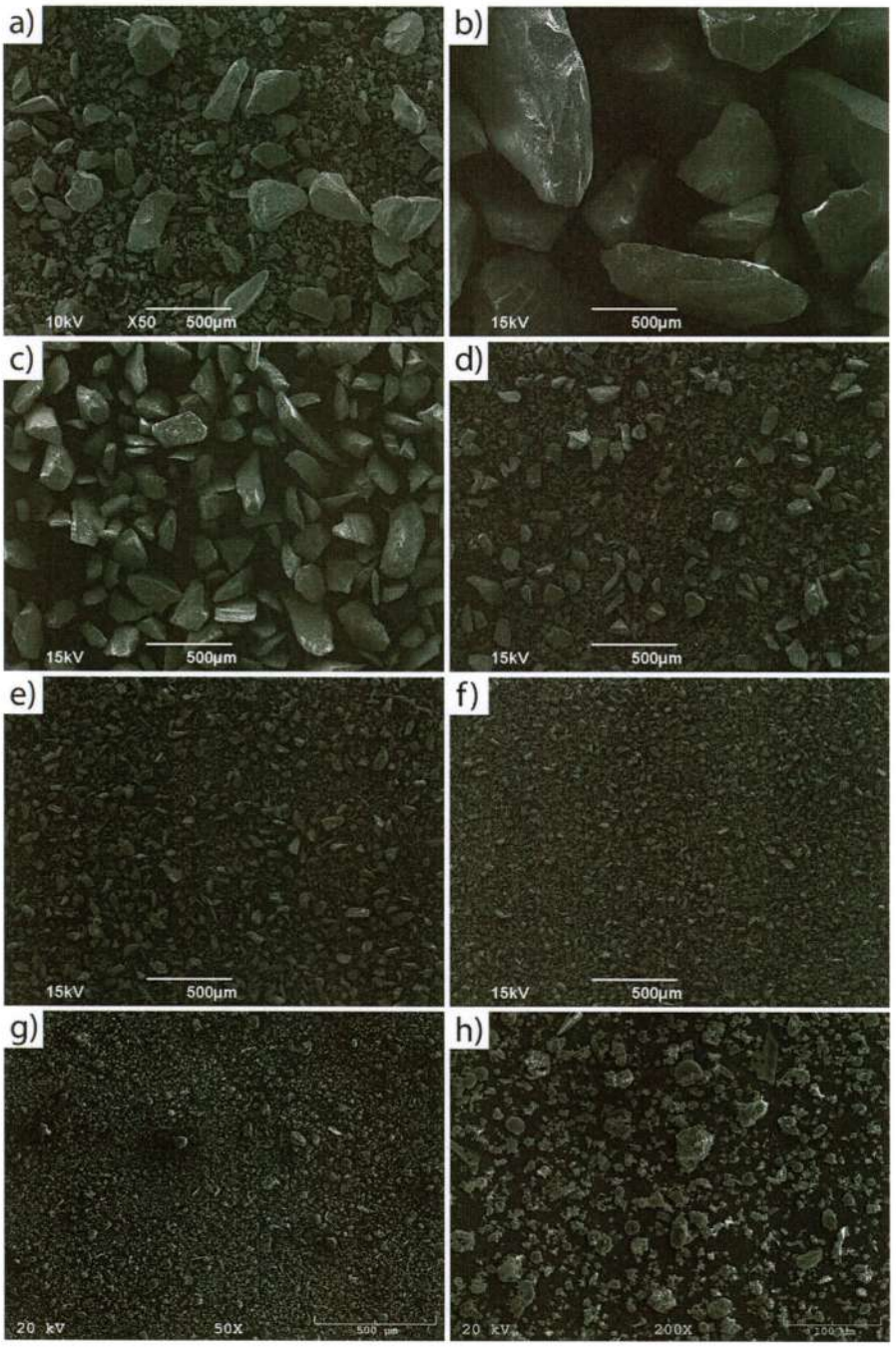

Figure 3. SEM images of waste glass with different particle sizes: (**a**) 0.1–1200 WG (all fractions), (**b**) 200–1200 WG, (**c**) 100–250 WG, (**d**) 63–120 WG, (**e**) 40–63 WG, (**f**) 0.1–40 WG and (**g**,**h**) coal fly ash.

The nitrogen adsorption-desorption isotherms of coal fly ash and the as-delivered waste glass (all fractions WG) are presented in Figure 4, whereas the isotherms of waste glass after separation into different fractions are shown in Figure S1 in Supplementary Materials. The specific surface area was determined by using the multi-BET method and was found to be 7.804 m^2/g and 0.152 m^2/g for coal fly ash and unsorted brown waste glass, respectively. Moreover, the specific surface area of waste glass after separation into five different fractions reached the following values: 0.048 m^2/g for 200–1200 WG, 0.114 m^2/g for 100–250 WG, 0.375 m^2/g for 63–120 WG, 0.594 m^2/g for 40–63 WG, and 0.693 m^2/g for 0.1–40 WG. Based on the IUPAC (International Union of Pure and Applied

Chemistry) classification, the N_2 isotherms of coal fly ash and waste glass correspond to type II isotherms with an H3-type hysteresis loop. Type II nitrogen adsorption-desorption isotherm indicates that the investigated material was non-porous or microporous, as well as having a comparatively low surface area [64,65].

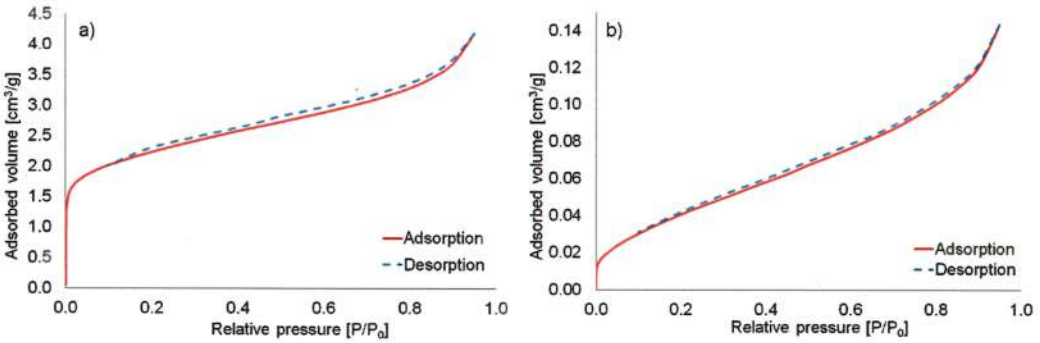

Figure 4. Nitrogen adsorption-desorption isotherms of (**a**) coal fly ash; (**b**) unsorted waste glass.

3.2. Properties of Produced Geopolymers

Figure 5 shows the density results of the produced geopolymer samples including waste glass determined using the geometrical method after 28 days of seasoning. The reference sample, not containing added waste glass, demonstrated a density of 0.69 ± 0.04 g/cm^3. On the basis of the obtained results, a visible effect of increasing density with higher content of waste glass was observed. A similar tendency was noticed by other authors [66–69]. Siddika et al. [47] observed that a higher content of waste glass increased the density and reduced the porosity of cement concrete. In contrast, regarding the effect of the particle size of the waste glass on the density of the materials produced, it was generally found that the use of a smaller additive size resulted in a decrease in geopolymer density. This effect was independent of the proportion of the introduced addition of glass waste to the matrix.

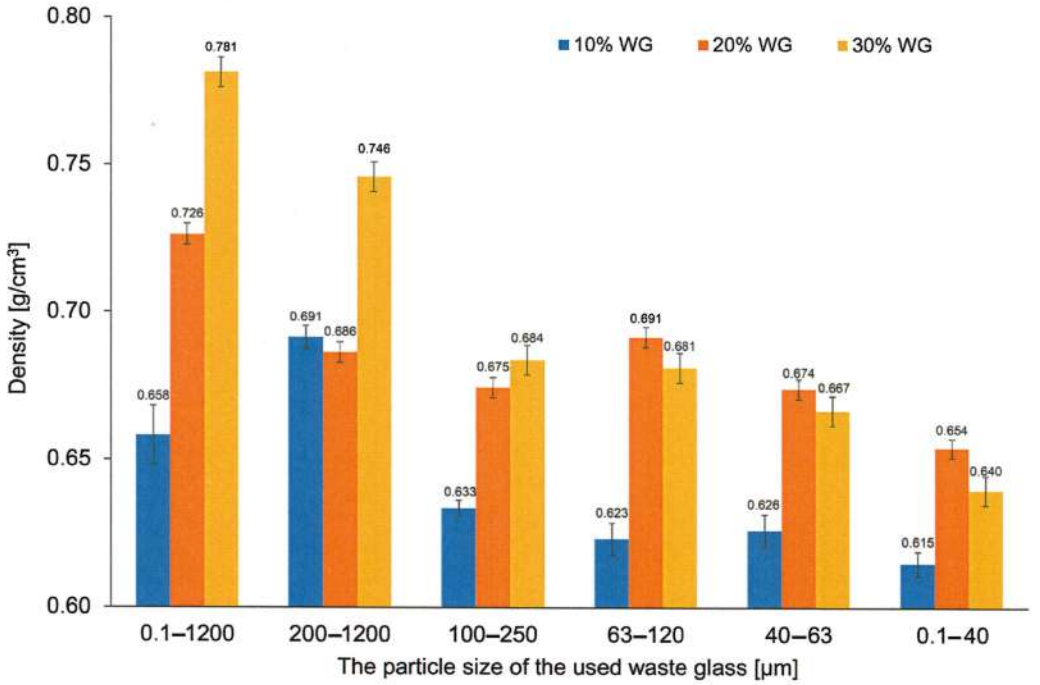

Figure 5. The density of geopolymers depending on the percentage and size of the fraction of the waste glass addition.

As can be seen, the density of geopolymers with added waste glass with a particle size up to 120 µm (0.1–40 WG, 40–63 WG, 63–120 WG) was the highest for samples containing 20% of waste. Similar findings were obtained by Ahmad et al. [70] who investigated the properties of concrete with the addition of waste glass with a particle size of up to 75 µm. It was concluded that waste glass undergoes a pozzolanic reaction, creating additional C-S-H gel resulting in an increase in the viscosity and density of the blends. At the same time, the higher content of waste glass hinders the compaction process, causing the formation of a larger number of pores and thereby decreasing material density.

The specific surface area (calculated using the BET equation) of the produced geopolymers was significantly higher than that of the raw materials and in the case of the reference sample, without the addition of waste glass, it reached a value of 22.772 m^2/g. The addition of unsorted waste glass caused an increase in the surface area by up to 65% in the case of the A20 sample. Moreover, it was found that the decrease in the size of the waste glass particles introduced into the matrix resulted in an increase in the specific surface area of the produced composite. Janowska-Renkas et al. [66] confirmed that waste glass with lower particle sizes is characterized by higher surface area. The decrease in particle sizes of waste glass, and therefore the increase in their specific surface area cause increased pozzolanic reactivity [47]. Coal fly ash has a higher surface area than waste glass; therefore, increasing the amount of used waste cullet and consequently reducing the applied coal fly ash in specimens with unsorted waste glass should increase their surface area, which would be entailed by the summation of their properties. However the specific surface area of the A20 and A30 samples amounts to 37.556 m^2/g and 36.435 m^2/g, respectively, and, therefore, this trend is not clearly visible here due to the wide and somewhat random range of particle sizes of waste glass or the structure of the samples. All the designated values of BET are shown in Table S2 in Supplementary Materials.

All the obtained adsorption-desorption isotherms (Figure 6) of produced geopolymers based on coal fly ash with the addition of waste glass can be qualified as IV type with an H3 hysteresis loop in compliance with IUPAC categorization [71]. The obtained IV type of adsorption-desorption isotherms is a typical result of the investigation of mesoporous samples with 2–50 nm diameter [72]. The presence of hysteresis is a result of condensation within the capillaries of slit-shaped mesoporous structures [73,74].

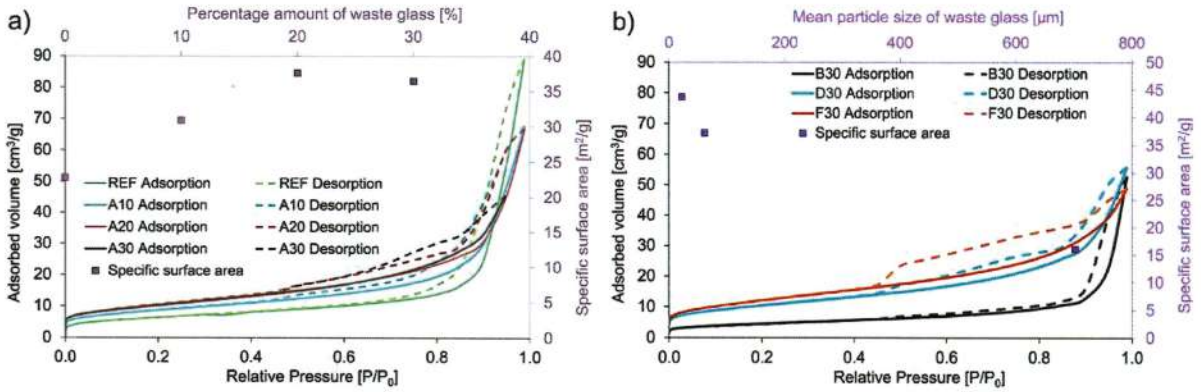

Figure 6. The nitrogen adsorption-desorption isotherms of geopolymers with the addition of waste glass with (**a**) various amounts by weight (0–30%); (**b**) different diameters of particle sizes.

The result of various amounts of waste glass addition on the mineralogical composition of the geopolymers is presented in Figure 7. After the geopolymerization process, the obtained samples contained crystallized phases, such as quartz (SiO_2, card no.: 01-075-8320) as the primary phase occurring in geopolymers because of the substantial silica amount [75], as well as mullite ($Al_6Si_2O_{13}$, card no.: 01-082-1237), and hematite (Fe_2O_3, card no.: 01-079-0007), which indicate the presence of unreacted elements from the raw materials [76,77]. However, the diffuse broad hump between 20–40° 2θ in all specimens proves the presence

of an amorphous component in the form of C-S-H gel (as a Rosenhahnite, card no.: 00-029-0378). This is also confirmation that the geopolymerization process took place [78,79]. C-S-H gel developed due to the adequate content of calcium oxide in the starting materials [80]. On the basis of the obtained results, it can be concluded that the change in the amount of glass waste addition as well as the size of their fractions had a negligible effect on the type of mineralogical composition present in the produced geopolymers. The degree of crystallinity of the geopolymers based on their XRD pattern was also determined, and it reached the following levels: 0.324 for REF, 0.322 for A10, 0.308 for A20, 0.248 for A30, 0.230 for B30, 0.248 for D30, and 0.270 for F30.

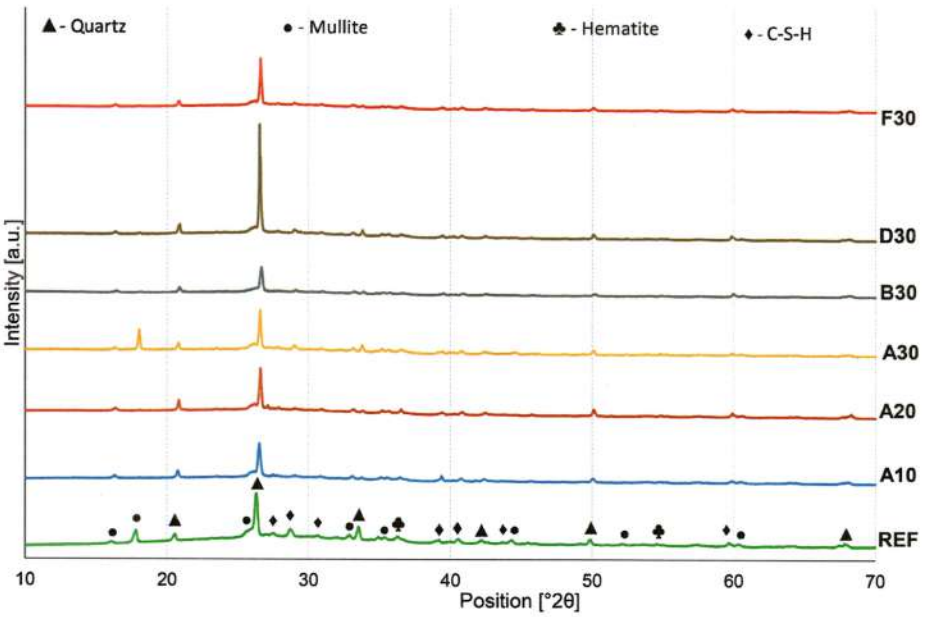

Figure 7. The XRD patterns of geopolymers with varying waste glass content.

It is well known that porosity depends on various factors, such as the type and fineness of the foaming agent [81], stabilizer [82], alkali content [83], curing temperature [84], and the type of raw materials [85]. The influence of waste glass on the obtained porosity of geopolymers is shown in Figure 8. An example of the determination of porosity is presented in Figure S2 in Supplementary Materials. In the presented study, the porosity of the geopolymers with waste glass ranged from 50.3% to 68.5%, whereas for reference specimens it was 50.5%. The application of unsorted waste glass in the amount of 30% resulted in a reduction in porosity of 9.5% in comparison to the reference material; while reducing the amount of additive introduced to 20% or 10% caused the opposite effect.

The effect of waste glass on the compressive strength of the geopolymers is shown in Figure 9. On the basis of the results, it was noticed that the highest results were obtained for foams containing unsorted waste glass. The addition of 20% as well as 30% of unsorted glass waste to the geopolymer increased the compressive strength of samples by 80% compared to the reference specimens, tested after 28 days of curing. In general, the higher compressive strength of geopolymers with the addition of waste glass may result from a more efficient pozzolanic reaction due to higher access to dissolved aluminum and silica [30]. Moreover, the application of this type of waste glass is also an environmentally and economically friendly solution due to the elimination of the necessity to use additional processing such as grinding or crumbling. At the same time, it should be noted that the use of the addition of waste glass in the same proportion but with a different particle size may result in obtaining different effects than for unsorted glass. For example, the use of waste glass with a particle size of up to 63 µm, initially up to 20% of the additive, increases

the compressive strength, however, the samples containing 30% of the additive showed a decrease in properties even below the values obtained for the reference materials.

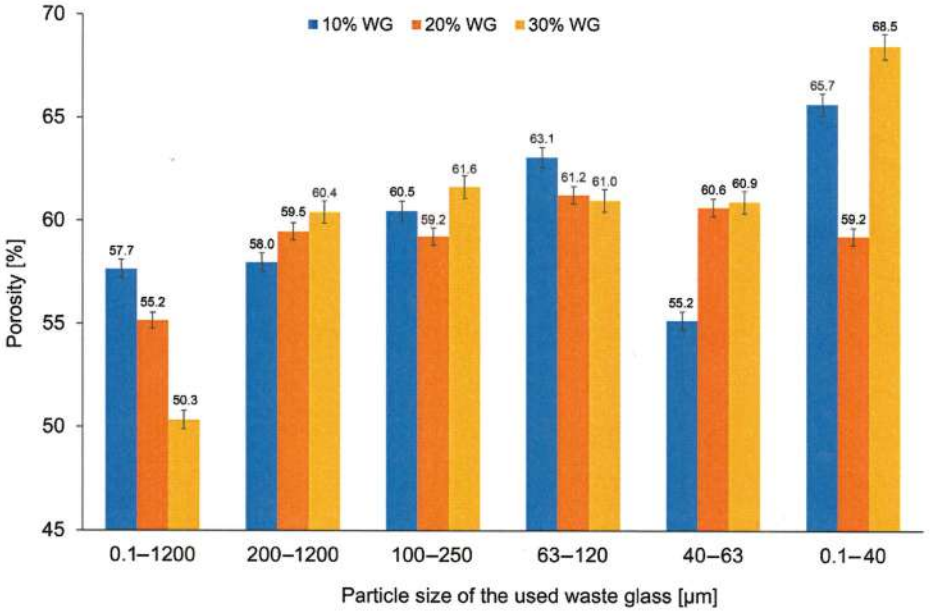

Figure 8. The porosity of geopolymers depending on the percentage and size of the fraction of the waste glass addition.

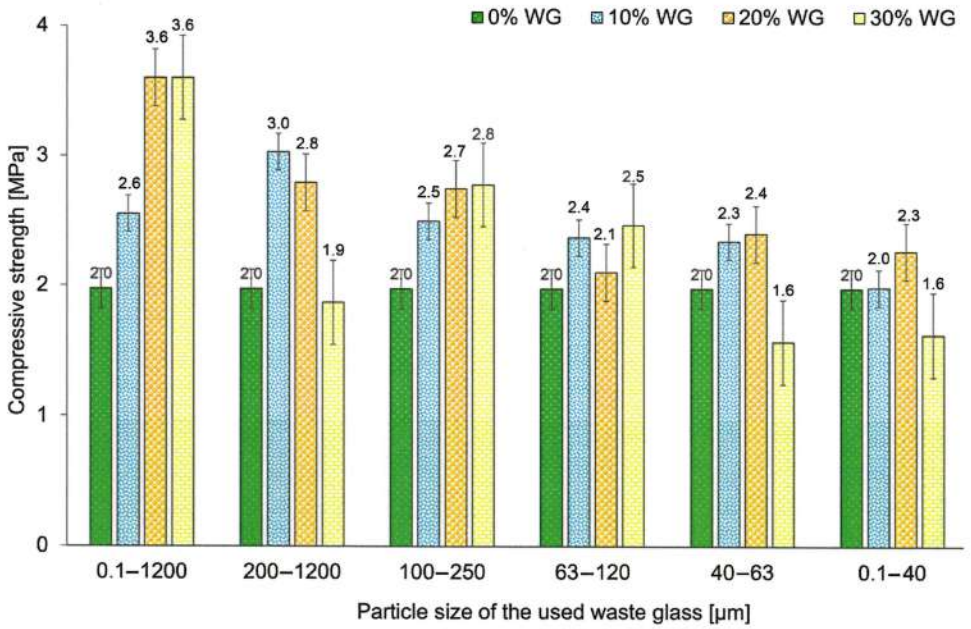

Figure 9. The compressive strength of geopolymers depending on the percentage and size of the fraction of the waste glass addition, after 28 days of curing.

The obtained results for compressive strength are consistent with the results of porosity presented earlier. Generally, it can be stated that increasing the porosity of the geopolymers decreased the compressive strength. A similar observation was made by Deng et al. [86], who noticed that the increase in strength was related to the filling of the existing porosity in the material by glass additive.

The influence of waste glass content and particle size on the flexural strengths of geopolymers is presented in Figure 10. The incorporation of waste glass reduced the

flexural strength of all samples, regardless of the particle size and amount of waste glass used for geopolymer synthesis. A similar effect was noticed by Ali et al. [87] and Toniolo et al. [88] in their studies. However, the effect of waste glass particle size is clearly visible here. The flexural strengths of samples tended to increase along with the application of smaller particle sizes of the introduced additive.

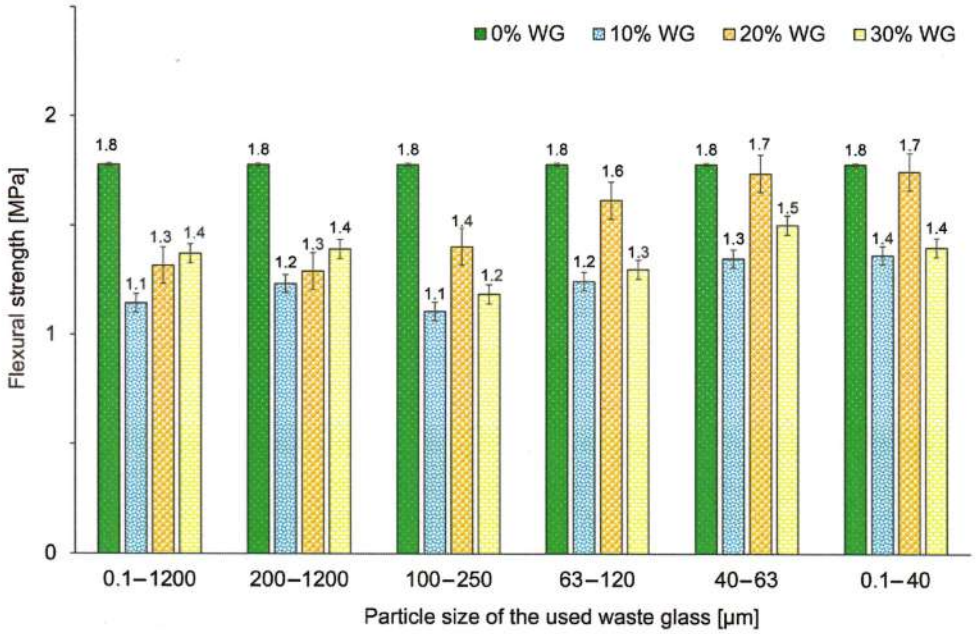

Figure 10. The flexural strength of geopolymers depending on the percentage and size of the fraction of the waste glass addition, after 28 days of curing.

Siddika et al. [47] indicated that the particle size of waste glass should be in the range of 38–75 µm to obtain the optimal value of pozzolanicity as well as silica dissolution in concrete. When considering the influence of waste glass with particle sizes ranging from 100–250 µm, 63–120 µm, 40–63 µm, and 0.1–40 µm on the flexural strength, the highest values were reached for 20% content of the cullet. A possible explanation for this phenomenon is the developing value of the Na_2O/SiO_2 ratio in the geopolymers. After exceeding the optimal value, the additional Na^+ ions may have resulted in excessive efflorescence, as well as a strength decrease [89]. The specimens containing bigger particle sizes of waste glass (0.1–1200 WG and 200–1200 WG) present an increasing trend in flexural strength with increasing incorporation of waste from 10% to 30%, but the obtained results are significantly lower than the reference material. Tahwia et al. [60] noticed that the incorporation of waste glass may result in the appearance of empty voids within the material due to their particle angularity and this may result in reduced mechanical properties. Even though the flexural strengths of the specimens are decreased due to the incorporation of waste glass, it should be noticed that samples included 20% of cullet with a particle size of up to 0.1 mm (D20, E20, F20) have results close to the values of the reference sample.

Based on the results obtained it can be concluded that the use of waste glass can significantly influence the mechanical properties of geopolymers by reducing their flexural strength and simultaneously increasing their compressive strength. Moreover, it was noticed that there is no correlation between compressive strength and flexural strength [90]. A similar effect, which is the opposite of the relations occurring in concrete technology in which compressive strength is associated with flexural strength, was also observed by other researchers [91–93]. The different fracture processes in both types of loads could be the reason for this phenomenon. Moreover, in the presented study, foamed samples were investigated. The pore size and their distribution affect the mechanical properties of

geopolymer, as well as the material's fracture resistance. Furthermore, the distribution of the additive has a crucial impact on the fracture properties of geopolymers.

Leaching test results from the geopolymer samples are presented in Table S3 in Supplementary Materials. Introducing a supplement in the form of waste glass particles into geopolymers proved to have an insignificant influence on the content of heavy metals such as Hg, Cd, Ni, Cr, Cu, Zn, and As in the leachates. Only the content of Pb is higher for geopolymers with the addition of the lowest particle size of waste glass than in the case of the reference material. The higher Pb content in the F30 leachates resulted from the dissolution of metals from the glass particle surface, which increases with the reduction in the particle size (Table S2 in Supplementary Materials) [94]. Shi et al. [95] noticed a similar tendency that, with increasing particle size, the content of Pb decreases, and it was concluded that it is related to the type of additives in the geopolymer structure. Bobirică et al. [96] investigated the leaching behavior of geopolymers with the addition of waste glass obtained from worn linear fluorescent lamps. It was found that Pb was leached in a larger amount in the case of geopolymers characterized by finer particle sizes.

The content of all examined hazardous metals in geopolymers was within the range of leaching limit values for inert waste in compliance with European Council Decision 2003/33/EC [57,97] except for the level of total dissolved substances, which is beyond the range of values for inert waste. However, it is below the limit of non-hazardous waste. It can be associated with the porosity and density of the produced geopolymers. Within samples with 30% of various sizes of waste glass, the highest concentration of TDS was reached for F30, which has the highest porosity and smallest density.

The influence of the content of unsorted waste glass (with particle size from 0.1 μm to 1200 μm) on the geopolymer structure depending on the percentage is presented in Figure 11, while the effect of the particle size for the samples containing 30% of the waste glass addition is presented in Figure 12. It was found that, with an increase in the content of the unsorted waste glass, the pores had smaller diameters and were more evenly distributed in the geopolymer structure. Moreover, the addition of waste cullet has a beneficial influence on the homogeneity of the porous structure of the samples. It is well known that porosity has a fundamental influence on a material's compressive strength [98]. Samples without the addition of waste cullet have large porous macrostructures, which can cause deterioration of mechanical properties. The pictures presented in Figure 12 show that a significant amount of large-sized pores was generated as a result of the application of waste glass with larger diameters. In general, the size of the pore reduces with the reduction in waste glass particle size.

The correlation between cell density and cell size is presented in Figure 13. In general, with the increase in the introduced waste glass, the cell size of geopolymers decreased. However, an opposite relationship existed between cell density and waste glass content, and with increasing waste glass addition, cell density also increased. A similar tendency was also noticed by Fei et al., who proved that introducing the additive into a polymer resulted in a larger average cell size and smaller cell density of the investigated material [99]. On the basis of the presented results for geopolymers with different percentage amounts of waste glass (D50 = 483.4 μm), it can be concluded that samples with 30% of WG have the highest density (0.079 cells/cm^3) and the smallest cell size (2233 μm).

Representative SEM images of foamed geopolymers with 0% and 30% content of unsorted waste glass (0.1–1200 WG) are shown in Figure 14. It was noticed that the reference geopolymer sample had a homogeneous porous compact microstructure. However, in the geopolymer microstructure with the addition of glass waste, one can observe spherical particles of unreacted coal fly ash and particles of undissolved waste cullet (with irregular shapes, smooth surfaces, and sharp edges) in the geopolymer matrix. The presence of such undissolved glass particles influenced the leachability results described earlier.

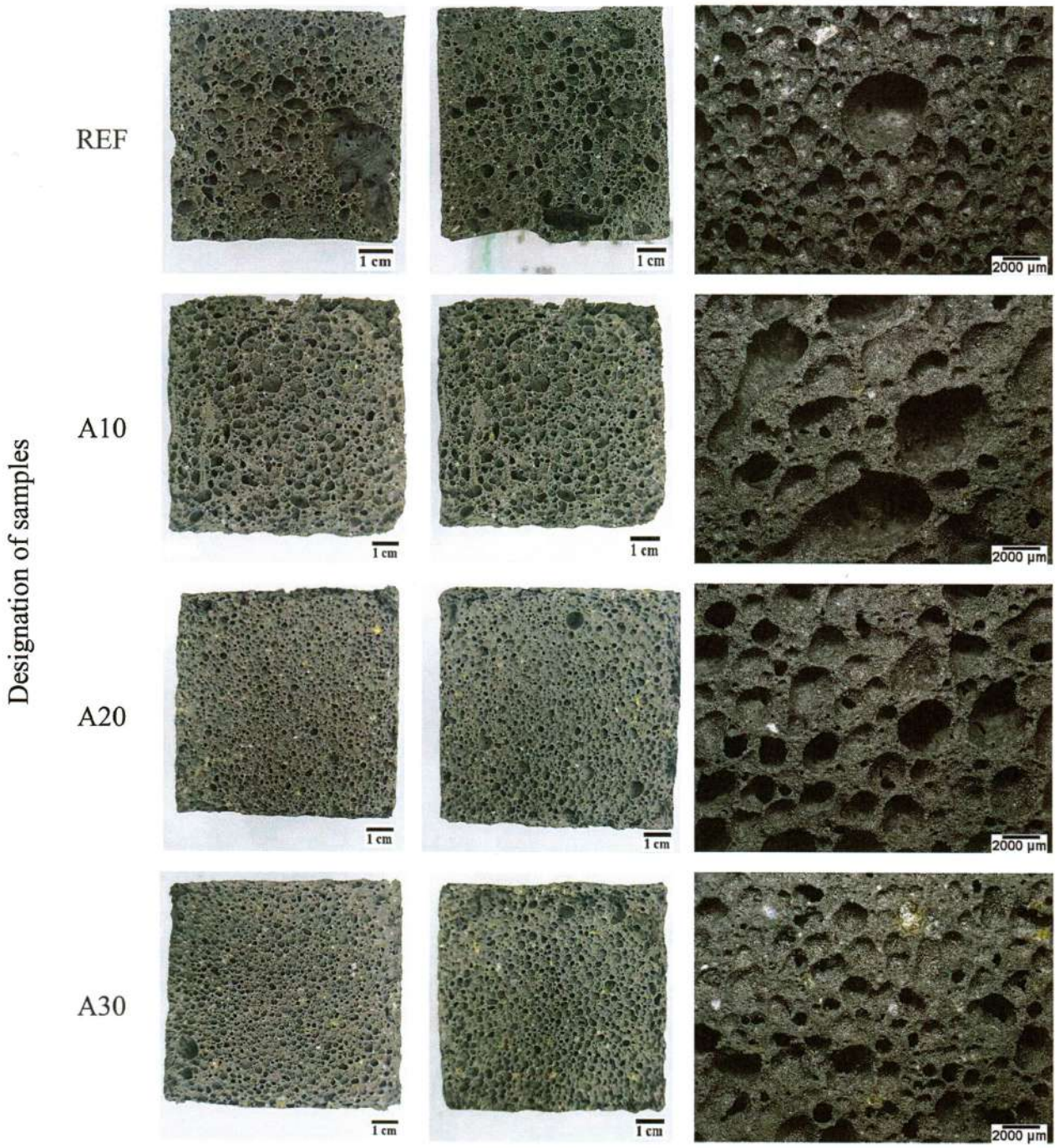

Figure 11. The structure of the geopolymer with waste glass with a particle size of 0.1–1200 µm, depending on the waste glass content.

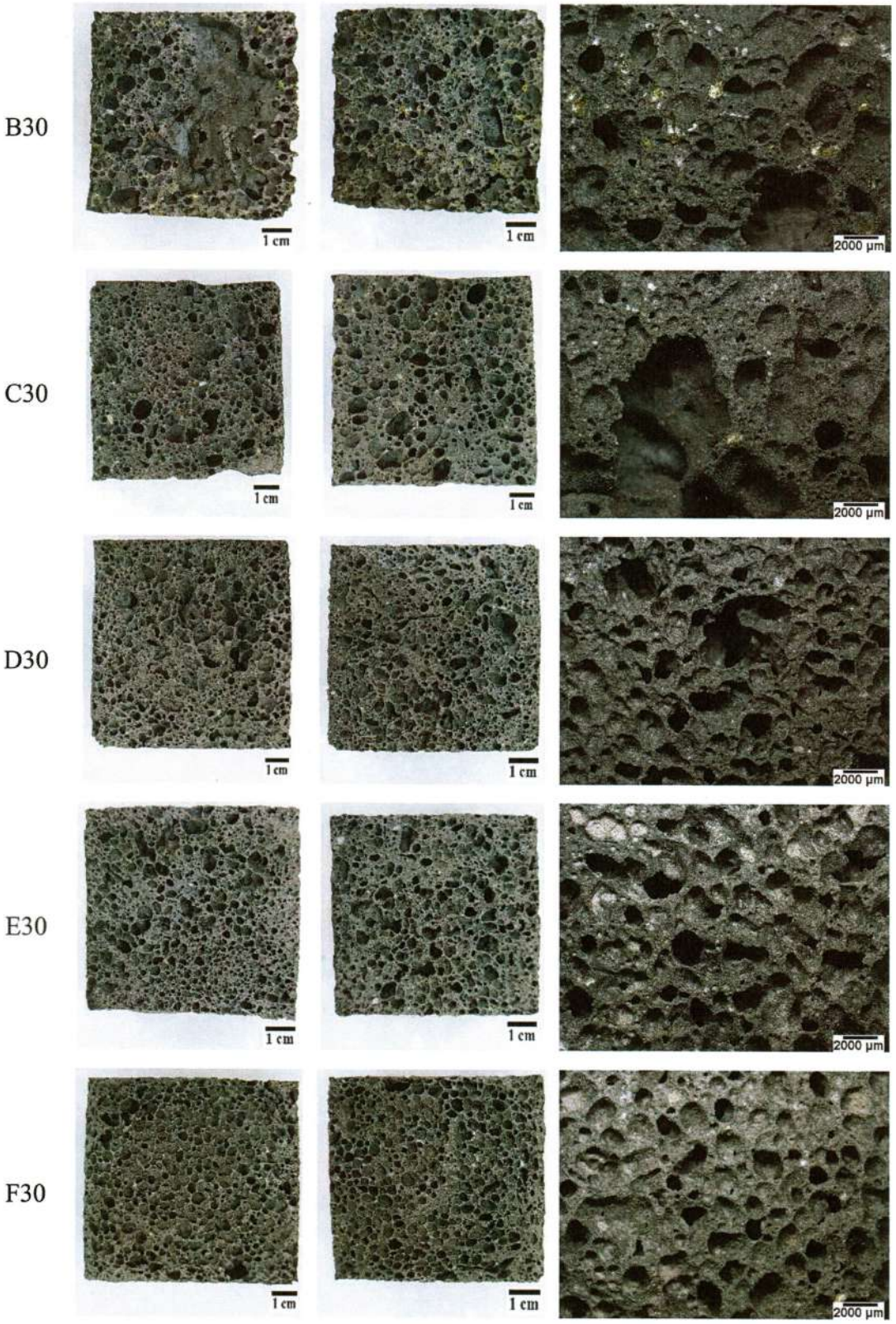

Figure 12. The structure of the geopolymer with the 30% addition of waste glass, depending on the particle size fraction.

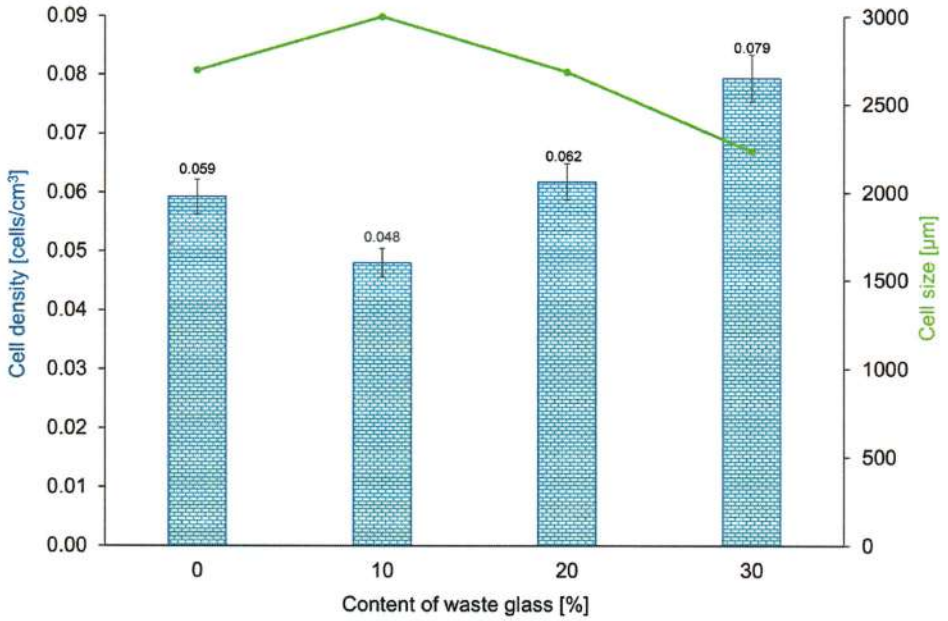

Figure 13. Cell size and cell density of geopolymers with the addition of waste glass with various amounts by weight (0–30%).

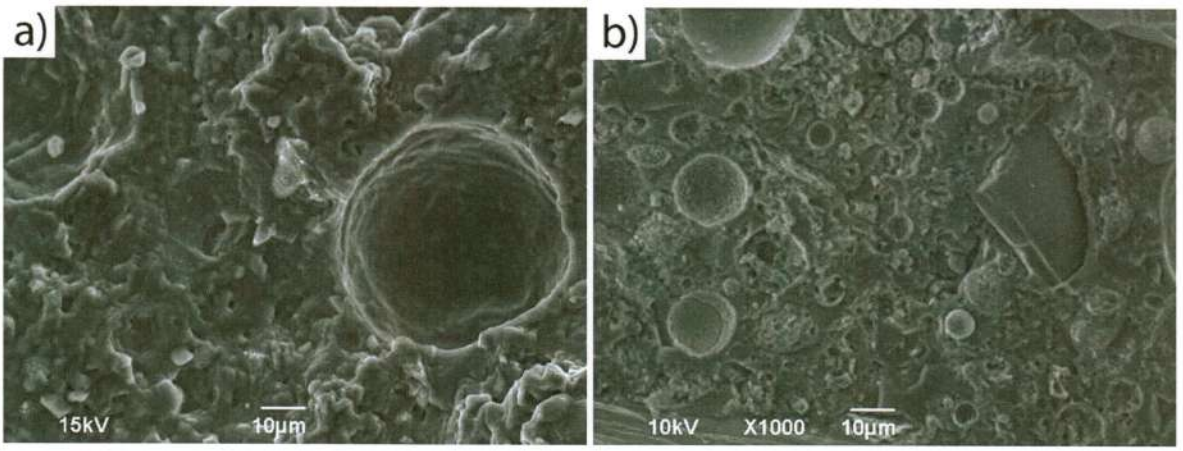

Figure 14. SEM microstructure of geopolymer samples: (**a**) REF; (**b**) A30%.

Figure 15 shows the water absorption results of the geopolymer samples containing varying amounts of waste glass. In general, water absorption depends on the voids content present in the examined materials [100]. On the basis of the obtained results, it was found that the water absorption of the geopolymers tends to decrease with increasing waste glass content. Thus, the addition of waste glass to the geopolymer matrix fills the pores formed, changes the porosity morphology, and influences capillary processes; it also increases the packing of particles in the geopolymerization process [101]. For the geopolymers with 10%, 20%, and 30% of unsorted waste glass, the decrease in water absorption relative to the reference sample was 15.8%, 22.5%, and 26.7%, respectively.

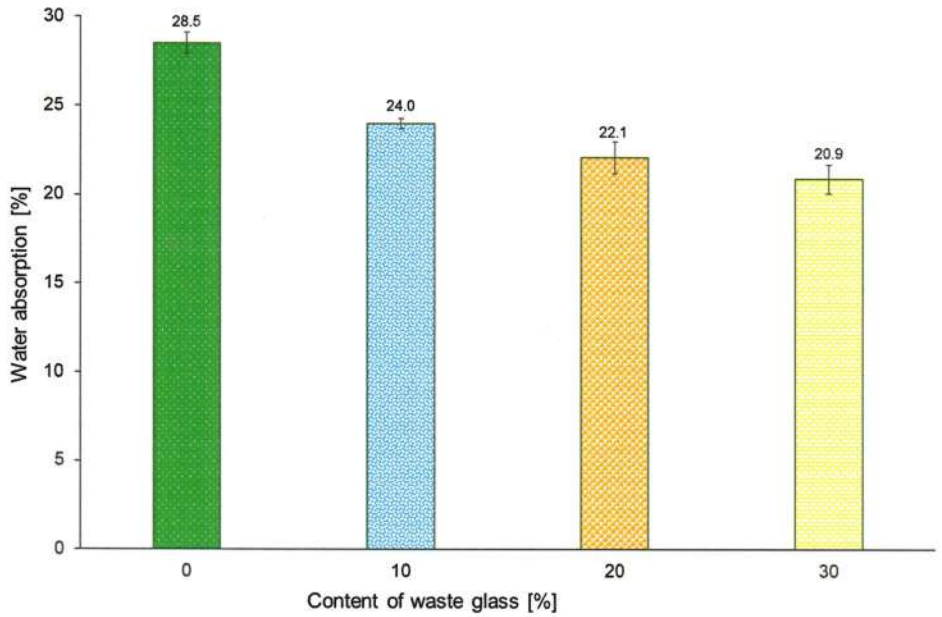

Figure 15. Water absorption of geopolymer samples containing varying amounts of unsorted waste glass.

4. Conclusions

For the first time, the impact of content and particle size of the addition of waste glass ranged between 0–1200 μm and divided into five fractions on foamed geopolymer composites was characterized. The density, specific surface area, mineralogical composition, compressive strength, flexural strength, leachability, water absorption, and porosity of foamed geopolymers were determined.

Based on the presented results, it was found that the content and particle size of waste glass both have a crucial impact on the porosity of the geopolymers. The formation of smaller, evenly distributed pores in the geopolymer structure can be achieved by increasing the content of waste glass with a particle size of 0.1 to 1200 μm or reducing the size of the added waste glass particles. The highest porosity (68.5%) was achieved by samples with 30% of waste glass with the smallest particle sizes (0.1–40 μm). Moreover, an increase in the weight share of waste glass, as well as a decrease in their particle size range, causes a higher BET surface area of the geopolymer. The compressive strength of coal fly ash-based geopolymers can be controlled by waste glass addition.

The application of 20–30% of unwashed and unsorted waste glass (550.1 μm mean particle size) μm to the geopolymer matrix resulted in 65–60% higher specific surface area, 6–9% higher density, and 80% higher compressive strength compared to the unmodified samples. Furthermore, it is an economical and environmentally friendly solution to use this type of waste glass, due to the reduced energy consumption and costs associated with grinding or sorting raw materials.

Moreover, the results of leaching tests confirm that these types of materials can be classified as non-hazardous waste in accordance with the European Council Decision 2003/33/EC. Potential applications of the geopolymer composites described in this paper include materials for the manufacture of porous prefabricated elements, as well as materials for hardening outdoor pavings. Future research will focus on determining environmental and fire resistance for these types of materials.

Supplementary Materials: The following supporting information can be downloaded at: https://www.mdpi.com/article/10.3390/ma16052044/s1.

Author Contributions: Conceptualization, C.Z., A.G. and M.H.; Formal analysis, C.Z., A.G. and M.H.; Funding acquisition, M.H.; Investigation, C.Z.; Methodology, C.Z., A.G. and M.H.; Resources, C.Z. and M.H.; Supervision, M.H.; Visualization, C.Z. and M.H.; Writing—original draft, C.Z. and M.H.; Writing—review & editing, C.Z. and M.H. All authors have read and agreed to the published version of the manuscript.

Funding: This research was supported by the POLI DOCTUS project: "ROAD TO EXCELLENCE—a comprehensive university support programme" implemented under the Operational Programme Knowledge Education Development 2014–2020 co-financed by the European Social Fund WND-POWR.03.05.00-00-Z214/18.

Institutional Review Board Statement: Not applicable.

Informed Consent Statement: Not applicable.

Data Availability Statement: Not applicable.

Conflicts of Interest: The authors declare no conflict of interest. The funders had no role in the design of the study; in the collection, analyses, or interpretation of data; in the writing of the manuscript, or in the decision to publish the results.

References

1. Belaïd, F. How Does Concrete and Cement Industry Transformation Contribute to Mitigating Climate Change Challenges? *Resour. Conserv. Recycl. Adv.* **2022**, *15*, 200084. [CrossRef]
2. Marey, H.; Kozma, G.; Szabó, G. Effects of Using Green Concrete Materials on the CO2 Emissions of the Residential Building Sector in Egypt. *Sustainability* **2022**, *14*, 3592. [CrossRef]
3. Gagg, C.R. Cement and Concrete as an Engineering Material: An Historic Appraisal and Case Study Analysis. *Eng. Fail. Anal.* **2014**, *40*, 114–140. [CrossRef]
4. Gibbs Michael, J.; Soyka, P.; Conneely, D. CO_2 Emissions from Cement Production. In *Good Practice Guidance and Uncertainty Management in National Greenhouse Gas Inventories*; IPCC: Geneva, Switzerland, 2000.
5. Strunge, T.; Naims, H.; Ostovari, H.; Olfe-Kräutlein, B. Priorities for Supporting Emission Reduction Technologies in the Cement Sector–A Multi-Criteria Decision Analysis of CO_2 Mineralisation. *J. Clean. Prod.* **2022**, *340*, 130712. [CrossRef]
6. Fletcher, W.D.; Smith, C.B. Introduction. In *Reaching Net Zero: What It Takes to Solve the Global Climate Crisis*; Elsevier: Amsterdam, The Netherlands, 2020; pp. 1–8. [CrossRef]
7. Ćirović, M.D. Risk Analysis of the European Union 2030 Greenhouse Gas Emission Target Compliance. *Int. J. Glob. Warm.* **2018**, *16*, 64. [CrossRef]
8. Strzałkowska, E. Morphology, Chemical and Mineralogical Composition of Magnetic Fraction of Coal Fly Ash. *Int. J. Coal. Geol.* **2021**, *240*, 103746. [CrossRef]
9. Cieślik, E.; Fabiańska, M.J. Preservation of Geochemical Markers during Co-Combustion of Hard Coal and Various Domestic Waste Materials. *Sci. Total Environ.* **2021**, *768*, 144638. [CrossRef]
10. Zhang, X.; Bai, C.; Qiao, Y.; Wang, X.; Jia, D.; Li, H.; Colombo, P. Porous Geopolymer Composites: A Review. *Compos. Part A Appl. Sci. Manuf.* **2021**, *150*, 106629. [CrossRef]
11. Grela, A.; Łach, M.; Bajda, T.; Mikuła, J.; Hebda, M. Characterization of the products obtained from alkaline conversion of tuff and metakaolin. *J. Therm. Anal Calorim.* **2018**, *133*, 217–226. [CrossRef]
12. Kumar Yadav, V.; Hiraman Fulekar, M. Advances in Methods for Recovery of Ferrous, Alumina, and Silica Nanoparticles from Fly Ash Waste. *Ceramics* **2020**, *3*, 384–420. [CrossRef]
13. Prabha, V.C.; Revathi, V. Geopolymer Mortar Incorporating High Calcium Fly Ash and Silica Fume. *Arch. Civ. Eng.* **2019**, *65*, 3–16. [CrossRef]
14. Doğan-Sağlamtimur, N.; Bilgil, A.; Szechyńska-Hebda, M.; Parzych, S.; Hebda, M. Eco-Friendly Fired Brick Produced from Industrial Ash and Natural Clay: A Study of Waste Reuse. *Materials* **2021**, *14*, 877. [CrossRef] [PubMed]
15. Bajpai, R.; Shrivastava, A.; Singh, M. Properties of Fly Ash Geopolymer Modified with Red Mud and Silica Fume: A Comparative Study. *SN Appl. Sci.* **2020**, *2*, 1846. [CrossRef]
16. Łach, M.; Gado, R.A.; Marczyk, J.; Ziejewska, C.; Doğan-Sağlamtimur, N.; Mikuła, J.; Szechyńska-Hebda, M.; Hebda, M. Process Design for a Production of Sustainable Materials from Post-Production Clay. *Materials* **2021**, *14*, 953. [CrossRef] [PubMed]
17. Feng, B.; Liu, J.; Chen, Y.; Tan, X.; Zhang, M.; Sun, Z. Properties and Microstructure of Self-Waterproof Metakaolin Geopolymer with Silane Coupling Agents. *Constr. Build. Mater.* **2022**, *342*, 128045. [CrossRef]
18. Yong, H.C.; Ming, L.Y.; al Bakri Abdullah, M.M.; Hussin, K. Fire Resistant Properties of Geopolymers: A Review. *Key Eng. Mater.* **2015**, *660*, 39–43. [CrossRef]

19. Lahoti, M.; Tan, K.H.; Yang, E.H. A Critical Review of Geopolymer Properties for Structural Fire-Resistance Applications. *Constr. Build. Mater.* **2019**, *221*, 514–526. [CrossRef]
20. Jiao, Z.; Li, X.; Yu, Q. Effect of Curing Conditions on Freeze-Thaw Resistance of Geopolymer Mortars Containing Various Calcium Resources. *Constr. Build. Mater.* **2021**, *313*, 125507. [CrossRef]
21. Verma, M.; Dev, N.; Rahman, I.; Nigam, M.; Ahmed, M.; Mallick, J. Geopolymer Concrete: A Material for Sustainable Development in Indian Construction Industries. *Crystals* **2022**, *12*, 514. [CrossRef]
22. Bakharev, T. Resistance of Geopolymer Materials to Acid Attack. *Cem. Concr. Res.* **2005**, *35*, 658–670. [CrossRef]
23. Szechyńska-Hebda, M.; Marczyk, J.; Ziejewska, C.; Hordyńska, N.; Mikuła, J.; Hebda, M. Neutral geopolymer foams reinforced with cellulose studied with the FT-Raman spectroscopy. *IOP Conf. Ser. Mater. Sci. Eng.* **2019**, *706*, 012017. [CrossRef]
24. Ahmad, J.; Zhou, Z.; Martínez-García, R. A Study on the Microstructure and Durability Performance of Rubberized Concrete with Waste Glass as Binding Material. *J. Build. Eng.* **2022**, *49*, 104054. [CrossRef]
25. Alhawat, M.; Ashour, A.; Yildirim, G.; Aldemir, A.; Sahmaran, M. Properties of Geopolymers Sourced from Construction and Demolition Waste: A Review. *J. Build. Eng.* **2022**, *50*, 104104. [CrossRef]
26. Guzmán-Carrillo, H.R.; Gasca-Tirado, J.R.; López-Romero, J.M.; Apátiga-Castro Luis, M.; Rivera-Muñoz Eric, M.; Pineda-Piñón, J.; Pérez-Bueno, J.J.; Feregrino-Montes, C.; López-Naranjo, E.J.; Manzano-Ramírez, A. Encapsulation of Toxic Heavy Metals from Waste CRT Using Calcined Kaolin Base-Geopolymer. *Mater. Chem. Phys.* **2021**, *257*, 123745. [CrossRef]
27. Roopchund, R.; Andrew, J.; Sithole, B. Using Cellulose Nanocrystals to Improve the Mechanical Properties of Fly Ash-Based Geopolymer Construction Materials. *Eng. Sci. Technol. Int. J.* **2022**, *25*, 100989. [CrossRef]
28. Refaie, F.A.Z.; Abbas, R.; Fouad, F.H. Sustainable Construction System with Egyptian Metakaolin Based Geopolymer Concrete Sandwich Panels. *Case Stud. Constr. Mater.* **2020**, *13*, e00436. [CrossRef]
29. Kretzer, M.B.; Effting, C.; Schwaab, S.; Schackow, A. Hybrid Geopolymer-Cement Coating Mortar Optimized Based on Metakaolin, Fly Ash, and Granulated Blast Furnace Slag. *Clean. Eng. Technol.* **2021**, *4*, 100153. [CrossRef]
30. Hamada, H.; Alattar, A.; Tayeh, B.; Yahaya, F.; Thomas, B. Effect of Recycled Waste Glass on the Properties of High-Performance Concrete: A Critical Review. *Case Stud. Constr. Mater.* **2022**, *17*, e01149. [CrossRef]
31. Li, S.; Zhang, J.; Du, G.; Mao, Z.; Ma, Q.; Luo, Z.; Miao, Y.; Duan, Y. Properties of Concrete with Waste Glass after Exposure to Elevated Temperatures. *J. Build. Eng.* **2022**, *57*, 104822. [CrossRef]
32. Feng, J.; Wu, D.; Long, M.; Lei, K.; Sun, Y.; Zhao, X. Diopside Glass-Ceramics Were Fabricated by Sintering the Powder Mixtures of Waste Glass and Kaolin. *Ceram. Int.* **2022**, *48*, 27088–27096. [CrossRef]
33. Jiang, X.; Xiao, R.; Ma, Y.; Zhang, M.; Bai, Y.; Huang, B. Influence of Waste Glass Powder on the Physico-Mechanical Properties and Microstructures of Fly Ash-Based Geopolymer Paste after Exposure to High Temperatures. *Constr. Build. Mater.* **2020**, *262*, 120579. [CrossRef]
34. Xiao, R.; Huang, B.; Zhou, H.; Ma, Y.; Jiang, X. A State-of-the-Art Review of Crushed Urban Waste Glass Used in OPC and AAMs (Geopolymer): Progress and Challenges. *Clean. Mater.* **2022**, *4*, 100083. [CrossRef]
35. Jochem, L.F.; Casagrande, C.A.; Onghero, L.; Venâncio, C.; Gleize, P.J.P. Effect of Partial Replacement of the Cement by Glass Waste on Cementitious Pastes. *Constr. Build. Mater.* **2021**, *273*, 121704. [CrossRef]
36. Fu, C.; Liang, J.; Yang, G.; Dagestani, A.A.; Liu, W.; Luo, X.; Zeng, B.; Wu, H.; Huang, M.; Lin, L.; et al. Recycling of Waste Glass as Raw Materials for the Preparation of Self-Cleaning, Light-Weight and High-Strength Porous Ceramics. *J. Clean. Prod.* **2021**, *317*, 128395. [CrossRef]
37. Maitlo, G.; Ali, I.; Maitlo, H.A.; Ali, S.; Unar, I.N.; Ahmad, M.B.; Bhutto, D.K.; Karmani, R.K.; Naich, S.U.R.; Sajjad, R.U.; et al. Plastic Waste Recycling, Applications, and Future Prospects for a Sustainable Environment. *Sustainability* **2022**, *14*, 11637. [CrossRef]
38. Pickin, J.; Wardle, C.; O'farrell, K.; Stovell, L.; Nyunt, P.; Guazzo, S.; Lin, Y.; Caggiati-Shortell, G.; Chakma, P.; Edwards, C.; et al. National Waste Report 2022. Available online: https://www.dcceew.gov.au/environment/protection/waste/national-waste-reports/2022 (accessed on 26 February 2023).
39. Novais, R.M.; Ascensão, G.; Seabra, M.P.; Labrincha, J.A. Waste Glass from End-of-Life Fluorescent Lamps as Raw Material in Geopolymers. *Waste Manag.* **2016**, *52*, 245–255. [CrossRef]
40. Si, R.; Dai, Q.; Guo, S.; Wang, J. Mechanical Property, Nanopore Structure and Drying Shrinkage of Metakaolin-Based Geopolymer with Waste Glass Powder. *J. Clean. Prod.* **2020**, *242*, 118502. [CrossRef]
41. Polat, D.; Güden, M. Processing and Characterization of Geopolymer and Sintered Geopolymer Foams of Waste Glass Powders. *Constr. Build. Mater.* **2021**, *300*, 124259. [CrossRef]
42. Senff, L.; Novais, R.M.; Carvalheiras, J.; Labrincha, J.A. Eco-Friendly Approach to Enhance the Mechanical Performance of Geopolymer Foams: Using Glass Fibre Waste Coming from Wind Blade Production. *Constr. Build. Mater.* **2020**, *239*, 117805. [CrossRef]
43. Xiao, R.; Ma, Y.; Jiang, X.; Zhang, M.; Zhang, Y.; Wang, Y.; Huang, B.; He, Q. Strength, Microstructure, Efflorescence Behavior and Environmental Impacts of Waste Glass Geopolymers Cured at Ambient Temperature. *J. Clean. Prod.* **2020**, *252*, 119610. [CrossRef]
44. Hajimohammadi, A.; Ngo, T.; Kashani, A. Sustainable One-Part Geopolymer Foams with Glass Fines versus Sand as Aggregates. *Constr. Build. Mater.* **2018**, *171*, 223–231. [CrossRef]
45. Du, Y.; Yang, W.; Ge, Y.; Wang, S.; Liu, P. Thermal Conductivity of Cement Paste Containing Waste Glass Powder, Metakaolin and Limestone Filler as Supplementary Cementitious Material. *J. Clean. Prod.* **2021**, *287*, 125018. [CrossRef]

46. Ulugöl, H.; Kul, A.; Yıldırım, G.; Şahmaran, M.; Aldemir, A.; Figueira, D.; Ashour, A. Mechanical and Microstructural Characterization of Geopolymers from Assorted Construction and Demolition Waste-Based Masonry and Glass. *J. Clean. Prod.* **2021**, *280*, 124358. [CrossRef]
47. Siddika, A.; Hajimohammadi, A.; Ferdous, W.; Sahajwalla, V.; Blanco, I.; Catauro, M. Roles of Waste Glass and the Effect of Process Parameters on the Properties of Sustainable Cement and Geopolymer Concrete-A State-of-the-Art Review. *Polymers* **2021**, *13*, 3935. [CrossRef]
48. Kiliçoglu, C.; Çoruh, S. Recycling of Waste Glass in Concrete Plant as Aggregate and Pozzolan Replacement. *Int. J. Glob. Warm.* **2017**, *11*, 250–262. [CrossRef]
49. Shi, C.; Wu, Y.; Riefler, C.; Wang, H. Characteristics and Pozzolanic Reactivity of Glass Powders. *Cem. Concr. Res.* **2005**, *35*, 987–993. [CrossRef]
50. Badanoiu, A.I.; al Saadi, T.H.A.; Stoleriu, S.; Voicu, G. Preparation and Characterization of Foamed Geopolymers from Waste Glass and Red Mud. *Constr. Build. Mater.* **2015**, *84*, 284–293. [CrossRef]
51. Tramontin Souza, M.; Onghero, L.; Batista Passos, A.; Simão, L.; Honorato Piva, R.; Longuini Repette, W.; Novaes de Oliveira, A.P. Sustainable Glass Foams Produced with Stone Waste as a Pore-Forming Agent: Assessing the Role of Heating Rate in Foamability and Glass Foams Recyclability. *J. Clean. Prod.* **2022**, *338*, 130596. [CrossRef]
52. Siddika, A.; Hajimohammadi, A.; Sahajwalla, V. Recycling of Automotive Vehicle's Waste Glass to Develop Sustainable Glass Foam Using a Curing-Sintering Process. In Proceedings of the Concrete Institute of Australia's Biennial National Conference (Concrete 2021), Perth, Australia, 8 September 2021.
53. Zhang, Y.; Xiao, R.; Jiang, X.; Li, W.; Zhu, X.; Huang, B. Effect of Particle Size and Curing Temperature on Mechanical and Microstructural Properties of Waste Glass-Slag-Based and Waste Glass-Fly Ash-Based Geopolymers. *J. Clean. Prod.* **2020**, *273*, 122970. [CrossRef]
54. Ruan, S.; Kastiukas, G.; Liang, S.; Zhou, X. Waste Glass Reuse in Foamed Alkali-Activated Binders Production: Technical and Environmental Assessment. *Front. Mater.* **2020**, *7*, 581358. [CrossRef]
55. Catauro, M.; Dal Poggetto, G.; Sgarlata, C.; Vecchio Ciprioti, S.; Pacifico, S.; Leonelli, C. Thermal and Microbiological Performance of Metakaolin-Based Geopolymers Cement with Waste Glass. *Appl. Clay. Sci.* **2020**, *197*, 105763. [CrossRef]
56. Mahesh, Y.; Lalitha, G. Durablilty Propeties of Geopolymer Concrete Partial Replacement of Fine Aggaregate with Waste Crushed Glass. *Mater. Today Proc.* **2022**, *51*, 2466–2470. [CrossRef]
57. Marczyk, J.; Ziejewska, C.; Gadek, S.; Korniejenko, K.; Łach, M.; Góra, M.; Kurek, I.; Dogan-Saglamtimur, N.; Hebda, M.; Szechynska-Hebda, M. Hybrid Materials Based on Fly Ash, Metakaolin, and Cement for 3D Printing. *Materials* **2021**, *14*, 6874. [CrossRef] [PubMed]
58. Chen, H.J.; Shih, N.H.; Wu, C.H.; Lin, S.K. Effects of the Loss on Ignition of Fly Ash on the Properties of High-Volume Fly Ash Concrete. *Sustainability* **2019**, *11*, 2704. [CrossRef]
59. Vafaei, M.; Allahverdi, A. High Strength Geopolymer Binder Based on Waste-Glass Powder. *Adv. Powder Technol.* **2017**, *28*, 215–222. [CrossRef]
60. Tahwia, A.M.; Heniegal, A.M.; Abdellatief, M.; Tayeh, B.A.; Elrahman, M.A. Properties of Ultra-High Performance Geopolymer Concrete Incorporating Recycled Waste Glass. *Case Stud. Constr. Mater.* **2022**, *17*, e01393. [CrossRef]
61. Azdast, T.; Hasanzadeh, R. Increasing Cell Density/Decreasing Cell Size to Produce Microcellular and Nanocellular Thermoplastic Foams: A Review. *J. Cell. Plast.* **2020**, *57*, 769–797. [CrossRef]
62. Mucsi, G. Mechanical Activation of Power Station Fly Ash by Grinding—A Review. *Epa.-J. Silic. Based Compos. Mater.* **2016**, *68*, 56–61. [CrossRef]
63. Shee-Ween, O.; Cheng-Yong, H.; Yun-Ming, L.; Abdullah, M.M.A.B.; Li Ngee, H.; Chan, L.W.L.; Wan-En, O.; Jaya, N.A.; Yong-Sing, N. Cold-Pressed Fly Ash Geopolymers: Effect of Formulation on Mechanical and Morphological Characteristics. *J. Mater. Res. Technol.* **2021**, *15*, 3028–3046. [CrossRef]
64. Ankrah, A.F.; Tokay, B.; Snape, C.E. Heavy Metal Removal from Aqueous Solutions Using Fly-Ash Derived Zeolite NaP1. *Int. J. Environ. Res.* **2022**, *16*, 17. [CrossRef]
65. Segneanu, A.E.; Marin, C.N.; Vlase, G.; Cepan, C.; Mihailescu, M.; Muntean, C.; Grozescu, I. Highly Efficient Engineered Waste Eggshell-Fly Ash for Cadmium Removal from Aqueous Solution. *Sci. Rep.* **2022**, *12*, 9676. [CrossRef] [PubMed]
66. Janowska-Renkas, E.; Kaliciak, A. Properties of Geopolymers from Conventional Fly Ash Activated at Increased Temperature with Sodium Hydroxide Containing Glass Powder Obtained from the Recycling of Waste Glass. *MATEC Web Conf.* **2020**, *322*, 01018. [CrossRef]
67. Abdallah, S.; Fan, M. Characteristics of Concrete with Waste Glass as Fine Aggregate Replacement. *Int. J. Eng. Technol.* **2014**, *2*, 11–17.
68. Barkauskas, K.; Nagrockienė, D.; Girnienė, I. The Effect of Glass Powder on Physical and Mechanical Properties of Hardened Cement Paste. In Proceedings of the 13th International Conference Modern Building Materials, Structures and Techniques, Vilnius, Lithuania, 16–17 May 2019. [CrossRef]
69. Mendes, B.C.; Pedroti, L.G.; Vieira, C.M.F.; Carvalho, J.M.F.; Ribeiro, J.C.L.; Albuini-Oliveira, N.M.; Andrade, I.K.R. Evaluation of Eco-Efficient Geopolymer Using Chamotte and Waste Glass-Based Alkaline Solutions. *Case Stud. Constr. Mater.* **2022**, *16*, e00847. [CrossRef]

70. Ahmad, J.; Aslam, F.; Martinez-Garcia, R.; de-Prado-Gil, J.; Qaidi, S.M.A.; Brahmia, A. Effects of Waste Glass and Waste Marble on Mechanical and Durability Performance of Concrete. *Sci. Rep.* **2021**, *11*, 21525. [CrossRef]
71. Rahman, M.M.; Muttakin, M.; Pal, A.; Shafiullah, A.Z.; Saha, B.B. A Statistical Approach to Determine Optimal Models for IUPAC-Classified Adsorption Isotherms. *Energies* **2019**, *12*, 4565. [CrossRef]
72. Henderson, J. The Analysis of Ancient Glasses Part I: Materials, Properties, and Early European Glass. *JOM* **1995**, *47*, 62–64. [CrossRef]
73. Lowell, S.; Shields, J.E.; Thomas, M.A.; Thommes, M. *Characterization of Porous Solids and Powders: Surface Area, Pore Size and Density*; Springer Science & Business Media: Berlin, Germany, 2004; Volume 16. [CrossRef]
74. Yurdakal, S.; Garlisi, C.; Özcan, L.; Bellardita, M.; Palmisano, G. (Photo)Catalyst Characterization Techniques: Adsorption Isotherms and BET, SEM, FTIR, UV–Vis, Photoluminescence, and Electrochemical Characterizations. In *Heterogeneous Photocatalysis: Relationships with Heterogeneous Catalysis and Perspectives*; Elsevier: Amsterdam, The Netherlands, 2019; pp. 87–152. [CrossRef]
75. Arokiasamy, P.; al Bakri Abdullah, M.M.; Rahim, S.Z.A.; Arif Zainol, M.R.R.M.; Salleh, M.A.A.M.; Kheimi, M.; Chaiprapa, J.; Sandu, A.V.; Vizureanu, P.; Razak, R.A.; et al. Metakaolin/Sludge Based Geopolymer Adsorbent on High Removal Efficiency of Cu2+. *Case Stud. Constr. Mater.* **2022**, *17*, e01428. [CrossRef]
76. Qiu, J.; Zhao, Y.; Xing, J.; Sun, X. Fly Ash/Blast Furnace Slag-Based Geopolymer as a Potential Binder for Mine Backfilling: Effect of Binder Type and Activator Concentration. *Adv. Mater. Sci. Eng.* **2019**, *2019*, 2028109. [CrossRef]
77. Sathonsaowaphak, A.; Chindaprasirt, P.; Pimraksa, K. Workability and Strength of Lignite Bottom Ash Geopolymer Mortar. *J. Hazard. Mater.* **2009**, *168*, 44–50. [CrossRef]
78. Toniolo, N.; Rincón, A.; Roether, J.A.; Ercole, P.; Bernardo, E.; Boccaccini, A.R. Extensive Reuse of Soda-Lime Waste Glass in Fly Ash-Based Geopolymers. *Constr. Build. Mater.* **2018**, *188*, 1077–1084. [CrossRef]
79. Wang, S.; Yu, L.; Xu, L.; Wu, K.; Yang, Z. The Failure Mechanisms of Precast Geopolymer after Water Immersion. *Materials* **2021**, *14*, 5299. [CrossRef] [PubMed]
80. Bagheri, A.; Moukannaa, S. A New Approach to the Reuse of Waste Glass in the Production of Alkali-Activated Materials. *Clean. Eng. Technol.* **2021**, *4*, 100212. [CrossRef]
81. Kozub, B.; Bazan, P.; Gailitis, R.; Korniejenko, K.; Mierzwiński, D. Foamed Geopolymer Composites with the Addition of Glass Wool Waste. *Materials* **2021**, *14*, 4978. [CrossRef]
82. Łach, M.; Pławecka, K.; Bąk, A.; Lichocka, K.; Korniejenko, K.; Cheng, A.; Lin, W.T. Determination of the Influence of Hydraulic Additives on the Foaming Process and Stability of the Produced Geopolymer Foams. *Materials* **2021**, *14*, 5090. [CrossRef]
83. Al-Bakri Abdullah, M.M.; Jamaludin, L.; Hussin, K.; Bnhussain, M.; Ghazali, C.M.R.; Ahmad, M.I. Fly Ash Porous Material Using Geopolymerization Process for High Temperature Exposure. *Int. J. Mol. Sci.* **2012**, *13*, 4388. [CrossRef]
84. Luna-Galiano, Y.; Fernández-Pereira, C.; Izquierdo, M. Contributions to the Study of Porosity in Fly Ash-Based Geopolymers. Relationship between Degree of Reaction, Porosity and Compressive Strength. *Mater. De Construcción* **2016**, *66*, e098. [CrossRef]
85. Szechyńska-Hebda, M.; Marczyk, J.; Ziejewska, C.; Hordyńska, N.; Mikuła, J.; Hebda, M. Optimal Design of PH-Neutral Geopolymer Foams for Their Use in Ecological Plant Cultivation Systems. *Materials* **2019**, *12*, 2999. [CrossRef]
86. Deng, Q.; Lai, Z.; Xiao, R.; Wu, J.; Liu, M.; Lu, Z.; Lv, S. Effect of Waste Glass on the Properties and Microstructure of Magnesium Potassium Phosphate Cement. *Materials* **2021**, *14*, 2073. [CrossRef]
87. Ali, E.E.; Al-Tersawy, S.H. Recycled Glass as a Partial Replacement for Fine Aggregate in Self Compacting Concrete. *Constr. Build. Mater.* **2012**, *35*, 785–791. [CrossRef]
88. Toniolo, N.; Taveri, G.; Hurle, K.; Roether, J.A.; Ercole, P.; Dlouhý, I.; Boccaccini, A.R. Fly-Ash-Based Geopolymers: How the Addition of Recycled Glass or Red Mud Waste Influences the Structural and Mechanical Properties. *J. Ceram. Sci. Technol.* **2017**, *8*, 411–419. [CrossRef]
89. Dadsetan, S.; Siad, H.; Lachemi, M.; Sahmaran, M. Extensive Evaluation on the Effect of Glass Powder on the Rheology, Strength, and Microstructure of Metakaolin-Based Geopolymer Binders. *Constr. Build. Mater.* **2021**, *268*, 121168. [CrossRef]
90. Korniejenko, K.; Figiela, B.; Miernik, K.; Ziejewska, C.; Marczyk, J.; Hebda, M.; Cheng, A.; Lin, W.-T. Mechanical and Fracture Properties of Long Fiber Reinforced Geopolymer Composites. *Materials* **2021**, *14*, 5183. [CrossRef]
91. Wielgus, N.; Kubica, J.; Górski, M. Influence of the Composition and Curing Time on Mechanical Properties of Fluidized Bed Combustion Fly Ash-Based Geopolymer. *Polymers* **2021**, *13*, 2527. [CrossRef]
92. Taher, S.M.S.; Saadullah, S.T.; Haido, J.H.; Tayeh, B.A. Behavior of Geopolymer Concrete Deep Beams Containing Waste Aggregate of Glass and Limestone as a Partial Replacement of Natural Sand. *Case Stud. Constr. Mater.* **2021**, *15*, e00744. [CrossRef]
93. Ercoli, R.; Laskowska, D.; Nguyen, V.V.; Le, V.S.; Louda, P.; Łoś, P.; Ciemnicka, J.; Prałat, K.; Renzulli, A.; Paris, E.; et al. Mechanical and Thermal Properties of Geopolymer Foams (GFs) Doped with By-Products of the Secondary Aluminum Industry. *Polymers* **2022**, *14*, 703. [CrossRef] [PubMed]
94. van Jaarsveld, J.G.S.; van Deventer, J.S.J.; Lorenzen, L. Factors Affecting the Immobilization of Metals in Geopolymerized Flyash. *Met. Mater. Trans. B* **1998**, *29*, 283–291. [CrossRef]
95. Shi, P.; Zhang, Y.; Sun, Q.; Ta, X. Eluviation and Leaching of Elements from Broken Fly-Ash-Based Porous Geopolymer. *Materials* **2021**, *14*, 6884. [CrossRef] [PubMed]
96. Bobirică, C.; Shim, J.H.; Park, J.Y. Leaching Behavior of Fly Ash-Waste Glass and Fly Ash-Slag-Waste Glass-Based Geopolymers. *Ceram. Int.* **2018**, *44*, 5886–5893. [CrossRef]

97. Council of the European Union. Council Decision Establishing Criteria and Procedures for the Acceptance of Waste at Landfills Pursuant to Article 16 of and Annex II to Directive 1999/31/EC. *Off. J. Eur. Communities* **2003**, *11*, 27–49.
98. Luhar, S.; Cheng, T.W.; Nicolaides, D.; Luhar, I.; Panias, D.; Sakkas, K. Valorisation of Glass Wastes for the Development of Geopolymer Composites–Durability, Thermal and Microstructural Properties: A Review. *Constr. Build. Mater.* **2019**, *222*, 673–687. [CrossRef]
99. Fei, Y.; Chen, F.; Fang, W.; Xu, L.; Ruan, S.; Liu, X.; Zhong, M.; Kuang, T. High-Strength, Flexible and Cycling-Stable Piezo-Resistive Polymeric Foams Derived from Thermoplastic Polyurethane and Multi-Wall Carbon Nanotubes. *Compos. B Eng.* **2020**, *199*, 108279. [CrossRef]
100. Jindal, B.B.; Jangra, P.; Garg, A. Effects of Ultra Fine Slag as Mineral Admixture on the Compressive Strength, Water Absorption and Permeability of Rice Husk Ash Based Geopolymer Concrete. *Mater. Today Proc.* **2020**, *32*, 871–877. [CrossRef]
101. Boum, R.B.E.; Kaze, C.R.; Nemaleu, J.G.D.; Djaoyang, V.B.; Rachel, N.Y.; Ninla, P.L.; Owono, F.M.; Kamseu, E. Thermal Behaviour of Metakaolin-Bauxite Blends Geopolymer: Microstructure and Mechanical Properties. *SN Appl. Sci.* **2020**, *2*, 1358. [CrossRef]

Article

Influence of Waste Glass Particle Size on the Physico-Mechanical Properties and Porosity of Foamed Geopolymer Composites Based on Coal Fly Ash

Celina Ziejewska[1], Agnieszka Grela[2], Marek Hebda[1*]

[1] Faculty of Materials Engineering and Physics, Cracow University of Technology, Warszawska 24, 31-155 Cracow, Poland

[2] Faculty of Environmental and Power Engineering, Cracow University of Technology, Warszawska 24, 31-155 Cracow, Poland

* Correspondence: marek.hebda@pk.edu.pl (M.H.)

Supplementary Materials

Table S1. Particle size distributions of fly ash and waste glass powders.

Raw materials	D_{10} [μm]	D_{50} [μm]	D_{90} [μm]	Mean [μm]	Span $(D_{90}-D_{10})/D_{50}$ [μm]
Fly ash	2.3 ± 0.1	12.3 ± 1.3	37.0 ± 6.0	17.3 ± 2.5	2.8 ± 0.2
0.1-1200 WG (all fractions)	112.8 ± 8.6	483.4 ± 19.7	896.7 ± 51.1	550.1 ± 18.9	1.6 ± 0.2
200-1200 WG	303.1 ± 1.6	584.9 ± 4.4	1123.3 ± 5.5	702.4 ± 1.6	1.4 ± 0.02
100-250 WG	30.4 ± 1.5	155.2 ± 0.5	248.6 ± 0.2	160.6 ± 0.6	1.4 ± 0.01
63-120 WG	6.3 ± 0.1	55.4 ± 1.2	118.5 ± 1.2	60.8 ± 0.9	2.0 ± 0.02
40-63 WG	4.9 ± 0.1	33.3 ± 0.1	63.1 ± 0.2	35.1 ± 0.1	1.7 ± 0.01
0.1-40 WG	3.9 ± 0.8	19.8 ± 0.3	39.2 ± 0.2	22.0 ± 0.3	1.8 ± 0.2

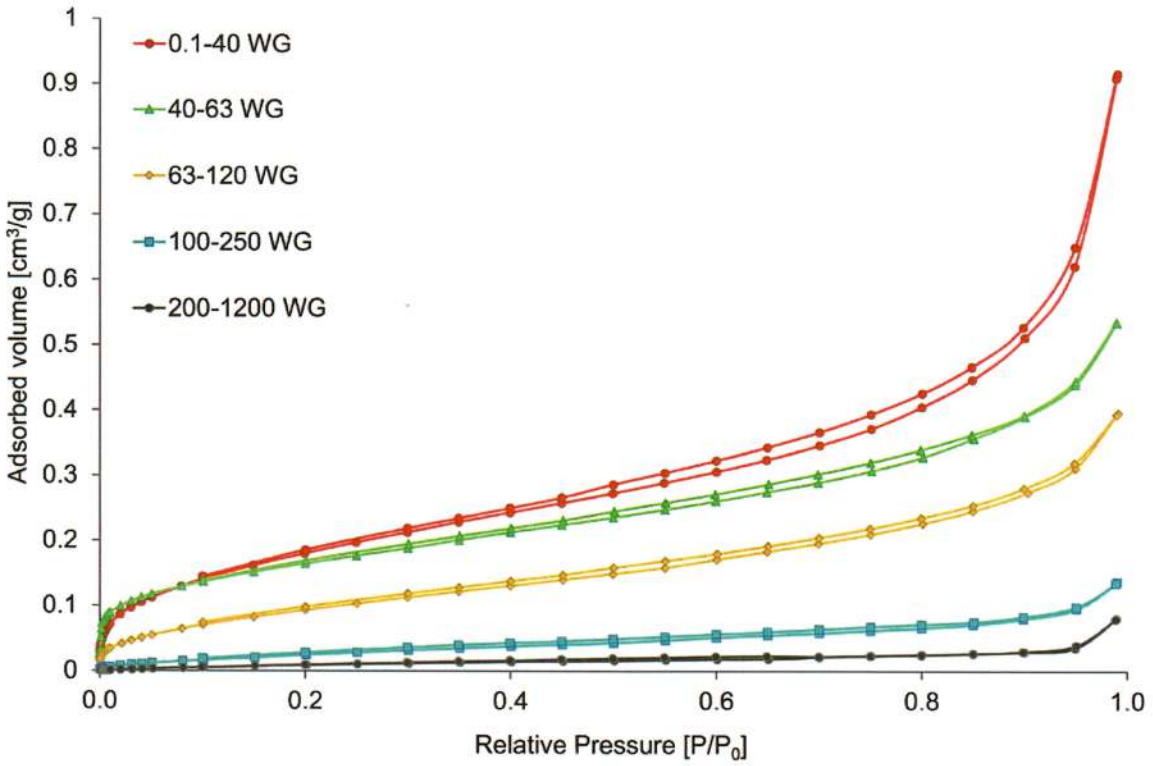

Figure S1. Nitrogen adsorption-desorption isotherms of waste glass after separation into five different fractions.

Table. S2. The specific surface area of geopolymers, depending on the used amount and particle diameters of waste glass.

Designation of samples	BET Surface area [m^2/g]
REF	22.772
A10	30.881
A20	37.556
A30	36.435
B30	16.089
D30	37.207
F30	43.711

Figure S2. The determination of porosity of geopolymers using ImageJ software. The best channel for analysed photography was chosen by means of the "Split Channels" option. After that, the maximum possible part of the image was selected using the rectangular section tool. The threshold tool was used to determine the porosity areas. Then the photograph was converted into a binary image. Finally, an analysis of particles option was chosen, and the obtained area fraction value was saved. All of the steps were repeated for each sample. The porosity results were the average of the image analysis of a minimum of three samples.

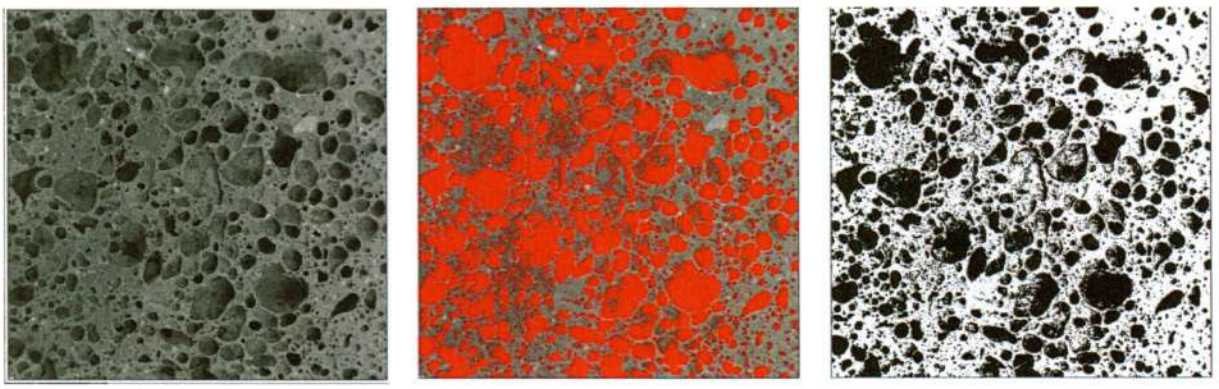

Table S3. The results of the leaching test conducted for geopolymer samples.

Designation of samples	Unit	REF	A30	B30	D30	F30
pH of the water extract	-	10.97 ± 0.08	10.84 ± 0.08	10.84 ± 0.08	10.83 ± 0.08	11.00 ± 0.08
total dissolved substances	mg/dm^3	5884 ± 231	5805 ± 228	5352 ± 210	6521 ± 256	8518 ± 334
chlorides		26.4 ± 2.2	11.2 ± 0.9	11.6 ± 1.0	11.9 ± 1.0	13.6 ± 1.1
fluorides		3.4 ± 0.3	2.7 ± 0.3	2.8 ± 0.3	2.3 ± 0.2	2.2 ± 0.2
sulphates		479 ± 39	335 ± 27	357 ± 29	349 ± 28	345 ± 28
Zn		0.0010 ± 0.0002	< 0.001	< 0.001	0.0050 ± 0.0008	0.0020 ± 0.0003
Cd		< 0.001	< 0.001	< 0.001	< 0.001	< 0.001
Cu		< 0.001	< 0.001	< 0.001	< 0.001	< 0.001
Pb		0.023 ± 0.003	0.040 ± 0.006	0.069 ± 0.010	0.066 ± 0.010	0.276 ± 0.040
Ni		0.0020 ± 0.0002	0.0030 ± 0.0004	0.0020 ± 0.0002	0.0030 ± 0.0004	0.0040 ± 0.0005
Ba		0.016 ± 0.004	0.006 ± 0.001	0.0020 ± 0.0004	0.0010 ± 0.0002	0.012 ± 0.0003
Cr		0.019 ± 0.004	0.010 ± 0.002	0.012 ± 0.003	0.012 ± 0.003	0.007 ± 0.002
Cr(VI)		< 0.020	< 0.020	< 0.020	< 0.020	< 0.020
Hg		< 0.01	< 0.01	< 0.01	0.06 ± 0.01	< 0.01
As		1.06 ± 0.11	0.72 ± 0.07	0.66 ± 0.07	0.80 ± 0.08	0.87 ± 0.09
Se		0.12 ± 0.02	0.09 ± 0.01	0.09 ± 0.01	0.10 ± 0.01	0.12 ± 0.02
Mo		0.43 ± 0.05	0.28 ± 0.03	0.26 ± 0.03	0.29 ± 0.03	0.30 ± 0.03
Sb		< 0.02	< 0.02	< 0.02	< 0.02	< 0.02
dissolved organic carbon		8.28 ± 0.75	7.75 ± 0.70	5.24 ± 0.48	7.53 ± 0.68	6.55 ± 0.60

Załącznik 4 – oświadczenia współautorów dotyczące publikacji P2

Kraków, dn. 23.11.2023 r.

OŚWIADCZENIE – PUBLIKACJA P2

Oświadczam, iż mój wkład w powstanie publikacji pt.: „*Influence of waste glass particle size on the physico-mechanical properties and porosity of foamed geopolymer composites based on coal fly ash*" opublikowanej w czasopiśmie *Materials* w 2023 roku, nr DOI: 10.3390/ma16052044 jest zgodny z informacją zawartą w poniższej tabeli.

Jednocześnie oświadczam, iż wyrażam zgodę na wykorzystanie wyżej wymienionej publikacji jako część rozprawy doktorskiej mgr inż. Celiny Ziejewskiej.

Autor	Wkład w powstanie publikacji
Celina Ziejewska	Sformułowanie problemu badawczego, opracowanie koncepcji i metodyki badań. Przygotowanie materiałów bazowych, synteza geopolimerów. Przeprowadzenie badań i analiza wyników: rentgenowskiej jakościowej analizy fazowej materiałów kompozytowych (XRD), analizy wielkości cząstek surowców, obserwacji morfologii surowców i geopolimerów z zastosowaniem skaningowego mikroskopu elektronowego (SEM) oraz mikroskopu cyfrowego, porowatości geopolimerów, powierzchni właściwej surowców i geopolimerów, gęstości geopolimerów metodą geometryczną, wytrzymałości na ściskanie geopolimerów, wytrzymałości na zginanie geopolimerów, nasiąkliwości próbek. Przygotowanie materiałów i analiza wyników wymywalności wodnej geopolimerów. Interpretacja i opracowanie graficzne wyników, przygotowanie pierwszej wersji manuskryptu, przygotowanie ostatecznej wersji manuskryptu, korekta manuskryptu po recenzjach.
Agnieszka Grela	Sformułowanie problemu badawczego, opracowanie koncepcji badań, weryfikacja danych, opracowanie metodyki prowadzonych badań, walidacja uzyskanych danych i ich analizy, nadzór merytoryczny nad prowadzonymi badaniami. Potwierdzenie, że materiały i procesy były zgodne z przyjętymi założeniami.

Marek Hebda	Sformułowanie problemu badawczego, opracowanie koncepcji i metodyki badań, zarządzanie zespołem badawczym, walidacja uzyskanych danych i ich analizy, nadzór merytoryczny nad prowadzonymi badaniami, analiza wyników badań, opracowanie graficzne wyników, pozyskanie finansowania na poczet zrealizowanych badań i kosztów publikacyjnych, udział w pisaniu pierwszej wersji manuskryptu, dyskusja i udział w przygotowaniu ostatecznej wersji manuskryptu, korekta manuskryptu po recenzjach.

Celina Ziejewska

podpis oświadczającego
mgr inż. Celina Ziejewska

A. Grela

podpis oświadczającego
dr inż. Agnieszka Grela

podpis oświadczającego
dr hab. inż. Marek Hebda, prof. PK

materials

MDPI

Article

Influence of Waste Glass Addition on the Fire Resistance, Microstructure and Mechanical Properties of Geopolymer Composites

Celina Ziejewska [1], Agnieszka Grela [2], Dariusz Mierzwiński [1] and Marek Hebda [1,*]

[1] Faculty of Materials Engineering and Physics, Cracow University of Technology, Warszawska 24, 31-155 Kraków, Poland; celina.ziejewska@pk.edu.pl (C.Z.); dariusz.mierzwinski@pk.edu.pl (D.M.)
[2] Faculty of Environmental Engineering and Energy, Cracow University of Technology, Warszawska 24, 31-155 Kraków, Poland; agnieszka.grela@pk.edu.pl
* Correspondence: marek.hebda@pk.edu.pl

Abstract: Nowadays, humanity has to face the problem of constantly increasing amounts of waste, which cause not only environmental pollution but also poses a critical danger to human health. Moreover, the growth of landfill sites involves high costs of establishment, development, and maintenance. Glass is one of the materials whose recycling ratio is still insufficient. Therefore, in the presented work, the influence of the particle size and share of waste glass on the consistency, morphology, specific surface area, water absorption, setting time, and mechanical properties of geopolymers was determined. Furthermore, for the first time, the fire resistance and final setting time of such geopolymer composites were presented in a wide range. Based on the obtained results, it was found that the geopolymer containing 20% unsorted waste glass obtained a final setting time that was 44% less than the sample not containing waste glass, 51.5 MPa of compressive strength (135.2% higher than the reference sample), and 13.5 MPa of residual compressive strength after the fire resistance test (164.7% more than the reference sample). Furthermore, it was found that the final setting time and the total pore volume closely depended on the additive's share and particle size. In addition, the use of waste glass characterized by larger particle sizes led to higher strength and lower mass loss after exposure to high temperatures compared to the composite containing smaller ones. The results presented in this work allow not only for reducing the costs and negative impact on the environment associated with landfilling but also for developing a simple, low-cost method of producing a modern geopolymer composite with beneficial properties for the construction industry.

Keywords: fly ash; fire resistance; compressive strength; particle size; specific surface area

Citation: Ziejewska, C.; Grela, A.; Mierzwiński, D.; Hebda, M. Influence of Waste Glass Addition on the Fire Resistance, Microstructure and Mechanical Properties of Geopolymer Composites. *Materials* **2023**, *16*, 6011. https://doi.org/10.3390/ma16176011

Academic Editor: Michael I Ojovan

Received: 31 July 2023
Revised: 26 August 2023
Accepted: 29 August 2023
Published: 1 September 2023

1. Introduction

During the past few decades, building has been one of the fastest-growing industries worldwide, and this trend is expected to continue, with global construction output reaching 42% growth in 2030 compared to 2020 [1]. Concrete is the most common building material around the world [2], and it consists primarily of Ordinary Portland Cement, a widespread type of cement that has been used in the construction sector for many years [3]. It is worth mentioning that global cement production has been still increasing; for instance, in 2000 it amounted to 1600 million tons, whereas in 2019 it reached 4100 million tons [4]. Although cement has many advantages such as great mechanical properties and durability, its production process has a meaningfully negative impact on the environment due to its high energy consumption and substantial emission of CO_2 [5–8].

Glass is produced in around 100 million tons per annum, and it is a widespread material that is used worldwide in households, industries, laboratories, medicine, etc. Generally, it is believed to be an environmentally friendly material because it can be reused. However, the current global reuse rate for glass waste is only 26%, which results from the

high cost of recycling [9]. Therefore, most of this waste is disposed of in landfills, causing environmental and economic problems. Glass is a non-biodegradable material, and it is estimated that millions of years are needed to decompose it naturally [10]. Scientists have been alarmed that global waste production is constantly growing and will double by 2050 and even triple by 2100 if the current trend continues, in comparison to the amounts observed in 2016 [11]. Due to that, the possibility of the application of waste in the construction industry has a growing interest [12]. It has been proven that waste glass can show pozzolanic reactivity, but only when its particle size is equal to or smaller than 100 μm [13]. Waste glass can play a different role in a matrix of cement concrete depending on its particle sizes, such as coarse aggregates (particle size smaller than 14 mm), fine aggregates (particle size below 4.75 mm), and binders (particle size below 0.6 mm) [14]. Furthermore, authors in their previous works used waste glass as a partial replacement for cement [15], or as a fine type of aggregate in mortar [16], fly ash [17], and metakaolin [18]. In addition, the properties of waste glass depend on several factors, such as its chemical composition, type and share of contaminants, the color of the cullet, and its origin [19]. The addition of glass can positively impact on mechanical strength [20], the capacity of radiation shielding [21], workability [22], density [23], and water absorption [24].

Fly ash is a by-product received most of all from power plants as a result of coal combustion [25]. Millions of tons of coal fly ash are produced annually all over the world, including, among others, 120–150 million tons from India [26], more than 550 million tons from China [27], and 145 million tons from Europe [28]. Although fly ash can be used primarily as an additive in concrete, its utilization rate is still very low; for instance, in Europe, in 2016, it amounted to only 20.1% [28]. The remainder of the materials are deposited in ever-expanding landfill areas.

Geopolymer is an excellent alternative to cemental materials due to the possibility of using industrial by-products and waste in their production (e.g., fly ash [29,30], gangue [31], slag [32], clay [33]), which is in line with the effective reduction of production costs. Moreover, the cement industry is responsible for approximately 6–8% of the total anthropogenic CO_2 emission [34], whereas the geopolymer production process generates up to 5–6 times less quantity of greenhouse gas [35]. In general, geopolymers are inorganic polymers obtained by the reaction between aluminosilicate precursors and alkaline activators, which was invented by Joseph Davidovits in 1970 [36].

Despite the availability of many products reporting about the state of emergency, such as smoke detectors or temperature sensors, fires are still the key danger to people's health and lives nowadays. The NSC (National Safety Council) organization estimated that fire brigades in the United States react, on average, every 23 s to a fire occurrence, and every 3 h and 8 min, approximately, one person dies because of it. Therefore, fire resistance is one of the most important features of building materials, due to the necessity to ensure the stability of the construction during the fire [37]. Concrete manufactured using Ordinary Portland Cement shows significant deterioration of properties at temperatures above 400 °C because of the decomposition of portlandite. Moreover, in the range of 300–450 °C, spalling of such type of concrete is noted [38]. In contrast, geopolymers have good thermal stability and do not emit noxious vapor pending the fire, which is particularly important with regard to user safety [38]. Therefore, they can be applied as thermal insulation, as well as fire protection [3,39]. It was proven that even a small amount of geopolymer incorporated into a concrete matrix has a positive impact on fire resistance [40].

It was found that waste glass could have a beneficial impact on fire resistance due to the transition from the solid to liquid state, which is directly related to the melting point of waste glass. At a proportionately high temperature, waste glass can have the ability to fill pores, and can also fill microcracks that occur as a result of high temperatures [41]. Until now, many authors explored the fire resistance of concrete materials and cement mortars [42,43]. For instance, Chen et al. [44] examined the influence of the size of glass cullet on cementitious composites after higher temperature exposure using four various fractions of particles of the following sizes: less than 0.6 mm, 0.6–1.18 mm, 1.18–2.36 mm,

and 2.36–4.75 mm. The authors concluded that only samples containing two of the smallest fractions of particles improved the residual compressive strength after exposure to a temperature of 600 °C or higher, compared to the reference sample produced without adding the cullet. Moreover, they highlighted that the most positive effect was obtained by applying particles with sizes below 0.6 mm. However, in the case of geopolymers with the addition of waste glass, investigations about their fire resistance are very limited. Tahwia et al. [45] investigated the effect of high temperature on the properties of geopolymer concrete made with the addition of waste glass and ceramic after 56 days of curing. They incorporated waste glass particles into a matrix in the amount of 7.5 to 22.5% by volume and later subjected the samples to high temperatures of 200–800 °C for 1.5 h. The researchers noticed that the compressive strength of all the samples produced, even the control samples, was higher after exposure to 200 °C due to the further course of the geopolymerization process. However, after exposing the samples to a temperature of 800 °C, the authors noted the beneficial effect of glass waste, which resulted in an increase in residual compressive strength compared to the control mixture containing ceramic waste. Furthermore, Jiang et al. [46] explored fly ash-based geopolymers with the addition of waste glass (D_{50} = 18.21 μm) before and after exposure to 800 °C, 1000 °C, and 1200 °C. They concluded that the optimal level of incorporation of waste glass was 20% and after achieving the melting temperature of the glass, it can fill pores existing in the geopolymer matrix. Yu et al. [47] investigated the influence on the fire resistance of two types of waste glass with sizes of 4.9–10 mm and 4.9–16 mm, which were used as a coarse aggregate in the concrete columns. At the beginning of the test, samples were subjected to compressive loading, and then they were placed in the furnace and heated by up to 800 °C. The most positive effect was noted for samples containing 13% waste glass, and those samples exhibited longer endurance during the fire than concrete ones. Turkey et al. [47] tested lightweight geopolymer concrete with the addition of glass powder, which was ground to achieve particles of 10–30 μm. They found that after heating at 200 °C the mechanical strength was higher, and it decreased at 400 °C afterward. However, the most significant decrease was observed at 800 °C, which was caused by the loss of water from the structure of materials. Moreover, Chindaprasirt et al. [48] confirmed the profitable effect of the incorporation of fine auto glass on the fire-resistance performance of fly ash-based geopolymers.

Until now, the effect of incorporating waste glass with various particle sizes and shares on geopolymer fire resistance remains unknown. Therefore, the main objective of this work is to fill the existing research gap. The consistency of fresh geopolymer mortars was examined. The thermal effects occurring during the geopolymerization process were investigated using negative temperature coefficient thermistors. Mineralogical and mechanical analysis, microscopic observation, water absorption tests, density, and specific surface area of composites after curing depending on particle size and share of waste glass addition were carried out. Finally, a fire resistance test was performed, and then the loss mass, residual compressive strength, and chemical compositions of geopolymers were determined.

2. Materials and Methods

2.1. Materials

Fly ash from Skawina Power Plant was used as a primary material for the geopolymers synthesis. A commonly available quartz river sand (Swiętochłowice, Poland) was applied as an aggregate in the geopolymer matrix. Waste cullet glass of brown bottles after initial cleaning and crushing, used as a partial replacement of fly ash in geopolymer composites, was delivered by Grabowski Import Export Company (Sędziszowa, Poland). The glass cullet was sieved through a set of sieves with mesh sizes of 200 μm, 100 μm, 63 μm, and 40 μm to determine the influence of various ranges of waste glass particle size on the properties of the composites. As a result, there were six various ranges of particle sizes, such as 0.1–1200 μm (unsorted waste glass), 200–1200 μm, 100–250 μm, 63–120 μm, and 40–63 μm, 0.1–40 μm. The cullet was not subjected to additional cleaning before the

application due to economic and environmental reasons, including reducing the cost of geopolymers production, as well as water and electricity savings. The schematic of the waste glass preparation process is shown in Figure 1.

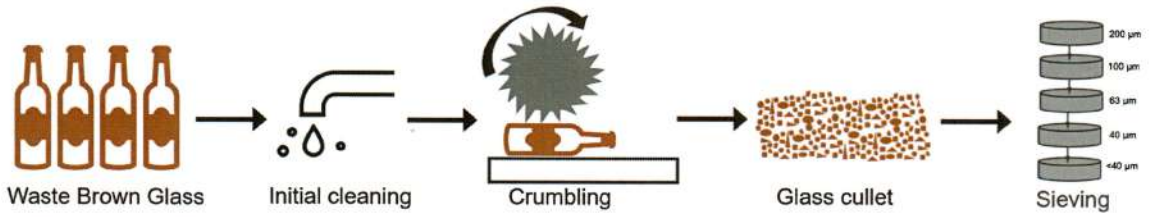

Figure 1. Preparation of waste glass for the experiments.

Furthermore, Table 1 presents the particle size distribution of raw materials, such as fly ash, sand, and various factions of waste glass.

Table 1. Particle size distribution for starting materials [49].

Raw Materials	D_{10} [µm]	D_{50} [µm]	D_{90} [µm]	Mean [µm]	Span $(D_{90}-D_{10})/D_{50}$ [µm]
Fly ash	2.3 ± 0.1	12.3 ± 1.3	37.0 ± 6.0	17.3 ± 2.5	2.8 ± 0.2
Sand	203.3 ± 13.6	416.2 ± 14.9	583.6 ± 17.2	450.1 ± 17.2	0.9 ± 0.02
0.1–1200 waste glass	112.8 ± 8.6	483.4 ± 19.7	896.7 ± 51.1	550.1 ± 18.9	1.6 ± 0.2
200–1200 waste glass	303.1 ± 1.6	584.9 ± 4.4	1123.3 ± 5.5	702.4 ± 1.6	1.4 ± 0.02
100–250 waste glass	30.4 ± 1.5	155.2 ± 0.5	248.6 ± 0.2	160.6 ± 0.6	1.4 ± 0.01
63–120 waste glass	6.3 ± 0.1	55.4 ± 1.2	118.5 ± 1.2	60.8 ± 0.9	2.0 ± 0.02
40–63 waste glass	4.9 ± 0.1	33.3 ± 0.1	63.1 ± 0.2	35.1 ± 0.1	1.7 ± 0.01
0.1–40 waste glass	3.9 ± 0.8	19.8 ± 0.3	39.2 ± 0.2	22.0 ± 0.3	1.8 ± 0.2

The alkaline activator consisted of an 8 M sodium hydroxide (NaOH) solution and an aqueous solution of sodium silicate mixed in the proportion 1:2.5. Sodium hydroxide (NaOH) in flake form, acquired from KRAKCHEMIA S.A. (Kraków, Poland), and tap water were used to obtain the NaOH solution, whereas an aqueous solution of sodium silicate (R-145) was bought from Chemi Kam Sp. z o.o. (Będzin, Poland).

2.2. Geopolymer Manufacturing

Fly ash, waste glass, and sand were stirred in a planetary mixer (GEOLAB, Warsaw, Poland) for 2 min, and then an alkali activator was slowly added to the mixture. The quantity of sand was equal in all produced samples, and it amounted to 10% by weight. This was decided on the basis of the literature review in order to increase the durability property of geopolymers, as well as reduce the shrinkage and porosity of manufactured samples [50]. The waste glass as a replacement for fly ash was added at a weight percent of 10%, 20%, and 30% for each fraction of particle size. Based on the literature information, it can be concluded that the optimal share of the addition of waste glass to building materials is usually between 10–30% [51]. The liquid-to-solid ratio was established based on the tested workability, and it was 0.4. Well-mixed homogeneous blends were cast into wood molds of appropriate dimensions, vibrated to dispose of inner air bubbles, and covered by stretch wrap. After drying, they were removed from the molds and then cured under laboratory conditions (at a temperature of 22 °C ± 3 °C and a humidity of 30% to 50%). Samples were designated in accordance with the applied share and the particle size of various fractions of waste glass in geopolymer blends (Table 2).

Table 2. The composition of geopolymer mixtures depending on the share and the fraction of waste glass particle size.

	Composition			Characterization of Used Waste Glass		
Sample Designation	**Fly Ash [%]**	**Sand [%]**	**Waste Glass [%]**	**The Particle Size of Waste Glass [μm]**	**D_{50} of Waste Glass [μm]**	**Specific Surface Area [m^2 g^{-1}]**
REF	90	10	-	-	-	-
10_0.1–1200	80	10	10	0.1–1200	483.4 ± 19.7	0.152
10_200–1200	80	10	10	200–1200	584.9 ± 4.4	0.048
10_100–250	80	10	10	100–250	155.2 ± 0.5	0.114
10_63–120	80	10	10	63–120	55.4 ± 1.2	0.375
10_40–63	80	10	10	40–63	33.3 ± 0.1	0.594
10_0.1–40	80	10	10	0.1–40	19.8 ± 0.3	0.693
20_0.1–1200	70	10	20	0.1–1200	483.4 ± 19.7	0.152
20_200–1200	70	10	20	200–1200	584.9 ± 4.4	0.048
20_100–250	70	10	20	100–250	155.2 ± 0.5	0.114
20_63–120	70	10	20	63–120	55.4 ± 1.2	0.375
20_40–63	70	10	20	40–63	33.3 ± 0.1	0.594
20_0.1–40	70	10	20	0.1–40	19.8 ± 0.3	0.693
30_0.1–1200	60	10	30	0.1–1200	483.4 ± 19.7	0.152
30_200–1200	60	10	30	200–1200	584.9 ± 4.4	0.048
30_100–250	60	10	30	100–250	155.2 ± 0.5	0.114
30_63–120	60	10	30	63–120	55.4 ± 1.2	0.375
30_40–63	60	10	30	40–63	33.3 ± 0.1	0.594
30_0.1–40	60	10	30	0.1–40	19.8 ± 0.3	0.693

2.3. *Characterization of Geopolymer Samples*

The consistencies of fresh geopolymer mortars were examined using two methods, the Novikov cone subsidence and the flow table test. The procedure for determining consistency is shown in Figure 2. Determination of consistency by the flow table was performed according to standard PN-EN 1015-3:1999/A2:2006 [52], whereas the Novikov cone test was acquired in accordance with PN-85/B-04500 standard [53].

The chemical composition of raw materials and geopolymers was determined using an EDX-7200 Energy Dispersive X-ray Fluorescence Spectrometer (Shimadzu Corporation, Kioto, Japan).

The nitrogen adsorption–desorption isotherms were determined using Autosorb—iQ/MP Quantachrome gas sorption analyzer (Anton Paar company, Graz, Austria). The test samples had been outgassed at 300 °C for 24 h prior to measurement to remove impurities from solid surfaces. The Brunauer–Emmett–Teller (BET) method was applied to calculate the specific surface area of geopolymers.

The density of geopolymer composites was calculated by dividing the samples' mass by volume (geometric method). The mass was measured by using a Radwag PS 200/2000R2 (RADWAG Wagi Elektroniczne, Radom, Poland) precision balance. The final result was the average of the measurements of the 3 samples.

The mineralogical composition of geopolymers was determined by X-ray diffraction using PANalytical Aeris Diffractometer (Malvern Panalytical, Almelo, The Netherlands, Cu Kα radiation) with the step size of 0.003° (2θ), a time per step of 340 s, and the 2θ angular range of 10–100°.

The mechanical properties of the samples were investigated using the concrete press MATEST 3000 kN (Matest, Treviolo, Italy). The compressive strengths were tested in accordance with the PN-EN 12390-3:2019 standard using at least three 50 mm cubical samples of each geopolymer composition after 56 days of curing [54].

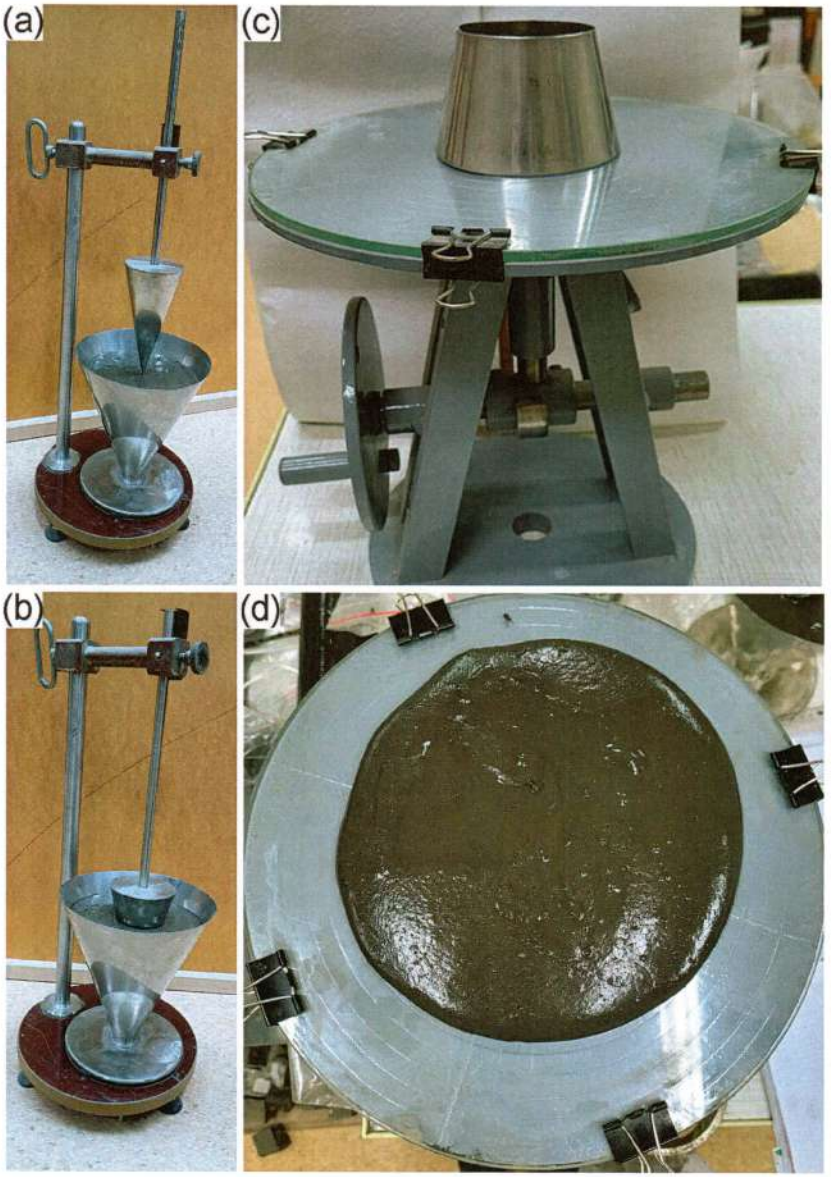

Figure 2. Consistency of geopolymers mortars determined by (**a**,**b**) the Novikov cone method and (**c**,**d**) the flow table test.

The microstructure of geopolymer composites was analyzed using a JEOL JSN5510LV model Scanning Electron Microscope. Before the investigation, the surface of the geopolymers was coated with a thin gold layer by using a JOEL JEE-4X vacuum evaporator (JEOL, Tokyo, Japan).

The fire resistance of geopolymers was determined in accordance with the PN-EN ISO 1182:2020 standard [55]. The samples were placed inside an electric furnace at a temperature of 750 °C. After the isothermal holding of the samples for 30 min, they were cooled together with the furnace to room temperature. Then, the mass loss of specimens was determined according to the following equation:

$$Loss\ of\ mass,\ \% = 100 \times \left[1 - \frac{mass\ after\ experiment}{mass\ before\ experiment}\right]$$

Moreover, the residual compressive strength of samples after the fire resistance test was examined and the result was the arithmetic average of a minimum 3 specimens for each type of geopolymer.

The water absorption test of geopolymers was performed in compliance with PN-88/B-06250 'ordinary concrete' standard. For performing this, three cubic samples for each type of geopolymer were immersed in water to half of their height. After 24 h, water was added in the proper amount to obtain a 10 mm higher water level than the height of samples, and this level was held until the end of saturation. Samples were removed from the water, and after wiping the surface, they were weighed every 24 h. The investigation was ended when two consecutive weighings showed a lack of increase in weight. Completely saturated samples were placed in a dryer until a constant mass was obtained.

The following dependence was applied to determine the water absorption:

$$n_w = \frac{G_2 - G_1}{G_1} \cdot 100\ [\%]$$

where G_1 and G_2 were the average mass of dry specimens and the average mass of the samples replete with water, respectively.

To explore the geopolymerization process depending on the waste glass addition, the fresh geopolymer mortars, and the geopolymers after 48 h of curing, were placed in a laboratory dryer at 75 °C, and distinctive effects were determined using a dedicated negative temperature coefficient system, as described in our previous work [56]. Samples were selected to test based on the most significant differences in the size of the waste cullet (20_0.1–40 and 20_200–1200) and its content in the geopolymer matrix (20_0.1–1200 and 30_0.1–1200). The reference sample contained no added glass. In addition, in order to determine the effect of sand addition on the geopolymerization process, a fly ash-only sample was analyzed.

3. Results and Discussion

The chemical compositions of fly ash, sand, and waste glass are presented in Table 3. Based on the obtained results, coal fly ash used in the experiment mainly consisted of silica, aluminium oxide, and iron oxide. The residual carbon content of fly ash expressed as LOI (the loss of ignition) reached the value of 3.284 [57]. Therefore, it can be classified as class F according to the ASTM C618-95 standard [58]. An extensive study of raw materials was provided in our previous work [49].

Table 3. Chemical compositions of fly ash, sand, and waste glass determined using an X-ray Fluorescence Spectrometer (XRF).

Compound [%]	Fly Ash	Sand	Waste Glass
SiO_2	52.861	89.099	68.814
Al_2O_3	26.561	6.589	1.598
Fe_2O_3	7.588	0.708	0.423
CaO	4.698	0.503	11.671
K_2O	1.567	2.260	0.500
MgO	1.567	0.416	1.325
TiO_2	1.370	0.141	0.083
SO_3	1.095	0.127	0.051
MnO	0.108	0.024	0.050
P_2O_5	0.220	-	-
V2O5	0.089	-	-
Cr_2O_3	0.038	-	0.047
SrO	0.081	0.018	0.024
ZrO_2	0.035	-	0.019
PbO	0.013	-	0.010

Table 3. *Cont.*

Compound [%]	Fly Ash	Sand	Waste Glass
ZnO	0.032	0.003	0.005
NiO	0.012	-	-
SnO_2	0.011	-	-
Ga_2O_3	0.006	0.005	-
Y_2O_3	0.012	0.002	0.002
Cs_2O	-	0.086	-
Na_2O	-	-	15.285
BaO	-	-	0.084

Figure 3 presents the morphology of (a,b), waste glass in the delivery condition, (b,c) fly ash, and (c,d) sand. The waste glass consisted of particles characterized by irregular shapes, diverse sizes, and sharp edges. The river sand had irregular angular structures with hollows, flutes, and protruding sections. The fly ash that was used as a base material in the experiment contained irregular and spherical particles, however, with a predominance of spherical ones, facilitating the geopolymerization process [59].

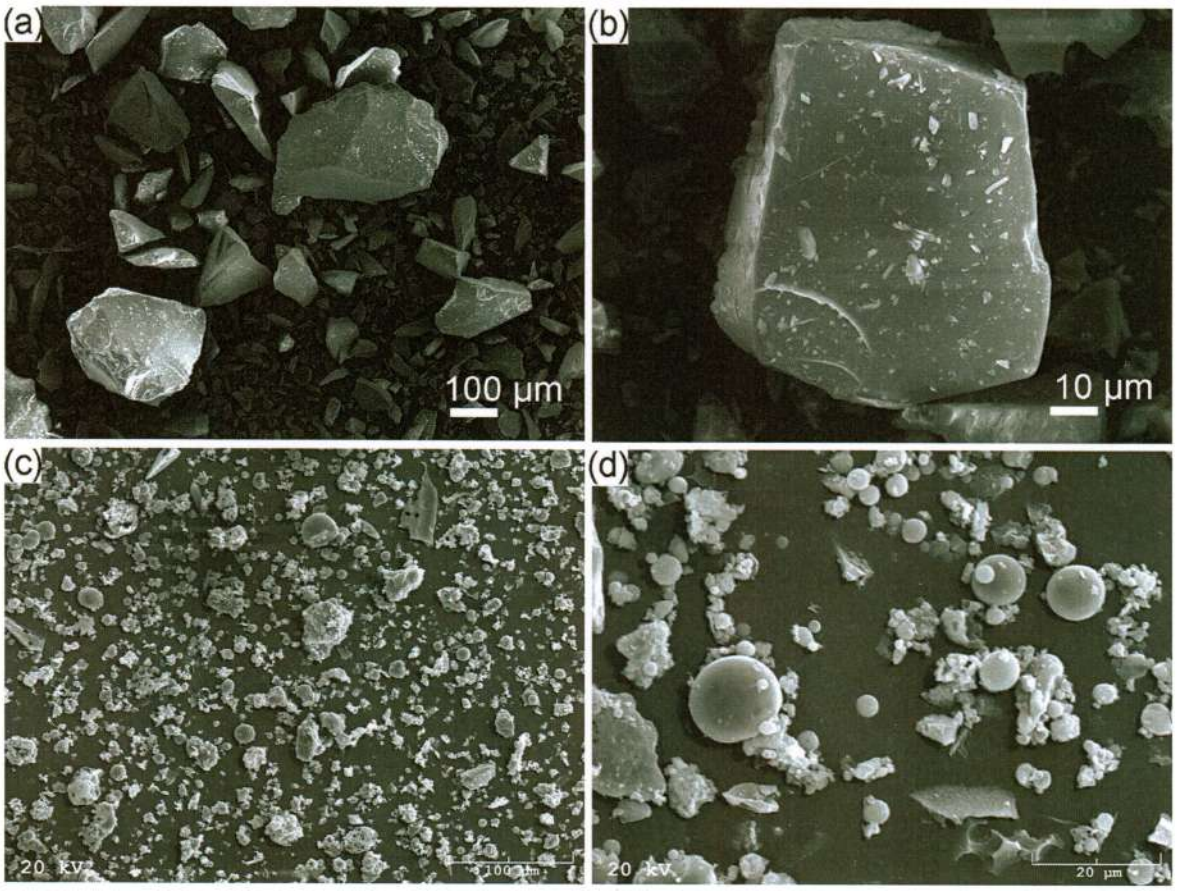

Figure 3. *Cont.*

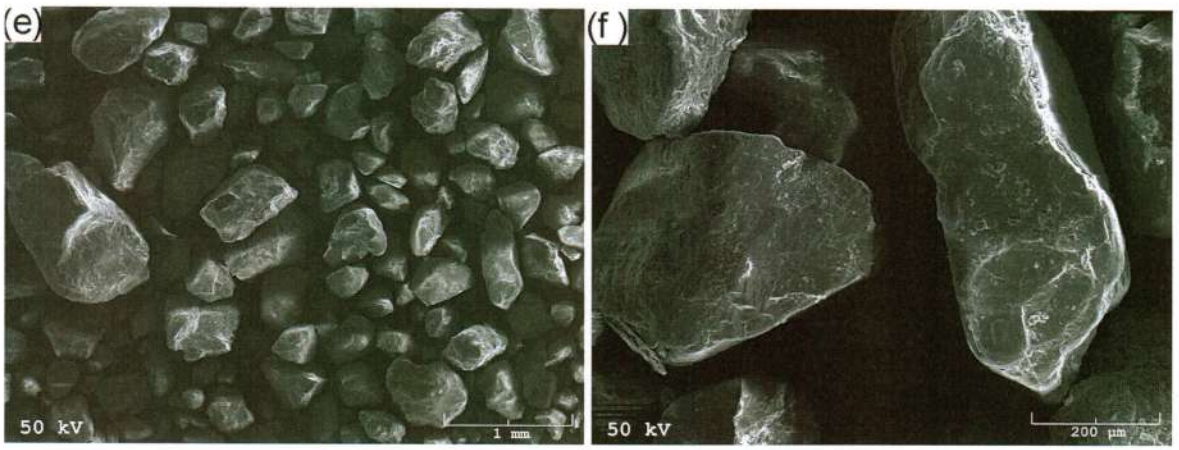

Figure 3. SEM micrographs of (**a**,**b**) waste glass, (**c**,**d**) fly ash, and (**e**,**f**) sand.

Figure 4 demonstrates the obtained results, and three curves were presented on the graph for each sample, representing thermal effects that took place pending the geopolymerization process of fresh geopolymer mortar (red curve), those that took place after 48 h of curing (blue curve), and the difference between these two curves (black curve).

Furthermore, Table 4 summarizes determined characteristic values, such as the maximum gained temperature during the geopolymerization process of fresh geopolymer mortar and the corresponding time, the final setting time, the energy of exothermic reaction, and the temperature difference between the maximum values of thermal effects recorded during the geopolymerization process of fresh geopolymer mortars and after 48 h of curing.

Table 4. Characteristic values for investigated geopolymer compositions calculated based on thermal effects recorded during the geopolymerization process of fresh geopolymer mortars, and after 48 h of curing.

Sample Designation	Maximum Temperature during the Geopolymerization Process [°C]	Time Corresponding to the Highest Temperature [s]	Difference between the Maximum Values of Thermal Effects [°C]	Final Setting Time [s]	Energy of Exothermic Reaction [J (m × K)$^{-1}$]
REF	77.62	7797	3.19	26,580	0.66
REF without sand	77.25	7687	3.09	28,440	0.69
20_0.1–1200	76.65	7375	2.92	14,880	0.56
20_200–1200	77.00	7797	2.79	25,380	0.69
20_0.1–40	79.40	6943	6.36	24,240	2.60
30_0.1–1200	77.10	8446	2.23	56,880	0.62

In the comparison of materials containing various particle sizes of waste glass addition, it has been seen that applications of the smallest particles resulted in the following: (1) the highest reaction energy and the highest recorded temperature, (2) the largest difference between the maximum recorded values of thermal effects, and (3) the maximum thermal effect that was recorded earlier than for the other samples. These effects can be explained by the fact that smaller particles are characterized by larger specific surface areas, and, therefore, the larger area is accessible to the alkaline activator during the geopolymerization process [60]. The presence of exothermic effects results from the dissolution of the solid raw material in the alkaline activator and thus the formation of new material phases. Moreover, it is clearly visible that the energy of the exothermic reaction and achieved maximum temperature depended on the size of the waste glass and were the highest in the case of the sample containing the smallest particles (20_0.1–40), which testified to the highest soluble of these raw materials during the geopolymerization process [61]. During the

geopolymerization process, the amount of released heat is relatively small, indicating that occurring reactions are rather thermally stable [56].

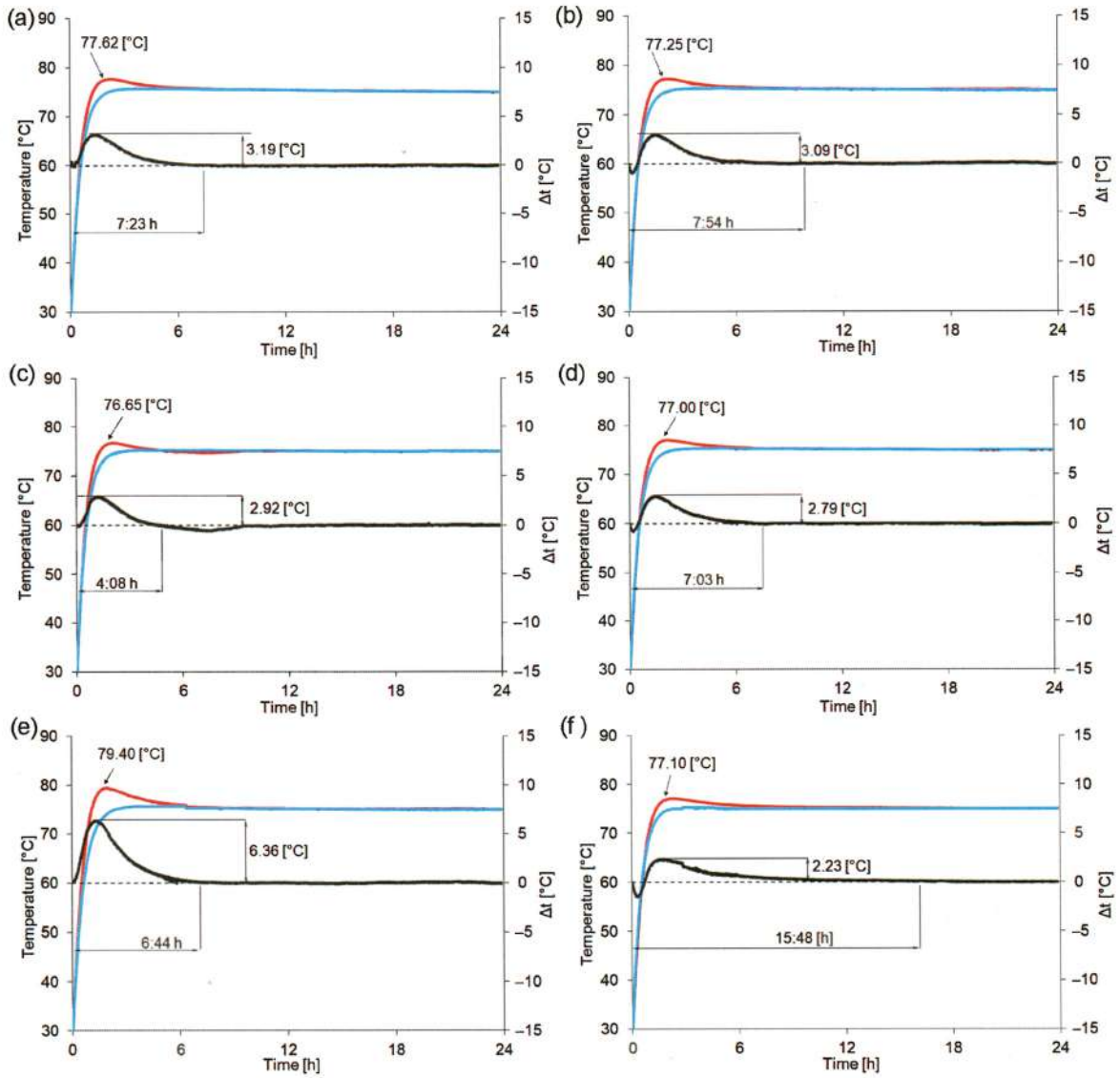

Figure 4. Thermal effects of (**a**) REF, (**b**) REF without sand, (**c**) 20_0.1–1200, (**d**) 20_200–1200, (**e**) 20_0.1–40, and (**f**) 20_0.1–1200 registered using a negative temperature coefficient thermistor device for fresh geopolymer mortars during the geopolymerization process (red curve), after 48 h of curing (blue curve), and the difference between these two curves (black curve).

In general, it was found that the addition of 20% waste glass decreased the final setting time regardless of the used fractions. Basically, the incorporation of starting materials including a higher content of calcium may impact the reduction of the setting time and, simultaneously, the increase of mechanical strength, and this was proven by the presented results [62]. Noteworthily, the 20_0.1–1200 sample, containing unsorted waste cullet, had the shortest final setting time, and, more specifically, it constituted the following part of the final setting time of other samples: 52% of REF without sand, 56% of REF, 59% of 20_200–1200, 61% of 20_0.1–40, and 8% of 30_0.1–1200. However, the elevation of the addition of unsorted waste glass to 30% (30_0.1–1200) caused a different effect, namely, the final setting time was the most extended and was more than twice as long as for the REF sample. The shorter final setting time of geopolymer could be beneficial in terms of future

industrial applications. Moreover, considering the effect of sand on the geopolymerization process, it was found that the use of 10% sand resulted in a decrease in the energy released during the exothermic reaction and a shortening of the final setting time.

As it is commonly known, consistency is defined as the ability of a fresh mixture to flow. Its properties depend on the type of raw materials used, particle size, number of components, and liquid-to-solid ratio [63]. Figure 5 shows the results of the consistency assessment of fresh geopolymer mortars measured by the flow table test and Novikov cone methods. The reference mortar, without the addition of waste glass, achieved values of 182 mm and 8.2 cm by using the Novikov cone and flow table methods, respectively. Moreover, on the basis of the recorded results, it can be seen that all of the fresh geopolymer mortars containing up to 20% of waste glass had plastic consistency. This effect was regardless of the particle size. However, the addition of 30% of waste cullet with particle sizes ranging between 0.1 and 1200 µm or 200 and 1200 µm resulted in a change in the consistency of the mortar to liquid/thin. The explanation of this phenomenon is related to the fact that waste glass particles with larger dimensions do not have the ability to absorb as much alkaline solution as fly ash. In contrast, the use of cullet in the same amount (30% by weight) but with a smaller particle diameter determined the formation of a mixture with a plastic consistency. It should be noted that decreasing the particle size of waste glass addition reduces the flow diameter and Novikov's cone immersion depth of fresh geopolymer mortars. This effect can be explained by the increase of the specific surface area of smaller particle waste glass, which absorbed a larger quantity of alkaline solution. Other authors noticed a similar phenomenon. The results clearly indicate that the flowability of composite with the addition of glass depends on a few factors, including the type, size, and roughness of the incorporated addition [64,65].

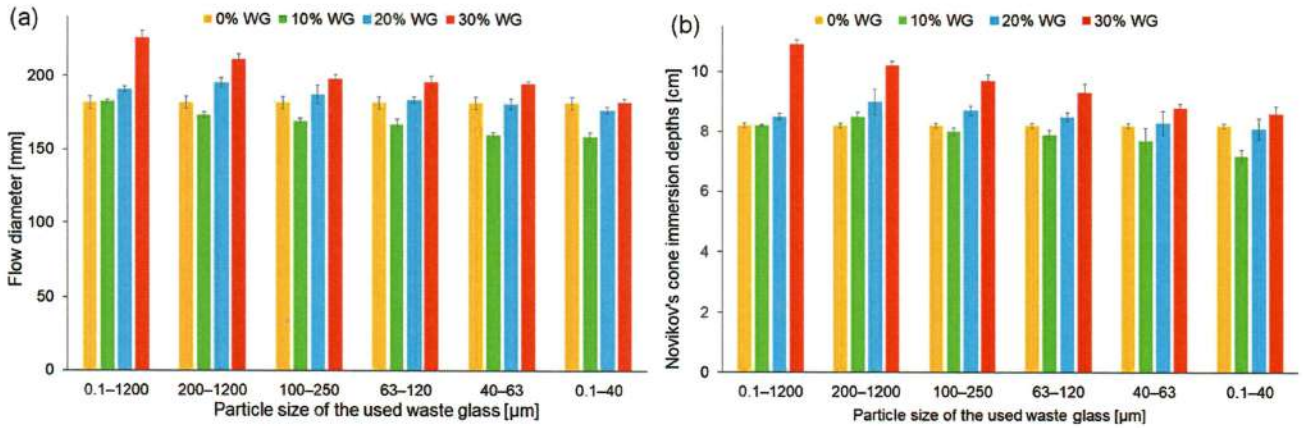

Figure 5. The consistency of fresh geopolymer mortars depending on the share and the fraction of waste glass particle size determined by (**a**) the flow table test and (**b**) the Novikov cone method.

Water absorption is an important feature of construction materials, which shows the resistance of concrete materials to sulphate, chloride ions, carbonation, and freeze-thaw cycles [66]. Water absorption is strongly connected to pore size and volume in the investigated materials [67]. Figure 6 presents the results of the water absorption and density test of reference geopolymers and composites containing unsorted waste glass, corresponding to the particle size of 0.1–1200 µm. There was a strong dependence between the share of waste glass in geopolymers and their water absorption. As predicted, the water absorption decreases with the increase of waste glass share in geopolymers. The reason for this is the water absorption of waste glass, which is close to zero [68,69]. Furthermore, the addition of waste glass to the geopolymer matrix resulted in higher density as compared to the reference material.

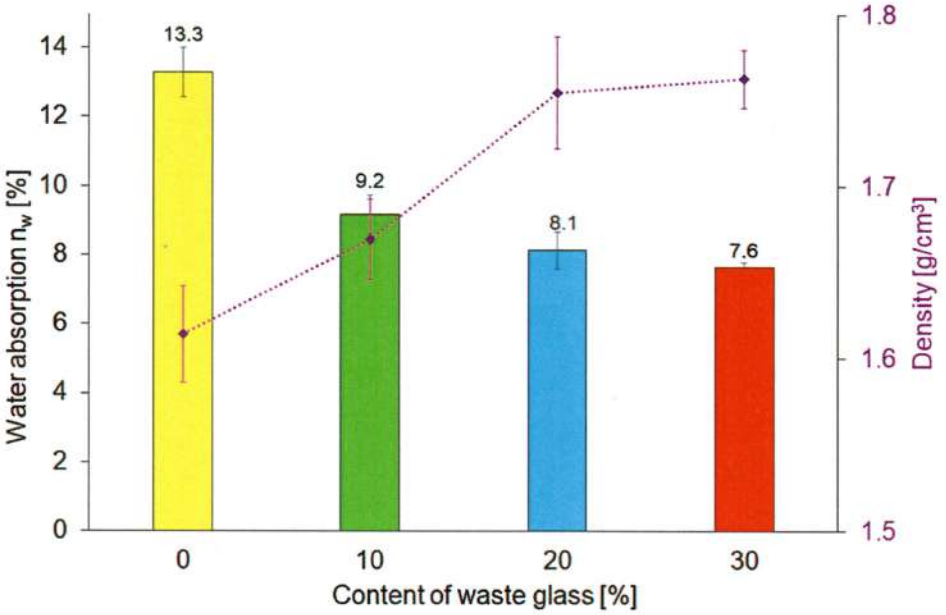

Figure 6. Water absorption and density of geopolymers depending on the composition of the samples.

In order to assess the influence of waste glass on the mineralogical composition of geopolymers containing different shares and sizes of the fraction of the waste glass addition, their XRD patterns were compared (Figure 7). The qualitative analysis revealed the following phases: quartz (SiO_2, ref. code: 01-075-8320), mullite ($Al_6Si_2O_{13}$, 01-082-1237), C-S-H as Rosenhanite (Ca_3 ($Si_3O_8(OH)_2$, ref. code: 00-029-0378), albite ($NaAlSi_3O_8$, ref. code: 01-071-1150), and anorthite ($CaAl_2Si_2O_8$, ref. code: 04-013-2357). In general, the peak locations of all investigated samples had almost no difference, pointing out that they consisted of the same phases. However, the XRD peaks of samples manufactured using waste glass addition had lower intensity as compared to the reference material. Similarly, the smaller the particle size, the lower the intensity of the peaks, which is especially evident for the sample containing the smallest particle size (20_0.1–40). This effect can be attributed to the decline in the degree of crystallinity. The appearance of the hump on the diffractogram at position 15–35° 2θ indicates the presence of an amorphous phase, which was identified as a C-S-H compound. Moreover, sharp diffraction peaks observed in particular positions on the diagram as a result of the use of X-rays were assigned to crystalline phases [70]. Albite and anorthite belong to plagioclase feldspar minerals, and due to their high stability, they can serve as a filler or reinforcing material [71].

The nitrogen adsorption–desorption isotherms of samples containing various shares and particle sizes of waste glass are presented in Figure 8a,b, respectively. According to the IUPAC (International Union of Pure and Applied Chemistry) classification, all obtained isotherms can be categorized as type IV isotherms with H3 hysteresis loops [72]. In this type of isotherm, a hysteresis loop occurs as a result of the filling or evacuating of mesopores (pores with a diameter of 2–50 nm) via capillary condensation [73,74].

The specific surface areas of geopolymers calculated by the single-point and multi-point Brunauer–Emmett–Teller (BET) methods, pore volume, and pore size are shown in Table 5. It can be noticed that the specific surface area of the 30_0.1–1200 sample achieved 33.26 $m^2\ g^{-1}$; therefore, it decreased by almost 27% compared to the reference sample, taking into account the result of the multi-point BET method. Furthermore, the smallest specific surface area of 5.35 m^2g^{-1} was obtained for the sample with the 30% addition of the smallest particle size (30_0.1–40), representing a decrease of around 88% and 84% in comparison with the sample without the additive and with 30% of waste glass characterized by the largest particle size, respectively. Geopolymers including the largest range of waste glass particle size (0.1–1200 μm) showed a decrease in specific surface area

with an increasing share of addition. Based on the recorded results, it was found that the specific surface of the samples decreased with the use of smaller particle sizes of glass waste, as well as with the share increase of glass addition to the composite.

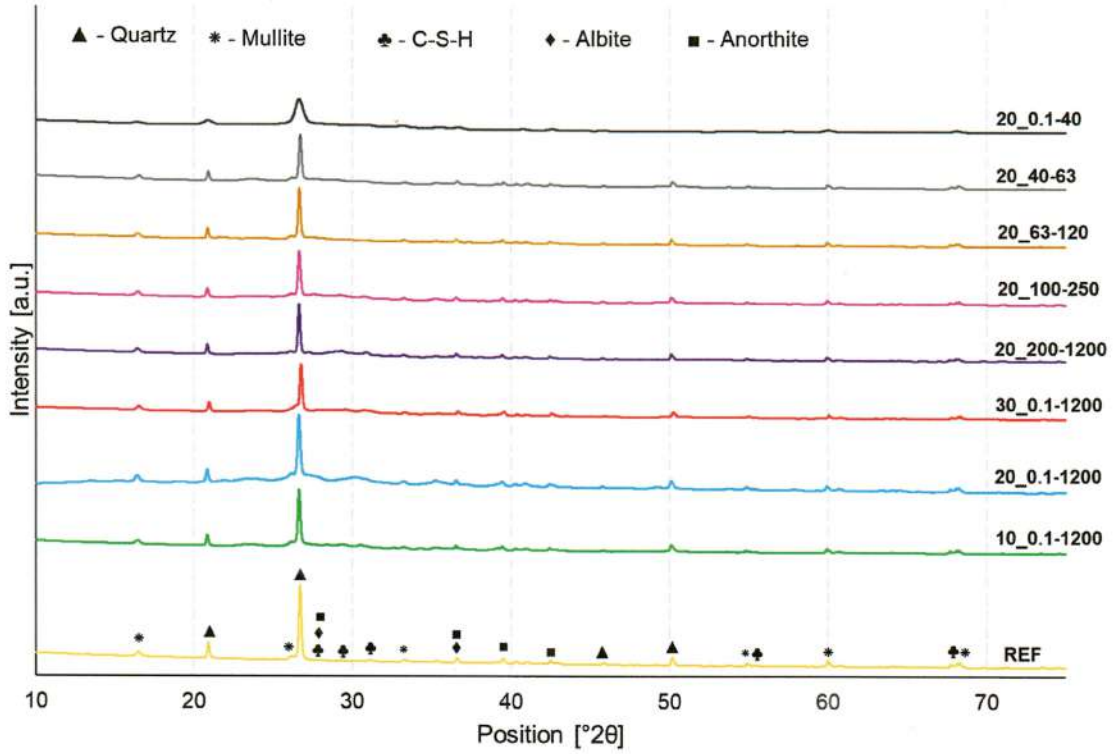

Figure 7. XRD analysis of reference samples and selected geopolymers depending on the share and the fraction of waste glass particle size.

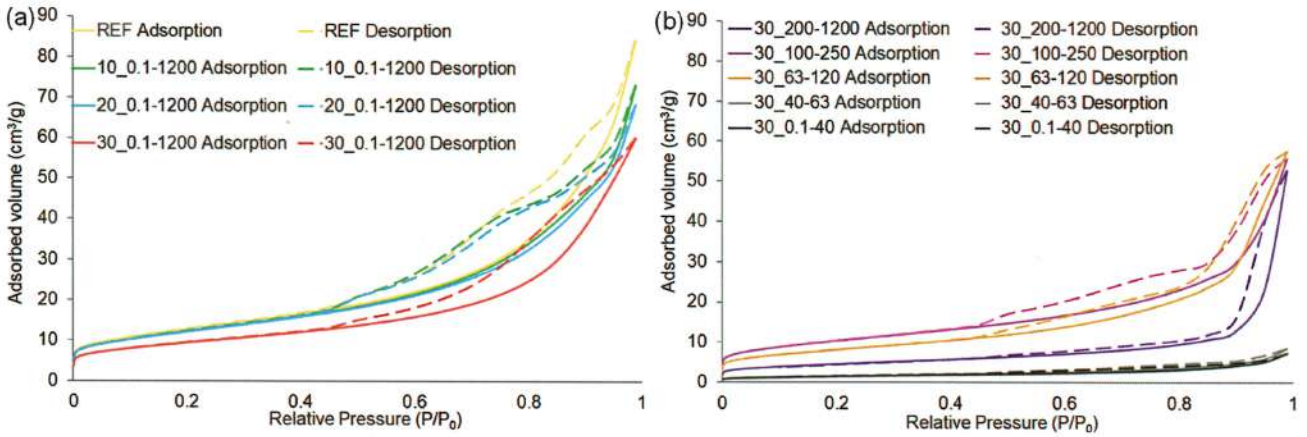

Figure 8. Nitrogen adsorption–desorption isotherms of geopolymers depending on: (**a**) the share and (**b**) the fraction of waste glass particle size.

The application of 30% of waste glass with particle sizes ranging from 0.1 to 1200 µm resulted in a decrease of 29% of the total pore volume as compared to the reference specimen. Furthermore, the total pore volume in the sample containing 30% waste characterized by the smallest particle sizes (30_0.1–40) was over 11 times lower than the reference material, indicating that this factor closely depended on the share and particle size of the additive. The obtained results also showed a certain, but not so clear, correlation in terms of the pore

diameter of geopolymers, i.e., the smaller particle size and higher share of the waste glass, the lower the diameter of pores were.

Table 5. The specific surface area of the selected geopolymers depending on the share and the fraction of waste glass particle size.

Sample Designation	Specific Surface Area [m^2 g^{-1}]		Pore Volume [cm^3 g^{-1}]		Pore Size [nm]	
	Multi Point BET Method	Single Point BET Method	Total Pore Volume at P/P0 = 0.99	BJH Pore Volume	Average Pore Diameter	BJH Average Pore Diameter
REF	45.44	42.03	0.1306	0.1293	11.50	6.551
10_0.1–1200	44.39	40.76	0.1133	0.1120	10.21	6.544
20_0.1–1200	43.74	40.43	0.1059	0.1043	9.682	5.630
30_0.1–1200	33.26	31.13	0.09313	0.09171	11.20	7.799
30_200–1200	33.67	30.80	0.1013	0.1004	12.03	6.549
30_100–250	33.13	30.28	0.09000	0.08903	10.87	4.908
30_63–120	28.65	26.63	0.08923	0.08820	12.46	5.626
30_40–63	5.91	5.43	0.01316	0.01276	8.917	1.690
30_0.1–40	5.35	5.16	0.01141	0.01085	8.529	2.744

The findings were consistent with the density and water absorption of geopolymer composites. The incorporation of waste glass caused a decrease in water absorption, a reduction in pore size and volume, a slight increase in density, and a cutting of specific surface area simultaneously. These results show that the addition of waste glass reduces the porosity of the fly ash-based geopolymer matrix, causing the formation of denser structures.

The compression strength of geopolymers depending on the share and particle size of the waste glass addition was demonstrated in Figure 9. The compressive strength of the geopolymers increased after the incorporation of waste glass into the matrix by 53% to 137%, depending on the composition of the samples. Similar results were obtained by Jiang et al. [46], who explained that glass contains SiO_2 and Al_2O_3, which can react and form aluminosilicate hydrates, which have a positive influence on compressive strength.

It is evident that the optimal level of the waste glass changed depending on the particle size of the addition, and it amounted to 20% for samples containing the following fractions: 0.1–1200 µm, 200–1200 µm, 100–250 µm, and 63–120 µm. However, in the case of using fractions with smaller particles, 63–40 and 0.1–40 µm, the optimal level was achieved with a 10% addition of waste glass. This phenomenon is related to the pozzolanic activity of waste glass, which depends mainly on the chemical composition and particle size. The crumbling of waste glass could lead to the enhancement of its pozzolanic reactivity and could react in the geopolymerization process afterward [23]. However, when the share of waste glass amounted to 30%, the Si/Al ratio was higher, resulting in the formation of low-crosslinked aluminosilicates, and therefore the deterioration of mechanical properties [75]. It is worth mentioning that all geopolymer composites, even with 30% of waste glass, had higher results than the reference material.

Fly ash showed a mean particle size of 17.3 ± 2.5 µm, whereas the fraction of waste glass containing the smallest particle size (0.1–40 µm) had a mean particle size of 22.0 ± 0.3 µm. On the other hand, the true density of fly ash and waste glass was 2.288 ± 0.001 g cm^{-3} and 2.507 ± 0.001 g cm^{-3}, respectively. In general, using smaller particle sizes of starting materials is beneficial due to the higher available specific surface area and therefore higher reactivity and more efficient course of geopolymerization process [57]. Even though fly ash had a smaller particle size, the replacement of it by waste glass in geopolymers was beneficial in terms of compressive strength, regardless of the used fraction of waste glass. It is evident that the main factor affecting the strength properties of samples was the ability to dissolve silica-rich waste glass particles. Furthermore, waste glass contained a higher amount of CaO (11.671%) than fly ash (4.698%), resulting

in the development of additional calcium silicate hydrate and therefore structures that are characterized by higher density and strength, and this was also noticed in previous work [76]. Regarding the particle size of waste glass, many earlier reports indicated that using the finer particles resulted in a higher strength of the final material due to their higher pozzolanic reactivity [77]. A similar tendency is also visible in the presented study, showing that the most positive effect of the incorporation of waste glass on the compressive strength was achieved for samples containing the smallest particle size (0.1–40 µm). However, it should be noted that surprisingly high compressive strength was obtained using unsorted waste glass, consisting of the widest size range of particles.

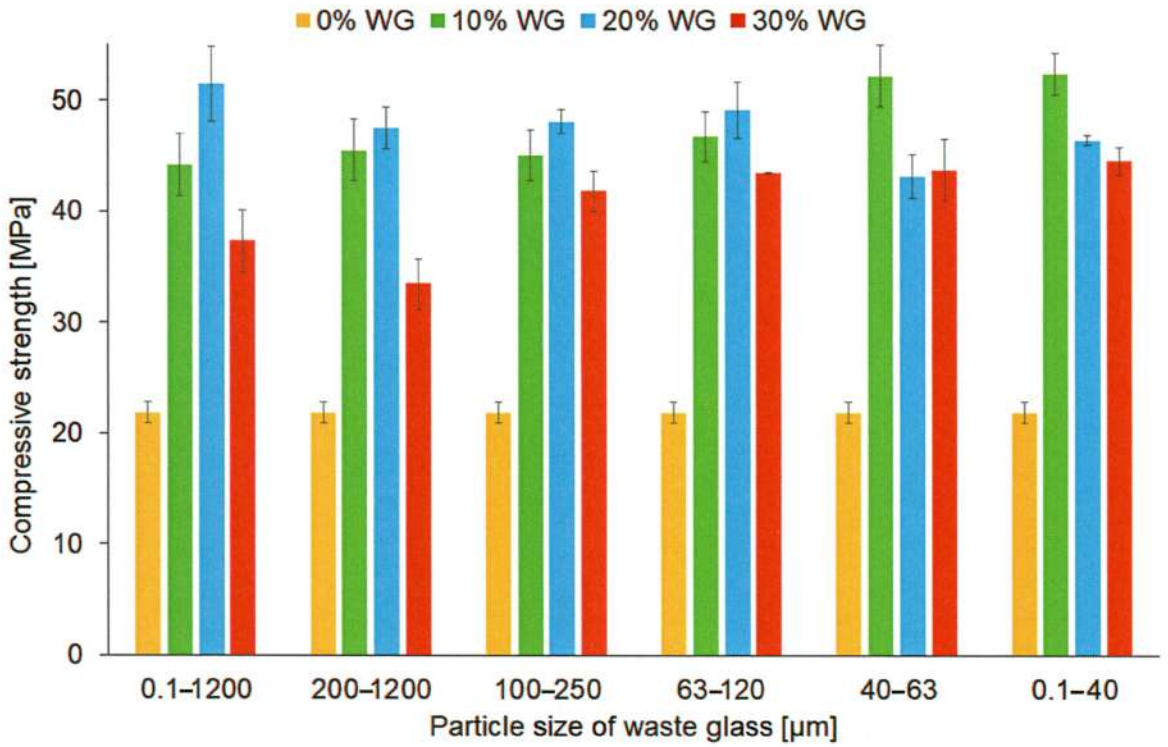

Figure 9. The compressive strength of geopolymers depending on the share and the fraction of waste glass particle size.

The morphology of the reference material and samples with 30% share and various sizes of the waste glass is presented in Figure 10. Because the samples were observed after the compressive strength test, cracks can be seen on their surface. A greater number of pores in the matrix of reference samples was clearly visible, compared to composites with the addition of glass waste. This observation was consistent with the geopolymer density results presented earlier. Moreover, unreacted particles of fly ash in small amounts have occurred in the geopolymer matrix, which adversely affects the compressive strength [78]. On the other hand, it is well-known that during the geopolymerization process, not all of the components are converted into geopolymers.

Figure 11 presents the mass loss of the geopolymer composites after the fire resistance test. The mass loss ranged from 11.7% (30_0.1–1200 sample) to 17.7% (20_0.1–40 sample). By comparing the mass loss of geopolymers, it can be concluded that reducing the particle size of addition caused a more significant weight loss of the samples after the fire resistance test. The explanation for this can be the amount of absorbed water inside the waste glass particles. As mentioned before, smaller particles of waste glass have a higher specific surface area and can absorb more water during the manufacturing process than coarse ones. The mass loss of geopolymers occurs at high temperatures mainly due to the effects of evaporation of adsorbed water, as well as the desquamation and chips of materials.

However, depending on the temperature, various changes in the material were observed. In the beginning, at temperatures up to 400 °C, the fly ash-based geopolymers showed an improvement in compressive strength due to the reaction of unreacted particles of waste glass and the shrinkage of the pores. In higher temperatures, further changes took place, such as the transformation of iron compounds (400–800 °C), the formation of new pores with different sizes (400–800 °C), and the removal of the porosity during the sintering process (600–1000 °C), cracking of samples (600–800 °C), and shrinkage (200–1000 °C) [38,79]. However, regardless of the share of the added glass waste and its particle size fraction, it was found that all investigated composites can be categorized as materials class $A1_{fl}$ according to the fire classification PN-EN ISO 1182:2020 standard.

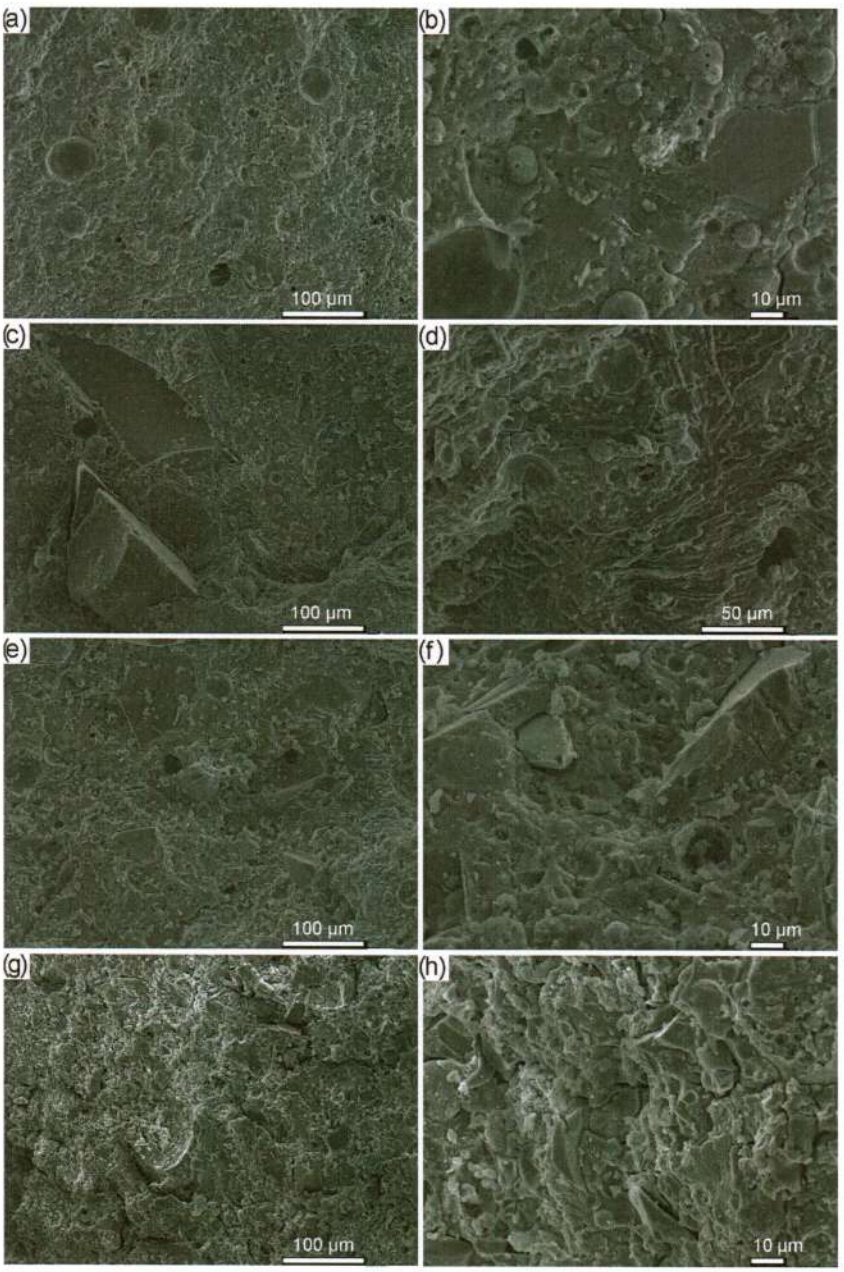

Figure 10. SEM images of geopolymers after the compressive strength test depending on the share and the fraction of the waste glass particle size: (**a**,**b**) REF, (**c**,**d**) 30_200–1200, (**e**,**f**) 30_63–120, (**g**,**h**) 30_0.1–40.

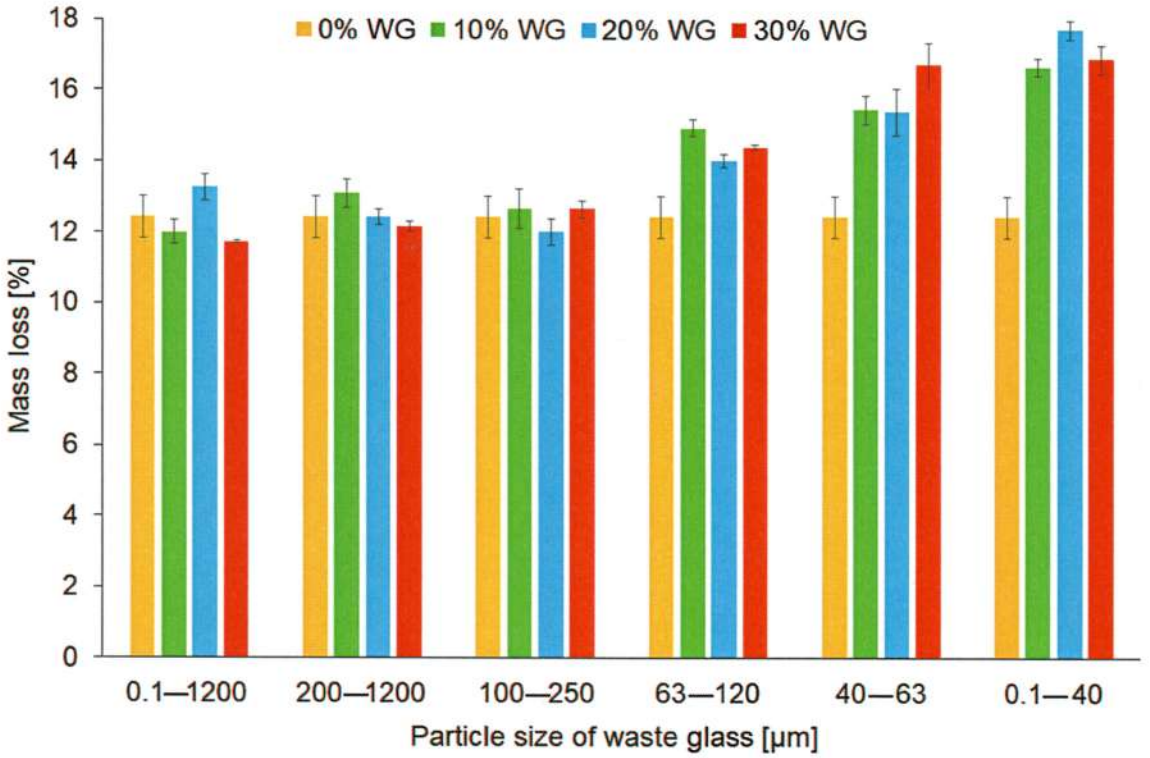

Figure 11. Mass loss of the geopolymers depending on the share and the fraction of waste glass particle size after the fire resistance test.

The influence of the high temperature on residual compressive strength changes of the samples after the fire resistance test was also investigated (Figure 12). The recorded results showed that, regardless of the size of the particle fraction and their share in the composite, the addition of glass waste had a beneficial effect on the residual compressive strength compared to the reference material. This effect was due to the introduction of an additional share of aluminium and silica into the material composition [80]. Bisht et al. [81] investigated the compressive strength of concrete mixes with the addition of waste glass after exposure to temperatures ranging from 200 °C to 800 °C. They noticed the beneficial impact of waste glass incorporation after exposure to 400 °C compared to the reference samples made without the glass addition.

It was noticed from the presented results (Figure 12) that the application of waste glass characterized by larger particle sizes led to reaching a higher strength than in the case of incorporating smaller particles. Similar observations regarding the influence of waste glass particle size on the compressive strength after exposure to high temperatures were made by Mao et al. [82], who investigated clay bricks with the addition of waste glass powder after heating at 950 °C for 3 h. They concluded that incorporating larger particle sizes of waste glass into brick resulted in higher compressive strength due to the formation of albite or glass–ceramic compounds. However, it should be emphasized that they investigated only the influence of waste glass with average sizes of 250, 100, 35, and 10 µm.

Interestingly, comparing the results of compressive strength before (Figure 9) and after (Figure 12) the fire resistance test it was found that the optimal share of waste glass for each fraction of particle size was the same. Considering the waste glass with particle sizes within the ranges of 0.1–1200 µm (unsorted cullet), 200–1200 µm, 100–250 µm, and 63–120 µm it can be seen that 20% of the additive resulted in achieving the best outcomes. Nevertheless, geopolymer composites with the addition of smaller particle sizes of the additive (fractions of 40–63 µm and 0.1–40 µm) achieved the best performance by applying 10% of waste.

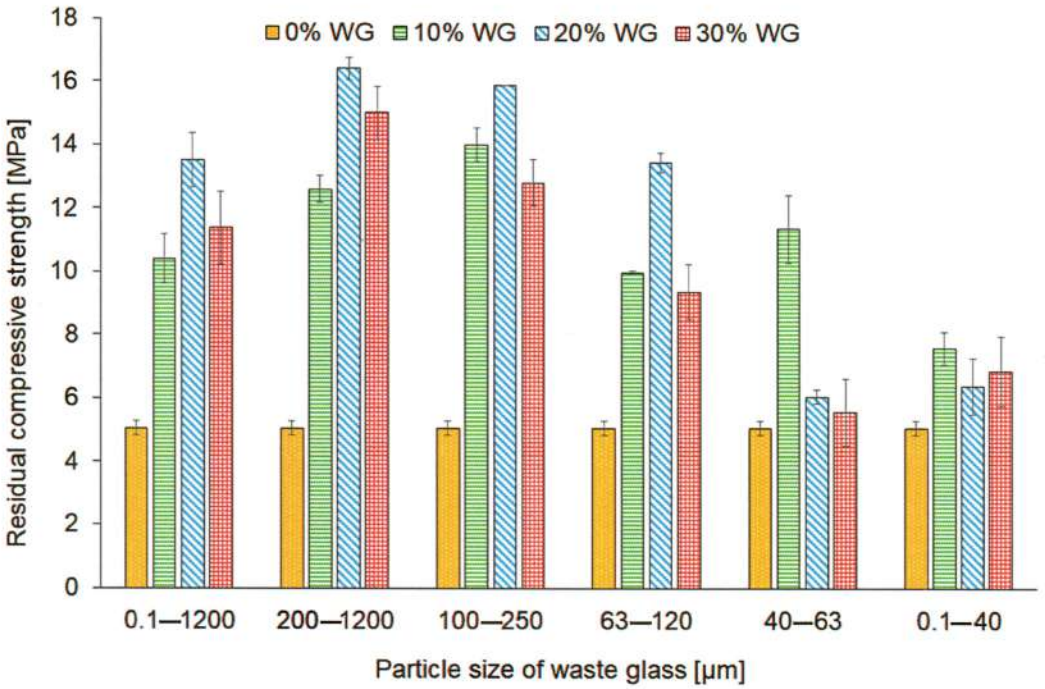

Figure 12. The residual compressive strength of geopolymers depending on the share and the fraction of waste glass particle size.

Moreover, on the basis of the results, it was observed that the application of waste containing fractions with the highest particles (200–1200 µm) and (0.1–1200 µm) caused the increase in residual compressive strength by about 221.6% and 164.7% as compared to the reference geopolymer. Considering future industrial applications, it should be noted that the sieving and dispensing of waste glass are associated with high costs and there is a necessity to use additional technological solutions. Therefore, the results obtained for geopolymers with the additive of unsorted waste glass are the most promising.

The residual compressive strength of the geopolymers constituted 26.2% and 23.3% of compressive strength before the fire resistance test in the case of 20_0.1–1200 and the reference samples, respectively. It could be clarified that waste glass with smaller particle sizes shows higher pozzolanic reactivity and could react in the geopolymerization process. After being heated to 750 °C, the glass waste particles could change their state from solid to liquid due to the exceeded melting threshold of waste glass (below 700 °C) and hence could fill pores inside the samples [48,83].

The chemical composition of the selected geopolymers depending on share and particle size fractions of waste glass before and after the fire resistance test is shown in Table 6.

All samples consisted of three main components, SiO_2, Na_2O, and Al_2O_3, either before or after the fire resistance test. The total share of these main chemical compounds ranged from 81.881% (REF sample before the test) to 86.430% (30_200 sample before exposure to high temperature).

Before the exposure of geopolymers to high temperatures, the SiO_2/Al_2O_3 ratio amounted to 3.45, 4.012, and 4.635 in REF, 30_200–1200, and 30_0.1–40 samples, respectively. Dehghani et al. [84] discovered that increasing the SiO_2/Al_2O_3 ratio caused a decrease in the BET-specific surface area in fly ash-based geopolymers, and this dependency is also clearly noticeable in the presented study. Furthermore, Klima et al. [38] indicated that in the temperature range of 600–800 °C, oxidation of iron oxides contained in unreacted particles of fly ash takes place, which was also proved in this work. The XRF analysis showed that the Fe_2O_3 share in geopolymers after the fire exposure decreased by 19.3%, 11.7%, and 35.9% for samples designated as REF, 30_200–1200, and 30_0.1–40, respectively,

as compared to the amount of this compound before treatment. In addition, it was noted that after the fire resistance test, SiO_2 content in geopolymers increased by 21.9%, 16.4%, and 15.5%, whereas the content of Na_2O decreased by 25.5%, 40.2, and 14.8% for REF, 30_200–1200, and 30_0.1–40, respectively.

Table 6. Chemical composition of geopolymers depending on the share and the fraction of waste glass particle size before and after the fire resistance test.

Compound [%]	Before the Fire Resistance Test			After the Fire Resistance Test		
	REF	30_200–1200	30_0.1–40	REF	30_200–1200	30_0.1–40
SiO_2	46.764	46.762	49.035	57.009	54.439	56.620
Na_2O	21.564	27.372	23.861	16.071	16.371	20.333
Al_2O_3	13.553	11.653	10.576	10.877	13.329	8.462
Fe_2O_3	6.481	5.041	5.598	5.232	4.453	3.586
CaO	5.726	4.541	5.535	3.314	3.883	5.341
K_2O	2.921	2.151	2.535	2.714	2.253	1.543
TiO_2	1.104	0.838	0.925	0.957	0.783	0.590
MgO	0.717	0.843	0.649	1.007	0.846	1.376
SO_3	0.435	0.291	0.715	2.217	3.020	1.749
P_2O_5	0.329	0.231	0.179	0.266	0.298	0.148
MnO	0.087	0.071	0.081	0.088	0.084	0.068
SrO	0.076	0.049	0.067	0.044	0.043	0.036
V_2O_5	0.067	0.053	0.073	0.066	0.096	0.046
ZrO_2	0.035	0.026	0.031	0.029	0.027	0.024
ZnO	0.029	0.018	0.024	0.027	0.024	0.018
Cr_2O_3	0.023	0.028	0.039	0.021	0.018	0.030

4. Conclusions

In this study, the influence of share (0, 10, 20, and 30%) and fractions of particle size of waste glass (0.1–1200, 200–1200, 100–250, 63–120, 40–64, and 0.1–40 μm) on the properties of coal fly ash-based geopolymers were determined. The thermal phenomena that occurred during the geopolymerization and curing process were characterized. The consistencies of fresh mortars were examined afterward. Next, the mineralogical composition, specific surface area, water absorption, density, compressive strength, and microstructure of geopolymer composites were investigated. Finally, for all variants of the investigated samples, a fire resistance test was performed after which weight loss, residual compressive strength, and chemical composition were determined. Based on the obtained results, the following was found:

1. Thermal phenomena occurring in coal fly ash-based geopolymers closely depended on the composition of the mix. Each fraction of the particle size of waste glass additive applied in an amount of 20% by weight reduced the final setting time of the geopolymer products. Furthermore, the highest energy of the exothermic reaction was released during the geopolymerization of the sample containing the smallest particles of waste glass addition (0.1–40 μm). It is noteworthy that the sample, containing 20% of unsorted waste cullet, had the shortest final setting time of all investigated materials.
2. Decreasing the particle size of waste glass reduced the flow diameter and Novikov's cone immersion depth of fresh geopolymer mortars. This effect was due to the increase of the specific surface area of decreasing waste glass, which showed a tendency to absorb a larger amount of alkaline solution. All fresh geopolymer mortars, containing up to 20% of waste glass, regardless of the particle size, had plastic consistency. In contrast, the addition of 30% of the waste cullet with particle sizes of 0.1–1200 μm or 200–1200 μm resulted in a change in the consistency of the mortar to liquid/thin.
3. Samples without the addition of waste glass were characterized by the largest specific surface area. Its decrease was observed with a decrease in the size of glass particles and an increase in its share in the composite. All nitrogen adsorption–desorption isotherms of geopolymers were classified as type IV isotherms with H3 hysteresis

loops, indicating the presence of mesopores. Furthermore, it was found that the smaller the particles and the higher the share of the waste glass, the lower the pore volume and diameter of the pores were.

4. The water absorption of geopolymers was approximately 31%, 39%, and 43% lower for samples containing 10, 20, and 30% of waste glass with particle sizes ranging between 0.1 and 1200 μm than for reference ones. Furthermore, the addition of waste glass resulted in an increase of density by 9% (from 1.61 to 1.76 g cm^{-3}), a decrease in the specific surface area by 26% (from 45.44 m^2 g^{-1} to 33.67 m^2 g^{-1}), and a reduction of the total pore volume by 22% (from 0.1306 to 0.1013 cm^3 g^{-1}) by comparing the reference sample with geopolymers containing 30% of waste glass with particle sizes of 0.1–1200 μm simultaneously
5. Compared to the reference samples without the addition of waste glass, the compressive strength before and after the fire resistance test of the specimens containing 20% of unsorted waste glass (particle size within the range of 0.1–1200 μm) was enhanced by 135.2% and 164.7%, respectively.
6. Despite the fact that the compressive strength of the geopolymer composites increased along with the reduction of waste glass size, the use of a larger fraction of glass cullet resulted in a higher residual compressive strength determined after exposure to high temperatures. Moreover, all geopolymer samples were qualified as materials class $A1_{fl}$ in terms of fire resistance.

The presented results are significant for the development of materials used as paving bricks, offshore structures, fireproof covers, and prefabricated elements that will characterize appropriate crucial properties such as consistency, density, water absorption, compression strength, and fire resistance while reducing the negative environmental impact. By changing the share and particle size of waste glass, the properties of fly ash-based geopolymer composites can be adapted to a certain extent to the individual requirements in the industrial sectors.

Author Contributions: Conceptualization, M.H. and C.Z.; data curation, A.G. and D.M.; formal analysis, M.H. and C.Z.; funding acquisition, M.H.; investigation, C.Z. and D.M.; methodology, M.H., C.Z., A.G. and D.M.; resources, M.H. and C.Z.; supervision, M.H.; validation, M.H. and A.G.; visualization, M.H. and C.Z.; writing—original draft, M.H. and C.Z.; writing—review and editing, M.H. and C.Z. All authors have read and agreed to the published version of the manuscript.

Funding: This research was supported by the "ROAD TO EXCELLENCE—a comprehensive university support programme" accomplished within the Operational Programme Knowledge Education Development 2014–2020 and co-financed by the European Social Fund; agreement no. POWR.03.05.00–00-Z214/18.

Institutional Review Board Statement: Not applicable.

Informed Consent Statement: Not applicable.

Data Availability Statement: Not applicable.

Conflicts of Interest: The authors declare no conflict of interest.

References

1. Oxford Economics Future of Construction. Available online: https://www.oxfordeconomics.com/resource/future-of-construction/ (accessed on 12 April 2023).
2. Luo, Y.; Jiang, Z.; Wang, D.; Lv, Y.; Gao, C.; Xue, G. Effects of Alkaline Activators on Pore Structure and Mechanical Properties of Ultrafine Metakaolin Geopolymers Cured at Room Temperature. *Constr. Build. Mater.* **2022**, *361*, 129678. [CrossRef]
3. Akarken, G.; Cengiz, U. Fabrication and Characterization of Metakaolin-Based Fiber Reinforced Fire Resistant Geopolymer. *Appl. Clay Sci.* **2023**, *232*, 106786. [CrossRef]
4. Rusănescu, C.O.; Voicu, G.; Paraschiv, G.; Begea, M.; Purdea, L.; Petre, I.C.; Stoian, E.V. Recovery of Sewage Sludge in the Cement Industry. *Energies* **2022**, *15*, 2664. [CrossRef]
5. Karakaş, H.; İlkentapar, S.; Durak, U.; Örklemez, E.; Özuzun, S.; Karahan, O.; Atiş, C.D. Properties of Fly Ash-Based Lightweight-Geopolymer Mortars Containing Perlite Aggregates: Mechanical, Microstructure, and Thermal Conductivity Coefficient. *Constr. Build. Mater.* **2023**, *362*, 129717. [CrossRef]

6. Ding, M.; Yu, R.; Feng, Y.; Wang, S.; Zhou, F.; Shui, Z.; Gao, X.; He, Y.; Chen, L. Possibility and Advantages of Producing an Ultra-High Performance Concrete (UHPC) with Ultra-Low Cement Content. *Constr. Build. Mater.* **2021**, *273*, 122023. [CrossRef]
7. Zhang, Y.; Liu, H.; Ma, T.; Gu, G.; Chen, C.; Hu, J. Understanding the Changes in Engineering Behaviors and Microstructure of FA-GBFS Based Geopolymer Paste with Addition of Silica Fume. *J. Build. Eng.* **2023**, *70*, 106450. [CrossRef]
8. Doğan-Sağlamtimur, N.; Bilgil, A.; Ertürk, S.; Bozkurt, V.; Süzgeç, E.; Akan, A.G.; Nas, P.; Çetin, H.; Szechyńska-Hebda, M.; Hebda, M. Eco-Geopolymers: Physico-Mechanical Features, Radiation Absorption Properties, and Mathematical Model. *Polymers* **2022**, *14*, 262. [CrossRef]
9. Nodehi, M.; Taghvaee, V.M. Sustainable Concrete for Circular Economy: A Review on Use of Waste Glass. *Glass Struct. Eng.* **2021**, *7*, 3–22. [CrossRef]
10. Khan, M.N.N.; Saha, A.K.; Sarker, P.K. Reuse of Waste Glass as a Supplementary Binder and Aggregate for Sustainable Cement-Based Construction Materials: A Review. *J. Build. Eng.* **2020**, *28*, 101052. [CrossRef]
11. Pasupathy, K.; Ramakrishnan, S.; Sanjayan, J. 3D Concrete Printing of Eco-Friendly Geopolymer Containing Brick Waste. *Cem. Concr. Compos.* **2023**, *138*, 104943. [CrossRef]
12. Yelemessov, K.; Sabirova, L.B.; Martyushev, N.V.; Malozyomov, B.V.; Bakhmagambetova, G.B.; Atanova, O.V. Modeling and Model Verification of the Stress-Strain State of Reinforced Polymer Concrete. *Materials* **2023**, *16*, 3494. [CrossRef]
13. Ali, M.H.; Dinkha, Y.Z.; Haido, J.H. Mechanical Properties and Spalling at Elevated Temperature of High Performance Concrete Made with Reactive and Waste Inert Powders. *Eng. Sci. Technol. Int. J.* **2017**, *20*, 536–541. [CrossRef]
14. Siddika, A.; Hajimohammadi, A.; Mamun, M.A.A.; Alyousef, R.; Ferdous, W. Waste Glass in Cement and Geopolymer Concretes: A Review on Durability and Challenges. *Polymers* **2021**, *13*, 2071. [CrossRef]
15. Ahmad, S.A.; Rafiq, S.K.; Ahmed, H.U.; Abdulrahman, A.S.; Ramezanianpour, A.M. Innovative Soft Computing Techniques Including Artificial Neural Network and Nonlinear Regression Models to Predict the Compressive Strength of Environmentally Friendly Concrete Incorporating Waste Glass Powder. *Innov. Infrastruct. Solut.* **2023**, *8*, 119. [CrossRef]
16. Ahmad, S.A.; Rafiq, S.K. Numerical Modeling to Predict the Impact of Granular Glass Replacement on Mechanical Properties of Mortar. *Asian J. Civ. Eng.* **2023**, *1*, 1–19. [CrossRef]
17. Toniolo, N.; Taveri, G.; Hurle, K.; Roether, J.A.; Ercole, P.; Dlouhý, I.; Boccaccini, A.R. Fly-Ash-Based Geopolymers: How the Addition of Recycled Glass or Red Mud Waste Influences the Structural and Mechanical Properties. *J. Ceram. Sci. Technol.* **2017**, *8*, 411–420. [CrossRef]
18. Novais, R.M.; Ascensão, G.; Seabra, M.P.; Labrincha, J.A. Waste Glass from End-of-Life Fluorescent Lamps as Raw Material in Geopolymers. *Waste Manag.* **2016**, *52*, 245–255. [CrossRef]
19. Ahmad, S.A.; Rafiq, S.K.; Faraj, R.H. Evaluating the Effect of Waste Glass Granules on the Fresh, Mechanical Properties and Shear Bond Strength of Sustainable Cement Mortar. *Clean. Technol. Environ. Policy* **2023**, *25*, 1989–2008. [CrossRef]
20. Henao Rios, L.M.; Hoyos Triviño, A.F.; Villaquirán-Caicedo, M.A.; de Gutiérrez, R.M. Effect of the Use of Waste Glass (as Precursor, and Alkali Activator) in the Manufacture of Geopolymer Rendering Mortars and Architectural Tiles. *Constr. Build. Mater.* **2023**, *363*, 129760. [CrossRef]
21. Gao, X.; Yao, X.; Xie, R.; Li, X.; Cheng, J.; Yang, T. Performance of Fly Ash-Based Geopolymer Mortars with Waste Cathode Ray Tubes Glass Fine Aggregate: A Comparative Study with Cement Mortars. *Constr. Build. Mater.* **2022**, *344*, 128243. [CrossRef]
22. Singh, S.; Srivastava, V.; Agarwal, V.C. Glass Waste in Concrete: Effect on Workability and Compressive Strength. *Int. J. Innov. Res. Sci. Eng. Technol.* **2007**, *4*, 8142–8150. [CrossRef]
23. Ahmad, J.; Zhou, Z.; Usanova, K.I.; Vatin, N.I.; El-Shorbagy, M.A. A Step towards Concrete with Partial Substitution of Waste Glass (WG) in Concrete: A Review. *Materials* **2022**, *15*, 2525. [CrossRef] [PubMed]
24. De Castro, S.; De Brito, J. Evaluation of the Durability of Concrete Made with Crushed Glass Aggregates. *J. Clean. Prod.* **2013**, *41*, 7–14. [CrossRef]
25. Alterary, S.S.; Marei, N.H. Fly Ash Properties, Characterization, and Applications: A Review. *J. King Saud. Univ. Sci.* **2021**, *33*, 101536. [CrossRef]
26. Dwivedi, A.; Jain, M. Fly Ash—Waste Management and Overview: A Review. *Recent. Res. Sci. Technol.* **2014**, *6*, 30–35.
27. Luo, Y.; Wu, Y.; Ma, S.; Zheng, S.; Zhang, Y.; Chu, P.K. Utilization of Coal Fly Ash in China: A Mini-Review on Challenges and Future Directions. *Environ. Sci. Pollut. Res.* **2020**, *28*, 18727–18740. [CrossRef]
28. Ćwik, A.; Casanova, I.; Rausis, K.; Zarębska, K. Utilization of High-Calcium Fly Ashes through Mineral Carbonation: The Cases for Greece, Poland and Spain. *J. CO_2 Util.* **2019**, *32*, 155–162. [CrossRef]
29. Yalcinkaya, B.; Spirek, T.; Bousa, M.; Louda, P.; Růžek, V.; Rapiejko, C.; Buczkowska, K.E. Unlocking the Potential of Biomass Fly Ash: Exploring Its Application in Geopolymeric Materials and a Comparative Case Study of BFA-Based Geopolymeric Concrete against Conventional Concrete. *Ceramics* **2023**, *6*, 1682–1704. [CrossRef]
30. Doğan-Sağlamtimur, N.; Bilgil, A.; Szechyńska-Hebda, M.; Parzych, S.; Hebda, M. Eco-Friendly Fired Brick Produced from Industrial Ash and Natural Clay: A Study of Waste Reuse. *Materials* **2021**, *14*, 877. [CrossRef]
31. Dong, C.; Zhou, N.; Zhang, J.; Lai, W.; Xu, J.; Chen, J.; Yu, R.; Che, Y. Optimized Preparation of Gangue Waste-Based Geopolymer Adsorbent Based on Improved Response Surface Methodology for Cd(II) Removal from Wastewater. *Environ. Res.* **2023**, *221*, 115246. [CrossRef]
32. Willson-Levy, R.; Peled, A.; Klein-BenDavid, O.; Bar-Nes, G. Development of One-Part Geopolymers Based on Industrial Carbonate Waste. *Constr. Build. Mater.* **2023**, *365*, 130009. [CrossRef]

33. Łach, M.; Hebdowska-Krupa, M.; Stefańska, A.; Stefanek, J.; Stanek, A.; Mikuła, J.; Hebda, M. Characterisation of Post-Production Raw Material from the Raciszyn II Deposit as a Material Suitable for the Production of Alkaline-Activated Materials. *J. Therm. Anal. Calorim.* **2019**, *138*, 4551–4559. [CrossRef]
34. Ge, X.; Hu, X.; Shi, C. Impact of Micro Characteristics on the Formation of High-Strength Class F Fly Ash-Based Geopolymers Cured at Ambient Conditions. *Constr. Build. Mater.* **2022**, *352*, 129074. [CrossRef]
35. McLellan, B.C.; Williams, R.P.; Lay, J.; van Riessen, A.; Corder, G.D.; Riessen, V.A. Costs and Carbon Emissions for Geopolymer Pastes in Comparison to Ordinary Portland Cement. *J. Clean. Prod.* **2011**, *19*, 1080–1090. [CrossRef]
36. Srividya, T.; Kannan Rajkumar, P.R.; Sivasakthi, M.; Sujitha, A.; Jeyalakshmi, R. A State-of-the-Art on Development of Geopolymer Concrete and Its Field Applications. *Case Stud. Constr. Mater.* **2022**, *16*, e00812. [CrossRef]
37. Li, S.; Liew, J.Y.R. Fire Resistance of Partially-Heated High Strength Composite Beam-Columns. *J. Constr. Steel Res.* **2023**, *204*, 107836. [CrossRef]
38. Klima, K.M.; Schollbach, K.; Brouwers, H.J.H.; Yu, Q. Thermal and Fire Resistance of Class F Fly Ash Based Geopolymers—A Review. *Constr. Build. Mater.* **2022**, *323*, 126529. [CrossRef]
39. Sakkas, K.; Panias, D.; Nomikos, P.; Sofianos, A.; Sakkas, K.; Panias, D.; Nomikos, P.; Sofianos, A. Comparison of Fire Resistant Geopolymers for Passive Fire Protection of Concrete Tunnel Linings. *Open Access Libr. J.* **2017**, *4*, 1–15. [CrossRef]
40. Ziejewska, C.; Marczyk, J.; Korniejenko, K.; Bednarz, S.; Sroczyk, P.; Łach, M.; Mikuła, J.; Figiela, B.; Szechyńska-Hebda, M.; Hebda, M. 3D Printing of Concrete-Geopolymer Hybrids. *Materials* **2022**, *15*, 2819. [CrossRef]
41. Luhar, S.; Luhar, I. Valorisation of Waste Glasses for the Development of Geopolymer Mortar—Properties and Applications. *J. Compos. Sci.* **2022**, *6*, 30. [CrossRef]
42. Yang, S.; Lu, J.X.; Poon, C.S. Recycling of Waste Glass in Cement Mortars: Mechanical Properties under High Temperature Loading. *Resour. Conserv. Recycl.* **2021**, *174*, 105831. [CrossRef]
43. Ling, T.C.; Poon, C.S.; Kou, S.C. Influence of Recycled Glass Content and Curing Conditions on the Properties of Self-Compacting Concrete after Exposure to Elevated Temperatures. *Cem. Concr. Compos.* **2012**, *34*, 265–272. [CrossRef]
44. Chen, B.; Zhu, H.; Li, B.; Sham, M.; Li, Z. Study on the Fire Resistance Performance of Cementitious Composites Containing Recycled Glass Cullets (RGCs). *Constr. Build. Mater.* **2020**, *242*, 117992. [CrossRef]
45. Tahwia, A.M.; Ellatief, M.A.; Bassioni, G.; Heniegal, A.M.; Elrahman, M.A. Influence of High Temperature Exposure on Compressive Strength and Microstructure of Ultra-High Performance Geopolymer Concrete with Waste Glass and Ceramic. *J. Mater. Res. Technol.* **2023**, *23*, 5681–5697. [CrossRef]
46. Jiang, X.; Xiao, R.; Ma, Y.; Zhang, M.; Bai, Y.; Huang, B. Influence of Waste Glass Powder on the Physico-Mechanical Properties and Microstructures of Fly Ash-Based Geopolymer Paste after Exposure to High Temperatures. *Constr. Build. Mater.* **2020**, *262*, 120579. [CrossRef]
47. Turkey, F.A.; Beddu, S.B.; Ahmed, A.N.; Al-Hubboubi, S.K. Effect of High Temperatures on the Properties of Lightweight Geopolymer Concrete Based Fly Ash and Glass Powder Mixtures. *Case Stud. Constr. Mater.* **2022**, *17*, e01489. [CrossRef]
48. Chindaprasirt, P.; Lao-un, J.; Zaetang, Y.; Wongkvanklom, A.; Phoo-ngernkham, T.; Wongsa, A.; Sata, V. Thermal Insulating and Fire Resistance Performances of Geopolymer Mortar Containing Auto Glass Waste as Fine Aggregate. *J. Build. Eng.* **2022**, *60*, 105178. [CrossRef]
49. Ziejewska, C.; Grela, A.; Hebda, M. Influence of Waste Glass Particle Size on the Physico-Mechanical Properties and Porosity of Foamed Geopolymer Composites Based on Coal Fly Ash. *Materials* **2023**, *16*, 2044. [CrossRef] [PubMed]
50. Agrawal, U.S.; Wanjari, S.P.; Naresh, D.N. Impact of Replacement of Natural River Sand with Geopolymer Fly Ash Sand on Hardened Properties of Concrete. *Constr. Build. Mater.* **2019**, *209*, 499–507. [CrossRef]
51. Hamada, H.; Alattar, A.; Tayeh, B.; Yahaya, F.; Thomas, B. Effect of Recycled Waste Glass on the Properties of High-Performance Concrete: A Critical Review. *Case Stud. Constr. Mater.* **2022**, *17*, e01149. [CrossRef]
52. EN 1015-3:1999/A2:2006—Methods of Test for Mortar for Masonry—Part 3: Determination of Consistence of Fresh Mortar (by Flow Table). Available online: https://standards.iteh.ai/catalog/standards/cen/fb7a5bb4-d8e4-4c91-a7f8-a5cc646ce3e9/en-1015-3-1999-a2-2006 (accessed on 29 March 2023).
53. PN-B-04500:1985—Construction Mortars—Tests of Physical and Strength Characteristics. Available online: https://sklep.pkn.pl/pn-b-04500-1985p.html (accessed on 29 March 2023).
54. Korniejenko, K.; Łach, M.; Chou, S.Y.; Lin, W.T.; Mikuła, J.; Mierzwiński, D.; Cheng, A.; Hebda, M. A Comparative Study of Mechanical Properties of Fly Ash-Based Geopolymer Made by Casted and 3D Printing Methods. *IOP Conf. Ser. Mater. Sci. Eng.* **2019**, *660*, 012005. [CrossRef]
55. EN ISO 1182:2020—Reaction to Fire Tests for Products—Non-Combustibility Test (ISO 1182:2020). Available online: https://standards.iteh.ai/catalog/standards/sist/36888eed-5e43-41c3-ad45-9078a16a66ba/sist-en-iso-1182-2020 (accessed on 29 March 2023).
56. Mierzwiński, D.; Łach, M.; Hebda, M.; Walter, J.; Szechyńska-Hebda, M.; Mikuła, J. Thermal Phenomena of Alkali-Activated Metakaolin Studied with a Negative Temperature Coefficient System. *J. Therm. Anal. Calorim.* **2019**, *138*, 4167–4175. [CrossRef]
57. Marczyk, J.; Ziejewska, C.; Gadek, S.; Korniejenko, K.; Łach, M.; Góra, M.; Kurek, I.; Dogan-Saglamtimur, N.; Hebda, M.; Szechynska-Hebda, M. Hybrid Materials Based on Fly Ash, Metakaolin, and Cement for 3D Printing. *Materials* **2021**, *14*, 6874. [CrossRef]

58. Law, D.W.; Adam, A.A.; Molyneaux, T.K.; Patnaikuni, I.; Wardhono, A. Long Term Durability Properties of Class F Fly Ash Geopolymer Concrete. *Mater. Struct. Mater. Constr.* **2014**, *48*, 721–731. [CrossRef]
59. Shee-Ween, O.; Cheng-Yong, H.; Yun-Ming, L.; Abdullah, M.M.A.B.; Li Ngee, H.; Chan, L.W.L.; Wan-En, O.; Jaya, N.A.; Yong-Sing, N. Cold-Pressed Fly Ash Geopolymers: Effect of Formulation on Mechanical and Morphological Characteristics. *J. Mater. Res. Technol.* **2021**, *15*, 3028–3046. [CrossRef]
60. Hidayati, R.E.; Faradilla, F.S.; Dadang, D.; Harmelia, L.; Nurlina, N.; Prasetyoko, D.; Fansuri, H. Setting Time and Compressive Strength of Geopolymers Made of Three Indonesian Low Calcium Fly Ash with Variation of Sodium Silicate Addition. *Arch. Metall. Mater.* **2021**, *66*, 1115–1121. [CrossRef]
61. Kim, B.; Lee, S.; Chon, C.M.; Cho, S. Setting Behavior and Phase Evolution on Heat Treatment of Metakaolin-Based Geopolymers Containing Calcium Hydroxide. *Materials* **2022**, *15*, 194. [CrossRef]
62. Zhang, Y.; Xiao, R.; Jiang, X.; Li, W.; Zhu, X.; Huang, B. Effect of Particle Size and Curing Temperature on Mechanical and Microstructural Properties of Waste Glass-Slag-Based and Waste Glass-Fly Ash-Based Geopolymers. *J. Clean. Prod.* **2020**, *273*, 122970. [CrossRef]
63. Dineshkumar, M.; Umarani, C. Effect of Alkali Activator on the Standard Consistency and Setting Times of Fly Ash and GGBS-Based Sustainable Geopolymer Pastes. *Adv. Civ. Eng.* **2020**, *2020*, 2593207. [CrossRef]
64. Gholampour, A.; Danish, A.; Ozbakkaloglu, T.; Yeon, J.H.; Gencel, O. Mechanical and Durability Properties of Natural Fiber-Reinforced Geopolymers Containing Lead Smelter Slag and Waste Glass Sand. *Constr. Build. Mater.* **2022**, *352*, 129043. [CrossRef]
65. Dong, W.; Li, W.; Tao, Z. A Comprehensive Review on Performance of Cementitious and Geopolymeric Concretes with Recycled Waste Glass as Powder, Sand or Cullet. *Resour. Conserv. Recycl.* **2021**, *172*, 105664. [CrossRef]
66. Zhuang, S.; Wang, Q.; Zhang, M. Water Absorption Behaviour of Concrete: Novel Experimental Findings and Model Characterization. *J. Build. Eng.* **2022**, *53*, 104602. [CrossRef]
67. Ding, Z.; Quy, N.X.; Kim, J.; Hama, Y. Evaluations of Frost and Scaling Resistance of Fly Ash Concrete in Terms of Changes in Water Absorption and Pore Structure under the Accelerated Carbonation Conditions. *Constr. Build. Mater.* **2022**, *345*, 128273. [CrossRef]
68. Ibrahim, K. Recycled Waste Glass [WG] in Concrete. *Glob. J. Eng. Sci.* **2020**, *6*, 1–8. [CrossRef]
69. Abellan-Garcia, J.; Redondo-Mosquera, J.; Khan, M.I.; Abbas, Y.M.; Castro-Cabeza, A. Development of a Novel 124 MPa Strength Green Reactive Powder Concrete Employing Waste Glass and Locally Available Cement. *Arch. Civ. Mech. Eng.* **2023**, *23*, 1–17. [CrossRef]
70. Gill, P.; Jangra, P.; Roychand, R.; Saberian, M.; Li, J. Effects of Various Additives on the Crumb Rubber Integrated Geopolymer Concrete. *Clean. Mater.* **2023**, *8*, 100181. [CrossRef]
71. Sunjidmaa, D.; Batdemberel, G.; Takibai, S.; Sunjidmaa, D.; Batdemberel, G.; Takibai, S. A Study of Ferrospheres in the Coal Fly Ash. *Open J. Appl. Sci.* **2019**, *9*, 10–16. [CrossRef]
72. Sultan, M.; Miyazaki, T.; Koyama, S. Optimization of Adsorption Isotherm Types for Desiccant Air-Conditioning Applications. *Renew. Energy* **2018**, *121*, 441–450. [CrossRef]
73. Muttakin, M.; Mitra, S.; Thu, K.; Ito, K.; Saha, B.B. Theoretical Framework to Evaluate Minimum Desorption Temperature for IUPAC Classified Adsorption Isotherms. *Int. J. Heat. Mass. Transf.* **2018**, *122*, 795–805. [CrossRef]
74. Yurdakal, S.; Garlisi, C.; Özcan, L.; Bellardita, M.; Palmisano, G. (Photo)Catalyst Characterization Techniques: Adsorption Isotherms and BET, SEM, FTIR, UV–Vis, Photoluminescence, and Electrochemical Characterizations. In *Heterogeneous Photocatalysis: Relationships with Heterogeneous Catalysis and Perspectives*; Elsevier: Amsterdam, The Netherlands, 2019; pp. 87–152. [CrossRef]
75. Luhar, I.; Luhar, S. A Comprehensive Review on Fly Ash-Based Geopolymer. *J. Compos. Sci.* **2022**, *6*, 219. [CrossRef]
76. Tho-In, T.; Sata, V.; Boonserm, K.; Chindaprasirt, P. Compressive Strength and Microstructure Analysis of Geopolymer Paste Using Waste Glass Powder and Fly Ash. *J. Clean. Prod.* **2018**, *172*, 2892–2898. [CrossRef]
77. Siddika, A.; Hajimohammadi, A.; Ferdous, W.; Sahajwalla, V. Roles of Waste Glass and the Effect of Process Parameters on the Properties of Sustainable Cement and Geopolymer Concrete—A State-of-the-Art Review. *Polymers* **2021**, *13*, 3935. [CrossRef] [PubMed]
78. Skare, M.; Porada-rochon, M.; Blazevic-buric, S. Energy Cycles: Nature, Turning Points and Role in England Economic Growth from 1700 to 2018. *Acta Montan. Slovaca* **2021**, *26*, 281–302. [CrossRef]
79. Rickard, W.D.A.; Van Riessen, A.; Walls, P. Thermal Character of Geopolymers Synthesized from Class F Fly Ash Containing High Concentrations of Iron and α-Quartz. *Int. J. Appl. Ceram. Technol.* **2010**, *7*, 81–88. [CrossRef]
80. Uysal, M.; Aygörmez, Y.; Canpolat, O.; Cosgun, T.; Faruk Kuranlı, Ö. Investigation of Using Waste Marble Powder, Brick Powder, Ceramic Powder, Glass Powder, and Rice Husk Ash as Eco-Friendly Aggregate in Sustainable Red Mud-Metakaolin Based Geopolymer Composites. *Constr. Build. Mater.* **2022**, *361*, 129718. [CrossRef]
81. Bisht, K.; Ramana, P.V. Experimental Investigation of Strength, Drying Shrinkage, Freeze and Thaw and Fire Attack Properties of Concrete Mixes with Beverage Glass Waste as Fine Aggregate. *Structures* **2022**, *36*, 358–371. [CrossRef]
82. Mao, L.; Zhou, H.; Peng, M.; Hu, L.; Zhang, W. Effects of Waste Glass Particle Size on Improving the Property and Environmental Safety of Fired Brick Containing Electroplating Sludge. *Constr. Build. Mater.* **2020**, *257*, 119583. [CrossRef]

83. Lu, J.X.; Poon, C.S. Use of Waste Glass in Alkali Activated Cement Mortar. *Constr. Build. Mater.* **2018**, *160*, 399–407. [CrossRef]
84. Dehghani, A.; Aslani, F.; Ghaebi Panah, N. Effects of Initial SiO_2/Al_2O_3 Molar Ratio and Slag on Fly Ash-Based Ambient Cured Geopolymer Properties. *Constr. Build. Mater.* **2021**, *293*, 123527. [CrossRef]

Załącznik 6 – oświadczenia współautorów dotyczące publikacji P3

Kraków, dn. 23.11.2023 r.

OŚWIADCZENIE – PUBLIKACJA P3

Oświadczam, iż mój wkład w powstanie publikacji pt.: „*Influence of waste glass addition on the fire resistance, microstructure and mechanical properties of geopolymer composites*" opublikowanej w czasopiśmie *Materials* w 2023 roku, nr DOI: 10.3390/ma16176011 jest zgodny z informacją zawartą w poniższej tabeli.

Jednocześnie oświadczam, iż wyrażam zgodę na wykorzystanie wyżej wymienionej publikacji jako część rozprawy doktorskiej mgr inż. Celiny Ziejewskiej.

Autor	Wkład w powstanie publikacji
Celina Ziejewska	Sformułowanie problemu badawczego, opracowanie koncepcji badań, przygotowanie materiałów bazowych, synteza geopolimerów, przeprowadzenie badań i analiza wyników: analiza wielkości cząstek surowców, badanie konsystencji metodą stożka Novikowa, badanie konsystencji metodą stolika rozpływowego, określenie składu chemicznego surowców (XRF), wyznaczenie gęstości próbek, przeprowadzenie rentgenowskiej jakościowej analizy fazowej materiałów kompozytowych (XRD), określenie wytrzymałości na ściskanie geopolimerów, badanie morfologii surowców i geopolimerów z zastosowaniem skaningowego mikroskopu elektronowego (SEM), badanie ognioodporności, określenie resztkowej wytrzymałości na ściskanie po testach ognioodporności, wyznaczenie nasiąkliwości próbek, badania z zastosowaniem analizatora sorpcji fizycznej (określenie powierzchni właściwej, rozmiarów i objętości porów), badanie składu chemicznego geopolimerów przed i po testach odporności na ogień, interpretacja i opracowanie graficzne wyników, przygotowanie pierwszej wersji manuskryptu, przygotowanie ostatecznej wersji manuskryptu, korekta manuskryptu po recenzjach.
Agnieszka Grela	Weryfikacja danych, opracowanie metodyki prowadzonych badań, potwierdzenie, że materiały i procesy były zgodne z przyjętymi założeniami.
Dariusz Mierzwiński	Opracowanie metody badawczej z wykorzystaniem termistora typu NTC, przeprowadzenie badań zjawisk termicznych zachodzących podczas procesu polikondensacji materiałów aktywowanych alkalicznie oraz analiza wyników badań ze szczególnym uwzględnieniem czasu wiązania materiałów aktywowanych alkalicznie.

Marek Hebda	Sformułowanie problemu badawczego, opracowanie koncepcji i metodyki badań, zarządzanie zespołem badawczym, walidacja uzyskanych danych i ich analizy, nadzór merytoryczny nad prowadzonymi badaniami, analiza wyników badań, opracowanie graficzne wyników, pozyskanie finansowania na poczet zrealizowanych badań i kosztów publikacyjnych, udział w pisaniu pierwszej wersji manuskryptu, dyskusja i udział w przygotowaniu ostatecznej wersji manuskryptu, korekta manuskryptu po recenzjach.

Celina Ziejewska
.....
podpis oświadczającego
mgr inż. Celina Ziejewska

A. Grela
.....
podpis oświadczającego
dr inż. Agnieszka Grela

Dariusz Mierzwiński
.....
podpis oświadczającego
dr inż. Dariusz Mierzwiński

.....
podpis oświadczającego
dr hab. inż. Marek Hebda, prof. PK

materials

MDPI

Article

Eco-Friendly Coal Gangue and/or Metakaolin-Based Lightweight Geopolymer with the Addition of Waste Glass

Celina Ziejewska [1], Agnieszka Bąk [1], Krzysztof Hodor [2] and Marek Hebda [1,*]

[1] Faculty of Materials Engineering and Physics, Cracow University of Technology, Warszawska 24, 31-155 Cracow, Poland; celina.ziejewska@pk.edu.pl (C.Z.); agnieszka.bak@pk.edu.pl (A.B.)
[2] NETZSCH (Netzsch Instrumenty Sp. z o.o.), Halicka 9, 31-036 Cracow, Poland; krzysztof.hodor@netzsch.com
* Correspondence: marek.hebda@pk.edu.pl

Abstract: Massive amounts of deposited coal gangue derived from the mining industry constitute a crucial problem that must be solved. On the other hand, common knowledge about the recycling of glass products and the reuse of waste glass is still insufficient, which in turn causes economic and environmental problems. Therefore, this work investigated lightweight geopolymer foams manufactured based on coal gangue, metakaolin, and a mix of them to evaluate the influence of such waste on the geopolymer matrix. In addition, the effect of 20% (wt.) of waste glass on the foams was determined. Mineralogical and chemical composition, thermal behaviour, thermal conductivity, compressive strength, morphology, and density of foams were investigated. Furthermore, the structure of the geopolymers was examined in detail, including pore and structure thickness, homogeneity, degree of anisotropy, porosity with division for closed and open pores, as well as distribution of additives and pores using micro-computed tomography (microCT). The results show that the incorporation of waste glass increased compressive strength by approximately 54% and 9% in the case of coal-gangue-based and metakaolin-based samples, respectively. The porosity of samples ranged from 67.3% to 58.7%, in which closed pores constituted 0.3–1.8%. Samples had homogeneous distributions of pores and additions. Furthermore, the thermal conductivity ranged from 0.080 W/(m·K) to 0.117 W/(m·K), whereas the degree of anisotropy was 0.126–0.187, indicating that the structure of foams was approximate to isotropic.

Keywords: micro-computed tomography (microCT); TG-FTIR; thermal conductivity; foam; porosity

Citation: Ziejewska, C.; Bąk, A.; Hodor, K.; Hebda, M. Eco-Friendly Coal Gangue and/or Metakaolin -Based Lightweight Geopolymer with the Addition of Waste Glass. *Materials* **2023**, *16*, 6054. https://doi.org/10.3390/ma16176054

Academic Editor: Sukhoon Pyo

Received: 4 August 2023
Revised: 28 August 2023
Accepted: 30 August 2023
Published: 3 September 2023

1. Introduction

A continuous increase in the global population is associated with growing housing needs and the demand for building materials [1]. Due to its ease of manufacture, low cost, versatility, and easy accessibility, concrete is the most commonly used construction material around the world [2]. However, it is noteworthy that the cement industry is responsible for emitting an enormous amount of carbon dioxide released during cement manufacturing, which constitutes 6–8% of total global anthropogenic emissions worldwide, even reaching 12% in China [3,4].

On the other hand, civilization progress and simultaneous technological development cause an increased demand for energy. Glushkov et al. [5] noticed that in recent years, energy consumption has grown by around 2–3% annually. Despite many efforts undertaken by the European Union countries, coal is still the most commonly used fossil fuel around the world [6]. In many countries, such as China [7], Australia [8], India [9], Poland [10], and the Czech Republic [11], this conventional energy source is one of the most significant constituents of domestic energy structure.

Coal gangue is a widespread inert solid waste developed from coal extraction, constituting about 15–20% of coal output, which in practice means that the production of 1 t of coal is associated with obtaining about 0.12 to 0.20 t of coal gangue [12]. Therefore, it

is considered the most significant industrial type of waste in China, where over 6 billion tons of it is deponed annually [13]. Overall, coal gangue is mostly deposited, and therefore occupies a significant surface area on the one hand; on the other hand, it leads to soil degradation and the formation of geologic danger [14]. Many reports in the literature emphasised the capacity for combustion of coal gangue as a result of self-heating and reactions under air conditions, which is a threat to coal mines and all society as well due to the releasing of noxious gases into the atmosphere [15,16].

Another source is municipal waste, defined as waste of various origins, which is collected from households, factories, or institutional buildings. Their number is constantly growing due to economic development and the commonly accepted consumer lifestyle. One of them is waste glass, which constitutes 5.8% of all types of generated waste [17]. Glass is a well-known material, which is commonly used all over the world, and according to the literature data, every person consumes approximately 21 kg of glass per year [18]. Obviously, glass waste can be subjected to recycling and reusing, but statistics show that the global recycling rate reached only 21% [19]. The cause for this outcome lies in multiple colours of waste glass, which represent a crucial impediment in the recycling process and generates high costs due to the various chemical composition of each colour of waste glass. Furthermore, contamination occurring in the waste can also affect the chemical composition, hindering the recycling process [20]. Therefore, a huge amount of waste glass is constantly deposited, which in turn is connected with indispensability to bear the high costs.

Geopolymers constitute a group of modern and continuously developed materials, fabricated during the geopolymerisation process and more precisely through alkaline activation of silica-aluminous starting materials [21]. The geopolymer term was invented by Davidovits in 1972, who described them as aluminosilicate, characterised by a three-dimensional structure and formed as a result of activation by means of an alkaline solution [22,23]. Besides their environmental friendliness, geopolymers exhibit up-and-coming properties, proving the possibility of widespread prospective application [24]. Nevertheless, it should be highlighted that waste materials can be used for geopolymer production, such as construction and demolition waste [25], magnetic mining waste [26], brick waste [27], waste glass [28], and coal gangue [29].

Nowadays, geopolymer foams are applicable in a wide range of sectors of industries as thermal insulation of buildings, acoustic insulation, catalyst support, fire resistance, pH regulators, filters, and even flowerpots [30–32]. In general, one of the most popular methods for foam production relies on introducing chemical substances called foaming agents or surfactants into the material, which most often are aluminium powder, silicon powder, and hydrogen peroxide H_2O_2 [33]. However, it is worth mentioning that the properties of foams depend on many factors, such as type of base material [34] and its particle size [35], stabilizing agent [36], applied additive [37], curing conditions [38], and sintering application [39].

In recent years, the production of lightweight foam ceramics is becoming more and more popular in the scientific community. For instance, Zhang et al. [40] developed new glass-ceramic foams based on vitrified municipal solid waste incineration ashes, which were heated at 1150 °C for 2 h in the last stage of the manufacturing process. Researchers obtained materials characterised by porosity in the range of 79.23–88.35% and compressive strength of 0.36 to 5.55 MPa [40]. On the other hand, Li et al. [41] investigated glass-ceramic foams consisting mainly of recycled fluorite tailings and waste glass, which were produced at 1100 °C for 90 min. da Costa et al. [42] in their work applied waste glass, bentonite, and alumina in glass-ceramic foams, which were sintered at temperatures ranging from 750 °C to 800 °C, achieving porosity at the level of 52 to 85% and flexural strength of 0.2–3.7 MPa simultaneously. Overall, there is a lot of novel research focused on the application of waste glass in foams production, but the sintering process that requires high energy consumption and generates carbon dioxide is key in the great majority of them to obtain appropriate high porosity, low density, and at the same time relatively high mechanical properties [43–45]. However, it should be emphasised that the application

of such high temperatures is connected with high energy consumption, which in turn negatively affects economic and ecological aspects. Therefore, it was shown that waste glass can also be used as an additive to the geopolymer matrix with the omitting of the sintering process [46]. Furthermore, it was proven that the most beneficial is to use waste glass with particle size below 75 μm due to the high pozzolanic reactivity; however, it also causes energy consumption related to its fragmentation [47].

Although it was proved that in general coal gangue is an appropriate raw material for geopolymer production, its utilization of it is still insufficient [48]. The possibility of waste application in the production of construction materials, which are characterised by an appropriate thermal conductivity, will be beneficial with regard to environmental protection. On the other hand, such a solution could have a positive effect on energy saving, especially concerning components intend for energy-saving buildings [49,50].

This work presented for the first time the possibility to obtain eco-friendly lightweight coal-gangue-based geopolymer foams reinforced with glass waste. Moreover, in order to compare the influence of metakaolin and coal gangue on the geopolymer properties, samples based on them both, as well as the metakaolin-based geopolymer, were thoroughly examined. The mineralogical and chemical composition, thermal conductivity, compressive strength, surface area, density, porosity, morphology, and thermal behaviour of foams were determined.

2. Materials and Methods

2.1. Materials

The coal gangue was received from the PG Silesia hard coal mine located in Czechowic-Dziedzice, Poland. The preparation of raw coal gangue included the following stages: preliminary disintegrating in a jaw crusher; grinding in the mill (Fritsch, Idar-Oberstein, Germany) to powder with particle size below 75 μm; and calcination at 800 °C for 24 h in a laboratory oven.

Metakaolin was bought from KERAMOST, Plc. company (Most, Czech Republic), whereas Portland cement with the commercial name CEM I 42,5R was purchased from Górażdże Cement S.A. company (Heidelberg Cement Group, Chorula, Poland).

Waste glass obtained from brown bottles was received from the local company Grabowski Export-Import (Sędziszowa, Poland), who crashed and initially cleaned them. However, there was no used additional cleaning; therefore, the bottles still contained contamination, such the remnants of labels. Furthermore, considering the energy-saving idea, the received waste glass did not undergo any additional milling.

A mixture consisting of 8 M sodium hydroxide solution and sodium silicate aqueous solution (R-145, ChemiKam, Będzin, Poland) mixed in a ratio of 1:2.5 was used as an alkaline solution. In geopolymer manufacturing, the liquid to solid ratio was established at 0.4.

The solution of hydrogen peroxide H_2O_2 (Chempur, Piekary Śląskie, Poland) with a concentration of 35% and density of 1.133 g/mol was used as a foaming agent.

2.2. Geopolymer Manufacturing Process

The first step in geopolymer manufacturing was mixing dry components, such as metakaolin, calcined coal gangue, cement, waste glass, and syringaldehyde, in order to obtain a homogeneous mix. The substitution level of waste glass was fixed based on a previous study, indicating that the optimal amount of this material in the geopolymer foams reached 20% by weight [51]. Commercially available cement with a high CaO content in the amount of 10% by weight was added to enhance pozzolanic reactiveness [52]. Moreover, syringaldehyde (chemical formula: $HOC_6H_2(OCH_3)_2CHO$) was added in the amount of 0.15% (wt.) as a stabiliser, which was selected based on the literature review [53].

Subsequently, the alkaline solution was added, and all components were mixed until the appropriate consistency of blends was acquired. The alkaline activator was prepared 24 h before use in pursuit to provide the entire course of the exothermic reaction and

eliminate the possibility of fast setting because of heat hydration [54]. In the next step, the 35% solution of H_2O_2 in the amount of 3% (wt.) to the dry components was added. After that, the mixtures were poured into moulds and placed in a laboratory dryer (Chemland, Stargard, Poland) for 24 h at 75 °C. Geopolymers were tested after 28 days of curing at room temperature. Five types of geopolymer samples were investigated in this explorational work, and their compositions are given in Table 1.

Table 1. Mix design of geopolymer samples.

Samples Designation	Coal Gangue (%)	Metakaolin (%)	Cement (%)	Waste Glass (%)
C	90	-	10	-
CG	70	-	10	20
M	-	90	10	-
MG	-	70	10	20
CMG	35	35	10	20

2.3. Methods

Thermogravimetric analysis (TG/DTG) and Fourier-transform infrared spectroscopy (FT-IR) were performed using a TG-FTIR device NETZSCH TG 209F1 Libra equipped with an integrated FT-IR system (Erich NETZSCH GmbH & Co. Holding KG, Selb, Germany). Samples were heated in the temperature range from 25 °C to 1000 °C with a heating rate of 10 °C/min in an argon atmosphere. FTIR spectra were registered in the region of 600–4000 cm^{-1}.

An X-ray fluorescence (XRF) spectrometer EDX-7200 (Shimadzu Corporation, Kioto, Japan) was applied to determine the chemical compositions of raw materials and geopolymers. Particle Size Analyser PSA 1190 LD (Anton Paar, Graz, Austria) was utilised to determine the particle size distribution.

Determination of mineralogical composition was carried out using a Panalytical Aeris diffractometer (Malvern Panalytical, Almelo, The Netherlands). Measurements were recorded in the range 10° to 100° 2θ, applying Cu Kα radiation, time per step of 340, and step size of 0.003° (2θ). Subsequently, the results were analysed using the High Score Plus software version 4.8 (Panalytical) and the ICDD database (International Center for Diffraction Data, PDF4+). The quantitative analysis of mineral phases existing in raw materials and geopolymers were realised using the Rietveld refinement method.

Nitrogen adsorption–desorption measurements were conducted using Autosorb-iQ/MP Quantachrome Instruments (Anton Paar, Graz, Austria). The specific surface areas of investigated materials were determined by the Brunauer–Emmett–Teller (BET) method.

The density of the starting materials and geopolymers was assessed using a helium pycnometer Pycnomatic ATC Thermo Fisher Scientific (Waltham, MA, USA).

The morphological observation of geopolymers was performed by Keyence VHX-E100 digital microscope (Keyence, Osaka, Japan).

The thermal conductivity (λ) of geopolymers was explored using the heat flow meter HFM 446 Lambda Series (NETZSCH, Selb, Germany). Measurements were carried out in 3 different temperature ranges: 0–20 °C, 20–40 °C, and 30–50 °C, in accordance with DIN EN 12667 standard [55].

The compressive strength of geopolymers was evaluated after 28 days of curing in room conditions using the MTS Criterion Model 43 device (MTS Systems, Eden Prairie, MN, USA) in accordance with EN 12390:2019 standard [56], and each type of material was tested using at least 3 cubic samples.

Examination of geopolymers by means of X-ray micro-computed tomography was performed using Phoenix nanotom s (Skaneateles, NY, USA). Quantitative analysis of obtained data was carried out using the Fij open-source software version 1.53f51 and Bone J plugin intended for the investigation of porous structures. The central part of the specimens

was used as a region of interest (ROI) for the analysis with dimensions of approximately 27 mm × 27 mm × 27 mm.

3. Results and Discussion

3.1. Raw Materials

The raw crushed coal gangue was examined using TG–FTIR thermogravimetric analysis to determine the optimal calcination temperature and explore the gas products emitted during the heating. The 3D surface plot for TG-FTIR spectra of released gases, the thermogravimetric curve (TG) and its first derivative (DTG), and the 2D FTIR spectra for distinctive temperatures are shown in Figure 1a–c, respectively. On the basis of the obtained three-dimensional graph (Figure 1a), it is evident that the intensities of individual absorption bands changed depending on the temperature. The majority of gas products were released in the temperature range of about 200 °C to 1000 °C, and this was in line with the course of TG-DTG curves (Figure 1b). In general, the weight loss of coal gangue was a four-stage process, as marked on the diagram. These phenomena occurred in the following temperature ranges: from room temperature to 186 °C, 186 to 631 °C, 631 to 864 °C, and 86 to 1049 °C, and that corresponded with mass losses of 0.83%, 11.10%, 2.97%, and 1.48%, respectively. The first stage was connected with the dehydration process of water and desorption of gases trapped on the coal gangue surface, and it can be seen that the maximal effect of these was registered at 71.6 °C. After that, the oxidation process started with the maximum achieved at 205.8 °C [57]. Furthermore, the most significant change in mass was registered at the temperature between 186 and 631 °C, with the maximum temperature peak at 457.7 °C in the DTG curve, which occurred as a result of dehydroxylation of kaolinite and the constituting of metakaolinite [58]. However, it should be noted that after that stage, two consecutive smaller mass loss steps were observed at the temperature ranges of 631–864 °C and 863–1049 °C. They could be attributed to the combustion process, including the decomposition of organic matter [59]. The residual mass of coal gangue registered at the end of the measurement at 1050 °C was 83.62%. As shown in Figure 1c, all of the FTIR spectra corresponding to the characteristic temperatures consisted mainly of CO_2, H_2O, and CO, and this is compliant with the previous work [60]. The difference in the intensity of the spectra obtained for individual samples can be explained by the amount of gas released at a specific temperature.

On the basis of the described result, 800 °C was fixed as an optimal calcination temperature of coal gangue. In general, metakaolin can be obtained below this temperature; nonetheless, this choice was made due to the necessity to remove carbon from the raw material dedicated to geopolymer manufacturing.

The chemical composition of raw materials is presented in Table 2. Coal gangue in both stages (before and after calcination) and metakaolin had a quite similar composition, with two main compounds, SiO_2 and Al_2O_3, which is consistent with previous research [61,62]. The difference between these materials was the Fe_2O_3 content, which was much higher in the case of coal gangue compared to metakaolin. On the other hand, ordinary Portland cement contained CaO in the most enormous quantity, and simultaneously it had about content of SiO_2 that was three times lower than that of coal gangue and metakaolin. Moreover, taking into account the effect of the used treatment on the coal gangue, it can be concluded that the calcination process resulted in an increase in Fe_2O_3 and reduction in SO_3 content. The summary content of SiO_2, $A1_2O_3$, and Fe_2O_3 amounted to 90.168%, 96.680%, and 97.76% for raw coal gangue, calcinated coal gangue, and metakaolin, respectively, and consequently, they can be applied as cement material [63].

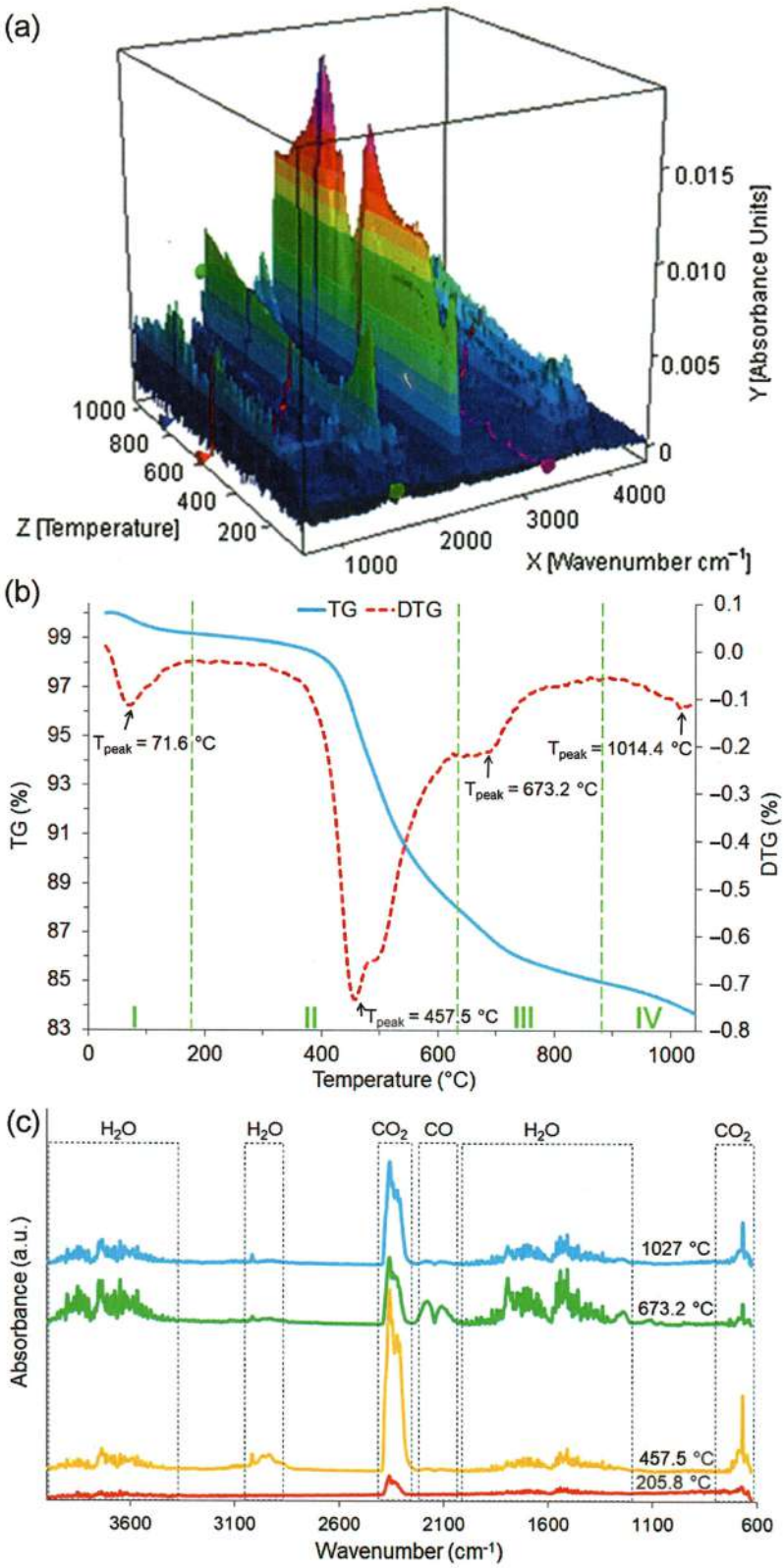

Figure 1. Thermal analysis results of coal gangue: (**a**) the 3D TG-FTIR spectra of emitted gas products; (**b**) TG and DTG curves; (**c**) 2D TG-FTIR spectra of gas products for representative temperatures.

Table 2. Chemical composition of raw materials used for geopolymer production.

Compound Formula	Raw Material				
	Coal Gangue before Calcination	Coal Gangue after Calcination	Metakaolin	Cement	Waste Glass
	Content (%)				
SiO_2	56.540	53.501	54.851	18.339	81.355
Al_2O_3	26.180	26.683	41.841	3.673	1.587
Fe_2O_3	7.448	12.496	1.068	4.524	1.030
K_2O	3.898	3.092	1.163	0.745	0.703
SO_3	2.437	0.878	0.076	4.202	0.003
CaO	1.677	1.325	0.426	67.745	14.929
TiO_2	1.410	1.179	0.309	0.293	0.084
MnO	0.078	0.120	-	0.202	0.068
V_2O_5	0.075	0.055	0.016	0.017	
P_2O_5	0.062	0.515	0.097	-	
SrO	0.044	0.038	0.011	0.130	0.035
Cr_2O_3	0.033	0.042	-	0.036	0.070
ZrO_2	0.030	0.025	0.010	0.010	0.028
ZnO	0.019	0.016	0.006	0.055	0.007
SnO_2	0.014	0.012	-	-	
CuO	0.011	0.010	0.004	0.024	0.007
Y_2O_3	0.010	0.008	0.002	0.002	0.001
BaO	-	-	-	-	0.079

The particle size distribution curves for raw materials are presented in Figure 2, which points out that metakaolin consisted of the smallest particle size of all investigated materials. However, the course of obtained curves was fairly similar in the case of metakaolin and coal gangue, and it consisted of the peak with top constituting particles with sizes of 25 µm and 32 µm for metakaolin and coal gangue, respectively. In contrast, the curve for waste glass has a bimodal distribution, suggesting that it consisted of particles with a more significant variation than the previously discussed materials.

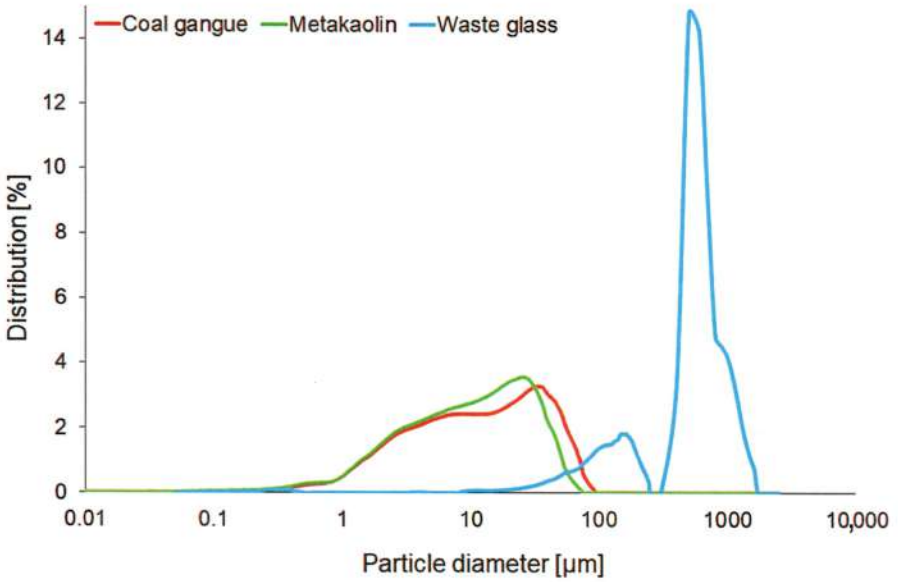

Figure 2. The particle size distribution of waste glass, metakaolin, and coal gangue before the calcination process.

Table 3 shows the particle size distribution parameters for all starting materials. The influence of particle size on the properties of the coal-gangue-based geopolymer was earlier examined by Li et al. [64], and they concluded that the optimal particle size was obtained by means of grinding and sieving using 200 mesh (74 µm), and the achieved average particle size (D_{50}) was 10.79 µm. Similarly, in the presented work, D_{50} of coal gangue amounted to 11.17 µm, and it was measured before calcination. However, for metakaolin, a lower value of D_{50} (9.60 µm) by approximately 16% was registered. On the other hand, waste glass was

characterised by the most enormous particle size (D_{50} 474.9 µm), but the calculated span was small (1.6 µm).

Table 3. Particle size distribution parameters of waste glass, metakaolin, and coal gangue before the calcination process.

Material	D_{10} [µm]	D_{50} [µm]	D_{90} [µm]	Mean Size [µm]	Span $(D_{90} - D_{10})/D_{50}$ [µm]
Coal gangue	1.82 ± 0.05	11.17 ± 0.36	44.32 ± 2.09	18.85 ± 0.81	3.80 ± 0.07
Metakaolin	1.63 ± 0.02	9.60 ± 0.12	32.50 ± 0.81	14.55 ± 0.29	3.21 ± 0.04
Waste glass	111.4 ± 11.7	474.9 ± 18.6	885.2 ± 66.5	541.1 ± 15.30	1.6 ± 0.2

The XRD patterns of raw materials are demonstrated in Figure 3, whereas the results of the quantitative analysis are summarised in Table 4. However, it is worth noticing that the presented results of the quantitative analysis were estimated due to the occurrence of an amorphous phase, which was visible as a diffuse halo between 15° and 40° 2θ on the diagram [65]. As a result of the qualitative analysis of coal gangue, the following phases were identified: quartz (ICDD card numbers: 01-075-8320); Kaolinite-1Ad (ICDD card numbers: 01-078-2110); Illite-2M1 (ICDD card numbers: 00-026-0911); and Muscovite-2M1 (ICDD card numbers: 00-006-0263). In the comparison of the results of coal gangue before and after treatment, it was noticed that the difference was in the contents of kaolinite and quartz. These findings were consistent with the other studies [66,67]. The kaolinite was still detectable in very low quantities after calcination of coal gangue, indicating that applied treatment did not cause entire dehydroxylate kaolinite, but it was still highly efficient as expected. Increasing the content of quartz (SiO_2) was also beneficial in terms of the geopolymerisation process [68]. Moreover, mullite was detected in the metakaolin structure, which existed as a result of high-temperature treatment [69].

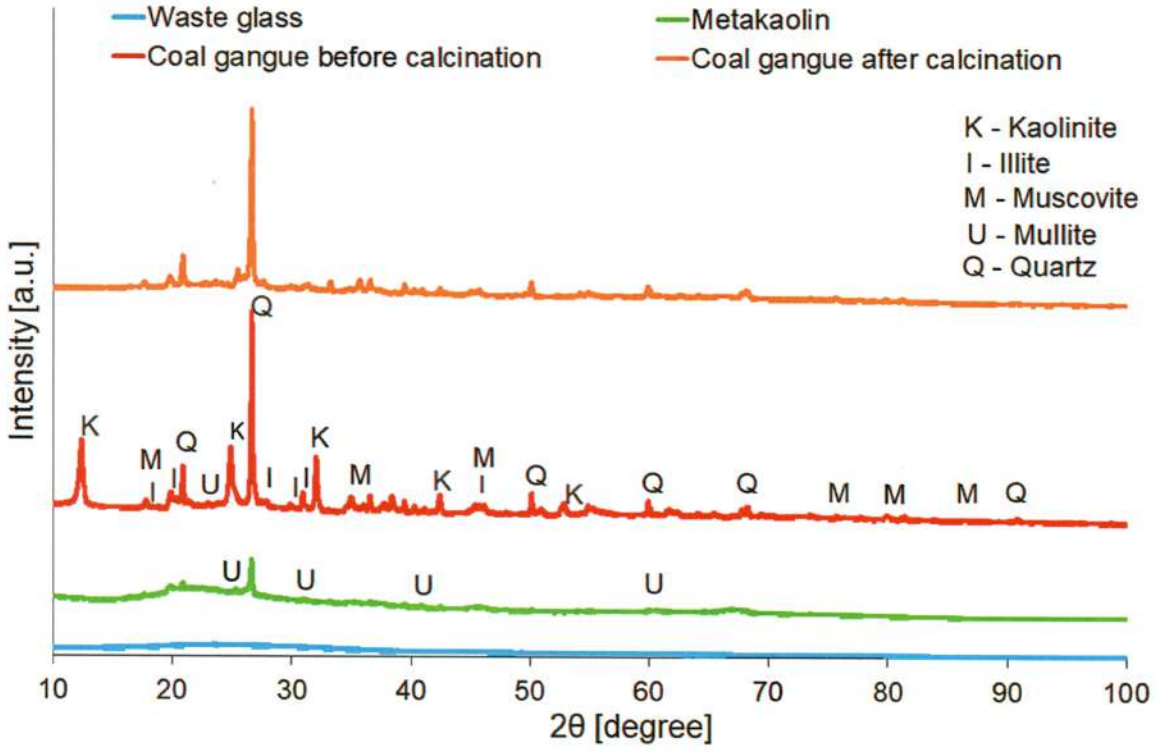

Figure 3. XRD patterns of waste glass, metakaolin, and coal gangue before and after calcination.

Table 4. Quantitative phase analysis of metakaolin and coal gangue before and after calcination.

Raw Material	Identified Mineralogical Compound (%)				
	Quartz	Kaolinite-1Ad	Illite-2M1	Muscovite-2M1	Mullite
	SiO_2	$Al_2Si_2O_5(OH)_4$	$(KH_3O)Al_2Si_3AlO_{10}(OH)_2$	$KAl_2(Si_3Al)O_{10}(OH,F)_2$	$Al_6O_5(SiO_4)_2$
Coal gangue before calcination	27.4	49.5	11.5	11.5	-
Coal gangue after calcination	57.1	0.1	21.4	21.4	-
Metakaolin	6.3	48.0	20.6	20.6	4.6

Furthermore, the true density of raw materials was examined, and it achieved 2.566 ± 0.001 g/cm^3 for metakaolin, 2.507 ± 0.001 g/cm^3 for waste glass, 2.273 ± 0.001 g/cm^3 for coal gangue before treatment, and 2.821 ± 0.001 g/cm^3 for calcinated coal gangue.

The obtained N_2 adsorption–desorption isotherms of raw materials are shown in Figure 4. According to IUPAC (International Union for Pure and Applied Chemistry) division, all of them can be classified as type IV, which is representative of mesoporous adsorbents [70]. Hysteresis loops enable the determination of the shape of pores occurring in the investigated material, and according to the classification, they exhibited H3 type, indicating the presence of slit-shaped pores. On the other hand, coal gangue in both stages showed H3-type hysteresis, which is attributed to slit-shaped pores [71].

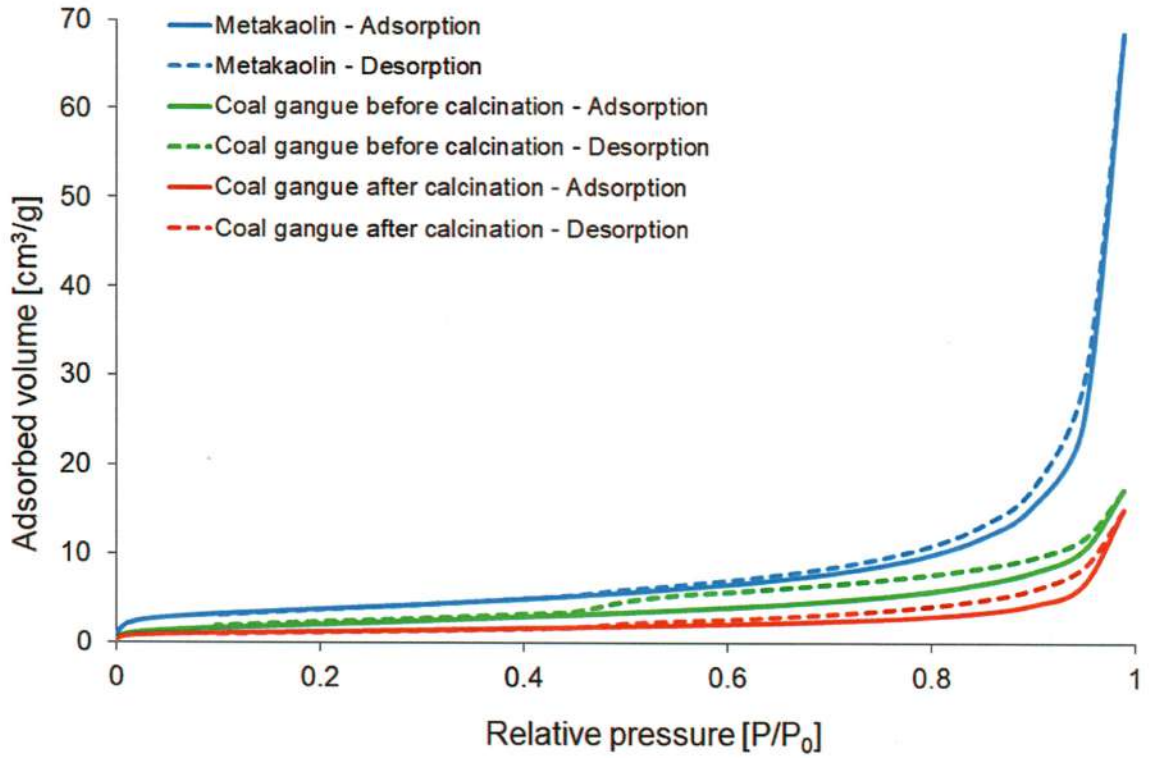

Figure 4. Nitrogen adsorption–desorption isotherms of metakaolin and coal gangue before and after calcination.

The specific surface area of metakaolin determined by means of the multi-BET method equalled 13.37 m^2 g^{-1} (Table 5), which is consistent with other studies [72,73]. The calcination process of coal gangue decreased hysteresis loops and specific surface area (by around 50%) and slightly reduced pore volume.

Table 5. Specific surface area, pore size, and volume of metakaolin and coal gangue before and after calcination.

Material	Specific Surface Area ($m^2\ g^{-1}$)		Pore Volume ($cm^3\ g^{-1}$)		Pore Size (nm)
	Single-Point BET	Multi-Point BET	BJH Pore Volume	Total Pore Volume at $P/P_0 = 0.99$	BJH Average Pore Diameter
Coal gangue before calcination	6.476	8.043	0.027	0.027	2.453
Coal gangue after calcination	3.819	4.150	0.023	0.023	3.056
Metakaolin	12.590	13.370	0.106	0.106	4.317

3.2. Geopolymers

On the basis of the results of the diffraction pattern shown in Figure 5, the mineral composition of geopolymers consisted of quartz, kaolinite, muscovite, mullite, albite, and C-S-H existing in the form of rosenhanite. Different from the raw material, all of the geopolymers contained mullite, albite, and a C-S-H phase. Moreover, the characteristic diffraction peak derived from quartz at 26.6° 2θ had the highest intensity in the case of the coal-gangue-based sample (C). Cheng et al. [74] suggested that the reduction in its intensity can be associated with a beneficial impact on compressive strength and therefore it can be assumed that the addition of waste glass, as well as metakaolin, was profitable. Furthermore, it can be seen that the intensity of quartz decreased with increasing content of metakaolin raw material. The quantitative analysis of coal-gangue-based geopolymer foams did not detect the kaolinite phase, which confirmed that during treatment the inner hydroxyl structure of kaolinite was reduced, and as a result, an amorphous substance material was formed [75]. Qualitative analysis of geopolymer (Table 6) showed new phases, which were albite and C-S-H, proving the reaction between raw materials and alkaline activator during geopolymerisation [76]. Similarly, results also revealed the mullite phase in all foams, whereas it was identified only in metakaolin from among raw materials. In addition, obtaining C-S-H gel, which is characterised by a dense structure, was beneficial due to the possibility to increase the strength of geopolymers [77]. Furthermore, Table S1 in the Supplementary Materials shows the influence of waste glass, coal gangue, and metakaolin on the chemical composition of samples. X-ray fluorescence confirmed that geopolymers mainly consisted of SiO_2, Al_2O_3, Fe_2O_3, and CaO regarding chemical composition. According to the results, the incorporation of waste glass slightly changed the content of SiO_2 in foams, as expected. On the other hand, the Al_2O_3 content, which is crucial in terms of geopolymerisation process, was higher in metakaolin-based samples.

Representative structures of the produced foams observed under an optical microscope are shown in Figure 6. The porous structure of geopolymers was formed as a result of the application of hydrogen peroxide, which exhibits thermal instability in basic media and then decomposes according to equations the following: $H_2O_2 + OH^- \longrightarrow HO_2^- + H_2O$ and subsequently $HO_2^- + H_2O_2 \longrightarrow H_2O + O_2 + OH^-$ [78,79]. Based on observation, it was noted that metakaolin-based samples contained smaller pores than their coal-gangue-based counterparts. Unreacted particles of waste glass are visible in the pore structure, which can lead to a decrease in mechanical properties. The pore distribution was relatively homogenised in foams; however, coal-gangue-based samples included voids heading along the height, and their shape is more irregular than that of samples containing metakaolin. In general, the macropores were visible in examined samples, and the pore distribution was quite homogeneous for each type of foam. It should be noted that slightly different pore shapes were around the edges of the sample, and this can be explained by boundary conditions and the influence of the applied mould [80].

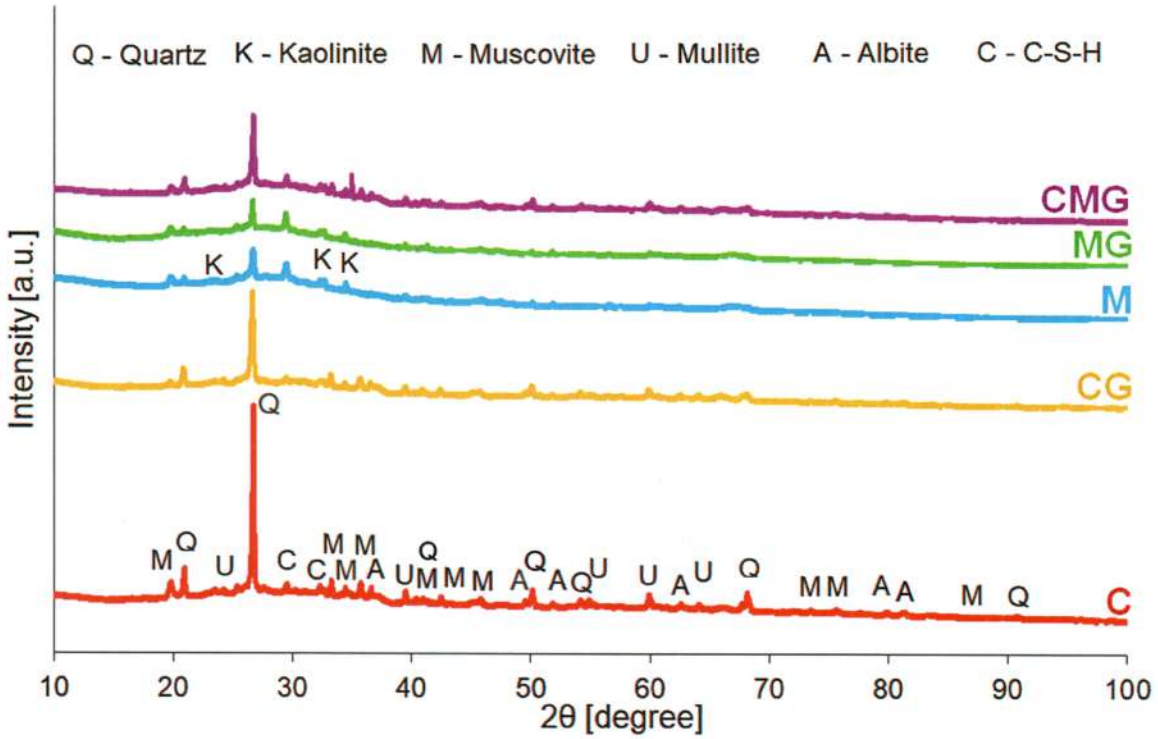

Figure 5. XRD patterns of geopolymer foams.

Table 6. Phase composition of investigated geopolymers.

Sample	Identified Mineralogical Compound					
	Quartz	Kaolinite	Muscovite	Mullite	Albite	CSH
	SiO_2	$Al_2Si_2O_5(OH)_4$	$KAl_2(Si_3Al)O_{10}(OH,F)_2$	$Al_6O_5(SiO_4)_2$	$NaAlSi_3O_8$	$Ca_3Si_3O_9 \cdot H_2O$
C	27.9	0.0	35.4	10.1	0.2	26.4
CG	22.5	0.0	29.5	11.8	11.3	24.9
M	3.0	0.3	41.2	4.2	21.0	30.3
MG	2.6	0.6	58.9	3.0	16.8	18.0
CMG	9.7	1.0	21.7	9.7	25.0	32.9

Thermal conductivity measurements were conducted in three various temperature ranges, namely 0–20 °C, 20–40 °C, and 30–50 °C, which are demonstrated in Figure 7. In general, the thermal coefficient (λ) of geopolymers was in the range of 0.079–0.117 W/(m·K). The thermal conductivity increased with the rising temperature, which is a well-known dependence for insulators [81]. The difference in results in thermal conductivity depending on complied temperature ranged up to 9%, which is visible in the diagram. Moreover, it was found that the thermal coefficient increased with the addition of waste glass. Furthermore, metakaolin-based samples showed lower values of the thermal coefficient than foams manufactured using coal gangue. It is well known that the thermal conductivity of geopolymer foams is dependent on the porosity of samples. The increase in sample porosity results in obtaining lower thermal conductivity. Based on the morphology analysis, it can be stated that pores can be open or closed. There was a tendency of closed-cell foams to demonstrate a lower value of the thermal coefficient than open-cell foams at a similar density [82]. For example, Smiljanić et al. investigated the thermal conductivity of waste glass, and they obtained λ coefficients of 1.30 W/(m·K) and 1.28 W/(m·K) for powder in the delivery condition (D_{50} 17 μm) and after 35 min of milling (D_{50} 8 μm) [83]. The particle size of the waste glass was too high to dissolve completely in the geopolymer matrix, and this was also confirmed by microscopy analysis. Therefore, it can be assumed that for the part quantity of added waste glass, thermal conductivity was close to the state of delivery and thus higher than for the geopolymer matrix without an additive.

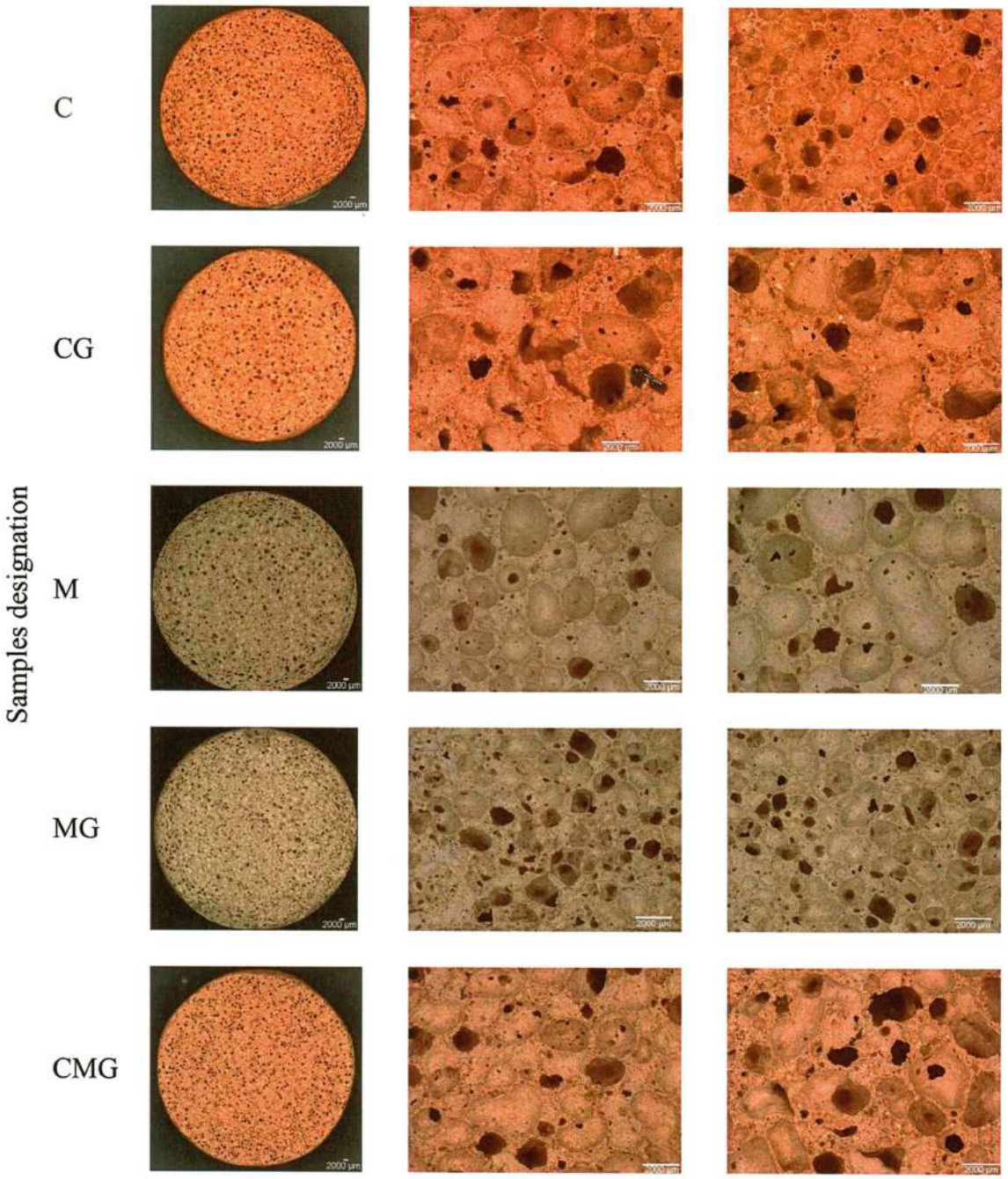

Figure 6. Optical micrographs of geopolymer foams.

Moreover, the conducted observations revealed that small inconsistencies, seemingly cracks, were observed in the coal gangue samples. This phenomenon can explain that the geopolymerisation process, in the case of using coal gangue, was not as effective as with using metakaolin.

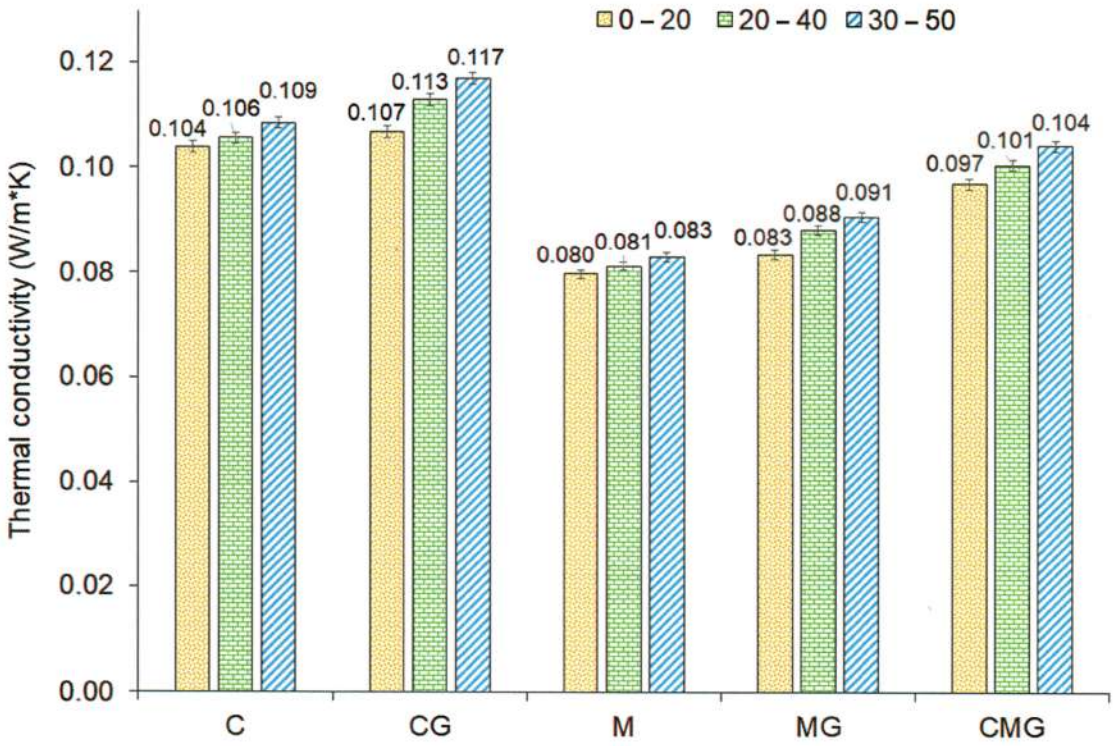

Figure 7. Thermal conductivity of geopolymer foams determined at different temperature ranges.

Figure 8 displays the density and results of the compressive strength test of geopolymer foams. It is evident that the incorporation of waste glass had a positive and significant effect on the mechanical properties. Geopolymers reinforced by waste glass exhibited approximately 54% and 9% higher compressive strength in the case of coal-gangue-based and metakaolin-based samples, respectively, compared to samples without the addition. This visible reduction in the density of foams suggests that the structure pores have changed, which in turn had an impact on the physical and mechanical properties, such as compressive strength. Moreover, a dependence between the compressive strength and the density of foams was found. The waste glass addition resulted in a higher density of geopolymers as a result of the reduction in pore volume and simultaneously positively affected the compressive strength. It should be noted, however, that the metakaolin used as the base material had a positive effect on both reducing the density and increasing the compressive strength. This phenomenon may be the result of the better homogeneity of the structure of the metakaolin-based foams.

In order to evaluate the structural properties of the geopolymer, representative samples were selected and investigated using computer microtomography. The selection criterion was the content of coal gangue in the sample to evaluate the influence of metakaolin first, followed by waste glass. The individual characteristic features of the representative samples of the coal gangue, metakaolin, and the mix of them are presented in graphical form in Figure 9. Moreover, Table S2 in the Supplementary Materials presents a 3D view of the sample, a 2D view of the sample (first slice) with a yellow line, and the slice perpendicular to the marked yellow line.

Furthermore, quantitative analysis of geopolymer foams was performed using Fiji software. The following features were measured: porosity (including open and closed pores); inclusions (waste glass designated as WG and stabiliser (syringaldehyde) designed as S); structure thickness; pores thickness; degree of anisotropy; and homogeneity (considering three directions: XY, XZ, and YZ and an average value of them). Obtained results are summarised in Table 7.

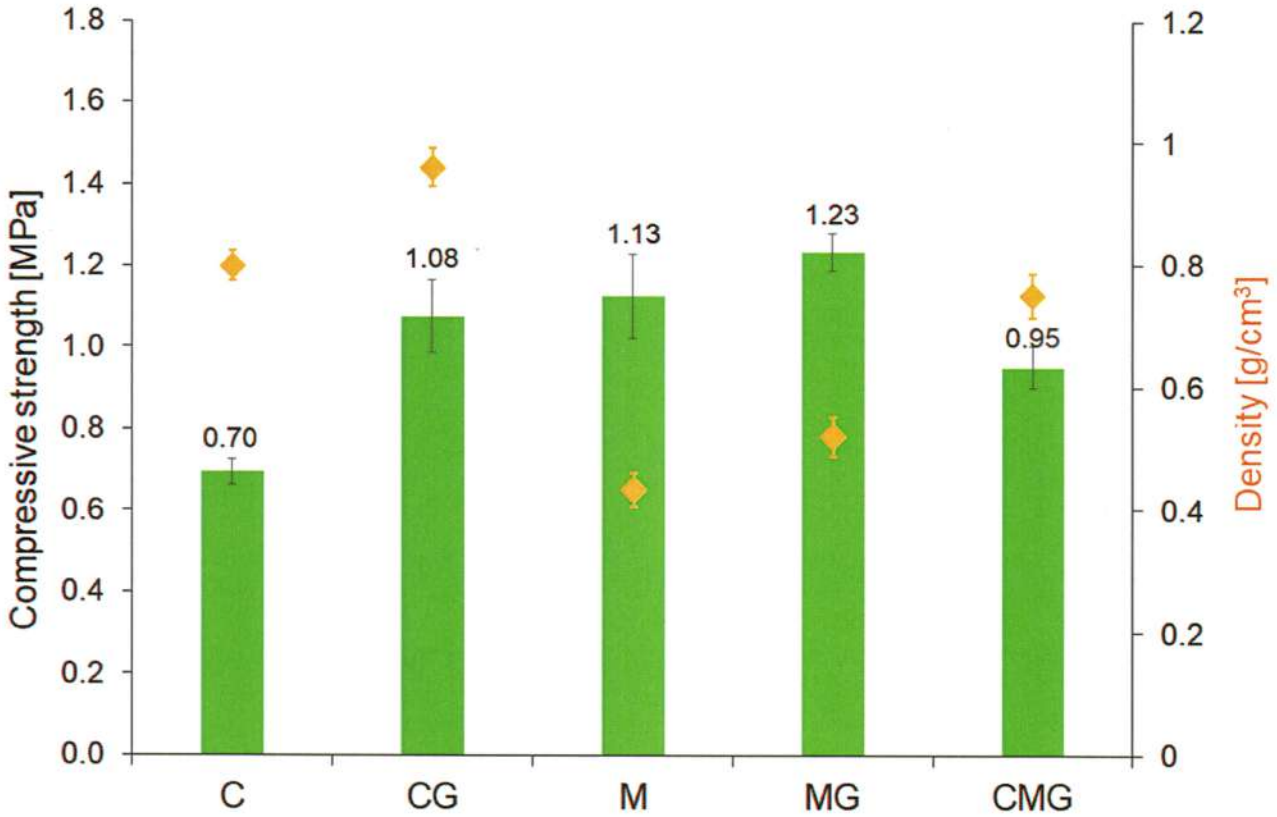

Figure 8. Compressive strength of geopolymer foams.

The porosity of the samples ranged from 69.0% to 58.7%. Comparing the influence of coal gangue and metakaolin, it can be concluded that a more porous structure was obtained using metakaolin as a raw material. Similarly, replacing 20% (wt.) of coal gangue with waste glass generated lower porosity of the geopolymers. In all analysed samples, open pores dominated the material structure, achieving 68.7%, 56.8%, and 66.9% for C, CG, and CMG, respectively. In general, two types of inclusions were detected in geopolymers, except for the C sample, which was consistent with the geopolymer manufacturing procedure, because only this sample did not include waste glass. The greatest results of structure thickness, as well as pores thickness were measured for the CG sample, which suggests that this material had the largest pores and, at the same time, the thickest wall structure. The smallest size of pores was attributed to the ample manufactured based on a mix, to wit coal gangue, metakaolin, and waste glass.

It is well known that the degree of anisotropy reaches 0 value for a fully isotropic structure, whereas a calculated value of 1 means that the structure is anisotropic. Therefore, it can be concluded that foams had structures approximate to isotropic. Moreover, the addition of waste glass to the geopolymer resulted in a lower degree of anisotropy, and this effect was also strengthened by introducing metakaolin. The homogeneity of foams was investigated in three directions, and it is certain that all fabricated samples had homogeneous structures, as can be seen from almost identical values of the obtained results.

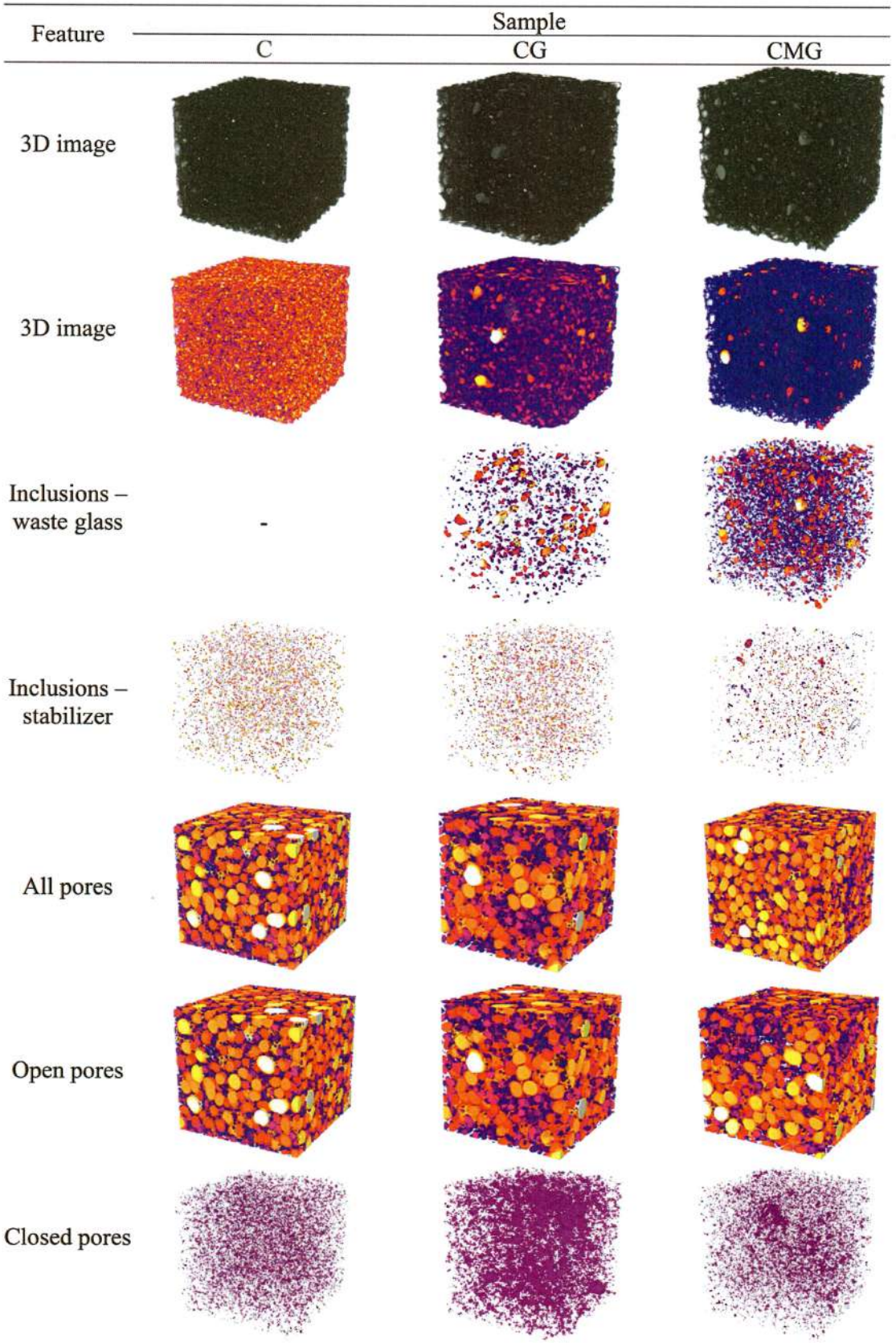

Figure 9. X-ray micro-computed tomography of geopolymers, showing individual features of foams.

Table 7. Characteristic parameters of geopolymer foams, calculated based on the X-ray micro-computed tomography results.

Sample	Porosity			Inclusions		Structure Thickness	Pores Thickness	Degree of Anisotropy	Homogeneity			
	Total [%]	Open [%]	Closed [%]	WG [%]	S [%]	[mm]	[mm]	-	XY [CTN]	XZ [CTN]	YZ [CTN]	Mean [CTN]
C	69.0	68.7	0.3	-	0.31	0.30 ± 0.08	1.62 ± 0.732	0.187	78.5 ± 15.4	78.5 ± 17.1	78.5 ± 16.3	78.5 ± 16.3
CG	58.7	56.8	1.8	1.08	0.26	0.62 ± 0.20	1.83 ± 0.658	0.156	104.9 ± 21.5	104.9 ± 21.3	104.9 ± 22.7	104.9 ± 21.8
CMG	67.3	66.9	0.4	3.74	0.21	0.33 ± 0.18	1.39 ± 0.569	0.126	82.9 ± 16.2	82.9 ± 17.1	82.9 ± 16.6	82.9 ± 16.6

In order to compare the porosity of all samples, porosity was calculated based on their apparent densities and true density in accordance with the formula: Porosity = 1 – (apparent density – true density) [84]. In Figure 10, the obtained results of porosity, as well as true density, are demonstrated. It can be noticed that the results obtained by micro-computed tomography and those determined on the basis of density measurements were highly consistent. Similar observations were made by other authors [85]. The highest porosity had metakaolin-based samples (M), as expected. Subsequently, the addition of 20% (wt.) of waste glass into metakaolin-based samples (MG) resulted in a decrease in porosity by around 5% compared to the designed M samples. It is clearly visible that using coal gangue resulted in lower porosity of geopolymer foams compared to metakaolin. However, the porosity tended to decrease with the addition of waste glass, regardless of the applied geopolymer raw material.

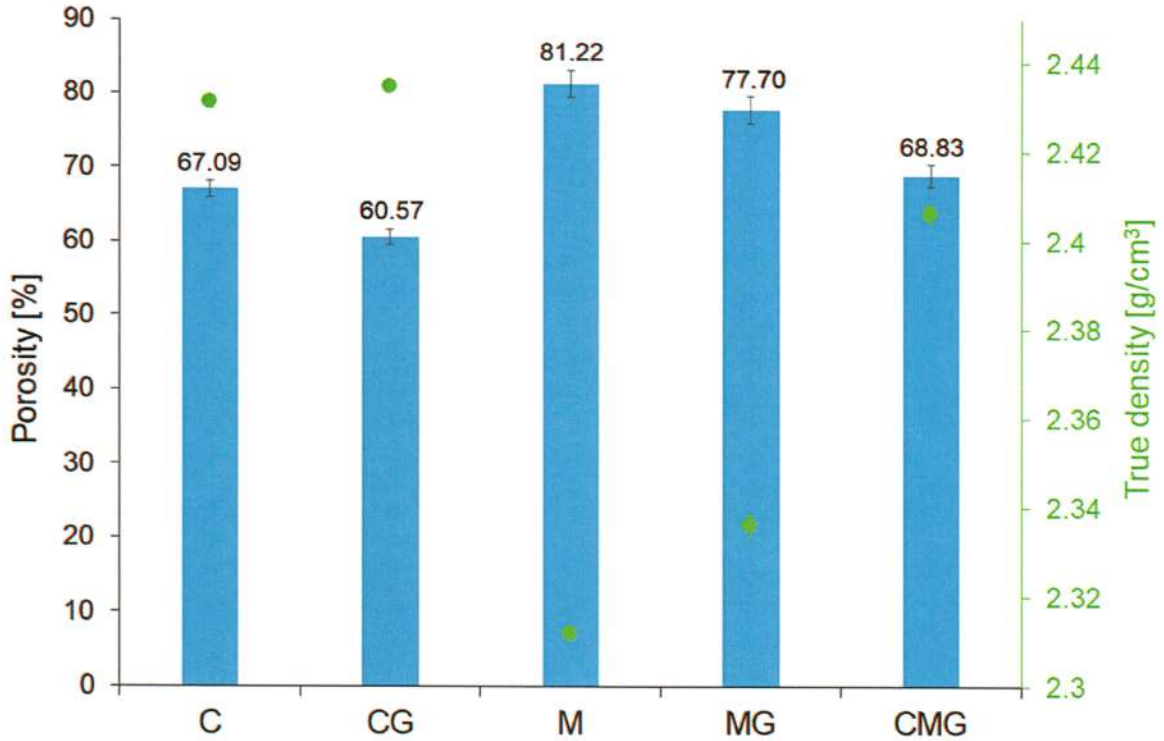

Figure 10. Comparison between the porosity and true density of the geopolymer foams.

Due to the lack of standards intended for geopolymers, the application of standards for concrete is a common practice [86]. In general, foam concrete is defined as a lightweight material that incorporates air voids. On the other hand, it is characterised by appropriate properties, such as density, thermal insulation, strength, and composition [87]. Based on the obtained results, it was found that the presented materials, with only one exception for CG due to the higher density, can be classified as lightweight concretes class III according to the division of the International Union of Laboratories and Experts in Construction Materials, Systems and Structures (RILEM). This means that foams comply with the following requirements: Lambda coefficient in the range of 0.065–0.22 W/(m·K); compressive strength

between 0.7 MPa and 3.4 MPa; and a density of 240–800 kg/m^3. Moreover, such materials were determined as insulating lightweight concrete [88,89].

4. Conclusions

In this work, the results of research focusing on eco-friendly, low-cost geopolymer foams characterised by low thermal conductivity are presented. Calcinated coal gangue and metakaolin were used as the starting materials; furthermore, waste glass was applied as an additive. Based on the obtained results, it was found that manufactured materials exhibited excellent potential for applications as insulating materials, for instance, of walls, roofs, and ceilings. Furthermore, the main gaseous products that evolved during the heating of the raw materials were CO_2, H_2O, and CO. Coal gangue in both stages (before and after calcination) and metakaolin had a quite similar composition, with two main compounds, namely SiO_2 and Al_2O_3, indicating that they can be used as geopolymer precursors. Metakaolin-based samples contained smaller pores than their coal-gangue-based counterparts. Pore distribution is relatively homogenised in foams, but notably, coal-gangue-based samples included voids heading along the height, and their shape is more irregular than in samples containing metakaolin. In addition, small inconsistencies, seemingly cracks, were observed in coal-gangue-based samples, which had a negative impact on their compressive strength. The thermal conductivity of geopolymers was dependent on the porosity of samples, indicating that the increase in porosity resulted in lower thermal conductivity. However, the addition of coal gangue, as well as waste glass, resulted in an increased thermal conductivity coefficient. Geopolymers reinforced by waste glass exhibited approximately 54% and 9% higher compressive strength in the case of coal-gangue-based and metakaolin-based samples, respectively, compared to samples without the addition. The porosity of the samples ranged from 58.7% to 67.3%, and closed pores constituted only 0.3–1.8% of it. Comparing the influence of coal gangue and metakaolin, it can be concluded that a more porous structure was obtained using metakaolin as a raw material. Moreover, the foams, which can be classified as lightweight concretes class III, had structures approximate to isotropic and they showed simultaneous homogeneous distribution of pores and additives. The presented research revealed the possibility of waste management from the mining industry in the building sector. Application of this type of materials complies with the circular economy concept and therefore should be developed in the future, especially on an industrial scale.

Supplementary Materials: The following supporting information can be downloaded at: https://www.mdpi.com/article/10.3390/ma16176054/s1, Table S1: Chemical composition of geopolymer foams; Table S2: 3D view of the sample, 2D view of the sample (first slice), slice perpendicular to the marked yellow line.

Author Contributions: Conceptualization, C.Z. and M.H.; Data curation, C.Z., A.B., K.H. and M.H.; Formal analysis, C.Z., K.H. and M.H.; Funding acquisition, M.H.; Investigation, C.Z., A.B. and M.H.; Methodology, C.Z., A.B., K.H. and M.H.; Resources, M.H.; Software, C.Z. and K.H.; Supervision, M.H.; Validation, M.H.; Visualization, C.Z. and M.H.; Writing—original draft, C.Z. and M.H.; Writing—review and editing, C.Z. and M.H. All authors have read and agreed to the published version of the manuscript.

Funding: This work was supported by the "ROAD TO EXCELLENCE—a comprehensive university support programme", accomplished within the Operational Programme Knowledge Education Development 2014–2020, co-financed by the European Social Fund; agreement no. POWR.03.05.00–00-Z214/18.

Institutional Review Board Statement: Not applicable.

Informed Consent Statement: Not applicable.

Data Availability Statement: Not applicable.

Conflicts of Interest: The authors declare no conflict of interest.

References

1. Sadigov, R. Rapid Growth of the World Population and Its Socioeconomic Results. *Sci. World J.* **2022**, *2022*, 8110229. [CrossRef] [PubMed]
2. Marczyk, J.; Ziejewska, C.; Gądek, S.; Korniejenko, K.; Łach, M.; Góra, M.; Kurek, I.; Doğan-Sağlamtimur, N.; Hebda, M.; Szechyńska-Hebda, M. Hybrid Materials Based on Fly Ash, Metakaolin, and Cement for 3D Printing. *Materials* **2021**, *14*, 6874. [CrossRef] [PubMed]
3. Zhou, C.; Xuan, D.; Miao, Y.; Luo, X.; Liu, W.; Zhang, Y. Accounting CO_2 Emissions of the Cement Industry: Based on an Electricity–Carbon Coupling Analysis. *Energies* **2023**, *16*, 4453. [CrossRef]
4. Li, L.; Shao, X.; Ling, T.C. Life Cycle Assessment of Coal Gangue Composite Cements: From Sole OPC towards Low-Carbon Quaternary Binder. *J. Clean. Prod.* **2023**, *414*, 137674. [CrossRef]
5. Glushkov, D.; Paushkina, K.; Shabardin, D.; Strizhak, P.; Gutareva, N. Municipal Solid Waste Recycling by Burning It as Part of Composite Fuel with Energy Generation. *J. Environ. Manag.* **2019**, *231*, 896–904. [CrossRef]
6. Xie, M.; Liu, F.; Zhao, H.; Ke, C.; Xu, Z. Mineral Phase Transformation in Coal Gangue by High Temperature Calcination and High-Efficiency Separation of Alumina and Silica Minerals. *J. Mater. Res. Technol.* **2021**, *14*, 2281–2288. [CrossRef]
7. Wang, L.; Wang, X.; Li, B. Data-Driven Model SSD-BSP for Multi-Target Coal-Gangue Detection. *Measurement* **2023**, *219*, 113244. [CrossRef]
8. Li, H.X.; Edwards, D.J.; Hosseini, M.R.; Costin, G.P. A Review on Renewable Energy Transition in Australia: An Updated Depiction. *J. Clean. Prod.* **2020**, *242*, 118475. [CrossRef]
9. Garg, A.; Shukla, P.R. Coal and Energy Security for India: Role of Carbon Dioxide (CO_2) Capture and Storage (CCS). *Energy* **2009**, *34*, 1032–1041. [CrossRef]
10. Li, Y.; Zhang, H.; Kang, Y. Will Poland Fulfill Its Coal Commitment by 2030? An Answer Based on a Novel Time Series Prediction Method. *Energy Rep.* **2020**, *6*, 1760–1767. [CrossRef]
11. Hupka, I.; Kotík, L. Dissolution Characteristics of Uranium and Lead in Simulated Lung Fluid Using Fly Ash Samples from Coal-Fired Power Plants in the Czech Republic. *J. Environ. Radioact.* **2023**, *256*, 107063. [CrossRef] [PubMed]
12. Feng, X.; Liu, N.; Lu, X. Investigation of Un-Calcined Coal Gangue Together with Ground Granulated Blast Furnace Slag and Fly Ash to Ambient-Curing Production High-Strength Geopolymer. *J. Mater. Res. Technol.* **2023**, *25*, 3985–3997. [CrossRef]
13. Wang, C.; Liu, C.; Zhang, L.; Wang, C.; Xu, S.; Yang, J. Exploring Calcined Coal Gangue Fines as the Total Substitute of Fly Ash in the Production of Alkali-Activated Slag/Fly Ash Materials. *Case Stud. Constr. Mater.* **2022**, *17*, e01332. [CrossRef]
14. Li, Y.; Yao, Y.; Liu, X.; Sun, H.; Ni, W. Improvement on Pozzolanic Reactivity of Coal Gangue by Integrated Thermal and Chemical Activation. *Fuel* **2013**, *109*, 527–533. [CrossRef]
15. Onifade, M.; Genc, B.; Wagner, N. Influence of Organic and Inorganic Properties of Coal-Shale on Spontaneous Combustion Liability. *Int. J. Min. Sci. Technol.* **2019**, *29*, 851–857. [CrossRef]
16. Munawer, M.E. Human Health and Environmental Impacts of Coal Combustion and Post-Combustion Wastes. *J. Sustain. Min.* **2018**, *17*, 87–96. [CrossRef]
17. Mohammadi, M.; Jämsä-Jounela, S.L.; Harjunkoski, I. Optimal Planning of Municipal Solid Waste Management Systems in an Integrated Supply Chain Network. *Comput. Chem. Eng.* **2019**, *123*, 155–169. [CrossRef]
18. Westbroek, C.D.; Bitting, J.; Craglia, M.; Azevedo, J.M.C.; Cullen, J.M. Global Material Flow Analysis of Glass: From Raw Materials to End of Life. *J. Ind. Ecol.* **2021**, *25*, 333–343. [CrossRef]
19. Fu, C.; Liang, J.; Yang, G.; Dagestani, A.A.; Liu, W.; Luo, X.; Zeng, B.; Wu, H.; Huang, M.; Lin, L.; et al. Recycling of Waste Glass as Raw Materials for the Preparation of Self-Cleaning, Light-Weight and High-Strength Porous Ceramics. *J. Clean. Prod.* **2021**, *317*, 128395. [CrossRef]
20. Hamada, H.; Alattar, A.; Tayeh, B.; Yahaya, F.; Thomas, B. Effect of Recycled Waste Glass on the Properties of High-Performance Concrete: A Critical Review. *Case Stud. Constr. Mater.* **2022**, *17*, e01149. [CrossRef]
21. Dan, H.; Li, M.; Tan, J.; Dan, H.; Ma, Z.; Ma, S. Nano- and Microscale Characterization for Interfacial Transition Zone of Geopolymer Stabilized Recycled Aggregate of Asphalt Pavement. *Constr. Build. Mater.* **2023**, *397*, 132368. [CrossRef]
22. Ziejewska, C.; Marczyk, J.; Korniejenko, K.; Bednarz, S.; Sroczyk, P.; Łach, M.; Mikuła, J.; Figiela, B.; Szechyńska-Hebda, M.; Hebda, M. 3D Printing of Concrete-Geopolymer Hybrids. *Materials* **2022**, *15*, 2819. [CrossRef] [PubMed]
23. Korniejenko, K.; Figiela, B.; Ziejewska, C.; Marczyk, J.; Bazan, P.; Hebda, M.; Choińska, M.; Lin, W.-T. Fracture Behavior of Long Fiber Reinforced Geopolymer Composites at Different Operating Temperatures. *Materials* **2022**, *15*, 482. [CrossRef]
24. Shee-Ween, O.; Cheng-Yong, H.; Yun-Ming, L.; Mustafa Al Bakri Abdullah, M.; Li-Ngee, H.; Pakawanit, P.; Suhaimi Khalid, M.; Hazim Bin Wan Muhammad, W.; Wan-En, O.; Yong-Jie, H.; et al. Green Development of Fly Ash Geopolymer via Casting and Pressing Approaches: Strength, Morphology, Efflorescence and Ecological Properties. *Constr. Build. Mater.* **2023**, *398*, 132446. [CrossRef]
25. Ilcan, H.; Sahin, O.; Unsal, Z.; Ozcelikci, E.; Kul, A.; Cağatay Demiral, N.; Ozkan Ekinci, M.; Sahmaran, M. Effect of Industrial Waste-Based Precursors on the Fresh, Hardened and Environmental Performance of Construction and Demolition Wastes-Based Geopolymers. *Constr. Build. Mater.* **2023**, *394*, 132265. [CrossRef]
26. Gier Della Rocca, D.; Santos e Sousa, F.A.; Domingos Ardisson, J.; Peralta, R.A.; Rodríguez-Castellón, E.; Peralta Muniz Moreira, R.d.F. Magnetic Mining Waste Based-Geopolymers Applied to Catalytic Reactions with Ozone. *Heliyon* **2023**, *9*, e17097. [CrossRef]

27. Pasupathy, K.; Ramakrishnan, S.; Sanjayan, J. 3D Concrete Printing of Eco-Friendly Geopolymer Containing Brick Waste. *Cem. Concr. Compos.* **2023**, *138*, 104943. [CrossRef]
28. Neeraj Varma, D.; Prasad Singh, S. Recycled Waste Glass as Precursor for Synthesis of Slag-Based Geopolymer. *Mater. Today Proc.* **2023**. [CrossRef]
29. Mao, N.; Wu, D.; Chen, K.; Cao, K.; Huang, J. Combining Experiments and Molecular Dynamics Simulations to Investigate the Effects of Water on the Structure and Mechanical Properties of a Coal Gangue-Based Geopolymer. *Constr. Build. Mater.* **2023**, *389*, 131556. [CrossRef]
30. Novais, R.M.; Pullar, R.C.; Labrincha, J.A. Geopolymer Foams: An Overview of Recent Advancements. *Prog. Mater. Sci.* **2020**, *109*, 100621. [CrossRef]
31. Boros, A.; Korim, T. Development of Geopolymer Foams for Multifunctional Applications. *Crystals* **2022**, *12*, 386. [CrossRef]
32. Utsumi, T.; Terasawa, T.; Kudo, I.; Suzuki, T.; Nakayama, T.; Suematsu, H.; Ogawa, T. Preparation of Potassium and Metakaolin Based Geopolymer Foam with Millimeter Sized Open Pores for Hydrogen Recombining Catalyst Supports. *J. Ceram. Soc. Jpn.* **2020**, *128*, 96–100. [CrossRef]
33. Li, X.; Zheng, J.; Shao, J.; Loutou, M.; Bai, C.; Qiao, Y.; Miao, Y.; Wang, X.; Zheng, T.; Colombo, P. Evaluation of Porosity, Mechanical and Thermal Properties of Self-Ignition Coal Gangue-Based Foams via Fast Microwave Foaming. *J. Build. Eng.* **2023**, *68*, 106062. [CrossRef]
34. Traven, K.; Češnovar, M.; Škapin, S.D.; Ducman, V. High Temperature Resistant Fly-Ash and Metakaolin-Based Alkali-Activated Foams. *Ceram. Int.* **2021**, *47*, 25105–25120. [CrossRef]
35. Szabó, R.; Gombköto, I.; Svéda, M.; Mucsi, G. Effect of Grinding Fineness of Fly Ash on the Properties of Geopolymer Foam. *Arch. Metall. Mater.* **2017**, *62*, 1257–1261. [CrossRef]
36. Korat, L.; Ducman, V. The Influence of the Stabilizing Agent SDS on Porosity Development in Alkali-Activated Fly-Ash Based Foams. *Cem. Concr. Compos.* **2017**, *80*, 168–174. [CrossRef]
37. Yan, S.; Ren, X.; Wang, W.; He, C.; Xing, P. Preparation of Eco-Friendly Porous Ceramic with Low Thermal Conductivity by High-Temperature Treatment of Foamed Solid Waste Based Geopolymer with Cenospheres. *Constr. Build. Mater.* **2023**, *398*, 131190. [CrossRef]
38. Dhasindrakrishna, K.; Pasupathy, K.; Ramakrishnan, S.; Sanjayan, J. Progress, Current Thinking and Challenges in Geopolymer Foam Concrete Technology. *Cem. Concr. Compos.* **2021**, *116*, 103886. [CrossRef]
39. Polat, D.; Güden, M. Processing and Characterization of Geopolymer and Sintered Geopolymer Foams of Waste Glass Powders. *Constr. Build. Mater.* **2021**, *300*, 124259. [CrossRef]
40. Zhang, J.; Liu, B.; Zhang, X.; Shen, H.; Liu, J.; Zhang, S. A Novel Approach for Preparing Glass Ceramic Foams from MSWI Fly Ash: Foaming Characteristics and Hierarchical Pore Formation Mechanism. *J. Mater. Res. Technol.* **2022**, *18*, 731–744. [CrossRef]
41. Li, H.; Wang, R.; Zhao, W.; Guo, H.; Yan, B.; Li, P. Sintered Glass-Ceramic Foams from Fluorite Tailings and Waste Glass with Calcium Phosphate Addition. *Constr. Build. Mater.* **2022**, *359*, 129528. [CrossRef]
42. da Costa, F.P.; Morais, C.R.d.S.; Pinto, H.C.; Rodrigues, A.M. Microstructure and Physico-Mechanical Properties of Al_2O_3-Doped Sustainable Glass-Ceramic Foams. *Mater. Chem. Phys.* **2020**, *256*, 123612. [CrossRef]
43. Hisham, N.A.N.; Zaid, M.H.M.; Matori, K.A.; Shabdin, M.K. Effect of Ark Clam Shell on Crystal Growth and Mechanical Evaluation of Foam Glass-Ceramic Derived from Cullet Glass Waste. *Mater. Sci. Eng. B* **2022**, *281*, 115730. [CrossRef]
44. Zhang, J.; Liu, B.; Zhao, S.; Shen, H.; Liu, J.; Zhang, S. Preparation and Characterization of Glass Ceramic Foams Based on Municipal Solid Waste Incineration Ashes Using Secondary Aluminum Ash as Foaming Agent. *Constr. Build. Mater.* **2020**, *262*, 120781. [CrossRef]
45. Zhang, C.; Wang, X.; Zhu, H.; Wu, Q.; Hu, Z.; Feng, Z.; Jia, Z. Preparation and Properties of Foam Ceramic from Nickel Slag and Waste Glass Powder. *Ceram. Int.* **2020**, *46*, 23623–23628. [CrossRef]
46. Siddika, A.; Hajimohammadi, A.; Mamun, M.A.A.; Alyousef, R.; Ferdous, W. Waste Glass in Cement and Geopolymer Concretes: A Review on Durability and Challenges. *Polymers* **2021**, *13*, 2071. [CrossRef]
47. Abdulazeez, A.S.; Idi, M.A.; Kolawole, M.A.; Hamza, B. Effect of Waste Glass Powder as A Pozzolanic Material in Concrete Production. *Int. J. Eng. Res.* **2020**, *9*, 589–594. [CrossRef]
48. Zhang, D.; Sun, F.; Liu, T. Study on Preparation of Coal Gangue-Based Geopolymer Concrete and Mechanical Properties. *Adv. Civ. Eng.* **2021**, *2021*, 5117584. [CrossRef]
49. Benazzouk, A.; Douzane, O.; Mezreb, K.; Laidoudi, B.; Quéneudec, M. Thermal Conductivity of Cement Composites Containing Rubber Waste Particles: Experimental Study and Modelling. *Constr. Build. Mater.* **2008**, *22*, 573–579. [CrossRef]
50. Du, Y.; Yang, W.; Ge, Y.; Wang, S.; Liu, P. Thermal Conductivity of Cement Paste Containing Waste Glass Powder, Metakaolin and Limestone Filler as Supplementary Cementitious Material. *J. Clean. Prod.* **2021**, *287*, 125018. [CrossRef]
51. Ziejewska, C.; Grela, A.; Hebda, M. Influence of Waste Glass Particle Size on the Physico-Mechanical Properties and Porosity of Foamed Geopolymer Composites Based on Coal Fly Ash. *Materials* **2023**, *16*, 2044. [CrossRef] [PubMed]
52. Łach, M.; Grela, A.; Komar, N.; Mikuła, J.; Hebda, M. Calcined Post-Production Waste as Materials Suitable for the Hydrothermal Synthesis of Zeolites. *Materials* **2019**, *12*, 2742. [CrossRef] [PubMed]
53. Łach, M.; Pławecka, K.; Bąk, A.; Lichocka, K.; Korniejenko, K.; Cheng, A.; Lin, W.T. Determination of the Influence of Hydraulic Additives on the Foaming Process and Stability of the Produced Geopolymer Foams. *Materials* **2021**, *14*, 5090. [CrossRef] [PubMed]

54. Kwek, S.Y.; Awang, H.; Cheah, C.B. Influence of Liquid-to-Solid and Alkaline Activator (Sodium Silicate to Sodium Hydroxide) Ratios on Fresh and Hardened Properties of Alkali-Activated Palm Oil Fuel Ash Geopolymer. *Materials* **2021**, *14*, 4253. [CrossRef] [PubMed]
55. *EN 12667:2001*; Thermal Performance of Building Materials and Products—Determination of Thermal. Available online: https://standards.iteh.ai/catalog/standards/cen/f845e9a0-09c4-43ef-955c-6478a0497fb4/en-12667-2001 (accessed on 29 August 2023).
56. *EN 12390-2:2019*; Testing Hardened Concrete—Part 2: Making and Curing Specimens for Strength Tests. Available online: https://standards.iteh.ai/catalog/standards/cen/ae7e6a86-1cbc-455e-8b2a-8964be9087f9/en-12390-2-2019 (accessed on 29 August 2023).
57. Deng, J.; Li, B.; Xiao, Y.; Ma, L.; Wang, C.P.; Lai-wang, B.; Shu, C.M. Combustion Properties of Coal Gangue Using Thermogravimetry–Fourier Transform Infrared Spectroscopy. *Appl. Therm. Eng.* **2017**, *116*, 244–252. [CrossRef]
58. Zhang, K.; Zhang, H.; Liu, L.; Yang, Y.; Liu, L.; Liu, Q.; Zhang, K.; Zhang, H.; Liu, L.; Yang, Y.; et al. Dispersibility of Kaolinite-Rich Coal Gangue in Rubber Matrix and the Mechanical Properties and Thermal Stability of the Composites. *Minerals* **2021**, *11*, 1388. [CrossRef]
59. Xu, B.; Liu, Q.; Ai, B.; Ding, S.; Frost, R.L. Thermal Decomposition of Selected Coal Gangue. *J. Therm. Anal. Calorim.* **2018**, *131*, 1413–1422. [CrossRef]
60. Bi, H.; Wang, C.; Lin, Q.; Jiang, X.; Jiang, C.; Bao, L. Combustion Behavior, Kinetics, Gas Emission Characteristics and Artificial Neural Network Modeling of Coal Gangue and Biomass via TG-FTIR. *Energy* **2020**, *213*, 118790. [CrossRef]
61. Choudhury, R.; Saikia, J.; Saikia, B.K. Mineralogical and Ash Geochemical Studies of Coal-Mine Shale and Its Hydrocarbon Potential: A Case Study of Shale from Makum Coalfield, Northeast India. *J. Geol. Soc. India* **2017**, *90*, 329–334. [CrossRef]
62. Mierzwiński, D.; Łach, M.; Hebda, M.; Walter, J.; Szechyńska-Hebda, M.; Mikuła, J. Thermal Phenomena of Alkali-Activated Metakaolin Studied with a Negative Temperature Coefficient System. *J. Therm. Anal. Calorim.* **2019**, *138*, 4167–4175. [CrossRef]
63. Li, J.; Wang, J. Comprehensive Utilization and Environmental Risks of Coal Gangue: A Review. *J. Clean. Prod.* **2019**, *239*, 117946. [CrossRef]
64. Li, Z.; Gao, Y.; Zhang, J.; Zhang, C.; Chen, J.; Liu, C. Effect of Particle Size and Thermal Activation on the Coal Gangue Based Geopolymer. *Mater. Chem. Phys.* **2021**, *267*, 124657. [CrossRef]
65. Grela, A.; Hebda, M.; Łach, M.; Mikuła, J. Thermal Behavior and Physical Characteristics of Synthetic Zeolite from CFB-Coal Fly Ash. *Microporous Mesoporous Mater.* **2016**, *220*, 155–162. [CrossRef]
66. Zhang, B.; Guo, H.; Deng, L.; Fan, W.; Yu, T.; Wang, Q. Undehydrated Kaolinite as Materials for the Preparation of Geopolymer through Phosphoric Acid-Activation. *Appl. Clay Sci.* **2020**, *199*, 105887. [CrossRef]
67. Aragaw, T.A.; Kuraz, F. Physico-Chemical Characterizations of Ethiopian Kaolin for Industrial Applications: Case Study WDP Propoxur Formulations. In *Lecture Notes of the Institute for Computer Sciences, Social-Informatics and Telecommunications Engineering, LNICST*; Springer International Publishing: Berlin/Heidelberg, Germany, 2019; Volume 274, pp. 122–134. [CrossRef]
68. Le, V.Q.; Do, Q.M.; Hoang, M.D.; Nguyen, H.T. The Role of Active Silica and Alumina in Geopolymerization. *Vietnam J. Sci. Technol. Eng.* **2018**, *60*, 16–23. [CrossRef]
69. Chargui, F.; Hamidouche, M.; Belhouchet, H.; Jorand, Y.; Doufnoune, R.; Fantozzi, G. Mullite Fabrication from Natural Kaolin and Aluminium Slag. *Bol. Soc. Esp. Cerám. Vidr.* **2018**, *57*, 169–177. [CrossRef]
70. Nishi, Y.; Inagaki, M. Gas Adsorption/Desorption Isotherm for Pore Structure Characterization. In *Materials Science and Engineering of Carbon: Characterization*; Butterworth-Heinemann: Oxford, UK, 2016; pp. 227–247. [CrossRef]
71. Xu, L.; Zhang, J.; Ding, J.; Liu, T.; Shi, G.; Li, X.; Dang, W.; Cheng, Y.; Guo, R. Pore Structure and Fractal Characteristics of Different Shale Lithofacies in the Dalong Formation in the Western Area of the Lower Yangtze Platform. *Minerals* **2020**, *10*, 72. [CrossRef]
72. Paiva, H.; Yliniemi, J.; Illikainen, M.; Rocha, F.; Ferreira, V.M. Mine Tailings Geopolymers as Awaste Management Solution for a More Sustainable Habitat. *Sustainability* **2019**, *11*, 995. [CrossRef]
73. Valášková, M.; Klika, Z.; Vlček, J.; Matějová, L.; Topinková, M.; Pálková, H.; Madejová, J. Alkali-Activated Metakaolins: Mineral Chemistry and Quantitative Mineral Composition. *Minerals* **2022**, *12*, 1342. [CrossRef]
74. Cheng, Y.; Hongqiang, M.; Hongyu, C.; Jiaxin, W.; Jing, S.; Zonghui, L.; Mingkai, Y. Preparation and Characterization of Coal Gangue Geopolymers. *Constr. Build. Mater.* **2018**, *187*, 318–326. [CrossRef]
75. Moghadam, M.J.; Ajalloeian, R.; Hajiannia, A. Preparation and Application of Alkali-Activated Materials Based on Waste Glass and Coal Gangue: A Review. *Constr. Build. Mater.* **2019**, *221*, 84–98. [CrossRef]
76. Jamil, N.H.; Abdullah, M.M.A.B.; Pa, F.C.; Mohamad, H.; Ibrahim, W.M.A.W.; Amonpattaratkit, P.; Gondro, J.; Sochacki, W.; Ibrahim, N. Self-Fluxing Mechanism in Geopolymerization for Low-Sintering Temperature of Ceramic. *Materials* **2021**, *14*, 1325. [CrossRef]
77. Matsimbe, J.; Dinka, M.; Olukanni, D.; Musonda, I. Geopolymer: A Systematic Review of Methodologies. *Materials* **2022**, *15*, 6852. [CrossRef] [PubMed]
78. Petlitckaia, S.; Poulesquen, A. Design of Lightweight Metakaolin Based Geopolymer Foamed with Hydrogen Peroxide. *Ceram. Int.* **2019**, *45*, 1322–1330. [CrossRef]
79. Szechyńska-Hebda, M.; Marczyk, J.; Ziejewska, C.; Hordyńska, N.; Mikuła, J.; Hebda, M. Optimal Design of PH-Neutral Geopolymer Foams for Their Use in Ecological Plant Cultivation Systems. *Materials* **2019**, *12*, 2999. [CrossRef]
80. Roviello, G.; Menna, C.; Tarallo, O.; Ricciotti, L.; Messina, F.; Ferone, C.; Asprone, D.; Cioffi, R. Lightweight Geopolymer-Based Hybrid Materials. *Compos. B Eng.* **2017**, *128*, 225–237. [CrossRef]

81. Zhang, H. Heat-Insulating Materials and Sound-Absorbing Materials. In *Building Materials in Civil Engineering*; Springer International Publishing: Cham, Switzerland, 2011; pp. 304–423. [CrossRef]
82. Amani, Y.; Takahashi, A.; Chantrenne, P.; Maruyama, S.; Dancette, S.; Maire, E. Thermal Conductivity of Highly Porous Metal Foams: Experimental and Image Based Finite Element Analysis. *Int. J. Heat. Mass. Transf.* **2018**, *122*, 1–10. [CrossRef]
83. Smiljanić, S.; Hribar, U.; Spreitzer, M.; König, J. Influence of Additives on the Crystallization and Thermal Conductivity of Container Glass Cullet for Foamed Glass Preparation. *Ceram. Int.* **2021**, *47*, 32867–32873. [CrossRef]
84. Sitarz, M.; Figiela, B.; Łach, M.; Korniejenko, K.; Mróz, K.; Castro-Gomes, J.; Hager, I. Mechanical Response of Geopolymer Foams to Heating—Managing Coal Gangue in Fire-Resistant Materials Technology. *Energies* **2022**, *15*, 3363. [CrossRef]
85. Sinico, M.; Jadhav, S.D.; Witvrouw, A.; Vanmeensel, K.; Dewulf, W. A Micro-Computed Tomography Comparison of the Porosity in Additively Fabricated CuCr1 Alloy Parts Using Virgin and Surface-Modified Powders. *Materials* **2021**, *14*, 1995. [CrossRef]
86. Zhang, P.; Wang, K.; Li, Q.; Wang, J.; Ling, Y. Fabrication and Engineering Properties of Concretes Based on Geopolymers/Alkali-Activated Binders—A Review. *J. Clean. Prod.* **2020**, *258*, 120896. [CrossRef]
87. Ramamurthy, K.; Kunhanandan Nambiar, E.K.; Indu Siva Ranjani, G. A Classification of Studies on Properties of Foam Concrete. *Cem. Concr. Compos.* **2009**, *31*, 388–396. [CrossRef]
88. Jaya, N.A.; Yun-Ming, L.; Cheng-Yong, H.; Abdullah, M.M.A.B.; Hussin, K. Correlation between Pore Structure, Compressive Strength and Thermal Conductivity of Porous Metakaolin Geopolymer. *Constr. Build. Mater.* **2020**, *247*, 118641. [CrossRef]
89. *ACI 318M-11*; Building Code Requirements for Structural Concrete (ACI 318M-11). American Concrete Institute: Farmington Hills, MI, USA, 2011.

materials

MDPI

Supplementary material

Eco-Friendly Coal Gangue and/or Metakaolin-Based Lightweight Geopolymer with the Addition of Waste Glass

Celina Ziejewska [1], Agnieszka Bąk [1], Krzysztof Hodor [2] and Marek Hebda [1,*]

[1] Cracow University of Technology, Faculty of Materials Engineering and Physics, Warszawska 24, 31-155, Kraków, Poland; celina.ziejewska@pk.edu.pl (C.Z.); agnieszka.bak@pk.edu.pl (A.B.)
[2] NETZSCH (Netzsch Instrumenty Sp. z o.o.), Halicka 9, 31-036 Kraków, Poland; krzysztof.hodor@netzsch.com (K.H.)
* Corresponding: marek.hebda@pk.edu.pl (M.H.)

Table S1. Chemical composition of geopolymer foams.

Chemical compound	C	CG	M	MG	CMG
SiO_2	55.957	56.680	61.012	61.026	61.299
Al_2O_3	18.075	14.622	28.684	27.562	21.301
Fe_2O_3	11.654	11.797	1.650	1.596	5.350
CaO	8.067	11.189	6.356	7.654	8.466
K_2O	2.823	2.700	1.253	1.139	1.690
SO_3	1.906	1.520	0.485	0.497	1.059
TiO_2	1.135	1.075	0.372	0.345	0.600
MnO	0.126	0.140	0.033	0.038	0.066
V_2O_5	0.065	0.061	0.021	0.017	0.033
SrO	0.061	0.063	0.027	0.029	0.041
Cr_2O_3	0.035	0.040	0.011	0.010	0.018
ZrO_2	0.033	0.034	0.016	0.016	0.025
ZnO	0.026	0.028	0.013	0.012	0.016
CuO	0.015	0.014	0.008	0.007	0.009
Ga_2O_3	0.007	-	0.010	0.007	0.007
NbO	0.003	-	0.003	0.002	0.002

Table S2. 3D view of the sample, 2D view of the sample (first slice), slice perpendicular to the marked yellow line.

Samples designation		
C		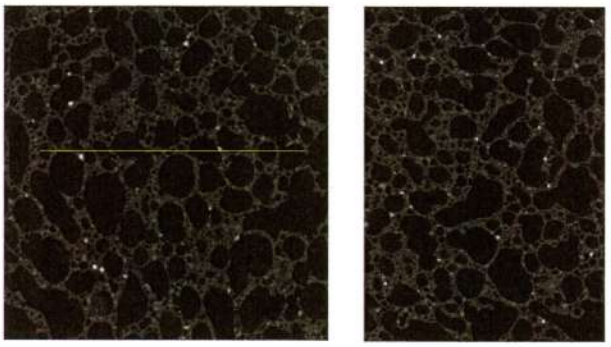
CG	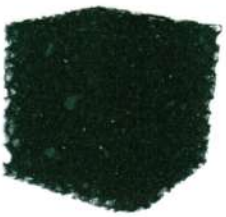	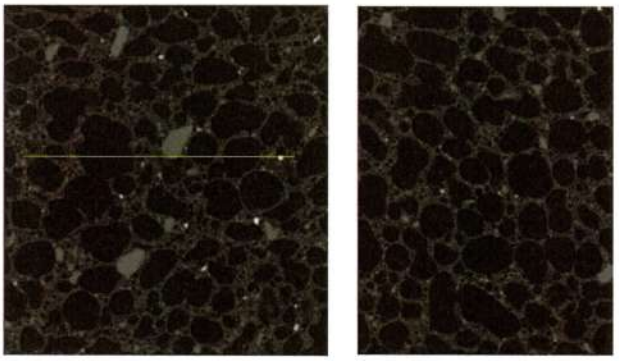
CMG	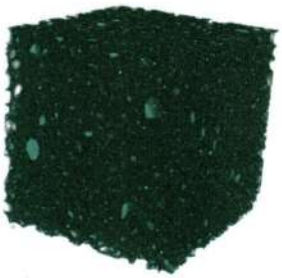	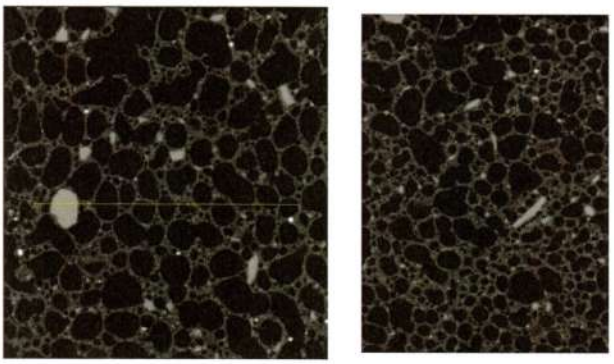

Załącznik 8 – oświadczenia współautorów dotyczące publikacji P4

Kraków, dn. 23.11.2023 r.

OŚWIADCZENIE – PUBLIKACJA P4

Oświadczam, iż mój wkład w powstanie publikacji pt.: „*Eco-Friendly coal gangue and/or metakaolin-based lightweight geopolymer with the addition of waste glass*" opublikowanej w czasopiśmie *Materials* w 2023 roku, nr DOI: 10.3390/ma16176054 jest zgodny z informacją zawartą w poniższej tabeli.

Jednocześnie oświadczam, iż wyrażam zgodę na wykorzystanie wyżej wymienionej publikacji jako część rozprawy doktorskiej mgr inż. Celiny Ziejewskiej.

Autor	Wkład w powstanie publikacji
Celina Ziejewska	Sformułowanie problemu badawczego, opracowanie koncepcji badań, przygotowanie materiałów bazowych, synteza geopolimerów, opracowanie metodyki badań, przeprowadzenie badań i analiza wyników: oznaczenia składu chemicznego materiałów metodą rentgenowskiej spektroskopii fluorescencyjnej (XRF), analizy wielkości cząstek surowców, rentgenowskiej jakościowej i ilościowej analizy fazowej surowców oraz materiałów kompozytowych (XRD), badań z zastosowaniem analizatora sorpcji fizycznej (określenie powierzchni właściwej, rozmiarów i objętości porów), gęstości właściwej surowców, obserwacji morfologii pianek geopolimerowych z zastosowaniem skaningowego mikroskopu elektronowego oraz mikroskopu cyfrowego, porowatości geopolimerów. Przygotowanie materiałów i analiza wyników: wytrzymałości na ściskanie geopolimerów, rezultatów uzyskanych za pomocą sprzężonych metod analizy termicznej oraz mikrotomografii komputerowej. Interpretacja i opracowanie graficzne wyników, przygotowanie pierwszej wersji manuskryptu, przygotowanie ostatecznej wersji manuskryptu, korekta manuskryptu po recenzjach.
Agnieszka Bąk	Realizacja części badań przewodności cieplnej pianek geopolimerowych.
Krzysztof Hodor	Opracowanie metodyki badań, realizacja badań surowców metodą sprzężonej analizy termicznej TG–FTIR, analiza uzyskanych rezultatów.

Marek Hebda	Sformułowanie problemu badawczego, opracowanie koncepcji i metodyki badań, zarządzanie zespołem badawczym, walidacja uzyskanych danych i ich analizy, nadzór merytoryczny nad prowadzonymi badaniami, analiza wyników badań, opracowanie graficzne wyników, pozyskanie finansowania na poczet zrealizowanych badań i kosztów publikacyjnych, udział w pisaniu pierwszej wersji manuskryptu; dyskusja i udział w przygotowaniu ostatecznej wersji manuskryptu, korekta manuskryptu po recenzjach.

Celina Ziejewska
podpis oświadczającego
mgr inż. Celina Ziejewska

Agnieszka Bąk
podpis oświadczającego
mgr inż. Agnieszka Bąk

Krzysztof Hodor
podpis oświadczającego
dr inż. Krzysztof Hodor

podpis oświadczającego
dr hab. inż. Marek Hebda, prof. PK